CRANFIELD UNIVERSITY

MAHDI ARABNEJAD

Development of an Impedimetric Biosensor for Lung Cancer Detection

School of Aerospace, Transport and Manufacturing

PhD THESIS

Academic Year: 2014 - 2018

Supervisor: Professor Ibtisam E. Tothill
Dr. Iva Chianella

CRANFIELD UNIVERSITY

SCHOOL OF AEROSPACE, TRANSPORT AND MANUFACTURING

PhD THESIS

Academic Year 2014 2018

MAHDI ARABNEJAD

DEVELOPMENT OF AN IMPEDIMETRIC BIOSENSOR FOR LUNG CANCER DETECTION

Supervisor: Professor Ibtisam E. Tothill
Dr Iva Chianella

Abstract

The promise of biosensors offering attractive features has kept the field active and growing. The aim is often to develop a device which is sensitive, specific, rapid, portable, cheap, and with the ability to capture an analyte in different matrices without cross-reactivity. The challenges increase when the aim is simultaneous multi-analyte detection on a single platform, without the need for complex procedures and expensive instruments. Such a system is invaluable in many clinical settings, where disease diagnosis and progression are multifactorial. Cancer is a good example of complex diagnosis requirements. This project is aimed at the development of biosensing platform to overcome the aforementioned problems and allow direct, simple analysis with the minimum of sample pre-treatment. The early detection of lung cancer has been chosen as there is no commercial biosensor available for detection of this disease and for lung cancer diagnosis multi-analyte recognition is necessary.

This project presents the development of impedimetric and magnetic sensing platform for early detection of lung cancer via detecting the neuron-specific enolase (NSE) and carcinoembryonic antigen (CEA) which are known as potential lung cancer biomarkers. The sensing platform developed here comprises of magnetic manipulation, screen printed electrode (SPE), and magnetic nanobeads. The magnetic nanobeads (MBs) were functionalised with antibodies to fish the analyte from the sample, and to move them over the sensing area. Moreover, magnetic nanobeads were used to increase the chance of antigen-antibody complex formation.

After cleaning the surface of electrodes with 50 mM KOH in 25% H_2O_2 (for 10 minutes), immunosensors were developed by immobilising the antibodies on the gold working electrode of SPEs through formation of self-assembled monolayer (SAM layer) due to its simplicity, stability, well-organised structure and low background noise.

The optimised NSE immunosensor with 10 µg/ml of 10-7937 antibody was successfully tested to measure various concentrations of NSE protein (0 – 100 ng/ml) in both PBS buffer and 100 % serum using functionalised MBs with 2.4 mg/ml of 10-7938

antibody. The optimised sensor achieved detection limit of 0.18 ng/ml (R^2 = 0.9848) in buffer and 0.52 ng/ml (R^2 = 0.9977) in 100 % serum with via EIS with the use of 10 mM potassium ferri/ferrocyanide as a redox probe.

The impedimetric CEA immunosensor was developed and optimised by use of 20 µg/ml of 12-140-01 antibody and was used to measure analyte with functionalised MBs with 2.4 mg/ml of 12-140-10 antibody. The CEA immunosensor was also able to measure various CEA concentrations (0 – 100 ng/ml) in both PBS buffer and 100 % serum in presence of 10 mM potassium ferri/ferrocyanide. The sensor achieved low limit of detection as 0.26 ng/ml (R^2 = 0.9924) and 0.76 ng/ml (R^2 = 0.9839) for CEA detection in buffer and 100 % serum, respectively.

In conclusion, both immunosensors developed here, using EIS and the magnetic sensing platform, were capable of detecting their corresponding biomarkers in serum in relatively short time (40 minutes) and in the appropriate concentration range, as serum concentrations higher than 12.5 ng/ml and 7 ng/ml for NSE and CEA respectively can indicate presence of cancer.

To the best of our knowledge, no one has reported a use of magnetic platform as the one developed in this thesis.

Keywords: Lung cancer, Magnetic nanobeads, MBs, CEA, NSE, EIS, Biosensor

Acknowledgements

I would like to convey my heartfelt gratitude and sincere appreciation to all who have helped and inspired me during my doctoral study. This PhD work and thesis would have not been possible without the support and care given by my family, friends, and colleagues at Cranfield University.

I would like to extend my sincerest gratitude to my supervisor, Professor Ibtisam E. Tothill, for her invaluable support, guidance, trust, enthusiasm and help through the last year of my PhD study. The completion of this PhD and thesis would have not been possible without her enormous help. I would also like to give warmest thanks to my co-supervisor Dr Iva Chianella for her availability, support, and constructive suggestions. My Special thanks also to my first-year supervisor Dr Mohammed Zourob and also to my second-year supervisor Dr Jeffrey D. Newman.

Special thanks to my dear lab mates: Dr Shayalini Wignarah, Antonio Rendon Romero, Roberta D'Aurelio, Dr Joanne Holmes, Dr Sinead Carr, Dr Stuart Collyer and Dr Sofia Foukaraki, who have all supported me throughout the process of my PhD and for all the fun we have had in the last three years. I also owe a special gratitude to all my friends especially Dr Ali S. Al-Turaihi, Dr Chrysi Karagiannaki, Navid Khallaghi and Dr Mohammadali Bahrami for all the support, unconditional friendship and caring they provided.

Last, but by no means least, my deep and sincere gratitude to my parents and family for their undying support and encouragement throughout my entire life. I am forever indebted to my parents for providing me the chance to do this PhD and for supporting me emotionally and financially through the hardest and pleasant parts of my PhD. Their guidance and support have allowed me to have the experience that made me who I am. Finally, I would especially like to thank my beautiful wife Saradokht Pournamdari for her enormous patience and never-ending care and love.

Table of Contents

List of Figures

List of Tables

List of Equations

List of Abbreviations

%CV	Percentage of coefficient variation
µA	Microampere
µg	Microgram
µl	Microliter
11-MUA	11-Mercaptoundecanoic acid
Ab	Antibody
Ag	Antigen
BSA	Bovine serum albumin
C_{dl}	Double layer capacitor
CE	Counter electrode
CEA	Carcinoembryonic antigen
CT Scan	Computerised demography scan
dH_2O	Deionised water
DMF	N,N-dimethyl formamide
DNA	Deoxyribonucleic acid
EDC	1-3-dimethylaminopropyl-3-ethylcarbodiimide hydrochloride
EIS	Electrochemical impedance spectroscopy
E_{pa}	Anodic peak potential
E_{pc}	Cathodic peak potential
g	Gram

H_2O_2	Hydrogen peroxide
HCl	Hydrochloric acid
Hz	Hertz
KDa	Kilodalton
KHz	Kilohertz
KOH	Potassium hydroxide
KΩ	Kilohm
LoD	Limit of detection
M	Molar
mA	Millianpere
mg	Milligram
ml	Millilitre
mM	Millimolar
MB	Magnetic nanobeads
MIP	Molecular imprinted polymer
MMP	Magnetic microparticle
MNP	Magnetic nanoparticle
MRI	Magnetic resonance imaging
ng	Nano gram
NHS	N-Hydroxysuccinide
NP	Nanoparticle

NSCLC	Non-small cell lung cancer
NSE	Neuron-Specific enolase
PBS	Phosphate buffer saline
PDITC	p,phenylene diisothiocyanate
PET Scan	Positron emission tomography scan
RE	Reference electrode
R_{et}	Resistance of electron transfer
RNA	Ribonucleic acid
R_s	Resistance of solution
S	Second
SAM	Self-assembled monolayer
SCLC	Small cell lung cancer
SD	Standard deviation
SPE	Screen printed electrode
SPR	Surface plasmon Resonance
V	Voltage
WE	Working electrode
Z_w	Warburg impedance
Ω	Ohm

Chapter 1:

INTRODUCTION & LITERATURE REVIEW

1.1. Introduction

The continual proliferation and spread of unregulated cells due to mistake(s) at the DNA/ RNA transcription, or protein translation stage is known as cancer disease that can affect more than 60 organs within the human body (Altintas et al., 2012; Chen et al., 2012; Arya & Bhansali, 2011). Cancer is the result of the interaction between genetic and environmental factors which can be categorised into 3 groups of chemical (*e.g.* arsenic), physical (*e.g.* ultraviolet radiation), and biological (*e.g.* viruses) carcinogens (WHO, 2017). Cancer Research UK reported >14 million cancer incidences occurred worldwide in 2012 (Figure 1.1), which led to 8.2 million deaths (Cancer Research UK, 2014a). They have also predicted an annual cancer morbidity of 23.6 million by 2030.

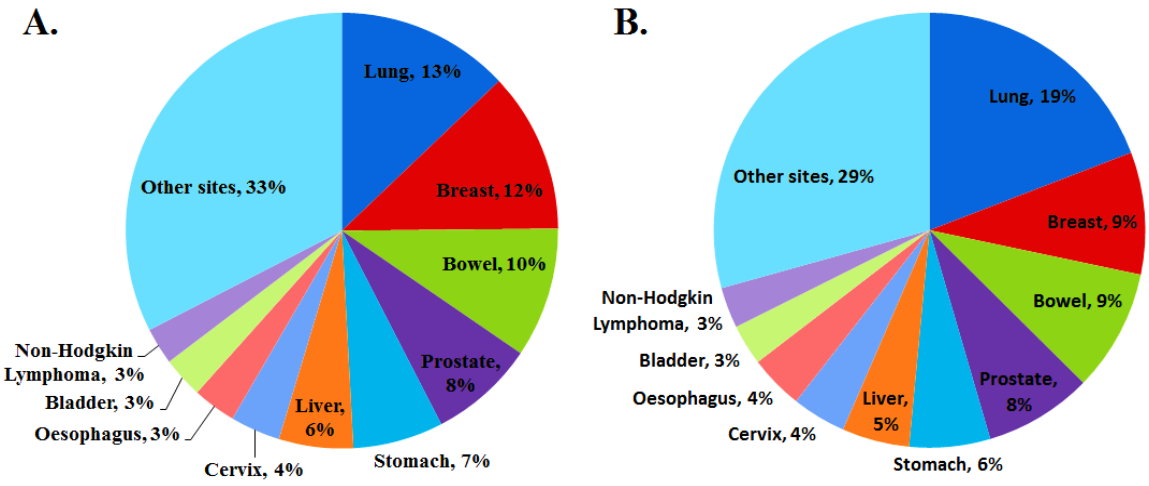

Figure 1.1: Worldwide Cancer Statistics (2012), A. Cancer Incidence Rate, B. Cancer Death Rate. (Data Extracted from www.cancerresearchuk.org (Cancer Research UK, 2014b, 2014c).

Figure 1.1, shows, that lung cancer was the most prevalent cancer in the world in 2012, which caused 13% (1.8 million) cancer incidences and 19% (1.6 million) cancer deaths. The rates of lung cancer morbidity and mortality are rapidly increasing annually which make lung cancer as one of the most serious health issue (Chen et al., 2015). Li & Hong (2013) reported that during the last 3 decades, lung cancer increased by 464.84%

(Li & Hong, 2013). The most of cancer-related death, about 90%, are caused by tumour metastases (Tian et al., 2017a).

1.2. Lung cancer

Uncontrolled cell proliferation of epithelial cells within the lung airways develops lung cancer disease (Kashyap et al., 2015). Lung cancer (Figure 1.2) is the most common type of cancer and the leading cause of cancer-related death in the world. It can be categorised into two main types by histology: Small Cell Lung Cancer (SCLC) and Non-Small Cell Lung Cancer (NSCLC) (Arya & Bhansali, 2011; Kalari et al., 2013; Cagle et al., 2013). Although there are lung cancer related symptoms, they may not appear until the advanced stage of the disease. The most general lung cancer symptoms are tiredness, shortness of breath, chest pain, persistent cough, coughing up blood, weight loss and difficulty in swallowing (Ettinger et al., 2015; Cancer Research UK, 2017). Lung cancer is classified into 4 stages based on the size of the tumour and whether it has spread out to other parts of the body. Depending on the stage of lung cancer, the treatment methods available are surgical excision, chemotherapy, and radiation therapy (Rang et al., 2007). Untreated lung cancer leads to the spread of cancer cells to other parts of the body in a process known as metastasis, and eventually this can lead to death.

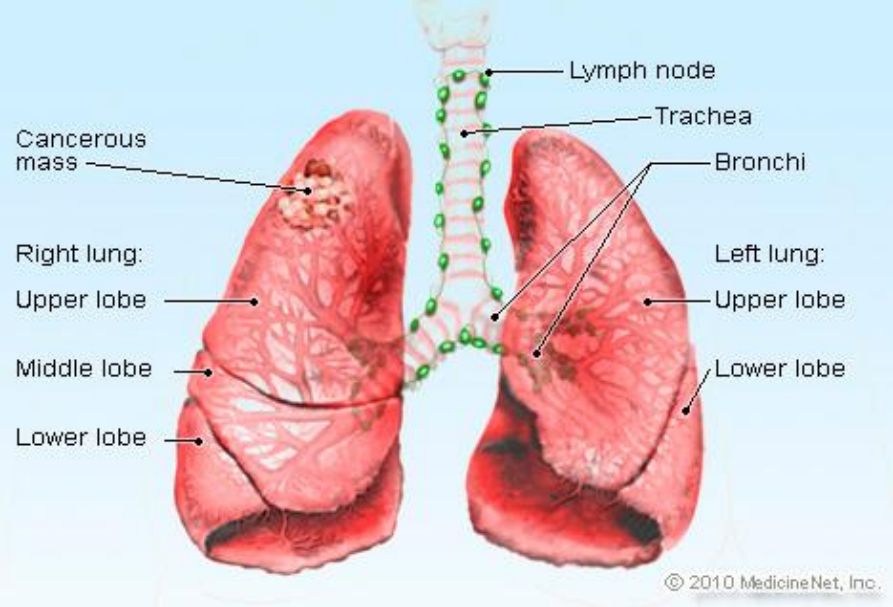

Figure 1.2: Image of lung cancer (MedicineNet, 2010).

1.2.1 Small Cell Lung Cancer (SCLC)

SCLC includes three groups: small cell cancer, mixed small/large cell cancer, and combined small cell cancer (Arya & Bhansali, 2011). Approximately 10 to 15% of lung cancer incidences are SCLCs which are normally originated from neuroendocrine cell precursors and they are closely linked to smoking habits. This type of lung cancer has a high growth rate and has the ability of spreading quickly at early stage of cancer. Hence 60% to 70% of patients are diagnosed at the metastasis stage of cancer. Although SCLC initially responds well to radiotherapy and chemotherapy, rapid drug resistance development might occur during treatment, which results in cancer recurring in most patients (Rossi et al., 2013; Früh et al., 2013; Byers & Rudin, 2015). The survival time of SCLC without treatment is between 2 to 4 months, whereas receiving the treatment can increase the survival time depending on the stage of cancer. The survival time for patients who received treatment with advanced SCLC is between 7 to 12 months, while it is 16 to 24 months for patients with earlier stage disease. Therefore, early diagnosis of the SCLC is essential (Kalari et al., 2013; Harmsma et al., 2013).

1.2.2 Non-Small Cell Lung Cancer (NSCLC)

NSCLC has the highest cancer related mortality rate. About 85% to 90% of lung cancer occurrence is caused by NSCLCs (Kashyap et al., 2015). Based on the pathological characterisation it can be further divided into three groups: large cell carcinoma (~10%), squamous cell carcinoma (~40%), and adenocarcinoma (~50%) (Cagle et al., 2013; Ali et al., 2016). Although NSCLC subtypes have different characterisation such as shape and size, they are categorised in the same group since they have almost the same prognosis and treatment procedure (Kashyap et al., 2015; Ali et al., 2016).

Once the patient has been diagnosed with NSCLC the treatment can be started based on the physical health of the patient and the stage of the disease. For instance, the standard treatment for stage one to three is surgery and combination chemotherapy; while for more locally advanced NSCLC radiotherapy and chemotherapy are suitable treatments (Chung & Christianson, 2014; Song et al., 2016; Tian et al., 2017b). However, the surgery is known as the most effective method for NSCLC treatment. Though for most patients, (70%) surgery cannot be used as the line of treatment as NSCLC is usually diagnosed at the late stage, *e.g.* metastatic stage (Cagle et al., 2013; Ettinger et al., 2015; Shin et al., 2015). Therefore, the treatment options will be limited to standard treatments such as chemotherapy and radiation therapy, with a response rates of 30 to 40%, for most of patients that cannot be cured by surgery. Moreover, late diagnosis of NSCLC also results in 5-year survival rate of about 15% of patients with a high chance of cancer recurring; while the 5-year survival rate for early stage disease is >50% (Hensing & Salgia, 2013; Zhang et al., 2013; Cagle et al., 2013; Shin et al., 2015; Najlah et al., 2017)

1.3. Diagnosis Methods Used for Lung Cancer Detection

Lung cancer can be diagnosed by the following methods: sputum cytology, computerised tomography scan (CT scan), positron emission tomography scan (PET), X-ray, bronchoscopy, magnetic resonance imaging (MRI), and immunohistochemistry (IHC) (Sharma et al., 2012; Altintas et al., 2012; Harmsma et al., 2013; Kashyap et al., 2015). Once the patient is suspected of having lung cancer, a series of tests and imaging

will be applied to confirm the lung cancer. Figure 1.3 shows the procedure used for lung cancer diagnosis.

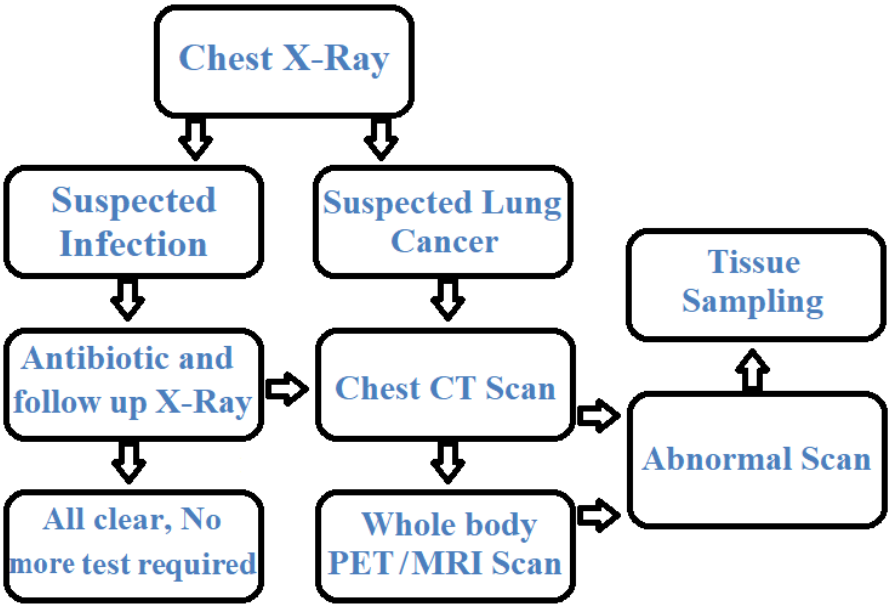

Figure 1.3: Lung Cancer Diagnosis Pathway.

As Figure 1.3 shows that infection can also result in having abnormal chest X-ray. Therefore, further scanning such as a CT scan is required. The chest CT scan is good in providing critical information such as the tumour location. Since, it is not accurate in distinguishing the benign from the malignant tumour, a whole body PET scan is required for staging lung cancer and checking the cancer metastatic. Even though the CT and PET scan have high specificity and sensitivity, false positive results might be obtained from other causes such as infection. Hence, tissue biopsy is an unavoidable part of lung cancer diagnosis (Silvestri et al., 2003).

The aforementioned methods have two main disadvantages. The first disadvantage is that most of them are invasive and rely on tissue biopsy especially in the case of SCLC, as cancer cells are located submucosally. The second one is that these methods are not able to detect lung cancer at an early stage. These methods are based on morphology of the cell and not designed for specific cancer detection.

The diagnosis of lung cancer through cancer biomarkers within body fluids, *e.g.* blood, can be effective, less invasive and helps in early diagnosis (Tothill, 2009; Sharma et al., 2012; Harmsma et al., 2013). The early lung cancer diagnosis is important as the highest cancer therapeutic potential is at its early stage of development, and the disease symptoms do not appear in patients until the late cancer stage (Arya & Bhansali, 2011; Zhang et al., 2013; Patra & Turner, 2014). Thus, early diagnosis of cancer increases the chance of respond to treatment and reduces the treatment cost.

1.4. Potential Lung Cancer Biomarkers (Analytes)

"Biomarker (biological marker) is an objectively measured characteristic that can be an indicator of a normal biological, pathologic process or pharmacologic response to a specified therapeutic intervention." (Atkinson et al., 2001).

As cancer cells start to grow and develop within the body, they release different types of biological substances such as metabolites, proteins, hormones, and nucleic acids (DNA and RNA) (Altintas & Tothill, 2013). Since the release of these biological substances is proportional to the stage of cancer, they can be used as cancer biomarkers (Arya & Bhansali, 2011). An individual with the same or higher biomarker concentration than the cut-off value is suspicious of having cancer. Detection of biomarkers within tumour cells, urine, sputum, or blood fluids not only allows cancer recognition at its early stage; but also can help in therapeutic processes (Su et al., 2008).

Cancer diagnosis via detection of biomarkers has the advantages of being less invasive and less painful in comparison with traditional methods of disease diagnosis such as tissue biopsy which is the gold standard (Tian et al., 2017a). Especially considering that sometimes multi-spot tissue biopsy is required, and the samples must be fresh. Among the sources of lung cancer biomarkers, blood might be the best choice. Ease of access, ability of continuously monitoring of the disease, and release of biomarkers at a very early stage of lung cancer development within the blood, are the advantages of using blood samples for cancer biomarker detection (Indovina & Marcelli, 2013; Altintas & Tothill, 2013; Hensing & Salgia, 2013).

Cancer biomarkers can be categorised into 3 categories. The first is diagnostic biomarkers which are normally used for detection and identification of the type of cancer, although they also can be used for therapeutic monitoring purposes. The second category is predictive biomarkers which can suggest therapeutic decisions; in other words, they can predict the treatment outcome as these biomarkers are the aim of therapy. Finally prognostic biomarkers, a third category, are used to provide information on patient outcome, for instance patient survival, independently from treatments (Grunnet & Sorensen, 2012; Chen et al., 2012; Chung & Christianson, 2014). Therefore, blood-based biomarkers provide key information which can be used for early diagnosis, staging and subtyping of the cancer, the therapeutic response, and patient survival. They are important lung cancer diagnostic tools which can also be applied for lung cancer patient management (Holdenrieder, 2016).

Table 1.1 presents the list of biomarkers for lung cancer diagnosis. The most used biomarkers for NSCLC diagnosis are carcinoembryonic antigen (CEA), cytokeratin 19 fragment antigen (CYFRA 21-1) and squamous cancer cell antigen (SCCA). The neuron-specific enolase (NSE) is the most famous biomarker for SCLC diagnosis (Holdenrieder, 2016). However, NSE protein may be found in blood of the patient with NSCLC which is an indicator of neuroendocrine property of the tumour that makes the cancer more aggressive. Although they normally respond well to chemotherapy (Kulpa et al., 2002).

CEA, NSE, and CYFRA 21-1 are well known biomarkers for early diagnosis of lung cancer. Cytokeratin 19 fragment antigen, also known as CYFRA 21-1, is a small soluble protein (40 kDa) from intermediate filaments family, present in epithelia cells. CYFRA 21-1 protein has been known as an epithelium cell-death indicator (Altintas & Tothill, 2013; Anderson et al., 2006; Arai et al., 2014; Kumar et al., 2016; Luo et al., 2013). Following cell apoptosis, caspase3 protease activity increases which degrades cytokeratin 19 and releases small fragments including CYFRA 21-1 into the body fluids and tissues during some pulmonary pathology, SCLC, and specially NSCLC (Ono et al., 2013; Xu et al., 2014). Hence, it is considered as one of the main biomarkers for cancer diagnosis.

Table 1.1: List of lung cancer biomarkers.

Type of Biomarker	Lung cancer biomarker	Reference
Protein	Carcinoembryonic antigen (CEA)	(Sawabata et al., 2002)
	Serum cytokeratin fragment 21-1 (CYFRA21-1)	(Pujol et al., 2004)
	Neuron specific enolase (NSE)	(Kulpa et al., 2002)
	p53	(Cheng et al., 2003)
	Epidermal growth factor receptor (EGFR)	(Mitsudomi et al., 2005)
	Human epithermal growth factor receptor 2 (HER2)	(Brabender et al., 2001)
	Squamous cell lung carcinoma antigen (SCC)	(Yu et al., 2013)
	Cyclin D1	(Gautschi et al., 2007)
	C-erbB2	(Kristiansen et al., 2001)
	Tissue polypeptide antigen (TPA)	(Foa et al., 1999)
	Carbohydrate antigen 19-9 (CA 19-9)	(Lin et al., 2012)
	Carbohydrate antigen 125 (CA125)	(Yu et al., 2013)
	Alpha-fetoprotein (AFP)	(Yoshimoto et al., 1987)
	Matrix metalloproteinase (MMP-9, MMP-7)	(Jumper et al., 2004) (Liu et al., 2007)
	Tissue inhibitor of matrix metalloproteinase (TIMP-1)	(Jumper et al., 2004)
	Interleukin 6 (IL-6); interferon γ (IFN-γ)	(Martin et al., 1999)
Genetic	Kirsten rat sarcoma (k-ras)	(Slebos et al., 1990)
	Fragile histidine triad (FHIT)	(Li et al., 2007)
	Methylation of tumour suppressor gene p16	(Hensing & Salgia, 2013)
	Circulating micro-RNAs (miR-25, miR-223)	(Kosaka et al., 2010)
	Krueppel-like factor 6 (KLF6)	(Ito et al., 2004)
	Myelocytomatosis (myc) family	(Little et al., 1983) (Nau et al., 1986, 1985)
	Ras association domain family 1A (RASSF1A)	(Liu et al., 2013)
	Cell division cycle 25 B (cdc25B)	(Sasaki et al., 2001)
	Kallikrein family (KLK5, 6, and 7)	(Planque et al., 2005) (Nathalie et al., 2009)

The overexpression of CYFRA 21-1, which occurs in more than 50% of NSCLC patients, is strongly linked with cancer stage, relapse of the disease, and survival time (Chen et al., 2015, 2017; Zeng et al., 2017). CYFRA 21-1 protein has been reported as highly sensitive and specific prognostic NSCLC biomarker which is overexpressed in approximately 70 to 85% of patients (Kulpa et al., 2002; Harmsma et al., 2013; He et al., 2013). Different studies have reported different CYFRA 21-1 cut-off levels in the blood and thus they obtained different sensitivity and specificity. For instance, Okamura et al. (2013) reported 3.5 ng/ml, Pujol et al. (2004) mentioned 3.6 ng/ml, and Swellam et al. (2008) indicated 5.6 ng/ml as cut-off level for the CYFRA 21-1 biomarker. Recently, research was carried out in the biosensor area toward the detection of CYFRA 21-1. For instance, Kumar et al. (2016) and Zeng et al. (2017) have used differential pulse voltammetry technique to measure CYFRA 21-1 and they have achieved the LoD of 0.122 ng/ml and 0.1 ng/ml, respectively.

In this thesis, CEA and NSE were selected as the biomarkers of interest to develop the biosensors. Therefore, these two biomarkers will be covered in more details.

1.4.1 Carcinoembryonic Antigen (CEA)

One of the potential prognostic biomarkers for lung cancer is carcinoembryonic antigen (CEA) (Figure 1.4) (Arrieta et al., 2009; Arya & Bhansali, 2011; Grunnet & Sorensen, 2012; Altintas & Tothill, 2013). CEAs are cell surface glycoproteins from immunoglobulin superfamily of cell adhesion molecules family (Moreira et al., 2016). These proteins have molecular weights of 180 kD and are usually produced during the fetal development and are not normally presents is the body of healthy individuals (Zhu et al., 2013).

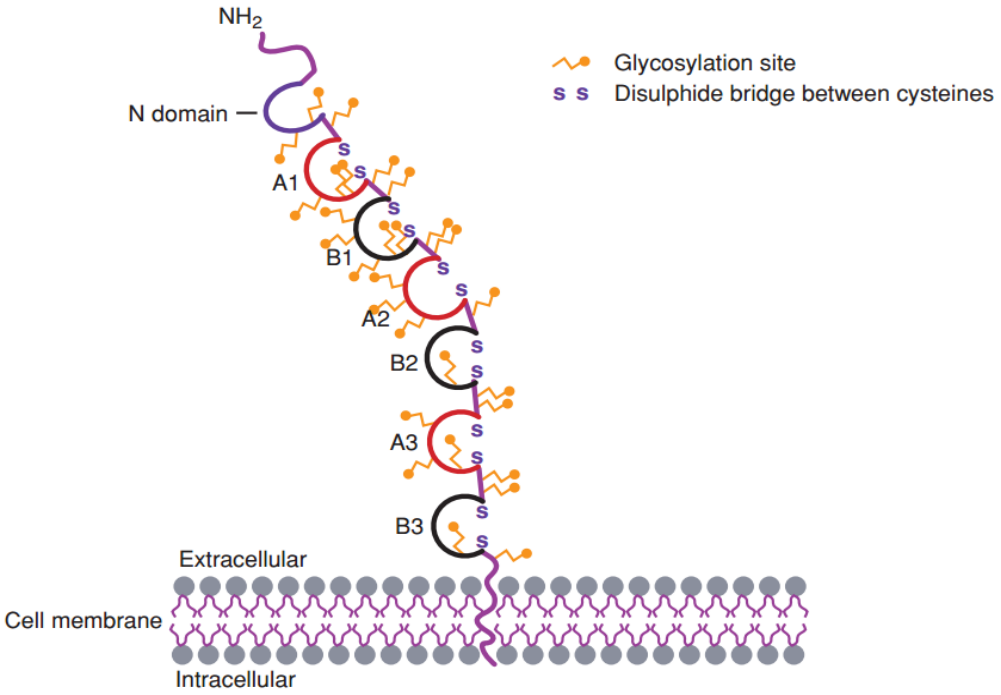

Figure 1.4: The Molecular Structure of CEA Protein; It consists of 7 domains as: N domain, 3 of A domains and 3 of B domains. Each domain is formed by disulphide bond between its four cysteine residues (Kaufman et al., 2000).

Although CEA can be found in the blood of people who smoke cigarettes (< 5 ng/ml), the concentration of CEA increase significantly in blood serum of patients with lung cancer (Yu & Cao, 2012). Elevated levels of CEA protein in the blood of patients can be an indicator of lung cancer, breast cancer, colon cancer, or ovarian carcinoma (Altintas & Tothill, 2013; Grunnet & Sorensen, 2012; Harmsma et al., 2013). The cut-off value for CEA detection is not the same in all studies. For instance, Su et al. (2008) indicated that CEA concentration in blood serum of healthy individuals is 2.5 – 5 ng/mL although its concentration in cancer patients is higher than 100 ng/mL; while Grunnet & Sorensen (2012) literature review shows the use of 5 to 7 ng/ml as the cut-off value for the majority of researches. In recent years numerous studies have been carried out to develop a biosensor for detection of CEA (Table 1.2) as a potential blood marker of lung cancer (Fragoso et al., 2010; Špringer & Homola, 2012; Zhu et al., 2013; Lei et al., 2013; Yeh et al., 2013; Altintas & Tothill, 2013).

Table 1.2: Developed biosensors for CEA detection.

Type of Sensor	Linear Range	Limit of Detection (LoD)	Reference
Amperometric	1 pg/ml–50 ng/ml	0.3 pg/ml	(Sun et al., 2014)
Anodic stripping voltammetry	0.05 pg/ml–1 ng/ml	0.024 pg/ml	(Lin et al., 2014)
Differential pulse voltammetry	1 fg/ml–100 pg/ml	0.001 pg/ml	(Wang et al., 2013)
Amperometric	0.1–2 ng/ml	60 pg/ml	(Gao et al., 2011)
Differential pulse voltammetry	0.1–750 ng/ml	~90 pg/ml	(Liu et al., 2015)
Differential pulse voltammetry	10 fg/ml–100 ng/ml	0.003 pg/ml	(Sun & Ma, 2012)
Surface plasmon resonance	0.4 – 25 ng/ml	100 pg/ml	(Špringer & Homola, 2012)
Impedimetric	1 pg/ml–80 ng/ml	0.64 pg/ml	(Hou et al., 2013)
Impedimetric	0.05 pg/ml–20 ng/ml	0.023 pg/ml	(Zhou et al., 2017)
Impedimetric	1.5 – 60 ng/ml	500 pg/ml	(Pan & Yang, 2007)
Impedimetric	0.5 – 20 ng/ml	100 pg/ml	(Tang et al., 2007)
Impedimetric	1 pg/ml – 0.5 ng/ml 1 – 40 ng/ml	0.03 pg/ml	(Zhou et al., 2016)
Impedimetric	1 pg/ml–100 ng/ml	0.1 pg/ml	(Zhou et al., 2014)
Impedimetric	0.1–1000 ng/ml	60 pg/ml	(Li et al., 2017)

1.4.2 Neuron-Specific Enolase (NSE)

Enolase is a 78 kDa glycolytic enzyme that consists of αα, ββ, γγ, αγ, and βγ isozyme (Holmes et al., 2011). Those isozymes with γ subunit are found in neurons and endocrine cells (Figure 1.5), and thus are called neuron-specific enolase (NSE) (Harmsma et al., 2013; Altintas & Tothill, 2013; Yang et al., 2014; Yang et al., 2014). NSE is known to be a reliable, sensitive and specific biomarker associated with SCLC, neuroendocrine cancer, and neuroblastoma (Wang & Ma, 2017). Although the stroke or cerebral injury can also cause elevation of NSE concentration within the blood serum, the concentration reached the normal level within a week of the event (Holmes et al., 2011).

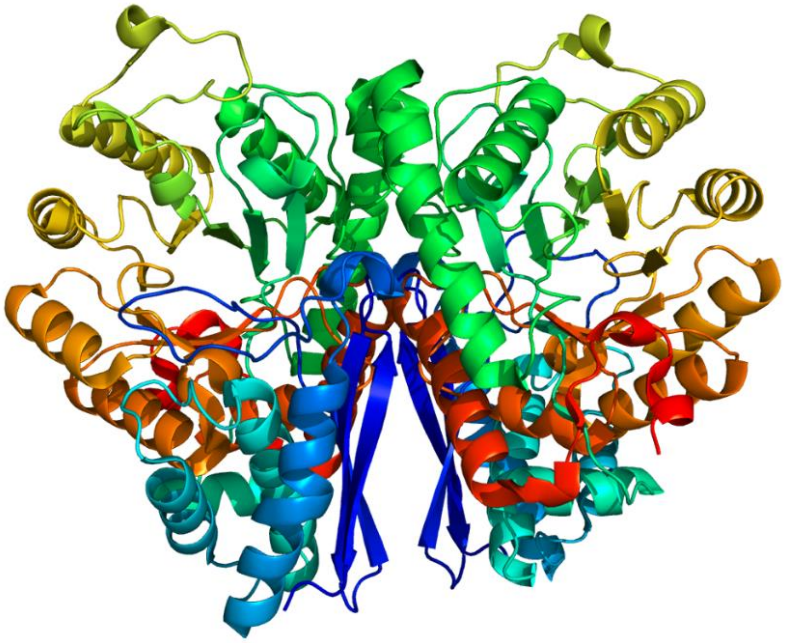

Figure 1.5: The structure of neuron-specific enolase (NSE).

Yang et al (2014), suggested NSE to be a good biomarker as the normal concentration range of NSE in serum of healthy individuals is between 5 to 12 ng/ml. NSE is also present in the cerebrospinal fluid of healthy individuals with a concentration of 20 ng/ml (Han et al., 2012). The percentage of NSCLC patients that have over expression of NSE was found to vary between 0 – 79% in various studies. As an example, Petrovic et al. (2012) reported the over expression of NSE in 31% of patients with NSCLC, while Harmsma et al. (2013) indicated NSE over expression in 5 – 11% of NSCLC patients. Another study in 2013 by Yu et al. showed that 63.6% (out of 481) of NSCLC patients had more than 12.5 ng/ml of NSE in their blood serum.

High levels of NSE (>100 ng/ml) is expressed in 60% – 81% of SCLC patients which often increases to nearly 1 µg/ml in a patient with late stages of cancer (Wang & Ma, 2017; Yu et al., 2012, 2015). Hence, the concentration of NSE protein in the serum can be used as an indicator for both early cancer diagnosis and response of patients to the treatment.

NSE might not be a suitable sole biomarker for detection of NSCLC although it has been suggested by several sources to be the best biomarker for the detection of SCLC. Thus, detection of NSE, and CEA or CYFRA 21-1 serum level of patients can help in distinguishing between SCLC and NSCLC. In recent years few studies have been reported on biosensors for NSE detection in blood serum and these are presented in Table 1.3.

Table 1.3: Developed biosensor for NSE detection.

Type of Sensor	**Linear Range**	**Limit of Detection (LoD)**	**Reference**
Forster resonance energy transfer	5 – 125 ng/ml	12 ng/ml	(Geißler et al., 2013)
Quantum dot	0.5 – 50 ng/ml	0.2 ng/ml	(Li et al., 2010)
Deferential pulse voltammetry	0 – 25 ng/ml	4.6 ng/ml	(Sánchez et al., 2016)
Field effect transistor	1 ng/ml – 1 µg/ml	100 ng/ml	(Cheng et al., 2015)
Square wave voltammetry	1 – 150 ng/ml	0.9 ng/ml	(Shan & Ma, 2016)
Optical	1 – 1000 ng/ml	N/A	(Aono et al., 2016)
Amperometric	0.01 – 100 ng/ml	0.0078 ng/ml	(Wang & Ma, 2017)
Optical	1 – 1000 ng/ml	0.05 ng/ml	(Li et al., 2017)
Impedimetric	1 – 50 pg/ml	0.0005 ng/ml	(Barton et al., 2008)
Square wave voltammetry	0.001 – 200 ng/ml	0.00026 ng/ml	(Wang et al., 2017)
Differential pulse voltammetry	0.1 – 2000 ng/ml	0.033 ng/ml	(Yu et al., 2012)
Voltammetric	0.001 – 100 ng/ml	0.0003 ng/ml	(Han et al., 2012)
Electrochemiluminescence	0.01 pg/ml – 10 ng/ml	0.00001 ng/ml	(Zhou et al., 2016)
Quantum dot	0.001 – 100 ng/ml	0.0002 ng/ml	(Yu et al., 2015)

1.5. Biosensors for Lung Cancer Diagnosis

It is crucial to diagnose lung cancer at an early stage to increase the survival time and the chance of successful treatment, especially for SCLC. Although, lung cancer can be detected with current methods such as X-ray, MRI and biopsy, these methods have disadvantages such as high cost, use of radiation and being invasive. Therefore, a low cost, rapid and non-invasive detection method with high sensitivity and specificity is required. A non-invasive and early diagnosis of lung cancer might be possible via detection of biomarkers (*e.g.* protein) within the body fluid (*e.g.* blood) as the level of these molecules changes (Harmsma et al., 2013; Altintas & Tothill, 2013). The low cost detection and simultaneously monitoring of the biomarker concentrations with an acceptable level of selectivity and sensitivity is possible using of biosensors (Aydın & Sezgintürk, 2017).

Biosensors are bioanalytical devices which recognise a specific analyte through the use of a bioreceptor, and convert the biological responses to electrical signals via the action of a transducer (Newman & Setford, 2006; Zhang et al., 2013). Figure 1.6 presents the principle of a biosensor.

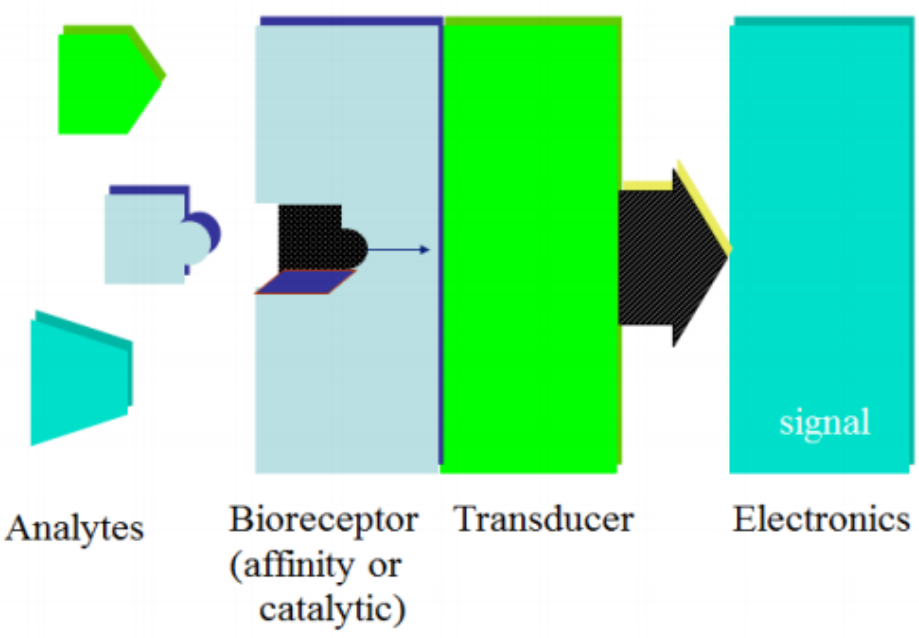

Figure 1.6: The Principle of Biosensors (Newman & Setford, 2006).

A bioreceptor is the biological recognition element of the biosensor. Antibody, enzyme, molecular imprinted polymer (MIP), and nucleic acids (*e.g.* ssDNA) can be used as bioreceptors to detect the analyte of interest. The binding of the analyte of interest to the bioreceptor causes changes in property of the transducer such as alteration of refractive index in optical biosensors, or resonant frequency of the crystal in piezoelectric biosensors. Biosensors can be classified based on the type of the transducer such as optical, electrochemical, piezoelectric, magnetic, or thermometric (Newman & Setford, 2006; Monošík et al., 2012). Each class of biosensor can be further classified into two groups. The response of a biosensor due to direct attachment of analyte is known as a label-free sensor, but if it is caused by recognition of a certain label (*e.g.* fluorescence) it is known as a labelled sensor.

It is crucial to validate the biosensors to make sure the obtained results are close enough to the true value. There are some measurable terms to validate the biosensors and to assure the quality of the obtained results. These including selectivity, sensitivity, limit of detection (LoD), and reproducibility (Justino et al., 2016).

The sensitivity is the amount of biosensor response to the slight change of the analyte concentration. The sensitivity value can be calculated by plotting the calibration curve and calculating the slop of the analyte linear range detection. The selectivity is how well the biosensor can detect and measure the concentration of the analyte of interest in the presence of other molecules. The LoD is defined as the smallest concentration of the analyte of interest which the biosensor can detect with an acceptable degree of certainty (Justino et al., 2016, 2010). The LoD can be calculated from Equation 1.

$$LoD = \frac{3 \times SD_B}{Slope} \qquad \text{Equation 1}$$

Where SD_B is standard deviation of the blank and the slope is the sensitivity of the biosensor. The reproducibility is defined as how close are the result of the same concentration of analyte by repeating the experiment with the same device and materials but different screen-printed electrode.

Below some of the most important transducers for lung cancer detection research will be discussed further.

1.5.1 Optical Biosensors

Optical transducers detect the presence of target molecule by measuring and converting into digital signals the changes within light amplitude, wavelength, frequency, or phase that are caused by biological events on the sensing layer of the biosensor (Justino et al., 2016). Although different types of optical transducers are available they can be subdivided in two main groups know as labelled, such as fluorescence and Chemiluminescence (Cl), and label-free (unlabelled), such as surface plasmon resonance (SPR) and waveguide (Fan et al., 2008; Bohunicky & Mousa, 2010; Narsaiah et al., 2012).

Many of the fluorescence labelled optical biosensors apply immunoassay as a common method for the detection of the analyte of interest. This type of immunoassay is based on the detection of fluorescence intensity changes that occurs after coupling of the target analyte to the bio-recognition element such as aptamers and antibodies (Monošík et al., 2012). Unlike the label-free optical biosensors, the labelled optical biosensors can detect biomolecules without labelling requirement. The principle of unlabelled optical immunoassays is based on the existence of sensing light near the sensing area which can change due to the presence of target molecules. Once the molecules of interest bind to the bio-recognition elements, the change in the refractive index will either cause changes in the angle of incidence or shift the wavelength which is proportional to the amount of analyte of interest (Fan et al., 2008; Scott & Peters, 2010). SPR (Figure 1.7) is known as one of the best label-free methods for detection of target molecules due its high sensitivity.

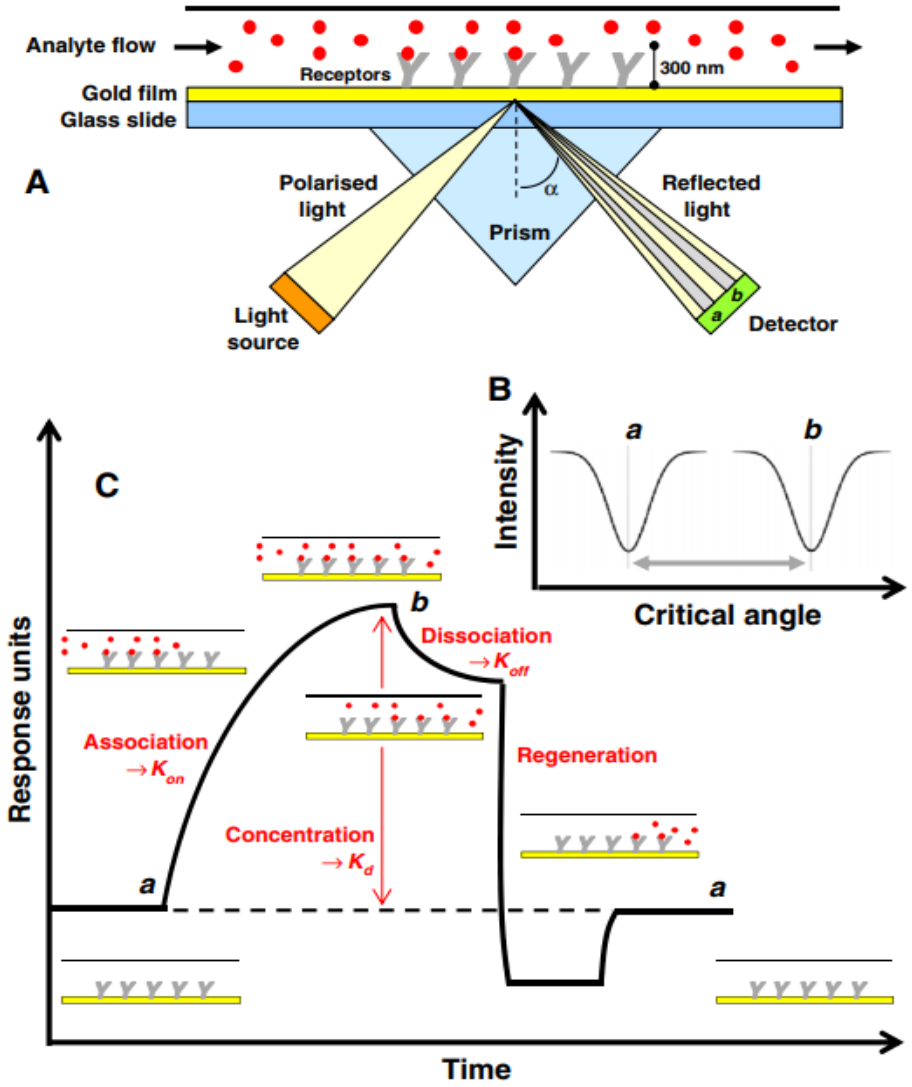

Figure 1.7: SPR illustration (A) The action mechanism of BIAcore Technology. The binding of analyte to the immobilised antibodies on the surface of the chip cause alteration of refractive index due to the mass of target molecule (detected light moved from a to b position). (B) Presents the change in critical angle. These changes are presented as a plot of resonance signal Vs. time (C). The amount of resonance signal is proportional to the concentration of analyte of interest (Cooper, 2002; Patching, 2014).

Optical biosensors can be highly selective and specific, immune to interference with a low limit of detection and minimally invasive. They can be used for multi-analyte detection by use of either various light wavelengths or different labels. Although optical detection has many of advantages, it usually relies on expensive readout devices which make optical sensing unsuitable for some field applications (Tothill 2009; Gauglitz, 2010; Narsaiah et al., 2012). Numerous studies have been published for the detection of lung

cancer biomarkers by optical biosensors. Some of these studies are summarised in Table 1.4.

Table 1.4: Published studies on optical recognition of lung cancer biomarkers. Cytokeratin 7 and 17 (CK7, CK 17), Annexin A3 (ANXA3), Serum collagen type IV (COLIV).

Method	Recognition element	Analyte	LoD	Reference
Optical fiber	Antibody	CK 7	0.4 nM	(Ribaut et al., 2016)
Chemiluminescence	Antibody	CYFRA 21-1	0.2 ng/ml	(Luo et al., 2013)
Quantum dots	Antibody	ANXA3	75 pg/ml	(Kim et al., 2013)
SPR imaging	Antibody	Podoplanin	15 pg/ml	(Gorodkiewicz et al., 2012)
Quantum dots	Antibody	HER2	N/A	(Ag et al., 2014)
SPR	Antibody	EGFR and CEA	N/A	(Teotia & Kaler, 2017)
SPR imaging	Antibody	COLIV	2.4 ng/ml	(Sankiewicz et al., 2016)
SPR	Antibody	CK 17	1 pg/ml	(Ribaut et al., 2017)
Localised SPR	Antibody	Exosome	194 ng/ml	(Thakur et al., 2017)

1.5.2 Magnetic Biosensors

The two main components of magnetic biosensors are bio-recognition elements and selective labelling of the analyte of interest with functionalised magnetic beads (Muluneh & Issadore, 2014). Based on the type of analyte, different sizes of magnetic beads from micro to nano can be used. Magnetic beads have two parts, a magnetic core and a polymer shell. The magnetic cores comprise 50 – 60% of magnetic beads and are commonly made from ferromagnetic substances such as iron oxide, cobalt, and nickel. Use of ferromagnetic materials allows magnetic beads to be magnetised only if an external magnet is applied. This property of ferromagnetic elements is due to their atoms arrangement. For instance, atoms of these materials will be in parallel arrangement when they are placed into an external magnetic field. Therefore, agglomeration of magnetic

beads will not occur in the absence of magnetic field. The second component of magnetic beads is the polymer shield which allows magnetic beads to be functionalised with bioreceptors (*e.g.* DNA probes or antibodies) (Tamanaha et al., 2008; Ríos et al., 2013).

Bio-recognition elements on the surface of magnetic beads are used to couple with analytes in the sample to form bio-complex molecules which can be detected via magnetic sensors through two common methods (Llandro et al., 2010; Li et al., 2012). The first is based on applying a magnetic field and voltage to the sample. Detection of changes in voltage, caused by a change of resistance due to binding of bio-complex molecules on magnetic sensor's surface is then monitored. Consequently, the amount of changes in voltage is proportional to the amount of bound bio-complex molecules (analytes) on the surface of magnetic biosensor (Figure 1.8). The second method of magnetic biosensor detection involves the use of two magnetic fields with different frequencies. The presence of target molecules alters the magnetic field frequency, thus the biosensor can detect and quantify the amount of analyte by measuring the differences between two magnetic field frequencies (Meyer et al., 2007; Grieshaber et al., 2008).

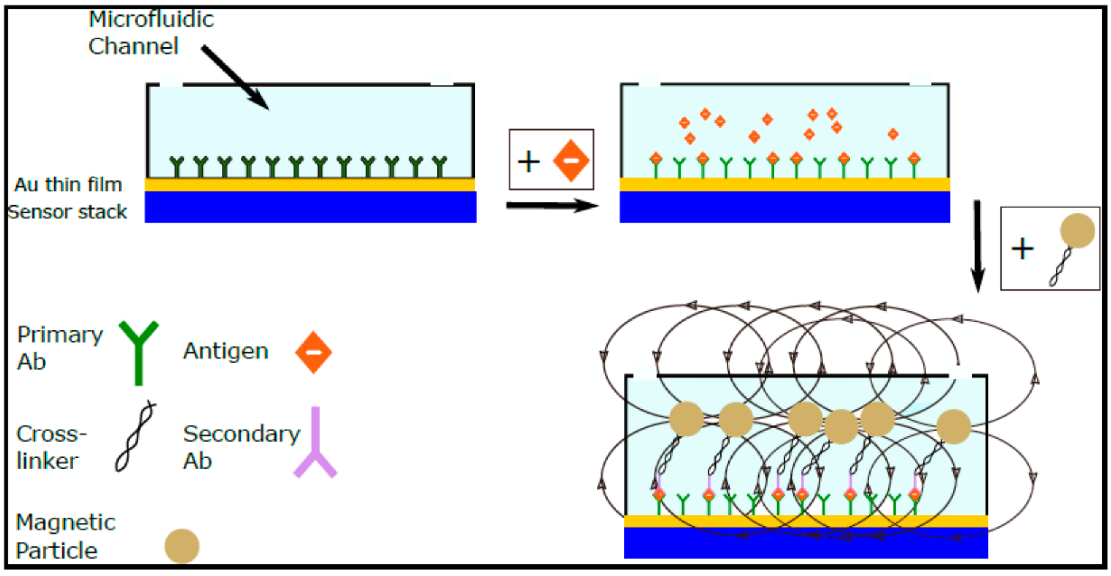

Figure 1.8: Most common mechanism of magnetic biosensors. The target molecules are detected by primary antibodies with are immobilised on the sensing area. Then, the magnetic particles will attach to the captured analyte. The transducer detects changes in stray magnetic field caused by magnetic particles (Giouroudi & Kokkinis, 2017).

Magnetic biosensors use magnetic forces which give them many advantages such as: simple sample preparation, rapid, small amount of sample and organic solvent requirement, low detection limit, and no effect of chemical variables (*e.g.* pH) on analyte quantification. However, sometimes the interaction of magnetic particles may lead to false positive results (Meyer et al., 2007; Xu & Wang, 2012; Ríos et al., 2013). Table 1.5 presents some of the published research for the detection of lung cancer biomarkers with magnetic biosensor.

Table 1.5: Published studies on detection of Interleukin-6 (IL-6) with giant magnetoresistive (MR) biosensor.

Method	Recognition element	Analyte	LoD	Reference
GMR	Antibody	IL-6		(Li et al., 2009)
GMR	Antibody	IL-6		(Srinivasan et al., 2009)
GMR	Antibody	IL-6	125 fM	(Li et al., 2010)

1.5.3 Electrochemical Biosensors

The history of biosensors began with Clark oxygen electrode transducer (1962) which is an electrochemical biosensor for glucose concentration measurement by measuring the oxygen concentration reduction (Grieshaber et al., 2008). Further attention was brought to electrochemical biosensor in clinical diagnosis such as Aizawa et al. (1979) that introduced the first electrochemical biosensor for cancer diagnosis (Wang, 2006).

Like other type of biosensors, different type of biorecognition elements such as antibodies (Du et al., 2010), aptamers (Song et al., 2008), enzymes (Shan et al., 2009), MIP (Piletsky & Turner, 2002), and nucleic acids (Ensafi et al., 2011) can be used to detect the target analyte in electrochemical biosensors. The attachment of the analyte to the biorecognition elements can be detected through the generation of measurable electrochemical signals as a current, potential, or impedance (resistance), which are

proportional to the concentration of the analyte. Based on the type of electrochemical detection, the electrochemical biosensors can be further classified as: voltammetric, potentiometric, and impedance (Perumal & Hashim, 2014).

These types of transducers have received considerable attention because of their many advantages such as quick response, selective, sensitive, highly miniaturised, inexpensive, and ease of use. The use of screen printed electrodes (SPEs) has helped in growing developments on the use of electrochemical biosensors because of their low cost, mass production, reliability, and reproducibility. Hence, this type of transducer has become one of the most successful transducer for analyte analysis in point-of-care devices. (Newman & Turner, 2005; Daniels & Pourmand, 2007; Tothill, 2009; Arya & Bhansali, 2011; Li et al., 2012;). Moreover, electrochemical biosensors based on SPE are able to detect the target molecules within small volume of analyte sample with excellent LoDs (Wilson & Nie, 2006).

The electrochemical biosensors have some limitations. The interaction of target molecule with bio-recognition might results in reduction of electronic signal because of the steric hindrance effect of large molecules, this affect is known as high interference from matrix effect. Moreover, since bio-recognition molecules are immobilised on the surface of electrode, the electrodes are not normally reusable (Xu & Wang, 2012).

1.5.3.1 Screen Printed Electrodes

The electrochemical biosensors generally use screen printed electrodes (SPEs) which consist of 3 electrodes: a working, a reference, and a counter or auxiliary electrode. Their working principle is based on recognition of target molecules by the immobilised bio-recognition elements on the working electrode, and measurement of signal difference before and after binding of target molecules (Newman & Setford, 2006; Xu & Wang, 2012). The biochemical reaction occurs on the surface of the working electrode and this results in producing the current. The working electrode is connected to both counter and reference electrode. The potential applied to the cell is applied against the reference electrode as it does have a constant potential that does not change. The reference electrode is normally made from Ag/AgCl, and since its constant potential should be stable during

the measurement, the reference electrode is placed in a distance from reaction site (Kimmel et al., 2012). The counter or auxiliary electrode is designed to detect any electrochemical signals which are not produced due to the redox reaction.

The SPEs are low cost and produced on a large scale. They can be produced in different shapes and with varied materials based on the type of application. The gold, platinum, and carbon are most common materials to use as working and counter electrodes as they need to be conductive and chemically stable (Grieshaber et al., 2008). Another advantage of SPEs is their small dimensions as it allows them to be used in portable point-of-care device and reduces the consumption of biological and chemical reagents. Since the signals are generated by occurrence of binding events close to the surface of transducer, using of SPEs can help to increase the assay sensitivity. Moreover, the small dimension of SPE reduces the assay performance time as the analytes and the biorecognition elements are in close distance (Arduini et al., 2016). Subsequently, the type of materials which SPEs are made of and the surface chemistry of the SPE play vital role in electrochemical biosensors.

i. Self-assembled monolayers (SAMs)

Self-assembled monolayers (SAMs) are defined as highly organised two-dimensional molecular assemblies which are formed spontaneously through the interaction of active precursors and solid surface (Figure 1.9) (Cheng & Hu, 2012; Jadhav, 2011). Formation of SAM layer on a metal substrate was reported for the first time by Zisman in 1946 (Watson et al., 2015). Since then, many studies have been done on development of different type of SAM layers and their applications. One of the most important studies in this area was done by Allara & Nuzzo in 1983, who for the first time reported the formation of alkanethiol SAM layer on gold surface (Jadhav, 2011).

There are two types of SAM layer formation methods on solid surface. The first and the most common way is through a solution, and the second way is via vapour deposition (Watson et al., 2015). The simple way of developing a SAM layer on the surface is immersing the solid substrate into the solution. The most common formed

SAMs are alkanethiolates and alkylsilanes on gold and silicon surfaces, respectively (Ko et al., 2015).

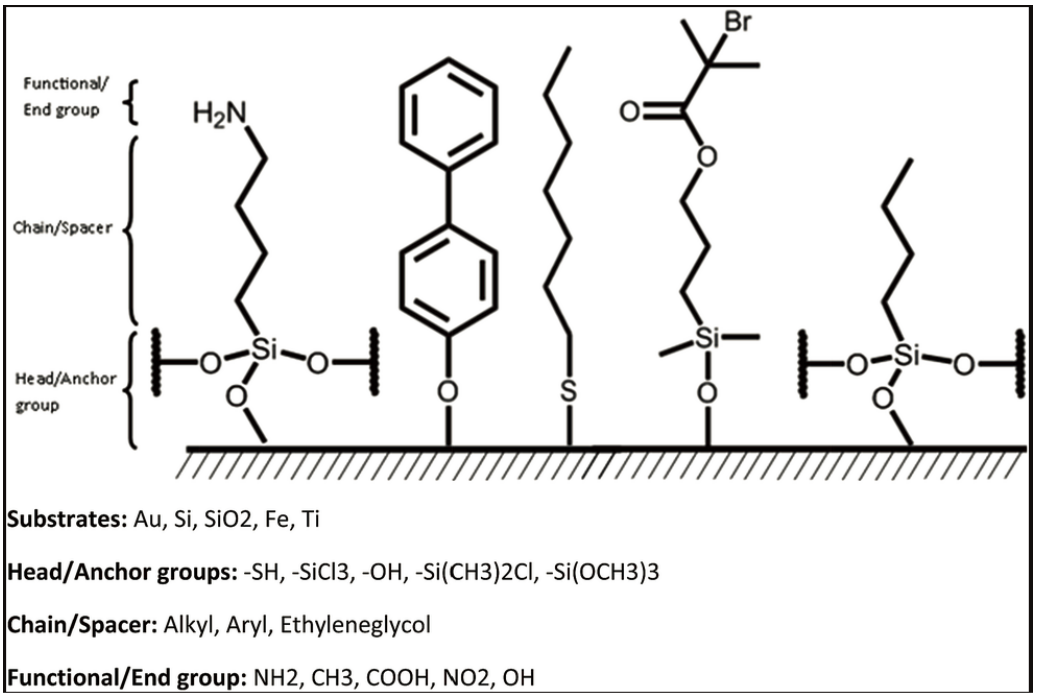

Figure 1.9: The formation of various type of SAMs on different type of materials (Watson et al., 2015).

The organic building-blocks for SAM have specific structures, as those in Figure 1.9. They consist of a head or anchor group, a chain or spacer part, and a functional or end group (Jadhav, 2011). All SAMs are normally formed through binding of the anchor group to the substrate. The anchor groups attach to the surface by forming either chemically or physically bonds. The strength of bonds between the anchor group and the surface is crucial. It must be reasonably strong to attach the molecule to the surface, but at the same time it needs to be sufficiently flexible as attached molecules to surfaces need mobility to form a dense SAM layer (Schmaltz et al., 2017). The process of thiol-based self-assembly formation is presented in Figure 1.10.

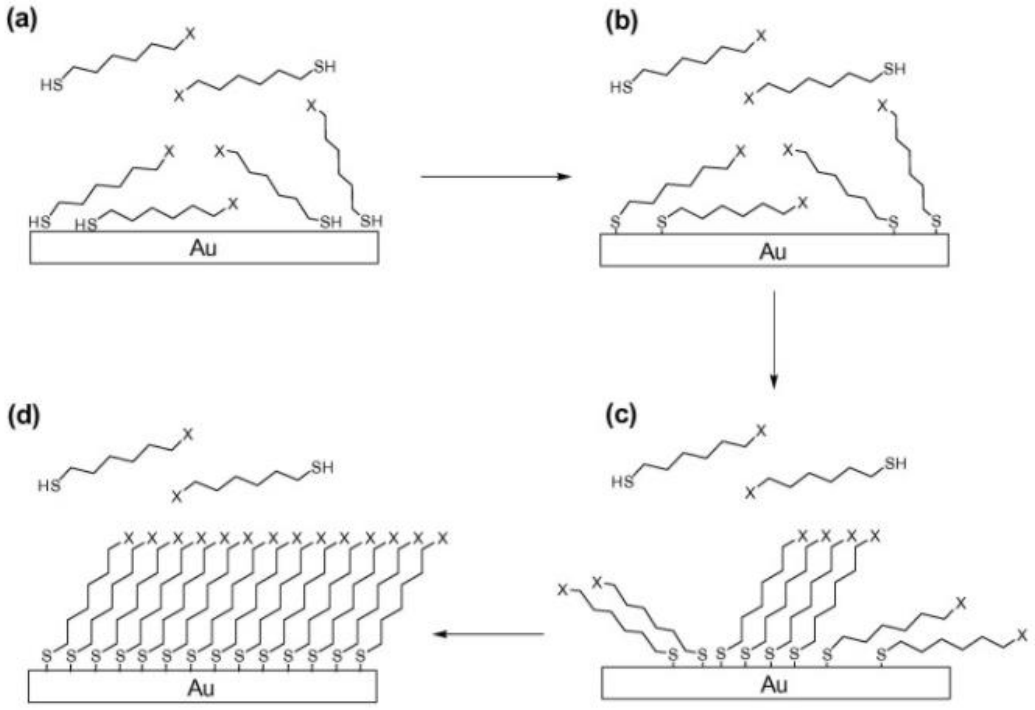

Figure 1.10: The illustration of thiol based SAM formation process on the gold surface (Ko et al., 2015). (a) physically adsorption of thiol molecules onto the gold surface; (b) formation of chemically bond between gold surface and lying down thiol molecules; (c) start of standing phase of thiol molecules as more thiol molecules are chemically adsorbed, (d) completion of SAM.

The quality of monolayer formation depends on many factors such as cleanliness of the surface, concentration of the molecules in the solution and the incubation time. Generally, the SAM formation process can be divided into two steps (Ko et al., 2015). The first step, binding of anchor end to the surface, is based on the concentration of substrate, takes up to few minutes and up to 85% surface coverage can be obtained, although it might not be well organised. During the second step, the self-organising process takes place, where the monolayer reaches its maximum compactness. Unlike the first step, the second is a slow process and takes hours (up to a day) to complete. The first step relies on formation of covalent bonds, while the second step mainly relies on weaker bonds such as van der Waals and hydrogen bonds to make a highly organised monolayer (Gooding & Ciampi, 2011; Watson et al., 2015) . The result of these steps is the formation of highly organised two-dimensional molecular assembly that has tilted alkanethiols at the angle of approximately 30^{o} from the surface. The compactness of SAM depends on intermolecular forces between

the thiol molecules. Thus, thiols with a longer chain or spacer unit can form more stable and organised monolayers as a result of their stronger van der Waals interactions. Although these interactions reduces the electron transfer across the surface which is an important factor in electrochemistry (Mandler & Kraus-Ophir, 2011). As Figure 1.9 shows, variety of functional or end groups of thiols, *e.g.* -NH_2, -OH -CH_3, and -COOH are used to couple biorecognition elements, *e.g.* antibodies.

The thiol based SAMs can be formed on various metal surfaces as platinum, silver, gold etc. Nevertheless, the strongest type of this monolayer is formed on the gold surface which makes gold the most common metal to use. Moreover, the gold surface is easy to clean which results in having better quality and more defined monolayer (Mandler & Kraus-Ophir, 2011; Manzanares-Palenzuela et al., 2015). The thiol based SAMs are robust and can tolerate high temperature (< 400 ^{o}C) and wide range of pH (1 – 12) (Samanta & Sarkar, 2011; Ko et al., 2015). The thiol based SAMs have become popular and attractive method to functionalise the electrode for electrochemical biosensors due to their ease of formation, stability, and well organised structure (Gooding & Ciampi, 2011).

1.5.3.2 Types of Electrochemical Transducers

Electrochemical transducers are devices that can convert the recognition signals to meaningful electrochemical signals of voltage, current, and impedance. They can be classified as: voltammetric, potentiometric, and impedimetric.

i. Voltammetric

Voltammetric measurement principle is based on measurement of voltage and current between two sets of reference – working electrodes, and working – counter electrodes. In the other words, if the target molecule is present on the sensing surface, by applying voltage to the working electrode, redox reaction will occur on the working electrode which will produce current. The produced current is correlated with the analyte concentration. The final results will be presented as graph which is plotted current against voltage and known as voltammogram (Grieshaber et al., 2008; Gu et al., 2012). Like other

electrochemical biosensors, voltammetric biosensors are highly selective and sensitive. Although they can be used for multi-analyte detection purpose, only if chosen analytes have different peak potential (Su et al., 2011).

ii. Potentiometric

Potentiometric biosensors are made of two electrodes; the indicator (or working) electrode is required for development of variable potential in case of analyte detection, and the reference electrode which is responsible for maintaining the constant potential. Potentiometric biosensors measure the concentration of substance through determination of potential or charge accumulation differences between the indicator and the reference electrodes, or two reference electrode which are separated by a permselective membrane, when a zero or significantly low current flows between them. The potential response of this type of devices is proportional to the logarithm of analyte concentration (Thévenot et al., 2001; Su et al., 2011; Perumal & Hashim, 2014).

Potentiometric biosensors are simple to use, cheap, and quick. Although potentiometric biosensors are highly sensitive and selective, they are less sensitive than amperometric one, and may give false-positive results if various types of charged species are contained into the sample (Zelada-Guillén et al., 2010; Perumal & Hashim, 2014). One of the challenges for use of potentiometric transducers is to choose the accurate reference to maintain the constant half-cell potential (Su et al., 2011).

iii. Impedimetric

The first impedimetric biosensor was reported in 1975 (Grieshaber et al., 2008). These biosensors measure the target molecule concentration through detection of changes in current vs a small amplitude sinusoidal voltage ratio spectroscopy which is known as the electrochemical impedance spectroscopy (EIS). The counter electrode produce the current while the working electrode is used to measure the current, and the reference electrode has voltage measurement function (Ates, 2011; Daniels & Pourmand, 2007). The impedimetric biosensors contains a frequency response analyser to establish voltage

and current phasor, and eventually measure the impedance; and a potentiostat to keep the voltage between electrodes (K'Owino & Sadik, 2005).

Impedance is like resistance when the current is applied. The resistance of ideal resistor is defined by the Ohm's law which is the ratio of voltage versus current which can be calculated by Equation 2.

$$R(\Omega) = \frac{E(v)}{I(A)} \qquad \text{Equation 2}$$

Where R is resistance, E is voltage, and I is current. Since in reality, the resistance of circuit element is complex and cannot be defined by simple equation, it has been replaced by impedance which is a complex resistance of a circuit made of capacitors, resistors, inductors or combination of these elements when the AC current is applied (Fernandez-Sanchez et al., 2005). Therefore, the impedance equation can be expressed as Equation 3.

$$Z = \frac{E}{I} = \frac{\Delta E \sin(\omega t)}{\Delta I \sin(\omega t + \varphi)} \qquad \text{Equation 3}$$

Where Z is impedance in ohm (Ω) ΔE is the amplitude of the sine wave, ω is the signal frequency in rad/s (=2πf, where f is the frequency in hertz), φ is the angle of phase shift. The Equation 3 can be transformed into Equation 4 based on the Euler's relationship.

$$Z = |Z|e^{j\varphi} = |Z|cos\varphi + j|Z|sin\varphi \qquad \text{Equation 4}$$

Where e is the natural logarithm and j is the imaginary unit. As Equation 4 presents, the total impedance consists of a real and an imaginary part. The real part of impedance, also known as resistor, is when the phase difference between the potential and current is zero. While the imaginary part of it, also called reactive, may be identified

with the contribution of interfacial elements such capacitor and mass transport (Fernandez-Sanchez et al., 2005).

By applying voltage, the current flows through the sample, which results in impedance spectroscopy. Attachment of analytes to bio-recognition elements causes a difference in magnitude and phase shift. The impedance measurements can be presented with the Nyquist diagram (Figure 1.11) which is the most common way of presenting impedance results. The Nyquist diagram is presented by the imaginary versus the real impedance; and shows the results as a curve that has two parts: a semicircle and a linear section. To obtain the curve the potentiostat applies 6 or 7 decades of frequency scan, from the highest to the lowest frequency.

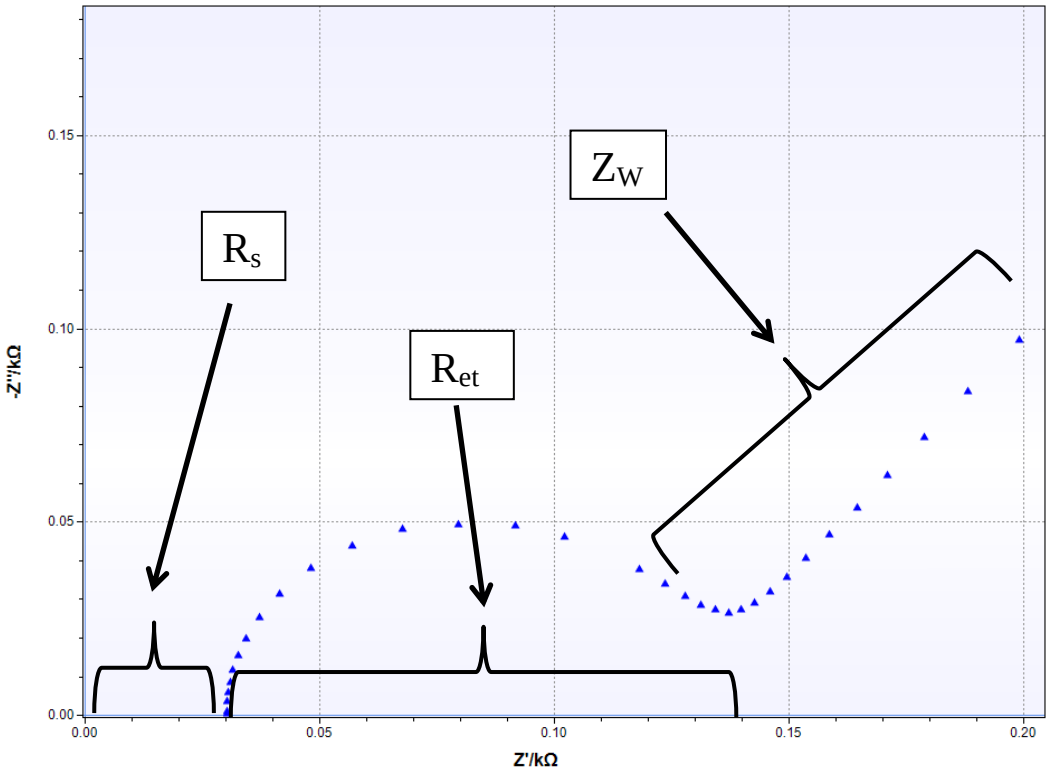

Figure 1.11: The Nyquist plot of Impedance Measurement; R_s: Resistance of bulk solution; R_{et}: Resistance of electron transfer; Z_W: Warburg impedance.

The Shape of the Nyquist plot can be explained by the Randles equivalent circuit. Figure 1.12 presents the Randles Circuit, which consists of the electrolyte solution resistance (R_s), the double layer capacitor (C_{dl}), the resistance of electron transfer (R_{et}), and the Warburg impedance (Z_W). R_s is obtained in impedance measurements when the applied frequency is very high at the beginning leading to prevention of effective electron conduction between the counter and the working electrode.

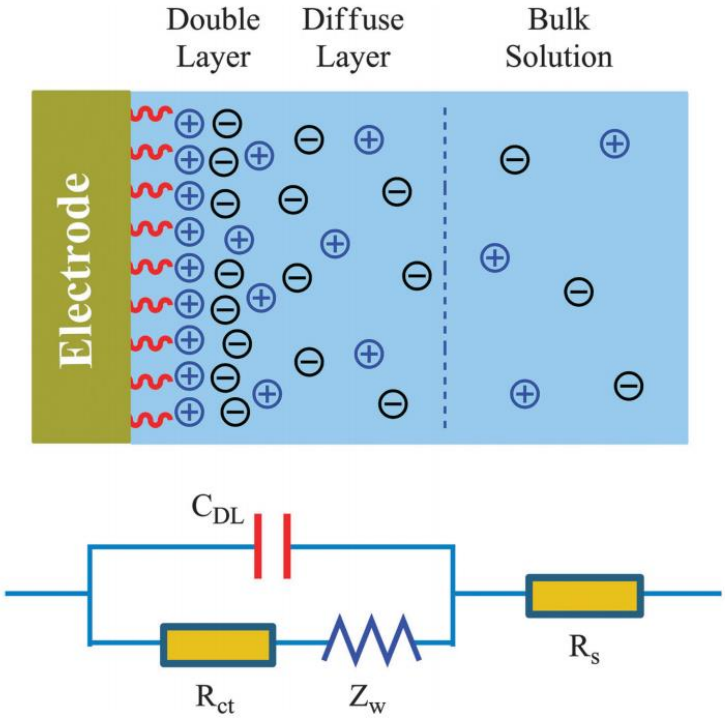

Figure 1.12: The illustration of Randles equivalent circuit and electrode-electrolyte interface. The C_{DL} is the double layer that forms on the surface of electrode when it has been immersed in an electrolyte solution; while the other elements of Randles circuit are arising from the ions diffusion. The C_{DL} and R_{et} are affected by attachment of analyte to the electrode surface, while the R_s and Z_w are the properties of the redox solution (Luo & Davis, 2013).

Due to the application of high frequency by the potentiostat at the beginning of impedance which gradually decreases and based on the presence of R_{et} in parallel to C_{dl}, the resistance at the SPE surface will happen which causes the semicircle section of the Nyquist plot. Therefore, the semicircle part represents the limitation of electron transfer

to the surface of electrode. Hence, larger semicircles in Nyquist plot present less amount of electron transferred from the redox solution to the electrode surface. The linear portion of the Nyquist plot obtains at low frequencies represents the frequencies at which diffusion of the redox solution ions occur to the surface of electrode. The linear portion also represents the Z_W of Randles circuit (Katz & Willner, 2003; Elshafey et al., 2013).

The EIS technique can be categorised as Faradaic and non-Faradaic methods. The main difference between two mentioned methods is the presence of redox probe. The Faradaic EIS analyte measurement is based on reversible reduction and oxidation process of the redox probe and movement of the electrons from the solution to the surface of WE (R_{et}); while the non-Faradaic EIS analyte measurement is based on changes in capacitance of electrode – electrolyte interface (C_{DL}). Non-Faradaic EIS can be used in miniaturised biosensor as it does not require redox solution, though it has been proven that Faradaic EIS is one of the most sensitive technique for investigating the events happening on the surface of electrodes such as surface electrode modifications and antigen-antibody interactions. The changes in Faradic EIS signals are due to the changes in amount of transferred electrons which can be altered because of the charges and/ or blockage of the electrode surface (Kazemi et al., 2015; Muñoz et al., 2017).

The EIS technique is a sensitive tool that is used by many researchers to investigate electrode modifications, *e.g.* antibody immobilisation to the surface (Hou et al., 2013; Aydın & Sezgintürk, 2017). One of the advantageous of impedimetric biosensors over the amperometric and voltammetric biosensors is the use of a small amplitude voltage (< 10 mV) that makes them non-destructive device. This means impedimetric biosensors can measure the analyte concentration without significantly disturbing the biomolecular probe layer (K'Owino & Sadik, 2005; Daniels & Pourmand, 2007).

Recently, impedimetric biosensors have attracted many attentions due to their various advantages such as label-free detection, cost effective, robust, no need of special reagent, portability, ability to be used for real time analysis, and not requiring skilled

person. However, they have not been explored in any commercial devices yet (Tothill, 2009; Lindholm-Sethson et al., 2010; Prodromidis, 2010; Perumal & Hashim, 2014).

1.6. Magnetic Nanoparticles (Beads)

Nanoparticles (NPs) are microscopic nanomaterials with the dimension of 1 – 100 nm. NPs are benefitting from their high surface to volume ratio which gives them multiple molecular interaction sites, and extraordinary chemical and physical properties in comparison with non-NP materials. Recently, due to tremendous properties of magnetic nanoparticles (MNPs) (*e.g.* low-cost production), MNPs are of great interest to be used in various research such as drug delivery, MRI, water purification, sample preparation, and biosensors (Rocha-Santos, 2014; Ali et al., 2016; Wang et al., 2017).

MNPs are normally made of iron, cobalt, nickel, and their oxides which are ferromagnetic particles. Magnetic particles are categorised based on their response to an applied external magnet into: ferromagnetic, antiferromagnetic, ferrimagnetic, and paramagnetic particles. Due to the sufficiently small size of MNPs, MNPs are superparamagnetic materials. Superparamagnetic materials are very small ferrimagnetic or ferromagnetic particles which are in non-magnetic state unless an external magnet is applied (Rocha-Santos, 2014; Ruffert, 2016). Figure 1.13 shows the difference between magnetic behaviour of MNPs in comparison with magnetic microparticles (MMPs).

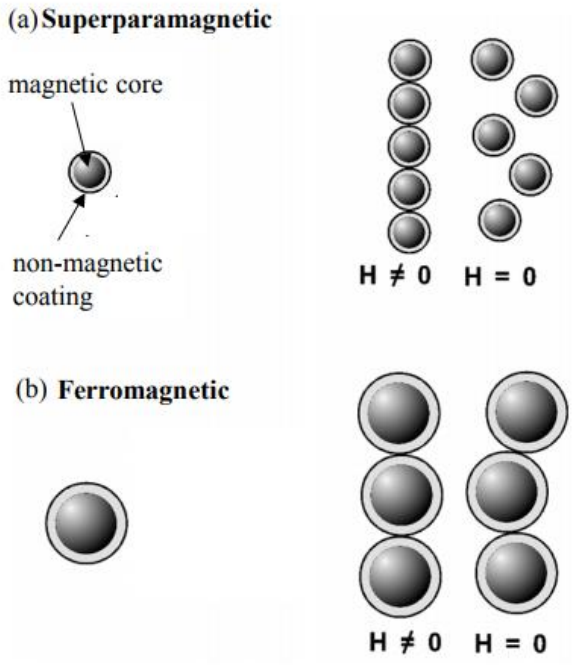

Figure 1.13: The comparison of magnetic behaviour of MNPs (a) and MMPs (b) in the presence and absence of external magnetic field (H) (Ruffert, 2016).

Although MNPs are superparamagnetic, a surface coating is required to make sure they separate and do not irreversibly agglomerate after removal of magnetic field. Further, the surface coating of MNPs protects them against, ions within the body fluids (*e.g.* Cl^-, K^+, Ca^{2+}), air and acids which are corrosive for MNPs (Rocha-Santos, 2014; Sobczak-Kupiec et al., 2016). The type of surface coating is crucial in functionalisation of MNPs with biological elements, *e.g.* antibodies. The materials that are used to coat the MNPs are transition-metal oxides, silica, gold, and carbon. Grass et al., (2007) suggests carbon coating as the best option to coat MNP as covalent bonds on transition-metal oxides and silica coat might be hydrolysed, and gold is not cost effective. The nanoparticles with coated magnetic core are known as magnetic beads (MB).

Since MNPs become strongly magnetic in the presence of an external magnetic field and this property does not exist in living systems, and also as they can be quickly removed from the sample matrix, they are great tools to be used for working in biomolecular systems (Ali et al., 2016; Grass et al., 2007). MNP have been used in biosensors to improve the stability, sensitivity, and LoD of assays, also to reduce the

detection time. They can be easily functionalised with biomolecules through their active parts, *e.g.* carboxyl, which enable them to detect diverse types of analyte. Thereby, they can be applied for several purposes such as signal amplification labelling, analyte detection in the surface of sensor, and preconcentration of analyte from complex media to minimise non-specific adsorption. MNPs ability to carry the target molecules to a sensor platform allows simultaneous detection of multi-analyte. In addition, MNPs can work as electro-catalysts for molecules, *e.g.* H_2O_2, which results in enhancing electron transfer between the electroactive solution and the surface of electrode (Holzinger et al., 2014; Rocha-Santos, 2014; Yáñez-Sedeño et al., 2016).

Jin et al. (2014) used MBs for label-free CEA detection by electrochemical biosensor, Figure 1.14. MBs functionalised with horseradish peroxide (HRP) were first mixed with sample to fish the analyte before adding the functionalised gold NPs on their surface. Then the whole MB-CEA-AuNP-HRP was added to the reaction cell to measure the analyte concentration. They achieved the LoD of 5 ng/ml for detection of CEA protein by testing various analyte concentration, 5 – 60 ng/ml, with use of cyclic voltammetry (CV).

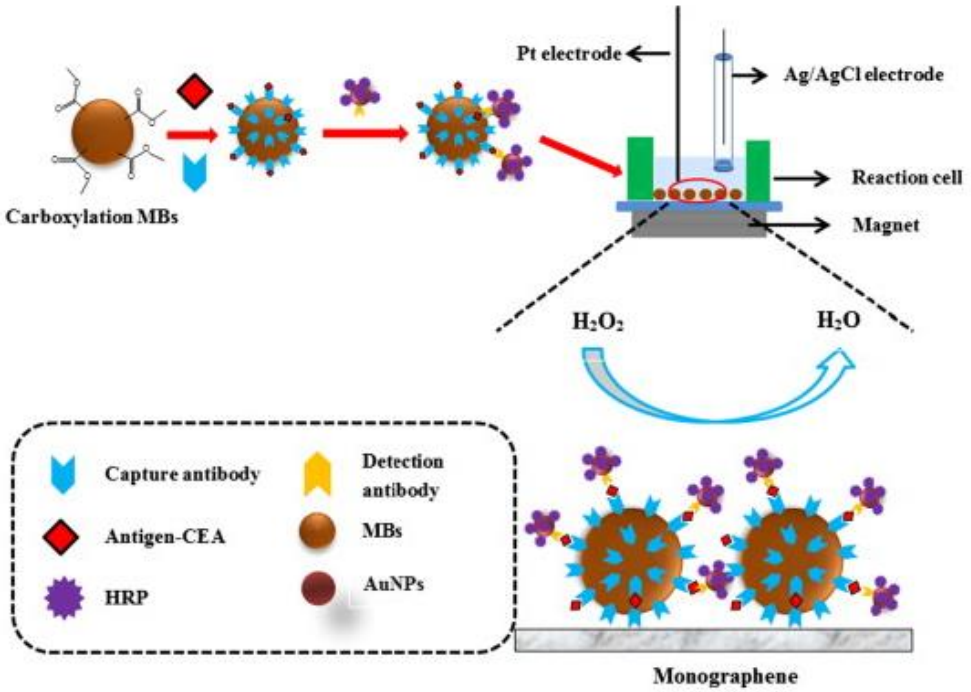

Figure 1.14: Schematic display of MB functionalisation and CEA detection. A magnet has been placed under the recognition cell to accumulate the MBs on the bottom of reaction cell, to increase the conductivity of graphene sheet (Jin et al., 2014).

1.6.1 Sample Preparation Platform

The concept of the sample prepration platform is based on using a rotational cylinder with implanted magnets for immunomagnetic sample preparation with use of functionalised magnetic beads followed by analyte detection on the sensing platform. The sample preparation technique (Figure 1.15) is known as trapping-and-releasing mechanism. The main part of this sample preparation platform is its three magnetic assemblies, which are used to continuously trap and release the magnetic beads at different part of the micro-channel.

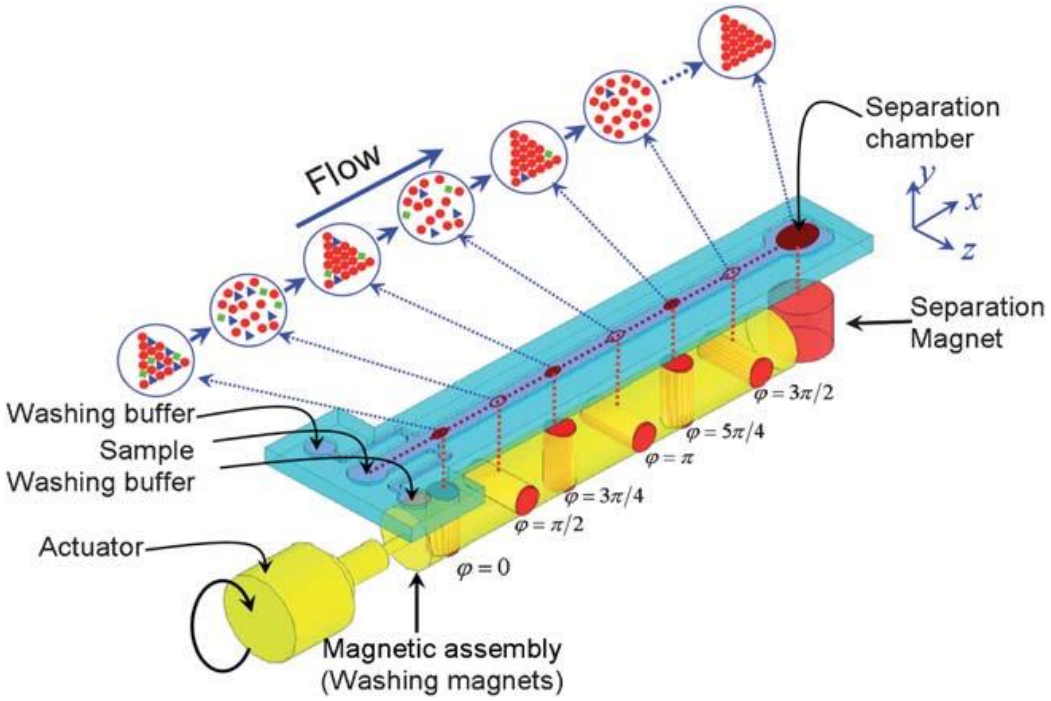

Figure 1.15: The Schematic Illustration of the Trapping-and-Releasing Sample Pre-concentration Mechanism (Ramadan et al., 2010).

In the sample preparation once the sample has been mixed with magnetic beads, the sample will flow over the platform through micro-channel. Magnetic beads will be trapped when the pole of cylinder's magnets face the channel, then magnetic beads will be released due to rotation of cylinder. The simultaneous trapping and releasing of magnetic carriers will result in separation of magnetic beads from the rest of molecules, which are present in the sample, as the flow speed of magnetic beads will be lower than the rest of molecules. The final purified sample can be collected from the separation chamber which is placed at the end of micro-channel on top of a strong permanent magnet (Ramadan & Gijs, 2011).

1.8. Aims and Objectives

Biosensors are facing numerous challenges which can be classified into two main groups, recognition receptors and device point of view. From a recognition point of view challenges are convenient storage condition, specificity, cross-reactivity, and multi-

analyte detection. Device challenges are portability, reliability, reversibility, sensitivity, rapidity, stability, low limit of detection, rapid sample treatment, and ability to be used for detection of analytes with different sizes (Perumal & Hashim, 2014).

This project aims at developing rapid, portable, highly sensitive and specific multi-analyte sensing platforms for lung cancer marker screening by use of magnetic platform for better and more sensitive detection of biomarkers. To achieve the goals of the project, we propose a magnetic sensing platform integrated with an impedimetric immunosensor to detect lung cancer biomarkers such as CEA, and NSE within human blood serum. Two types of monoclonal anti-cancer biomarker antibodies were used to detect each analyte of interest. The first antibody type, detection antibody, were immobilised on the sensing area and the second one, a capture antibody, were used to functionalise the magnetic nanobeads. The functionalised magnetic nanobeads were used to capture the analyte from the sample to increase the chance of analyte detection, and to enhance the immunosensor response. To accomplish the aims of the project, the objectives were divided into the sensing platform and analyte detection system. Figure 1.16 presents work included in this project in the form of a flow chart. The objectives of this project were:

- Designing and manufacturing of the platform.
- Programming the platform stepper motor (Ardiuno Uno kit).
- Testing the platform.
- Selection of the optional screen-printed electrode for use in this work.
- Functionalization of the screen-printed electrodes with detection antibody (anti-CEA, and anti-NSE antibody).
- Functionalisation of magnetic nanobeads with capture antibody (anti-CEA, and anti-NSE antibody).
- Detection of analyte in PBS buffer and optimisation of the immunoassay for both biomarkers.
- Specificity and non-specificity test of each type of immunosensor in blood serum samples.

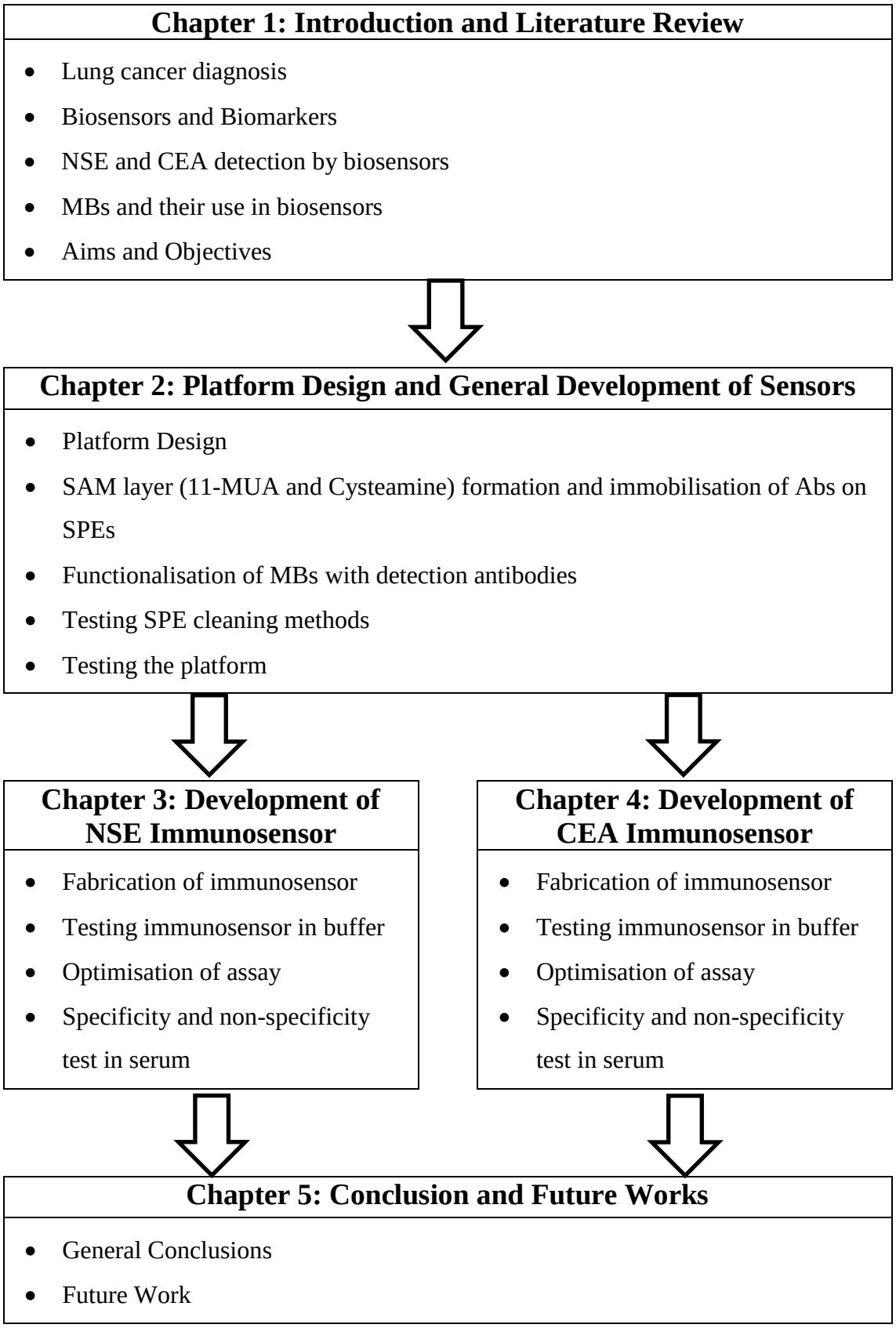

Figure 1.16: The flow chart of the thesis content.

Chapter 2:

PLATFORM DESIGN & GENERAL DEVELOPMENT OF SENSORS

2.1. Materials

2.1.1 Reagents and Chemical Products

11-Mercaptoundecanoic acid (11-MUA), 1-3-dimethylaminopropyl-3-ethylcarbodiimide hydrochloride (EDC), bovine serum albumin (BSA), cysteamine hydrochloride, hydrochloric acid (HCl), ethanol, ethanolamine, N,N-dimethyl formamide (DMF), N-Hydroxysuccinide (NHS), 1,4-phenylene diisothiocyanate (PDITC), potassium hexacyanoferrate(II) trihydrate, phosphate buffer saline tablet (PBS), potassium hexacyanoferrate(III), Potassium hydroxide, potassium phosphate monobasic, pyridine, sulphuric acid, turboBeads™ carboxy (50 nm), and tween 20 were purchased from Sigma-Aldrich (Dorset, UK). A 0.2 syringe filter was purchased from Sartorius (Germany).

10-7937-FIT anti-NSE mouse monoclonal antibody, 10-7938-FIT Anti-NSE mouse monoclonal antibody, 12-140-01 anti-CEA monoclonal antibody, 12-140-10 anti-CEA monoclonal antibody, native human CEA protein, and purified native human NSE protein were purchased from Fitzgerald Industries International (Acton, USA).

2.1.2 Solutions and Buffers

- **Coupling Buffer**
  Coupling buffer was prepared at pH 5.5 by mixing 136.1 mg of potassium phosphate monobasic and 877 mg of sodium chloride in 100 ml of deionised water, and adjusting the pH by 1M hydrochloric acid.

- **50 mM potassium hydroxide (KOH) 25% hydrogen peroxide (H_2O_2)**
  The 50 mM KOH H_2O_2 was prepared by, first, adding 20 ml of deionised water to 100 ml of H_2O_2 (30%) in order to make 25% H_2O_2. Then 0.2806 g of KOH was mixed in 100 ml of 25% H_2O_2.

- **1 M Hydrochloric Acid (HCl)**

  1 M HCl was prepared by adding 52 µl of HCl 37% to 10 ml of dH_2O.

- **Piranha Solution**

  Piranha solution was prepared by adding 10 ml of H_2O_2 35% with 30 ml of sulphuric acid in a glass container.

- **0.4 M EDC Solution**

  0.4M EDC was prepared by dissolving 7.2 mg of EDC in 9.387 ml of deionised water.

- **0.1 M NHS Solution**

  0.1 M NHS was prepared by dissolving 0.1151 g of NHS in 10 ml of deionised water.

- **PBS Buffer pH 7.4**

  PBS buffer pH 7.4 (10 mM phosphate buffer, 27 mM potassium chloride, and 137 mM sodium chloride) was prepared by dissolving PBS tablet in 200 ml of deionised water.

- **Standard Buffer (PBS pH 7.4 + 0.1 % BSA + 0.05% Tween 20)**

  The standard buffer was prepared by constituting 1.33 ml of 7.5% BSA and 50 µl of Tween 20 in prepared PBS buffer with pH 7.4.

- **10 mM Cysteamine Hydrochloride Solution**

  10 mM cysteamine hydrochloride was prepared by dissolving 11.36 mg of cysteamine hydrochloride into 10 ml of deionised water.

- **5 mM 11-Mercaptoundecanoic Acid (11-MUA)**

  5 mM 11-MUA was prepared by mixing 64 mg in 5.872 ml of ethanol.

- **Activation Solution (10 mM PDITC, in Pyridine and DMF [v/v 1:9])**

  The activation solution was prepared by dissolving 5 mg of PDITC in 2.25 ml of DMF solution, and then adding 250 µl of pyridine solution.

- **10 mM Ethanolamine Solution pH 7.6**

  10 mM ethanolamine was prepared by adding 61.08 µl of ethanolamine solution to 10 ml of deionised water and adjusting the pH to 8.6.

- **10 µg/ml Detection Antibody Solution**

  10 µg/ml of detection antibody for CEA detection sensor was prepared by adding 6.25 µl of anti-CEA antibody (12-140-01) to 1493.75 µl of PBS pH 7.4. The 10 µg/ml anti-NSE antibody solution was prepared by adding 12.5 µl of 10-7937 anti-NSE antibody in 1.2 ml of PBS pH 7.4 to make 100 µg/ml concentration. Then the 100 µg/ml antibody solution was diluted by 10 in PBS pH 7.4 to obtain the final concentration of 10 µg/ml of antibody solution.

- **10 mM Potassium Ferri/Ferro Cyanide Solution**

  10mM potassium ferri/ferro cyanide was prepared by mixing 65.86 mg of Potassium hexacyanoferrate (III) and 84.48 mg of Potassium hexacyanoferrate (II) trihydrate in 10 ml of PBS pH 7.4.

2.1.3 Equipment

Two types of potentiostat were used in this project for Voltametric and potentiometric measurements. The first device was an Auto GillAC analyser (ACM instrument, UK) (Figure 2.1, A) provided with ACM instrument software (version 5) and the second one was PalmSens^3 Potentiostat (PalmSens BV, Netherlands) (Figure 2.1, B) in conjugation with PSTrace software (Version 4.8).

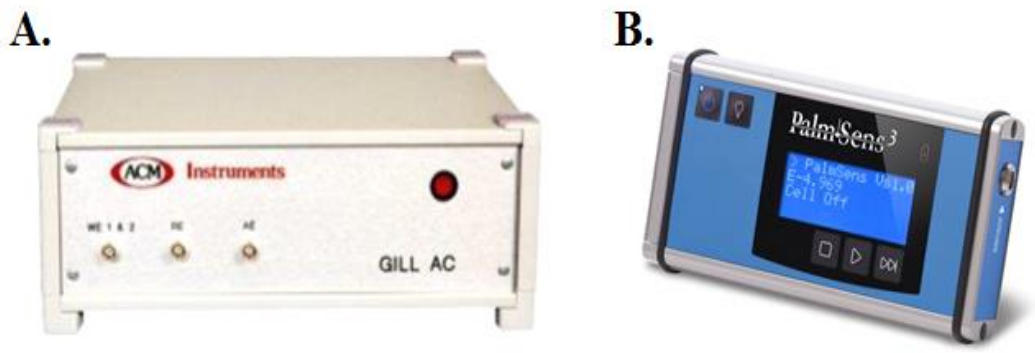

Figure 2.1: Used potentiostat in this project. A. Auto GillAC; B. PalmSens[3].

2.1.4 Screen Printed Electrodes

Three types of SPE including DRP-250AT, DRP-220AT, and DRP-220BT were investigated in this project. All SPE types were purchased from Dropsens (Austurius, Spain), and consisted of three electrodes: working (WE), reference (RE), and counter/ auxiliary (CE) (Figure 2.2).

Figure 2.2: Screen printed electrode used in this project and their configuration of their electrodes. A. counter electrode; B. working electrode; C. reference electrode.

The SPE electrodes in this investigation have the electrode configuration as follows:

- DRP-250AT: gold (WE). platinum (CE), and Ag/ AgCl (RE)
- DRP-220AT: gold (WE). gold (CE), and Ag/ AgCl (RE)
- DRP-220BT: gold (WE). gold (CE), and Ag/ AgCl (RE)

DRP-220AT and DRP-250AT SPE gold electrodes were printed using high temperature curing (900^{O}C) ink, while DRP-220BT SPEs gold electrodes were printed with a low temperature curing ink (150^{O}C) (Figure 2.3).

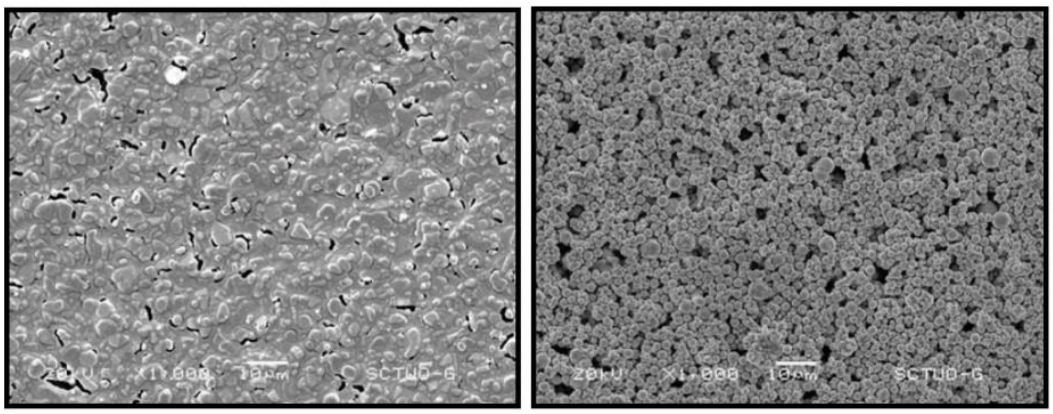

Figure 2.3: SEM Images of gold working electrodes; high temperature curing ink (AT model) is on the left side and low temperature curing ink (BT model) is on the right side (www.dropsens.com).

Figure 2.3 shows that the AT model SPEs have smoother surfaces than the BT model. According to the DropSens website, based on the type of surface modification and redox solution, they may have different behaviours. AT model SPEs benefit from better electron transfer than BT models in the presence of ferry/ ferro cyanide as the electrolyte solution, though BT model SPEs are cheaper to fabricate.

2.2. Methodology

Improvements in biosensor technology are required for the detection and analysis of multi-analytes for certain purposes, including cancer diagnosis through detection of multi-biomarkers (Tothill, 2009; Fragoso et al., 2010). The use of magnetic beads in biosensing platforms, *e.g.*, protein detection, has been successful because of the advantages these materials can have present such as a large surface area (Altintas et al., 2012; Li et al., 2012). Therefore, magnetic beads were used as a key component in this project.

This project includes development of a sensing platform. The experiments were initiated by with building the platform and testing the Trapping-and-Realising platform with CEA and NSE proteins for data analysis. Since the platform should have high sensitivity and specificity, for each protein two monoclonal antibodies were chosen which recognise two distinct sites of the CEA and NSE antigens. These antibodies were chosen as they have successfully been used in previous work reported by Fragoso et al. (2010).

2.2.1 Proposed Platform (Trapping and Releasing)

The idea of the detection platform proposed here was obtained from Ramadan et al. (2010), as explained in Chapter 1, Section 1.6.1. The trapping and releasing platform consists of magnetic assemblies, which will be placed underneath the functionalised SPEs. The analyte detection experiment begins by immobilising detection and recognition monoclonal antibodies on the surface of WEs and magnetic beads (MBs), respectively; and preparation of analyte samples with different concentrations.

Here SPEs were placed above the magnetic assemblies of the sensing platform. After mixing the functionalised MBs with the sample, the sample was dropped on the surface of the electrode. The purpose of using rotational magnetic cylinder was to accumulate MBs on the sensor surface for detection of the analyte *via* the immobilised antibodies. The magnetic cylinder was connected to a stepper motor to have a better control on the speed of magnetic beads movement over the sensor surface. The stepper

motor was connected to and controlled by an Arduino Uno kit (Arduino, Italy) which allows management of the motor speed and the number of steps. When the incubation time for binding of target molecules to recognition antibodies on WEs surface had been optimised, the magnetic beads that carry no analyte were eliminated from the sensing area with use of a magnet. The magnetic beads were attracted to the electrode surface several times to assure that the platform had detected all the captured analytes with the magnetic carriers. The principle of the proposed platform is shown in Figure 2.4.

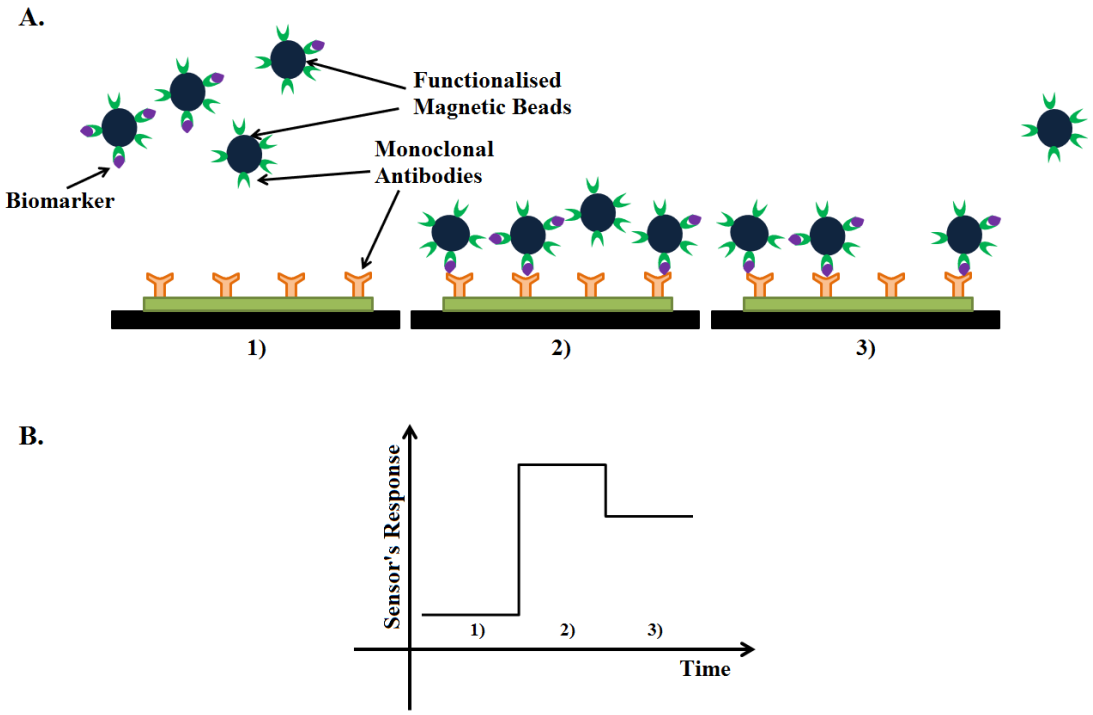

Figure 2.4: The platform measurement principle. A. the schematic of measurement process, 1) applying fished magnetic beads from the sample to the sensor, 2) attraction of magnetic beads to the sensing area 3) elimination of sensor surface from magnetic beads with no analyte via rotation of magnetic cylinder. B. the sensor response versus time graph, the signal difference between step 3) and 1) is proportional to the analyte concentration.

This shows that only the magnetic beads carrying the analyte will remain on the WE, and due to use of monoclonal antibodies the method of detection should be highly specific for the target analyte. It was assumed that the use of this this platform would

reduce false positive results as no unwanted materials would exposed to the sensing surface. Moreover, as MBs are used in the detection process, reduction of analyte measurement time and achievement of a low LoD could be optimised.

2.2.2 Functionalisation of Magnetic-NanoBeads with Capture Antibodies

Cobalt magnetic nanobeads (15 mg) (50 nm) were added to 400 µl of coupling buffer (potassium phosphate monobasic + sodium chloride) in 2 ml centrifuge tube and dispersed in the buffer by ultra-sonication using SONIC 6MX ultrasonic bath (James Products Europe, UK). Then washing step was applied, by separating magnetic beads with magnetic rack (Invitrogen, US), and then addition of 400 µl of coupling buffer. The beads were then dispersed in the buffer by placing the centrifuge tube in ultrasound water bath for 1 minute. After final washing step, the centrifuge tube was placed in a magnetic rack, the supernatant was removed, and the beads were resuspended in 400 µl of coupling buffer, with 400 µl of EDC solution, and 400 µl of NHS solution. The magnetic beads were then left under slow tilt rotation for 20 minutes.

The unreacted reagent solution was then removed before adding 400 µl of coupling buffer containing 10 µl of capture antibodies (12-140-10 for CEA immunosensor, and 10-7938 for NSE), the centrifuge tube was placed on slow tilt rotation for 30 minutes followed by three times washing with standard buffer (PBS 7.4 + 0.1% BSA + 0.05% tween 20) to remove unbounded antibodies. In the last step, standard buffer was removed from centrifuge tube and the conjugated magnetic beads with capture antibodies were resuspended in 400 µl of standard buffer.

2.2.3 Redox Probe Selection

To understand the effect of redox solution, potassium ferri/ ferrocyanide in PBS, on impedance measurements and selection of the best concentration, various concentration of potassium ferri/ ferrocyanide redox solutions were prepared in various concentration of PBS buffer. After preparation of redox solutions, 2 bare SPEs were used to test the effects of redox solution concentration. Before each impedance measurement, the SPEs

were washed by PBS pH 7.4 and dried with nitrogen gas. The impedance measurements were done by use of 50 µl of the redox solution. The auto GillAC potentiostat was used here to apply the impedance measurements.

2.2.4 Cyclic Voltammetry

In order to obtain the DC potential for impedance settings a cyclic voltammetry (CV) was done by PalmSens^3 potentiostat in conjugation with PSTrace software (Version 4.8) within the potential range of ±0.6 V at a scan rate of 0.1 V/S and using 50 µl of 10 mM $[K_3Fe(CN_6)]/[K_2Fe(CN_6)]$ in PBS pH 7.4 on a bare SPE.

2.2.5 Electrochemical Impedance Spectroscopy

Two types of potentiostat were used in this project, Auto GillAC and PalmSens^3. A redox probe (50 µl of 10 mM $[K_3Fe(CN_6)]/[K_2Fe(CN_6)]$ in 10 mM PBS pH 7.4) was used for all impedance measurements and all measurements were performed in a faraday cage. Both Auto GillAC and PalmSens^3 devices were connected to PC and were used alongside their software.

All the performed impedance measurements with both devices were done with frequency range between 50 kHz and 0.1 Hz and a number frequency of 51. The potential amplitude of 0.01 V, the applied potential of 0.12 V, and the current range of 10 µA to 10 mA, were used for PalmSens^3 potentiostat; while impedance measurements by the Auto GillAC were carried out by applying a wave amplitude of 10 mA and a DC offset of 0.1 mV.

2.2.6 Data Fitting Analysis

To be able to compare impedance measurements, conversion of impedance graphs (Nyquist plots) into meaningful numbers such as R_{et}, Z_W, C_{dl} needs to be performed according to the equivalent circuit. There are different programs which can be used to simulate the graph and calculate the above-mentioned values. In this project ACM

analysis V4 (GillAC software) and EIS spectrum analyser software (Bondarenko & Ragoisha, 2008) were used to analyse the impedance measurements.

The ACM analysis V4, Figure 2.5, can easily be used to calculate the desired values by placing the fitting circle on the semicircle part of impedance graph, and the software will calculate the R_{et}, C_{dl}, and R_s but not the Z_W. The second software, EIS spectrum analyser, Figure 2.6, calculates the required values based on the chosen equivalent circuit from its library.

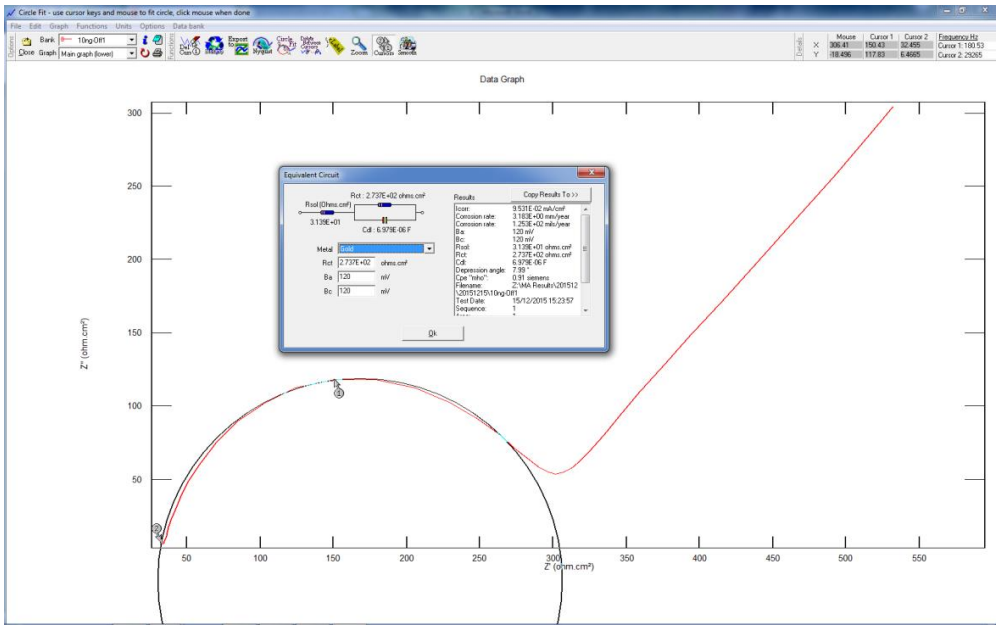

Figure 2.5: The Screen print of ACM analysis V4 software used for analysing obtained results from Auto GillAC instrument. The red graph is the impedance result. The black circle is used to determine analytical values.

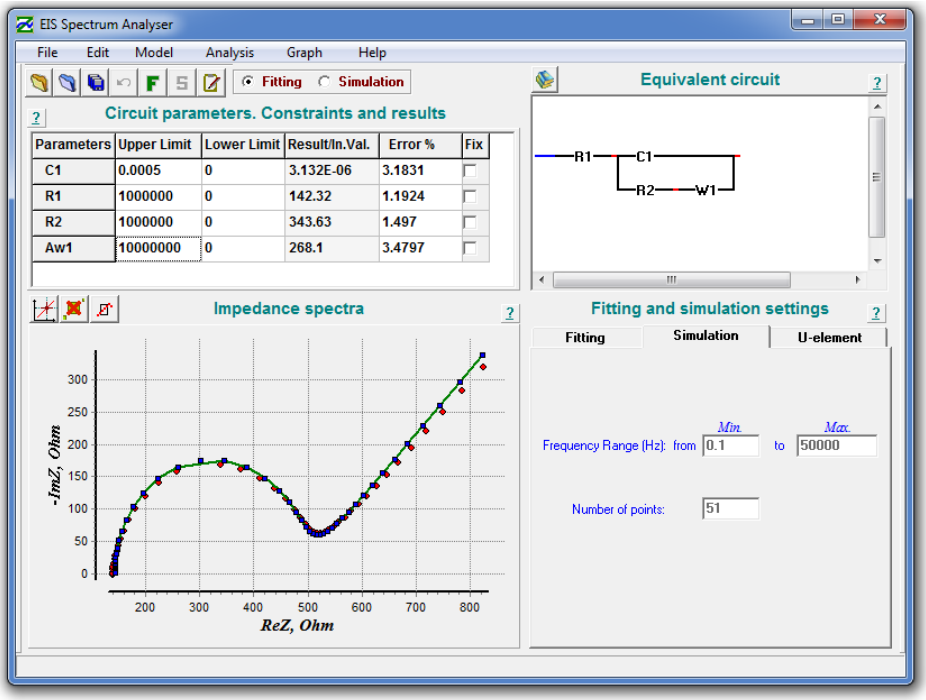

Figure 2.6: The Screen print of EIS Spectrum Analyser Software used for analysing obtained results from PalmSens[3] device. Experimental graph (Red), fitted curve (Green); simulation graph (Blue).

Figure 2.6 is a snapshot of EIS Spectrum Analyser software that has been used to simulate the best fitting curve to the obtained impedance results according to the equivalent Randles circuit, the circuit on the top corner. After fitting the results, the software shows the estimated value for each parameter above the plot area. The R1 and R2 are representing R_s and R_{et} respectively, and C1 and Aw1 are standing for C_{dl} and Z_W.

2.2.7 Immobilisation of Detection Antibodies on Gold Working Electrode

Two methods were tested to immobilise the antibody on the surface of the gold working electrode based on the formation of a self-assembled monolayer (SAM layer). This was conducted as it is important to reduce non-specific binding and increase the stability of immobilised recognition elements on the electrode surface. Use of SAM layer has been increased in biosensor development due to its simplicity, stability, well-organised structure, and production of low background noise (Cecchet et al., 2006; Ahmad & Moore, 2012; Zhang et al., 2013; Carter et al., 2015; Yang et al., 2016).

To confirm the success of antibody immobilisation process, the impedance measurements were performed before and after each step of immobilisation process. Both Auto GillAC and PalmSens^3 instruments were used to confirm the immobilisation steps with the cysteamine method while only the Auto GillAC was used for 11-MUA method confirmation.

2.2.7.1 Cysteamine SAM Layer

SPEs were placed on top of a wet tissue in a petri dish, and 10 µl of 10 mM Cysteamine hydrochloride was added on top of SPE's working electrodes and incubated at room temperature for 16 hours to allow SAM layer formation on WEs. The SPEs were then washed three times with 10 mM PBS pH 7.4 and dried with nitrogen gas.

To activate the amino group on SPEs, 10 µl of activation solution (PDITC, in pyridine and DMF [v/v 1:9]) was added on top of working electrodes and incubated at room temperature for 30 minutes followed by washing the electrode (×3) with DMF and PBS pH 7.4 before drying them by nitrogen gas. The activation solution contains 1,4-phenylene diisothiocyanate which is a homobifunctional crosslinking reagent and was used because of its stability and flexibility.

After incubation of electrodes in 20 µl of 10 µg/ml detection antibodies (12-140-01 for CEA immunosensor, and 10-7937 for NSE immunosensor) in PBS for two hours at room temperature, the SPEs were washed three times with 50 µl of PBS (pH 7.4) to eliminate unbound antibodies from the surface of SPE. Then 20 µl of 0.1 M of ethanolamine solution (pH 8.5) was added on WEs for 30 minutes, to deactivate thiocyanate terminal, followed by washing the electrodes three times with 50 µl of PBS pH 7.6. Then, the SPEs were incubated for 30 minutes in 100 µl of 1% BSA solution to minimise analytes non-specific binding to the surface of WEs, before rinsing the SPEs with PBS buffer pH 7.4. The immobilisation method of antibodies (Figure 2.7) through formation of a cysteamine SAM layer on gold surface has been successfully used by Elshafey *et al*, (2013).

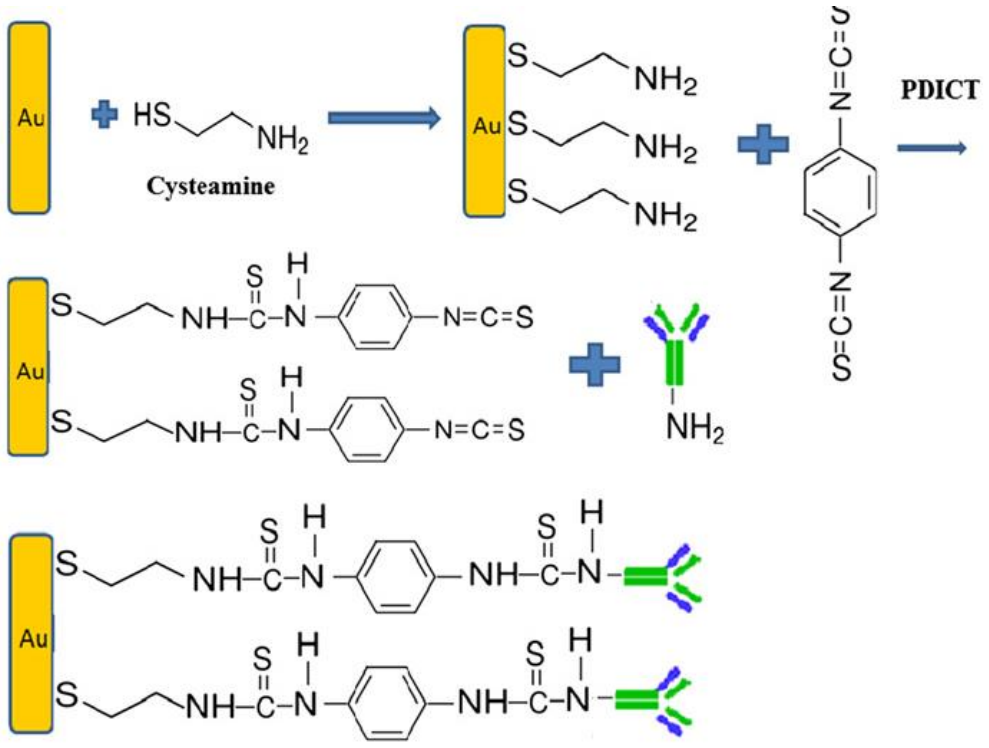

Figure 2.7: Schematic illustration of antibodies immobilisation on gold WEs through formation of cysteamine SAM layer (Elshafey et al., 2013).

2.2.7.2 11-Mercaptoundecanoic Acid (11-MUA) SAM Layer

SPEs were immersed in 2 ml of 5 mM 11-MUA prepared in ethanol and incubated in the dark for 16 hours at room temperature to form SAM layer on WEs. Then the washing step consisting of rinsing the SPEs with pure ethanol and dH_2O was applied three times to remove unbounded 11-MUA residues followed by drying the SPE with nitrogen gas.

Then, 10 µl of 0.4M EDC/ 0.1M NHS (1:1) solution was added on WEs at room temperature for 50 minutes. EDC was used as a crosslinker to link carboxylic end group of 11-MUA to primary amine. The coupling reaction is not highly stable and can be quickly hydrolyse into the solution; therefore, the NHS is required in coupling buffer (Conde et al., 2014).

Then 20 µl of 10 µg/ml detection antibodies (12-140-01 for CEA immunosensor, and 10-7937 for NSE immunosensor) in PBS (pH 7.4) was added on WEs with EDC/ NHS-activated SAM layer for 2 hours at room temperature before washing SPEs three times with PBS pH 7.4 and drying them with nitrogen gas. Later, 20 µl of 0.1M of ethanolamine (pH 8.5) was added on the WEs for 30 minutes to deactivate the remaining carboxyl groups. In the last step of antibody immobilisation, SPEs were washed again with PBS buffer and incubated in 1% BSA for 30 minutes at room temperature to block non-specific sites of electrodes. The process of antibody immobilisation on gold surface through formation of 11-MUA SAM layer is schematically reported on Figure 2.8.

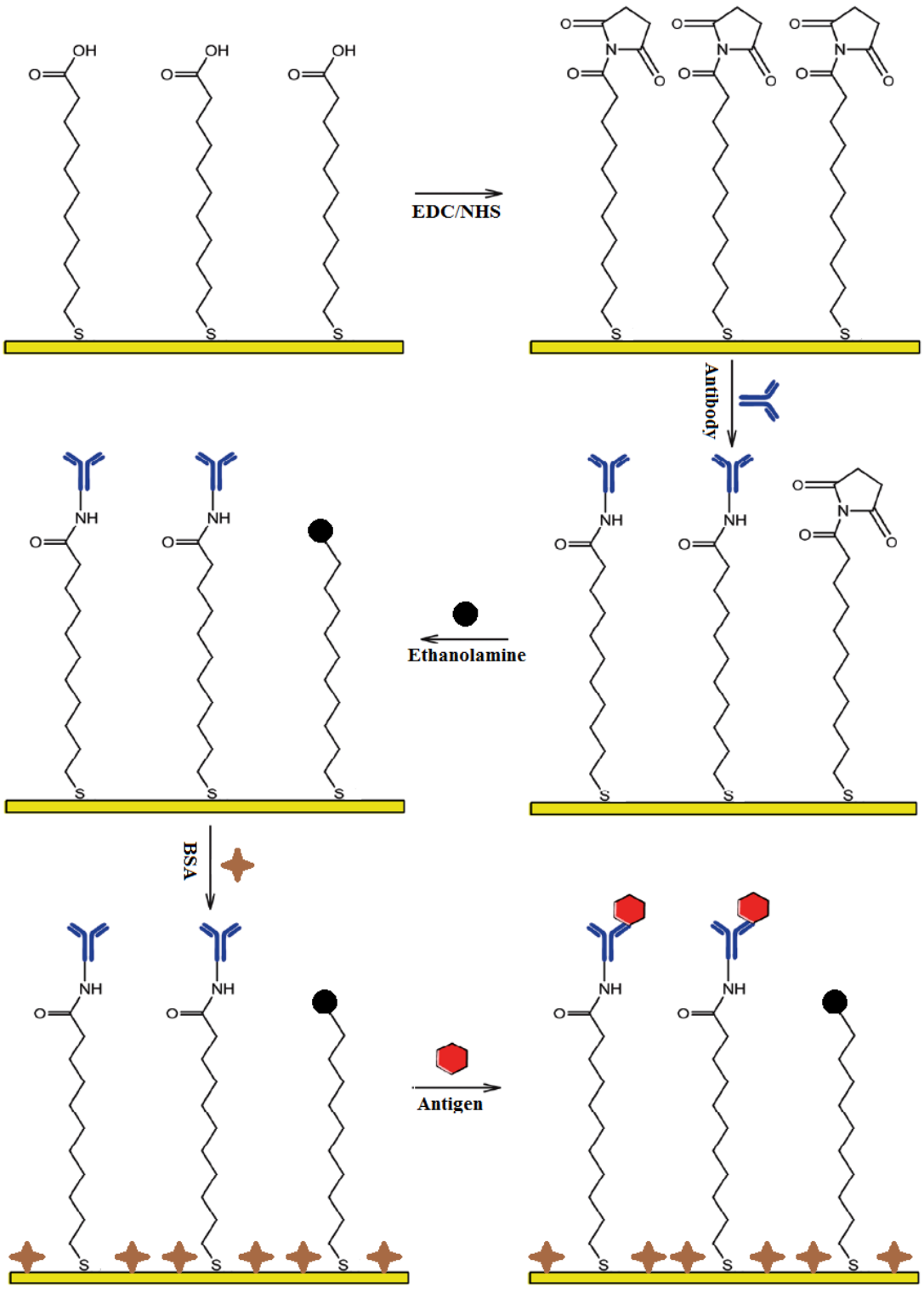

Figure 2.8: Schematic illustration of antibodies immobilisation on gold WEs through formation 11-MUA SAM layer.

2.2.8 SPE Selection

To investigate the effect of the SPE type and to choose the best one for this project, three types of SPEs (Section 2.1.4) were investigated.

Three SPEs, one of each type, were functionalised by 12-140-01 anti-CEA antibodies. Two CEA protein samples with 0 ng/ml and 100 ng/ml concentrations were prepared in 10 mM PBS pH 7.4. The signal measurements were done by incubating 50 µl of 0 ng/ml CEA on WEs for 20 minutes then washing the electrode with PBS pH 7.4 prior of recording the impedance signals in presence of 50 µl of potassium ferri/ ferrocyanide. Then, the electrodes were washed and dried before repeating the same procedure for 100 ng/ml sample. The impedance signals were measured by a PalmSens^3 instrument and its corresponding software.

2.2.9 Use of One SPE for Each Concentration *Vs.* One SPE for All Concentrations

This experiment was done by immobilising 12-140-10 anti-CEA antibodies on the MBs surface and functionalising SPEs with 12-140-01 anti-CEA antibody. The first part of the experiment was done by using of 3 SPEs. A single SPE was used to measure various concentrations of CEA protein from the lowest concentration, 0 ng/ml, to the highest concentration, 100 ng/ml. The electrode was washed with dH_2O and dried with nitrogen gas before using it for the next sample measurement. The second part of experiment was done by using each functionalised SPEs for the measurement of only one analyte.

All impedance measurements were done made with an Auto GillAC instrument and analysed by EIS spectrum analyser to calculate the R_{et} values. The calculated values were used to generate the $\%\Delta R_{et}$. The $\%\Delta R_{et}$ values were then normalised against the "0 ng/ml $\%\Delta R_{et}$" to plot the graphs.

2.2.10 Electrodes Cleaning Methods

The impedance measurements of bare SPEs are shown to vary from one electrode to another. The contamination of the electrode surface had an effect on thiol binding and electrochemical properties of the electrode (Fischer et al., 2009). Furthermore, chemical residues and dust might affect the quality of the SAM layer (Watson et al., 2015). Thereby, applying a cleaning method before constructing the immunosensor can help to improve the reproducibility. Five different electrode cleaning methods were tested to find the best compatible cleaning method with the chosen type of SPE. The cleaning methods included:

- Immersing the SPEs in 1 M hydrochloric acid (HCl) for 10 minutes.
- Immersing the SPEs in 50 mM potassium hydroxide in 25% hydrogen peroxide ($KOH+H_2O_2$) for 10 minutes.
- Immersing the SPEs in piranha solution for 1 minute.
- Immersing the SPEs in ultrasonic bath for 1 minute.
- Leaving the SPEs in the oven at 120^{o}C for 30 minutes.

All cleaning methods were applied on DRP-220BT, and a PalmSens^3 was used to measure the impedance signals. The cleaning methods were repeated three times with three different SPEs. All the cleaning methods had 4 steps: impedance measurement before cleaning process, cleaning process, rinsing SPEs with adequate amount of dH_2O and drying them with nitrogen gas, and impedance measurement after cleaning process.

2.2.11 Proposed Platform Test

This experiment was designed to check whether the MBs and proposed platform have an effect on the analyte detection. The SPEs were functionalised with an anti-NSE antibody (10-7937) and the anti-NSE antibody (10-7938) were immobilised on MBs surfaces. All functionalised SPEs were freshly prepared on the day of experiment, and were checked by impedance to confirm the attachment of antibodies to the surface of WEs. The impedance measurements of this section were performed by PalmSens^3 and its

corresponding software with settings mentioned on Section 2.2.5 in the presence of 50 µl of 10 mM potassium ferri/ ferrocyanide within the faradaic cage.

The impedance signals of functionalised SPEs were recorded and used as the baseline to compare impedance signals of analyte measurement. This experiment was divided into two parts, the proof of platform concept with specific analyte (NSE Protein) and the non-specificity test of the NSE immunosensor with non-specific analyte (CEA protein). For both experiments, specificity and non-specificity tests, consisted of three parts (Figure 2.9). Each step of the experiment was repeated three times with three freshly functionalised SPEs with an anti-NSE antibody. Various concentration of NSE and CEA antigens (0, 1, 10, and 100 ng/ml) in PBS at pH 7.4 were prepared and tested to compare each step of this experiment; and finally, to compare the results.

The first step of experiment was designed to check the ability of NSE immunosensor to detect the target molecules. This experiment was done by adding and incubating 45 µl of NSE protein solutions with various concentration to the WE of functionalised SPEs. After incubation on NSE solutions on SPEs for 20 minutes, the electrode was rinsed with 3 ml of PBS pH 7.4 and dried by nitrogen gas prior to reading the impedance. This step of the experiment was named “NSE”

The second step of experiment (“NSE+MB”) was done by use of MBs to see whether using nanoparticles (NPs) can help in increasing signals. Functionalised MBs (5 µl) were mixed with 45 µl of various concentrations of NSE protein solution in centrifuge tube for 20 minutes to form MB-NSE complex. Then, centrifuge tubes contents were added to the sensing area of SPEs and incubated for 20 minutes. The SPEs were rinsed with 3 ml of PBS pH 7.4 and dried by nitrogen gas prior to recording the impedance.

The third step of experiment (“NSE+MB+Platform”) was done by use of MBs with the proposed platform to check if an enhanced signal would be obtained. Functionalised MBs (5 µl) were mixed with 45 µl of various concentrations of NSE protein solution in centrifuge tubes for 20 minutes to allow formation of MB-NSE complex. Then, centrifuge tube contents were added to the surface of the SPEs far from

the sensing area where the magnet pole was facing toward the SPEs. The magnetic cylinders were rotated by the action of the stepper motor which resulted in pulling of both MBs and MB-NSE complex to the sensing area. MBs and MB-NSE complex were incubated on top of WEs for 20 minutes before rotating the magnetic cylinders to pull back the unbounded MBs. The SPEs were rinsed with 3 ml of PBS pH 7.4 and dried by nitrogen gas prior of reading the impedance.

The second part of experiment was non-specificity testing of the NSE immunosensors with specific functionalised MBs to NSE protein, the proposed platform, and various concentrations of CEA protein. All three steps of the first experiment were repeated with NSE immunosensors for non-specific analyte detection, CEA. Figure 2.9 shows each step of the experiment.

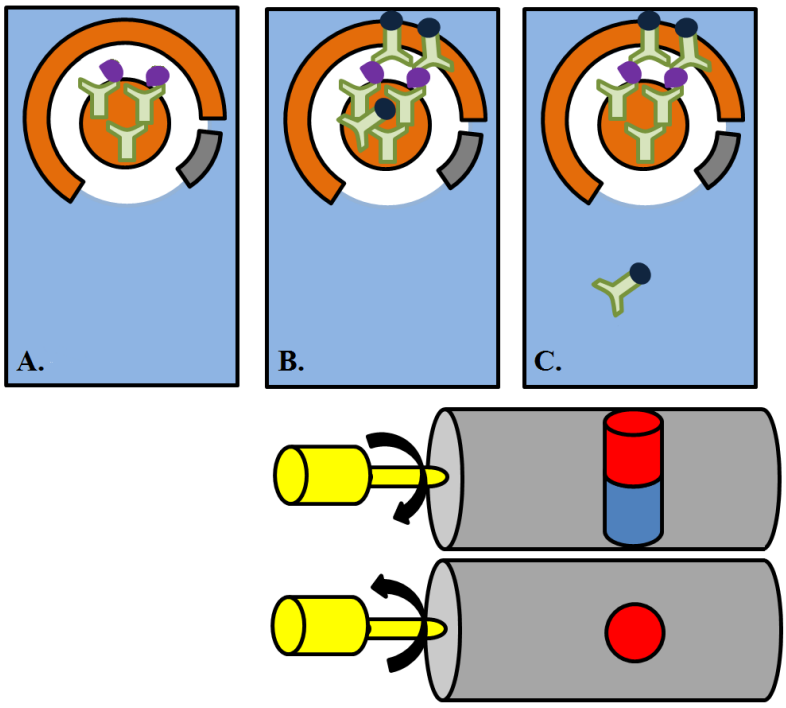

Figure 2.9: Schematic illustration of Proof of Platform experiment. A) The first step of experiment, measurement of NSE concentration, B) Second step of experiment, measurement of NSE concentration with use of MBs, C) Third step of experiment, measurement of NSE concentration with use of MBs and Proposed Platform.

2.3. Results and Discussion

2.3.1 Proposed Platform Construction

The proposed platform was designed and built by Cranfield University workshop. The sensing platform consisted of a cylinder which was connected to a stepper motor. The motor was controlled by an Arduino Uno kit which was programmed to automate the rotation of cylinder, Figure 2.10. Please refer to Appendix section (1 and 2) for platform blueprint and Arduino code.

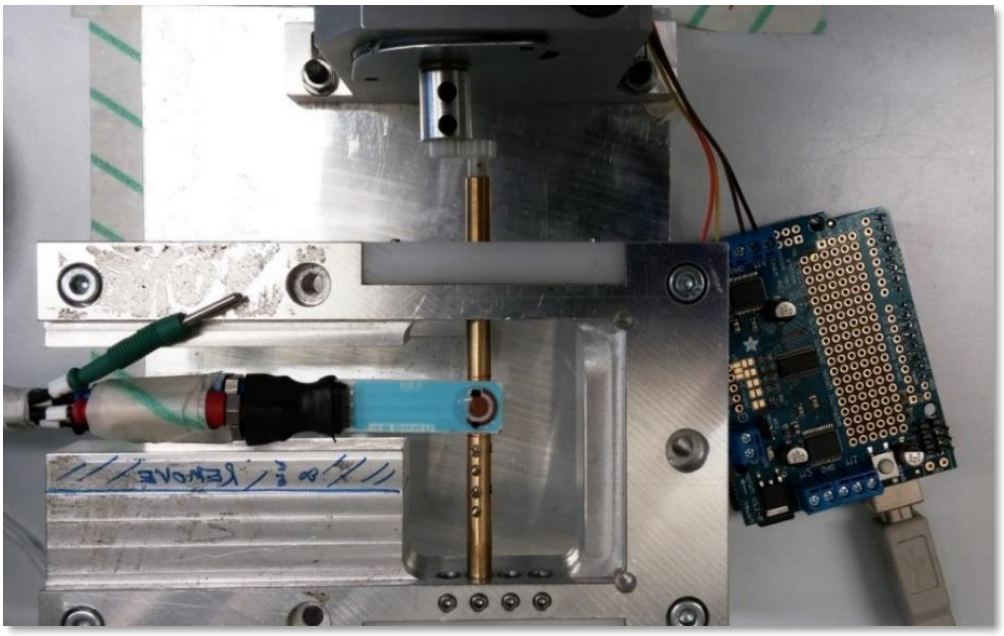

Figure 2.10: The proposed platform. A connected SPE to a potentiostat is placed on top of magnetic cylinder. The MBs on the sensing area of the SPE are placed on RE and CE as the side magnets are perpendicular to the SPE.

This shows that one cylinder with 3 implanted magnets were used in the platform. One magnet was placed under the WE and the other 2 magnets were placed on each side of the WE. To reduce the effects, unwanted material facing the sensing area of the SPEs, and also to reduce the effects of unbounded MBs which were facing reference and counter electrode, the magnets were rearranged. The arrangement of magnets was changed by

removing both of side magnets and adding another cylinder with one implanted magnet to pull away the magnetic beads to and from the sensing area. Figure 2.11 shows the rearrangement of the magnets.

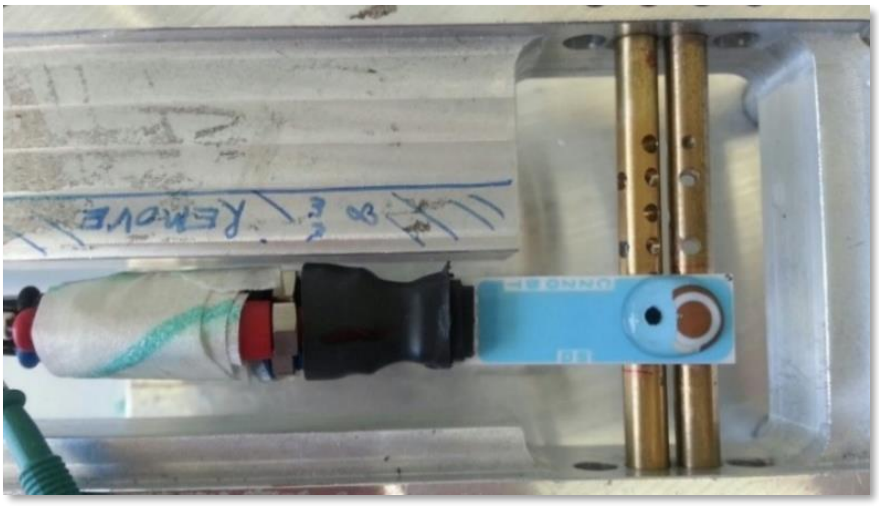

Figure 2.11: The proposed sensing platform with 2 cylinders.

2.3.2 Redox Probe selection

Different concentrations of ferri/ ferrocyanide such as 5 mM and 10 mM, have been used in different studies (Elshafey et al., 2013; Hou et al., 2013; Liu et al., 2015; Yang et al., 2016). To understantand the effect of redox solution and to choose the appropriate concentrations of ferri/ ferrocyanide and the PBS buffer for impedance measurements, various redox solutions were prepared and tested. The experimental results of different PBS concentrations and different ferri/ ferrocyanide concentrations are presented in Figure 2.12 and Figure 2.13, respectively.

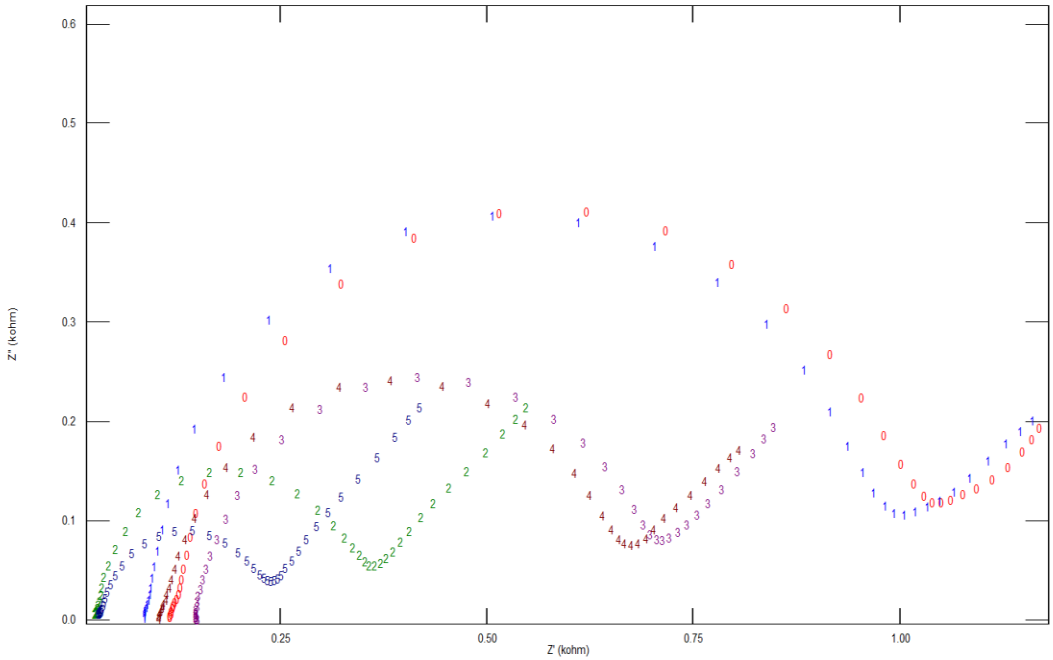

Figure 2.12: The Nyquist plot of impedance measurements of bare SPE1 and SPE2 with use of 10 mM potassium ferri/ferrocyanide in various concentration of PBS pH 7.4 SPE1 → 0.1 mM PBS (0), 1 mM PBS (1), 10 mM PBS (2), SPE2 → 0.1 mM PBS (3), 1 mM PBS (4), 10 mM PBS (5).

Figure 2.12, indicates that the PBS concentration of redox solution had an effect on impedance measurements. The resistance of electron transfer increased by reducing the concentration of PBS which may be caused by increasing the ion concentration. Since the bare electrode should have a low electron resistance and the prepared redox solution in 10 mM PBS was shown to have the lowest impedance signal in comparison with the other 2 redox solutions 10 mM PBS was chosen to prepare the redox solution.

The experimental data in Figure 2.13 shows that increasing the concentration of potassium ferri/ ferrocyanide in 10 mM PBS buffer pH 7.4 resulted in a reduction of the resistance of electron transfer, by increasing the concentration of ferri/ ferrocyanide, the amounts of electrons within the redox solution. This means that more electrons will be available to transfer from the redox solution to the surface of the electrode which results in reducing the resistance of the electrode.

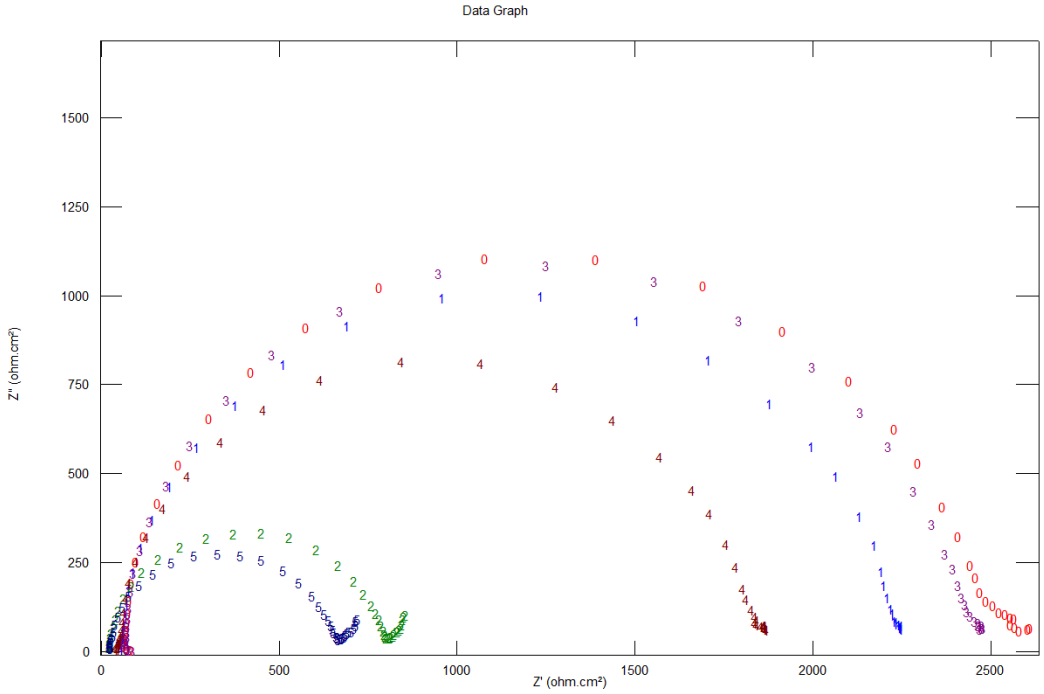

Figure 2.13: The Nyquist plot of impedance measurements of bare SPE1 and SPE2 with use of various concentration of potassium ferri/ferrocyanide in 10 mM of PBS pH 7.4 SPE1 → 0.1 mM (0), 1 mM (1), 10 mM (2), SPE2 → 0.1 mM (3), 1 mM (4), 10 mM (5).

Since 10 mM ferri/ ferrocyanide is the most common redox probe in analyte detection by EIS technique; and also based on the obtained results, 10 mM potassium ferri/ ferro cyanide in 10 mM PBS buffer pH 7.4 was selected for further experiments.

2.3.3 Cyclic Voltammetry

The CV technique was used to calculate one of the parameters required for impedance measurements. This parameter is called DC potential in PalmSens[3] and is named as DC offset in Auto GillAC instrument. It can be calculated from the Equation 5.

$$E_{DC} = \frac{(E_{pa} + E_{pc})}{2} \qquad \text{Equation 5}$$

Where E_{DC} is the DC potential, E_{pa} is anodic peak potential, and E_{pc} is cathodic peak potential.

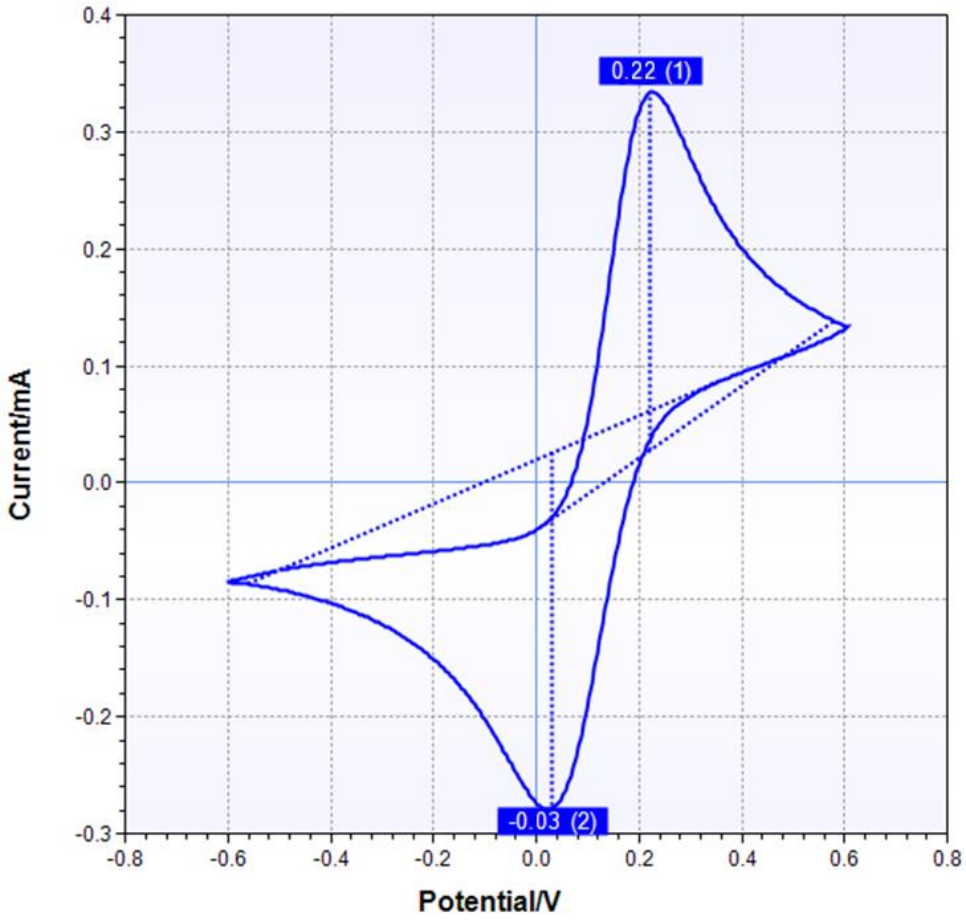

Figure 2.14: Cyclic Voltammogram Measurement with use of 10 mM $[K_3Fe(CN_6)]/[K_2Fe(CN_6)]$ in 10 mM PBS pH 7.4.

Figure 2.14 shows the obtained voltammogram where the E_{pa} and E_{pc} are 0.22 and 0.03, respectively. Therefore, DC potential was calculated as 0.12 by use of Equation 5.

$$E_{DC} = \frac{(0.22 + 0.03)}{2} = 0.12$$

2.3.4 Immobilisation of Detection Antibodies on Gold Working Electrode

As explained in Section 2.2.6, the SAM layer was used to immobilise the detection antibodies. Two methods of SAM formation on the gold surface were tested. The first one was by use of Cysteamine which produces a short chain SAM layer and the second was by use of 11-MUA which makes a longer chain SAM layer.

2.3.4.1 Cysteamine SAM Layer

The obtained impedance results by Auto GillAC for antibody immobilisation steps are shown in Figure 2.15.

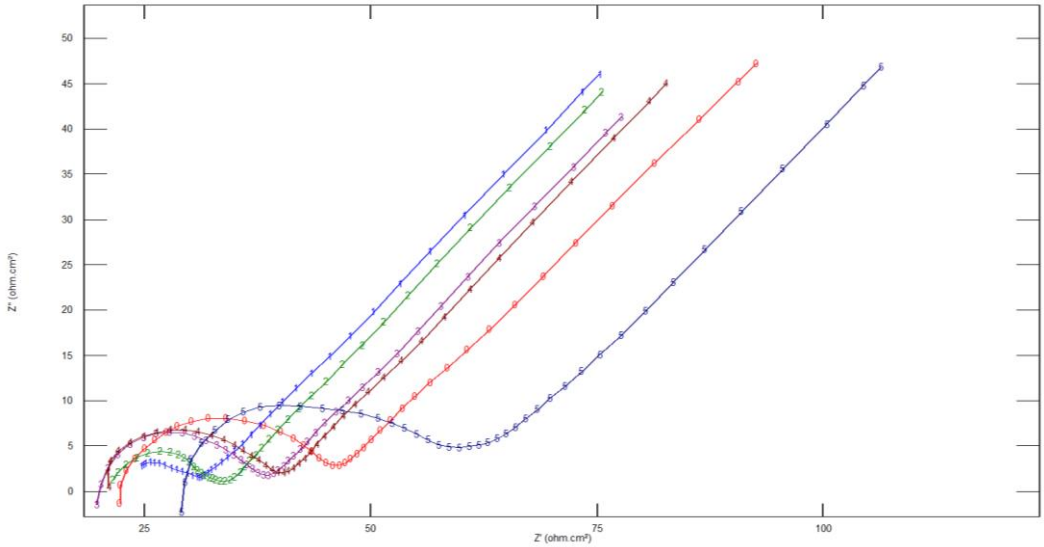

Figure 2.15: The Nyquist plot of impedance of antibody immobilisation through formation of cysteamine SAM layer (Auto GillAC instrument); Au (0); Au-Cys (1); Au-Cys-PDITC (2); Au-Cys-PDITC-Ab (3); Au-Cys-PDITC-Ab-Eth (4); Au-Cys-PDITC-Ab-Eth-BSA (5).

A previous study by Elshafey et al. (2013) showed that R_{et} is the best parameter to use for antibodies immobilisation confirmation, since it has the larger variation in comparison with C_{dl} and Z_W values. The R_{et} values of the impedance graphs are calculated by EIS Spectrum Analyser software and are shown in Table 2.1.

Table 2.1: Calculated R_{et} value for Each Step of antibody immobilisation process through formation of Cysteamine SAM layer (Auto GillAC Instrument).

Immobilisation Step	R_{et} (Ω)
Au	20.11
Au – Cysteamine	6.47
Au – Cysteamine – PDITC	9.89
Au – Cysteamine – PDITC – Ab	15.70
Au – Cysteamine – PDITC – Ab – Eth – BSA	25.21

The R_{et} values decreased from 20.11 Ω (Bare gold electrode surface) to 6.47 Ω (cysteamine modified gold electrode). Although the SAM layer must have formed on top of the gold WE, the R_{et} decreased. This might be due to the fact that the formation of the positively charged cysteamine layer on the electrode surface increases the electron transfer of the redox probe to the electrode surface (Li et al., 2011). Hence, by incubation of SPE in an activation solution the R_{et} increased to 9.89 Ω. After incubation of antibodies on WE, the R_{et} increased to 15.70 Ω which proved the attachment of antibodies to the SAM layer. Furthermore, the R_{et} value increased even more as a result of deactivation of the SAM layer by ethanolamine and surface blockage by 1% BSA.

This method of antibody binding to the surface of the gold electrode was also tested using the PalmSens^3 device and the results are presented as Figure 2.16 and Table 2.2.

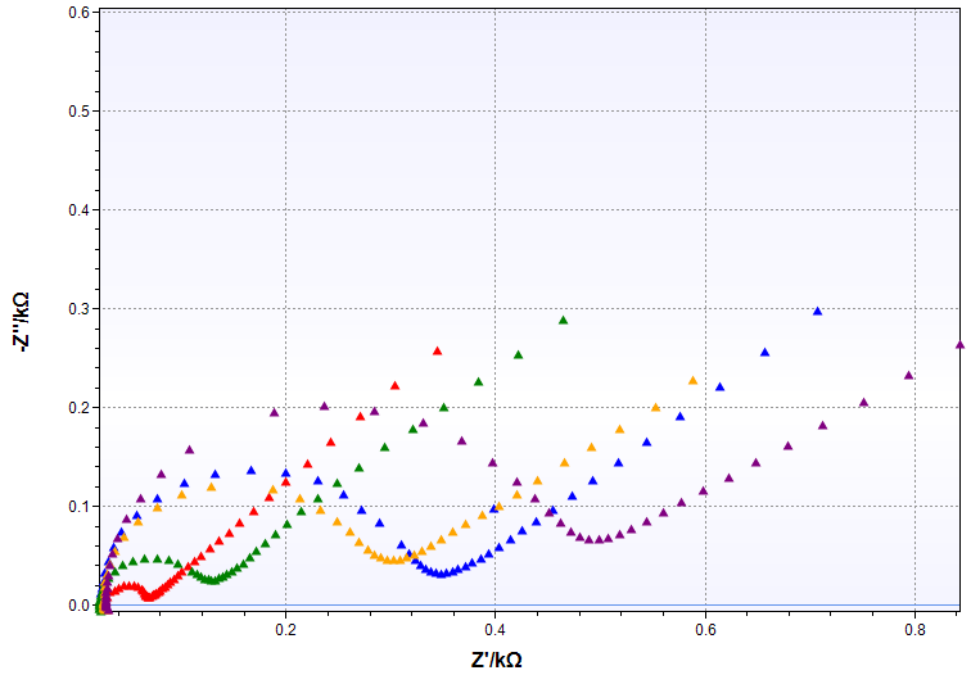

Figure 2.16: The Nyquist plot of impedance of antibody Immobilisation through formation of cysteamine SAM layer (PalmSens3); Au (Blue); Au-Cys (Red); Au-Cys-PDITC (Green); Au-Cys-PDITC-Ab (Yellow); Au-Cys-PDITC-Ab-Eth-BSA (Purple).

Table 2.2: Calculated R_{et} values for Each Step of antibody immobilisation process through formation of Cysteamine SAM layer (PalmSens^3 instrument).

Electrode	R_{et} (Ω)
Au	312.2
Au – Cysteamine	75.64
Au – Cysteamine – PDITC	152.8
Au – Cysteamine – PDITC – Ab	294.9
Au – Cysteamine – PDITC – Ab – Eth – BSA	492.1

The PalmSens^3 results showed the same pattern of decreasing and increasing of the impedance as for the data obtained by the Auto GillAC. For instance, the R_{et} value decreased from 312.2 Ω to 75.64 Ωafter cysteamine incubation step and increased to 152.8 Ω by activation of SAM layer. It then increases to 294.9 Ω after antibody immobilisation and to 492.1 Ω after blocking with ethanolamine and BSA.

2.3.4.2 11-MUA SAM Layer

Auto GillAC potentiostat was used to measure the impedance after each step of antibody immobilisation process and the results are shown in as Figure 2.17. EIS Spectrum Analyser was then used to simulate the impedance and calculate the R_{et} values (Table 2.3).

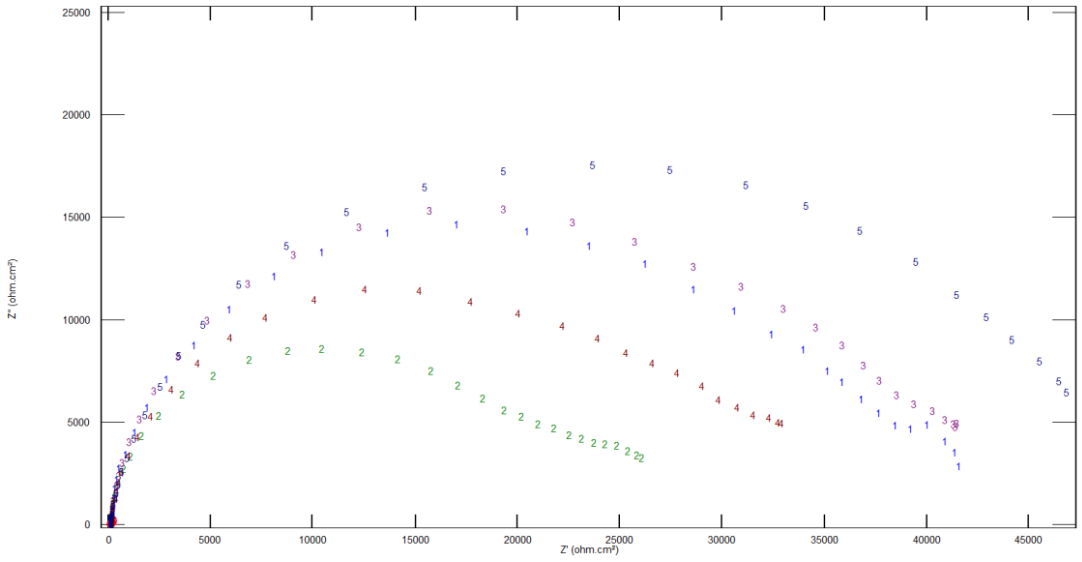

Figure 2.17: The Nyquist plot of impedance of antibody immobilisation by formation of 11-MUA SAM layer. Au (0); Au-MUA (1); Au-MUA-EDC (2); Au-MUA-EDC-Ab (3); Au-MUA-EDC-Ab-Eth (4); Au-MUA-EDC-Ab-Eth-BSA (5).

Comparing the results shows that the resistance of electron transfer enormously increased after incubation of SPEs in 5 mM 11-MUA, from 53.80 Ω to 34260 Ω, which prove the formation of SAM layer. Rajesh et al. (2010) indicated that the increase in R_{et} after formation of SAM layer is due to the negatively charged end of the SAM layer, which repulses the electron and therefore increases the resistance of the electrode surface.

Binding of the EDC/NHS to the SAM layer blocks most of polyanion end group of 11-MUA, which reduced the negatively charged ends of SAM layer, with a resultant reduction of impedance to 18293 Ω. The increase in R_{et} values from 18293Ω to 35550 Ω,

confirmed the attachment of antibodies to SAM layer through EDC/NHS. As Table 2.3 shows the R_{et} value decreased to 23129 Ω after blockage of repulsive activated SAM layer terminals by ethanolamine. The impedance signal increased again after blocking the SPE surface with 1% BSA. The BSA molecules cover the empty spaces of electrode and therefore reduced the amount of electron transfer from the redox solution to the WE surface.

Table 2.3: Calculated R_{et} value for each step of 11-MUA immobilisation process.

Electrode	R_{et} (Ω)
Au	53.80
Au – 11-MUA	34260
Au – 11-MUA – EDC/NHS	18293
Au – 11-MUA – EDC/NHS – Ab	35550
Au – 11-MUA – EDC/NHS – Ab – Eth	23129
Au – 11-MUA – EDC/NHS – Ab – Eth – BSA	45734

The obtained impedance signals during the 11-MUA immobilisation process are not semi-circular (Figure 2.17). These impedance signals are probably the result of SPE damage by ethanol. The SPEs becoming very fragile after dipping them in ethanol. During the immobilisation process the SPEs were damaged either during the washing steps or drying them with nitrogen gas. As Figure 2.18 shows, the CE, RE, and the insulating part of DRP-220BT SPE and the insulating part of DRP-250AT SPE were destroyed during or after the antibody immobilisation process. Therefore, immobilisation of antibody through formation of cysteamine based SAM layer was chosen.

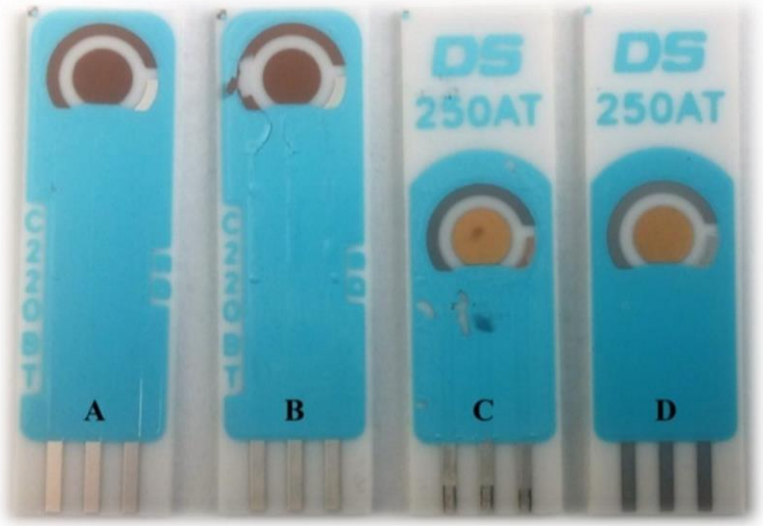

Figure 2.18: Effect of ethanol on SPEs. DRP-220BT before (A) and after (B); DRP-250AT before (D) and after (C) 11-MUA antibody immobilisation process.

2.3.5 SPE Selection

The Nyquist plot of impedance signals for CEA samples with 0 and 100 ng/ml measurements with three types of SPEs is shown in Figure 2.19.

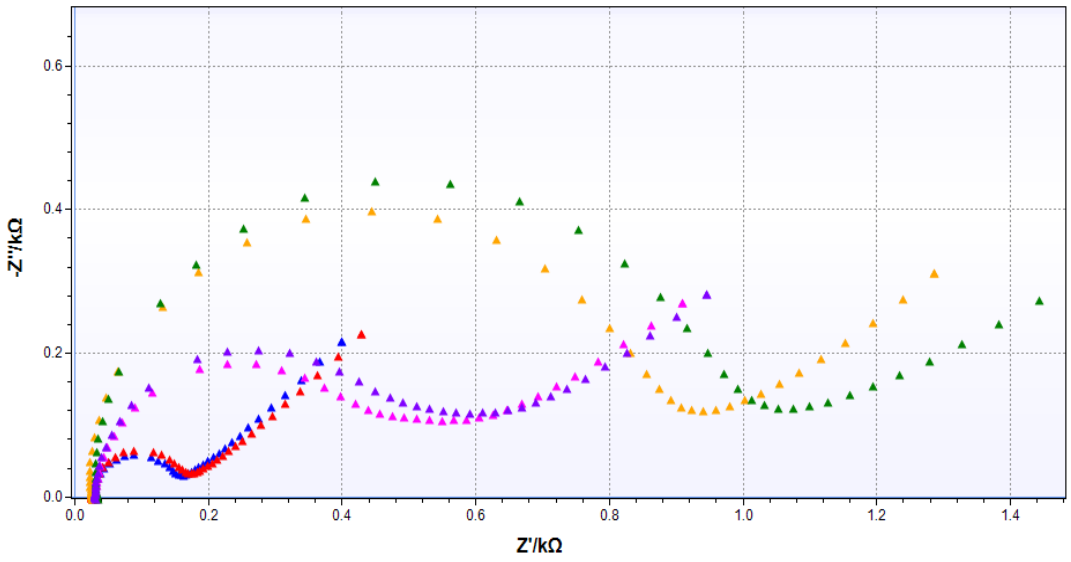

Figure 2.19: The Nyquist plot of CEA sample measurements with different type of SPEs in presence of 10 mM potassium ferri/ ferrocyanide. DRP-220AT 0 ng/ml (Blue), 100 ng/ml (Red); DRP-250AT 0 ng/ml (Pink), 100 ng/ml (Purple); DRP-220BT 0 ng/ml (Yellow), 100 ng/ml (Green).

Figure 2.19 shows an increase in impedance signal of all types of functionalised SPE by increasing the concentration of analyte from 0 ng/ml to 100 ng/ml. Since the impedance signals of the three SPE types for 0 ng/ml concentration of CEA antigen was different, to be able to compare the results the simulation of results was required. The R_{et} and the percentage of signal increase were calculated and are presented in Table 2.4.

As Table 2.4 shows, DRP-220BT has shown to have the largest signal difference, %12.20, for detection of 0 and 100 ng/ml of CEA; while the DRP-250AT had the lowest percentage of change in CEA detection signal. Therefore, DRP-220BT were selected as the best type of electrodes to develop the immunosensors.

Table 2.4: Calculated percentage of signal increase by increasing the concentration of analyte for each type of SPEs.

	R_{et} (Ω) of 0 ng/ml	R_{et} (Ω) 100 ng/ml	ΔR_{et} (Ω)	$\%\Delta R_{et}$
DRP-220AT	120.87	133.51	12.64	10.46
DRP-220BT	833.29	934.93	101.64	12.20
DRP-250AT	418.56	459.39	40.83	9.75

2.3.6 Use of One SPE for Each Concentration *Vs.* One SPE for All Concentrations

The generated data from simulation of impedance measurements in EIS spectrum analyser based on the Randles equivalent circuit were used to calculate percentage of changes in R_{et}. The calculated data are detailed in Table 2.5 and 2.6.

Table 2.5: Calculated $\%\Delta R_{et}$ One SPE was used for each set of samples.

Conc. (ng/ml)	$\%\Delta R_{et}$ Set 1	$\%\Delta R_{et}$ Set 2	$\%\Delta R_{et}$ Set 3	Mean	Mean - Mean (0)	SD	% CV
0	42.82	31.65	84.43	52.97	0.00	27.81	52.51
1	156.62	70.42	100.49	109.18	56.21	43.75	40.07
10	173.97	98.82	201.57	158.12	105.15	53.18	33.63
100	182.20	96.27	298.53	192.33	139.36	101.51	52.78

Table 2.6: One SPE was used for each analyte concentration measurement.

Conc. (ng/ml)	$\%\Delta R_{et}$ Set 1	$\%\Delta R_{et}$ Set 2	$\%\Delta R_{et}$ Set 3	Mean	Mean - Mean (0)	SD	% CV
0	29.84	31.94	42.02	34.60	0.00	6.51	18.82
1	38.44	68.18	114.39	63.67	29.07	43.93	68.99
10	65.69	19.01	71.24	51.98	17.38	28.69	55.19
100	131.45	35.82	97.51	88.26	53.66	48.48	54.93

Figures 2.20 and 2.21 show the $\%\Delta R_{et}$ value increased by increasing the analyte concentration in the first part of experiment, while an increase in $\%\Delta R_{et}$ value did not occur in the second part of experiment. Although the impedance signal of first part of the experiment increased more in comparison with the second part, $\%\Delta R_{et}$ values in the first part of experiment are actually $\%\Delta R_{et}$ values of that concentration plus its previous concentration(s). As an example, $\%\Delta R_{et}$ value of 100 ng/ml is the $\%\Delta R_{et}$ value of 0, 1, 10, and 100 ng/ml.

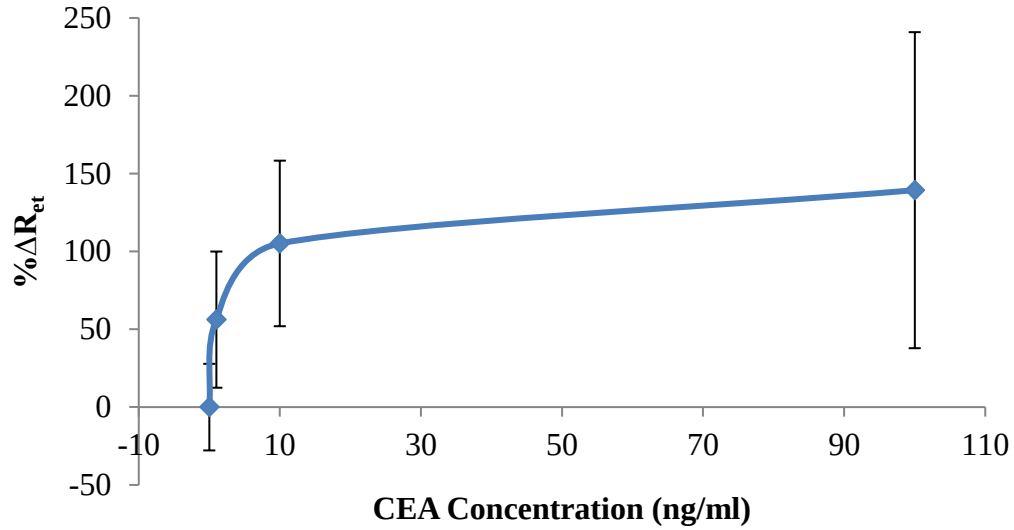

Figure 2.20: $\%\Delta R_{et}$ value Vs. CEA concentration for one SPE per set of concentration. The bars represent the average ± standard deviation of triplicates.

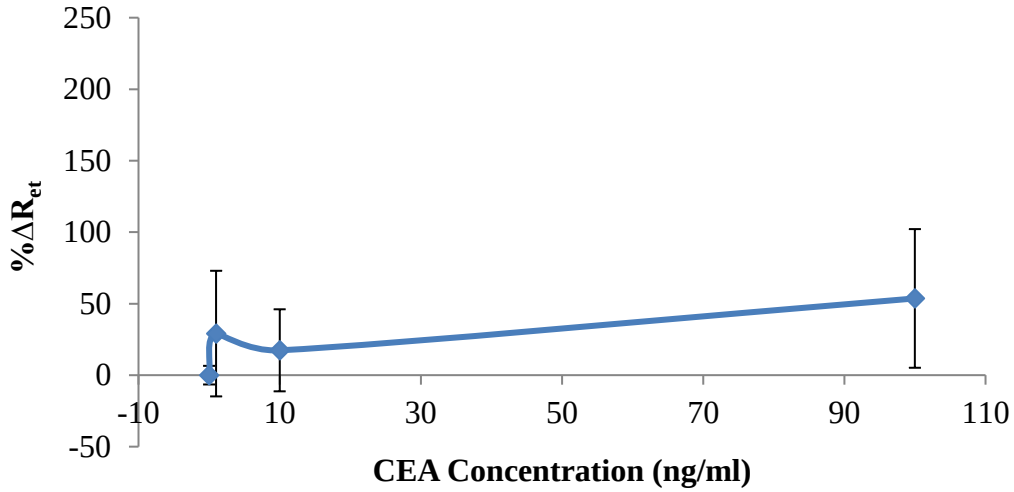

Figure 2.21: $\%\Delta R_{et}$ value Vs. CEA concentration for one SPE per analyte concentration Measurement. The bars represent the average ± standard deviation of triplicates.

Although the standard deviation (SD) of both graphs are quite high the first part of experiment had a lower coefficient of variation (%CV) in comparison with the second part of the experiment except for the 0 ng/ml measurement (Table 2.5 and Table 2.6). Thus, it seems that using the same electrode for a cumulative assay is better than using a

different electrode for each analyte concentration. This result can be explained by the intrinsic variability among SPEs, even when these are from the same batch.

2.3.7 Electrode Cleaning

The SPEs may contain a variety of unwanted materials, *e.g.* lipids, on their surface which will cause obtaining high and unstable impedance signal. Figure 2.22 shows the impedance measurements of single SPE, each measurement was recorded in every 1:30 minute. The impedance signal decreased by repeating the measurement. It is assumed that the signal reduction is caused by impedance measurements, due to use of frequency in this technique, which lead in having cleaner electrodes with less electron transfer resistance.

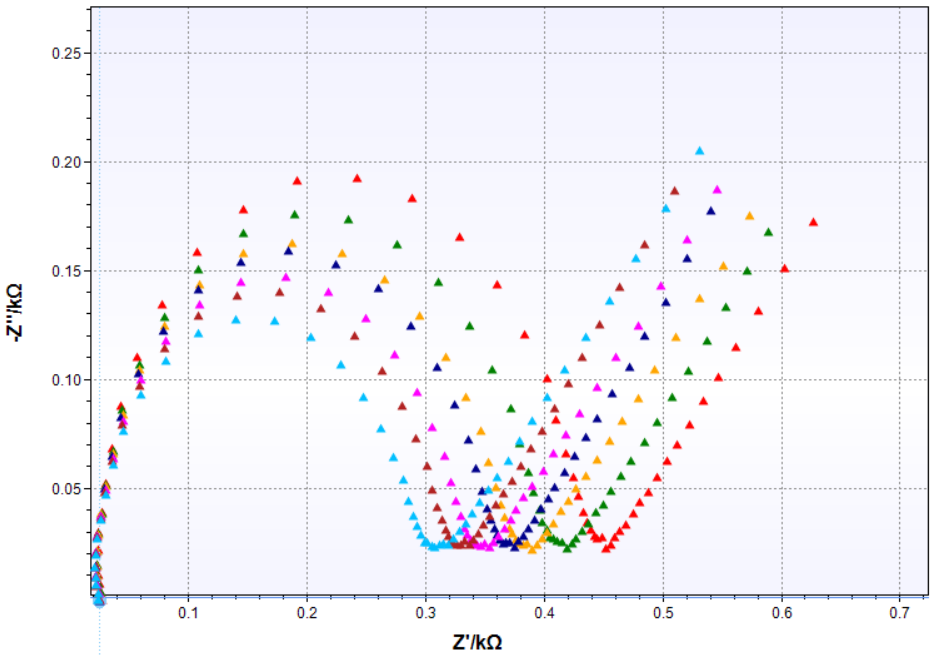

Figure 2.22: The Nyquist plot of impedance measurements of single bare electrode. The first measurement is red and the last one is light blue.

Thereby, different cleaning methods were applied, and the impedance measurements were recorded for all electrodes before and after applying the cleaning methods, and the impedance measurements are presented as Nyquist plots in Figure 2.23.

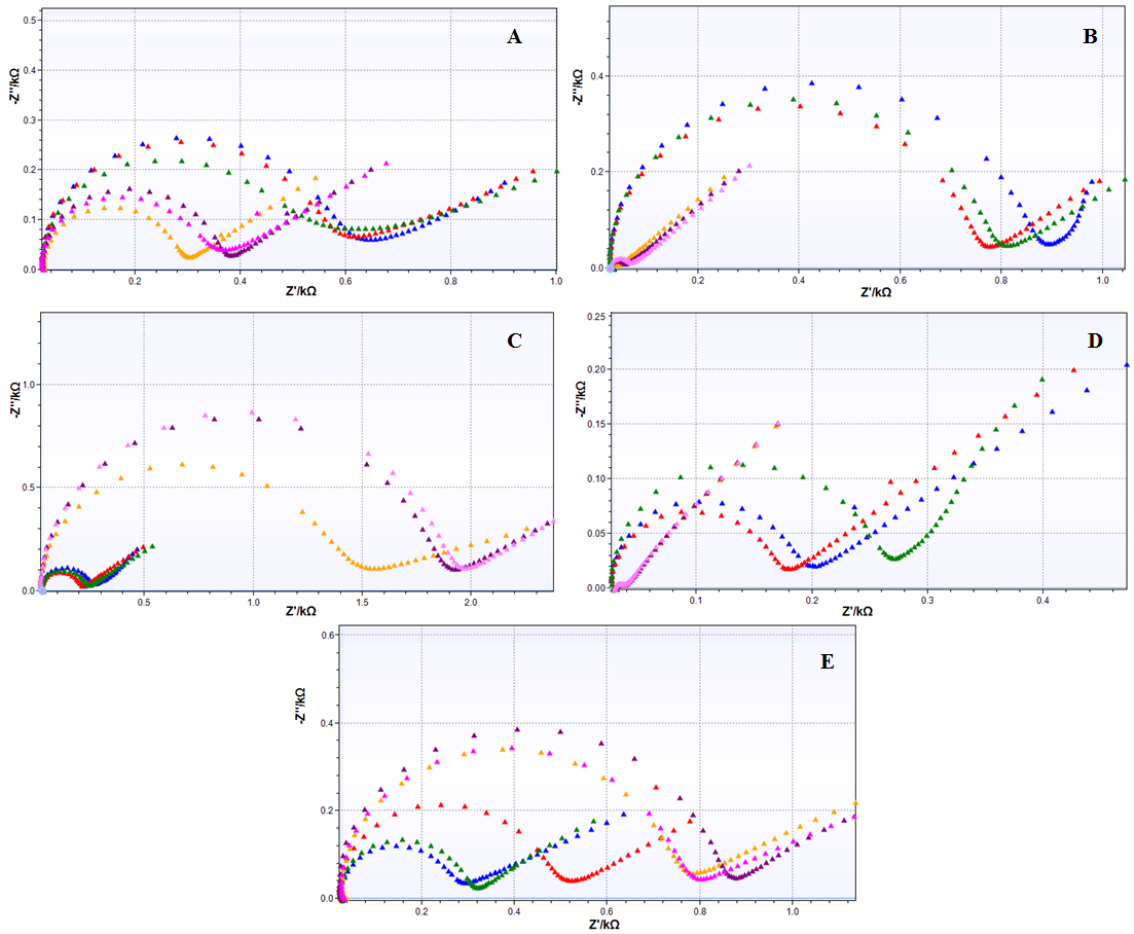

Figure 2.23: The Nyquist plot of impedance measurements of cleaning methods; (A) HCl, (B) KOH+H_2O_2, (C) Oven, (D) Piranha, (E) Ultrasonic Bath; Blue, Red, and Green graphs are recorded impedance signals before applying cleaning methods, while Yellow, Pink and Purple graphs are recorded impedance after applying cleaning methods. All the measurements were done by 10 mM ferri/ferrocyanide in 10 mM PBS.

The decrease in impedance signal after applying HCl, KOH+H_2O_2, and piranha solution cleaning methods (Figure 2.23) shows the success of the electrode cleaning process, since the working electrode is made of gold and gold resistance is low. The impedance signals before cleaning varies from one SPE to another which proves the difference in electrochemical properties of the electrode surface. Table 2.7 shown the calculated R_{et} values for all impedance measurements of both before and after applying cleaning methods. The average of R_{et} values were used to plot a comparison a graph, Figure 2.24.

Table 2.7: The R_{et} calculation of three SPEs before and after applying cleaning methods followed by calculation of % of R_{et} reduction.

	Methods	**HCl**	**KOH+ H_2O_2**	**Oven**	**Piranha Solution**	**Ultrasonic Bath**
R_{et} (Ω) before cleaning	SPE1	587.12	819.75	235.33	229.50	266.14
	SPE2	568.29	716.54	183.50	147.82	469.13
	SPE3	528.63	749.87	208.52	168.60	283.97
	Mean1	**561.35**	**762.05**	**209.14**	**181.99**	**339.75**
R_{et} (Ω) after cleaning	SPE1	264.55	15.89	1405.90	4.40	727.46
	SPE2	344.07	28.90	1802.50	3.64	817.55
	SPE3	322.91	38.84	1849.10	3.49	738.56
	Mean2	**310.51**	**27.88**	**1685.83**	**3.84**	**761.19**
	M1 –M2	**250.84**	**734.18**	**-1476.69**	**178.15**	**-421.44**
	% of R_{et} Reduction	**44.68**	**96.34**	**-706.07**	**97.89**	**-124.05**

Although the impedance signal decreased after performing HCl, KOH+H_2O_2, and piranha solution cleaning methods, it is not possible to choose the best cleaning procedure by looking at the amount of R_{et} reduction because their mean R_{et} values are not the same. Thus, the percentage of reduction in R_{et} values were calculated by subtracting the mean R_{et} value of after cleaning from the mean R_{et} value of before cleaning, dividing by the mean R_{et} value of before cleaning, and finally times by hundred. Table 2.7 indicates that the use of KOH+H_2O_2 and piranha solution as cleaning methods resulted in highest signal reduction with percentage reduction of 96.34 and 97.89 respectively.

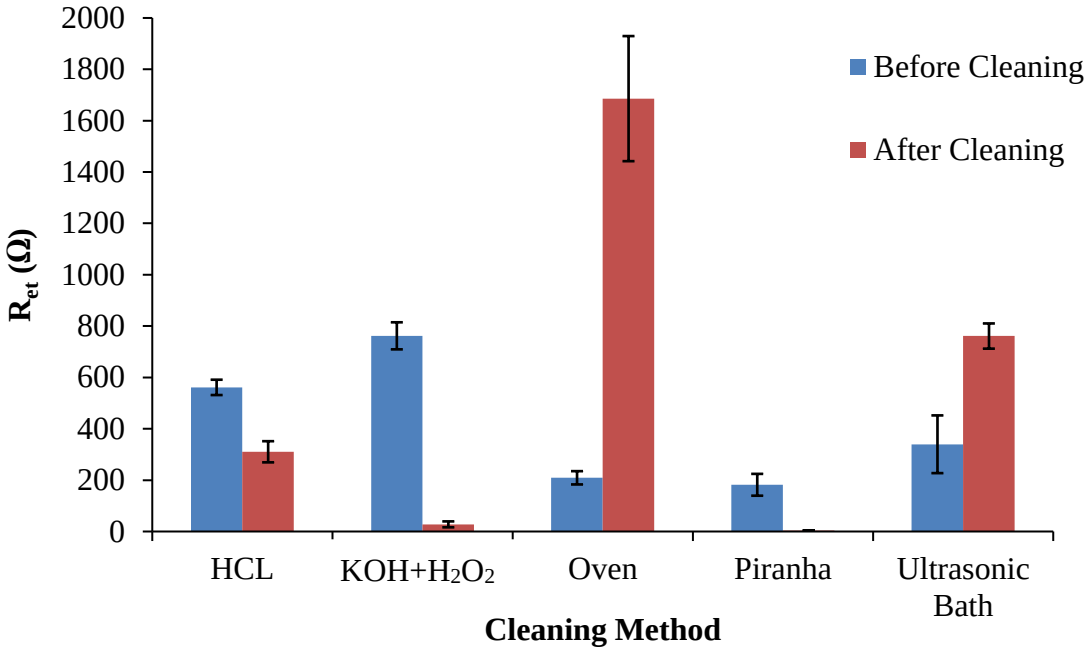

Figure 2.24: The comparison of ΔMean R_{et} values before and after applying the cleaning methods. The bars represent the average ± standard deviation of triplicates.

The cleaner the gold electrode is the quicker the charge transfer will take place. The impedance signal increased after use of oven and ultrasonic bath cleaning methods indicating an increase in resistance of electron transfer (Liu et al., 2015). These results might be obtained due to electrode damage.

2.3.8 Proposed Platform

After functionalising the SPEs with primary anti-NSE monoclonal antibody, the immunosensors were used to detect and measure the concentration of NSE and CEA protein samples in two experiments. The first experiment was designed to check the effects of MBs and the proposed platform on specific analyte detection, and the second experiment was designed to check the effect of MBs and the proposed platform on non-specific detection of analyte. Each part of both experiments was done by use of 3 functionalised SPEs and 5 impedance measurements were taken per SPE such as baseline, 0, 1, 10, and 100 ng/ml of antigen.

2.3.8.1 Specific Analyte Detection

The first part of this experiment is called “NSE” experiment. The impedance measurements of “NSE” part of experiment is presented in Nyquist plot as Figure 2.25.

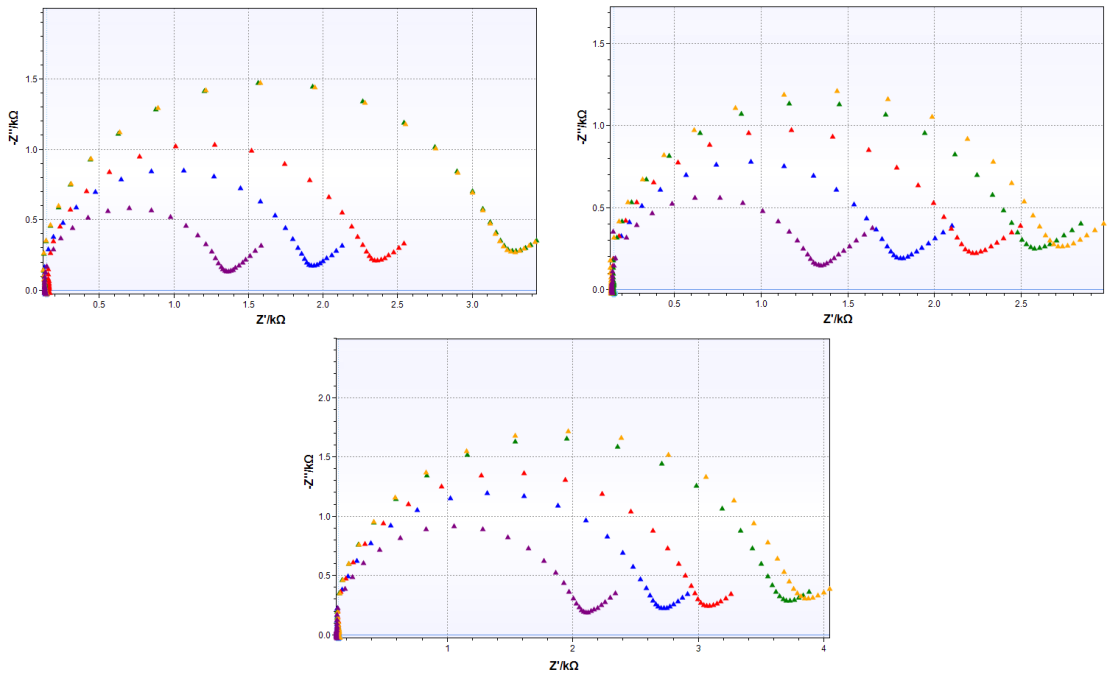

Figure 2.25: The Nyquist plots for impedance of “NSE” part of specific analyte experiment. Each plot represents the impedance of single functionalised SPE. Functionalised SPE (Purple), 0 ng/ml NSE (Blue), 1 ng/ml NSE (Red), 10 ng/ml NSE (Green), 100 ng/ml NSE (Yellow).

The impedance signal of the electrodes increased by increasing the analyte concentration except the impedance measurements of 10 ng/ml and 100 ng/ml of the first SPE (Figure 2.25). Table 2.8 presents the R_{et}, ΔR_{et}, and ΔR_{et} values of the “NSE” part of the experiment which were calculated via fitting the obtained impedance data in EIS spectrum analyser.

Table 2.8: Calculated R_{et}, ΔR_{et}, $\%\Delta R_{et}$ and values for impedance measurements of "NSE" part of specific analyte experiment.

		Baseline	0 ng/ml	1 ng/ml	10 ng/ml	100 ng/ml
R_{et} (Ω)	SPE1	1147.0	1701.0	2089.2	2996.0	2995.6
	SPE2	1120.1	1559.4	1959.9	2298.6	2448.0
	SPE3	1868.9	2447.5	2790.6	3405.8	3535.4
ΔR_{et} (Ω)	SPE1	N/A	554.0	942.2	1849.0	1848.6
	SPE2	N/A	439.3	839.8	1178.5	1327.9
	SPE3	N/A	578.6	921.7	1536.9	1666.5

Conc. (ng/ml)	$\%\Delta R_{et}$ SPE1	$\%\Delta R_{et}$ SPE2	$\%\Delta R_{et}$ SPE3	Mean	Mean – Mean (0)	SD	%CV
0	32.57	39.22	30.96	34.25	0.00	4.38	12.79
1	45.10	74.98	49.32	56.46	22.21	16.17	28.64
10	61.72	105.21	82.24	83.05	48.80	21.76	26.20
100	61.71	118.55	89.17	89.81	55.56	28.43	31.65

As the NSE concentration increased, the Mean values of $\%\Delta R_{et}$ also increased which is probably due to the binding of NSE protein to anti-NSE antibodies of the sensor surface.

The next step of the experiment was to check whether use of MBs can improve the impedance signals. This part of the experiment is called "NSE+MB" which consists of mixing the protein sample with functionalised MBs prior of adding the analyte samples to the sensing area. The impedance results are presented as Figure 2.26. Since the MBs and SPEs were functionalised with two different anti-NSE antibodies, sandwich assay should have formed on the WE surface. Hence, higher resistance of electron transfer was expected.

The same as the previous part of experiment, the impedance signals increased by increasing the concentration of analyte. The obtained data were used to calculate ΔR_{et} and $\%\Delta R_{et}$ to compare with other part of experiment. The calculated data are presented as Table 2.9.

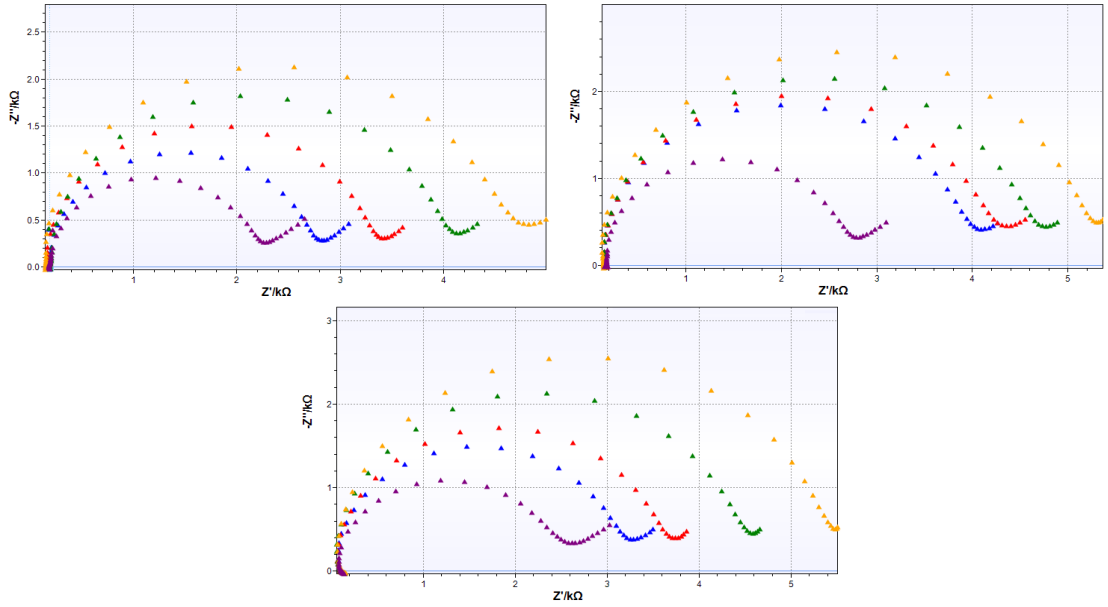

Figure 2.26: The Nyquist plots for impedance of "NSE+MB" part of specific analyte experiment. Each plot represents the impedance of single functionalised SPE. Functionalised SPE (Purple), 0 ng/ml NSE (Blue), 1 ng/ml NSE (Red), 10 ng/ml NSE (Green), 100 ng/ml NSE (Yellow).

Table 2.9: Calculated R_{et}, ΔR_{et}, and $\%\Delta R_{et}$ values for "NSE+MB" part of specific analyte experiment.

		Baseline	0 ng/ml	1 ng/ml	10 ng/ml	100 ng/ml
R_{et} (Ω)	SPE1	1913.6	2453.6	3183.7	3688.5	4363.6
	SPE2	2455.1	3727.1	3954.9	4318	5425.2
	SPE3	2271.8	2950	3487.7	4361.7	5353.3
ΔR_{et} (Ω)	SPE1	N/A	540	1270.1	1774.9	2450.0
	SPE2	N/A	1272	1499.8	1862.9	2970.1
	SPE3	N/A	678.2	1215.9	2089.9	3081.5

Conc. (ng/ml)	$\%\Delta R_{et}$ SPE1	$\%\Delta R_{et}$ SPE2	$\%\Delta R_{et}$ SPE3	Mean	Mean – Mean (0)	SD	%CV
0	28.22	51.81	29.85	36.63	0.00	13.17	35.97
1	66.37	61.09	53.52	60.33	23.70	6.46	10.71
10	92.75	75.88	91.99	86.87	50.24	9.53	10.97
100	128.03	120.98	135.64	128.22	91.59	7.33	5.72

The third part of experiment is called “NSE+MB+Platform”. Functionalised MBs were mixed with analyte samples prior of adding to the Functionalised SPEs apart from the sensing area. The proposed platform was used to move the MBs to the WEs and to pull away the unbounded MBs from the WEs.

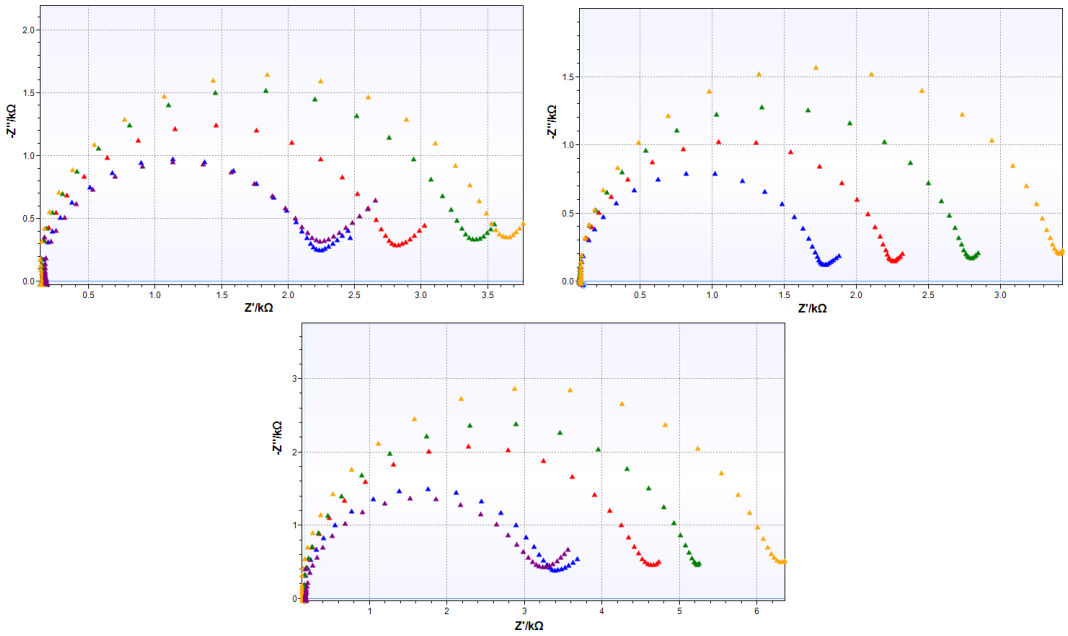

Figure 2.27: The Nyquist plots for impedance of “NSE+MB+Platform” part of specific analyte experiment. Each plot represents the impedance of single functionalised SPE. Functionalised SPE (Purple), 0 ng/ml NSE (Blue), 1 ng/ml NSE (Red), 10 ng/ml NSE (Green), 100 ng/ml NSE (Yellow).

Figure 2.27 shows the increase in impedance signal the same as previous parts of this experiment. The R_{et}, ΔR_{et}, and $\%\Delta R_{et}$ values are shown in Table 2.10. According to Table 2.10, the mean values of $\%\Delta R_{et}$ increased by increasing the NSE concentration from 0 ng/ml, 28.91, to 100 ng/ml, 126.42. The calculated $\%\Delta R_{et}$ values of all three parts of this experiment were used to plot a graph against the concentrations of NSE (ng/ml), which is presented in Figure 2.28.

Table 2.10: Calculated R_{et}, ΔR_{et} and $\%\Delta R_{et}$ values for "NSE+MB+Platform" part of specific analyte experiment.

		Baseline	0 ng/ml	1 ng/ml	10 ng/ml	100 ng/ml
R_{et} (Ω)	SPE1	1784.3	2028.3	2669.2	3217.2	3538.3
	SPE2	1188.6	1599.2	2073.2	2586.6	3171.6
	SPE3	2751.2	3810.7	4498.8	4870.4	5890.9
ΔR_{et} (Ω)	SPE1	N/A	244	884.9	1432.9	1754
	SPE2	N/A	410.6	884.6	1398	1983
	SPE3	N/A	1059.5	1747.6	2119.2	3139.7

Conc. (ng/ml)	$\%\Delta R_{et}$ SPE1	$\%\Delta R_{et}$ SPE2	$\%\Delta R_{et}$ SPE3	Mean	Mean – Mean (0)	SD	%CV
0	13.67	34.54	38.51	28.91	0.00	13.34	46.15
1	49.59	74.42	63.52	62.51	33.60	12.45	19.91
10	80.31	117.62	77.03	91.65	62.74	22.55	24.60
100	98.30	166.83	114.12	126.42	97.51	35.88	28.38

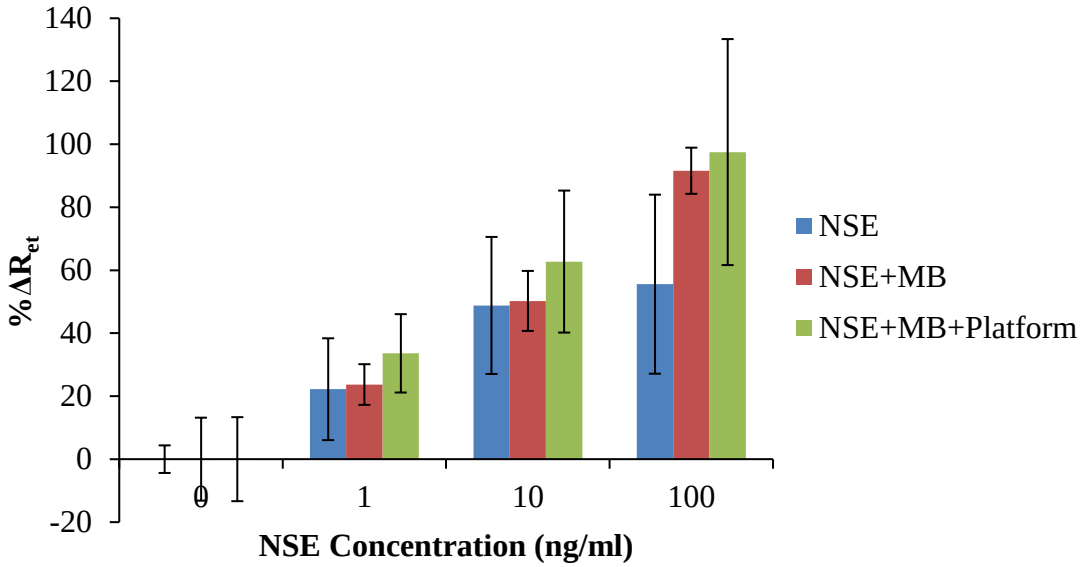

Figure 2.28: The $\%\Delta R_{et}$ of NSE immunosensors against the concentration of NSE protein for specific analyte experiment. The bars represent the average ± standard deviation of triplicates.

As Figure 2.28 shows, the NSE immunosensors could detect the NSE protein and the signal increases by increasing the concentration of the analyte. The second part of experiment, "NSE+MB", showed that there was a higher signal in comparison with the first part of experiment, which is probably due to the formation of sandwich assay on WEs. The highest percentage of change in R_{et} values are obtained in the third part of experiment, "NSE+MB+Platform", which might be the result of using the sensing platform. As the sensing platform pull the functionalised magnetic beads close to the surface. Since some of the magnetic beads were attached to the NSE proteins, pulling the MBs down to the sensing area surface which increased the chance of analyte to be captured by the anti-NSE antibodies of the SPEs. Nevertheless, the standard deviations in the graphs are generally very high, which indicates that the assays need further optimisations to achieve the optimal results.

2.3.8.2 Non-Specific Analyte Detection

The second experiment was to check the non-specificity and whether using non-specific analyte to the sensor will cause the same sensor response in the presence of MBs and the proposed platform. The functionalised MBs and SPEs with anti-NSE antibodies were used to detect the CEA protein with various concentrations in the same three step procedure as NSE protein detection. The impedance measurements of the first part of non-specific experiment which is called "CEA" are presented as Figure 2.29.

Figure 2.29 shows, the impedance signal increased when the analyte concentration was increased. However, the signal did not increase much by increasing the CEA concentration from 10 ng/ml to 100 ng/ml in SPE2 and SPE3. Table 2.11 shows the calculated R_{et}, ΔR_{et}, and $\%\Delta R_{et}$ values of the "CEA" part of non-specific experiment.

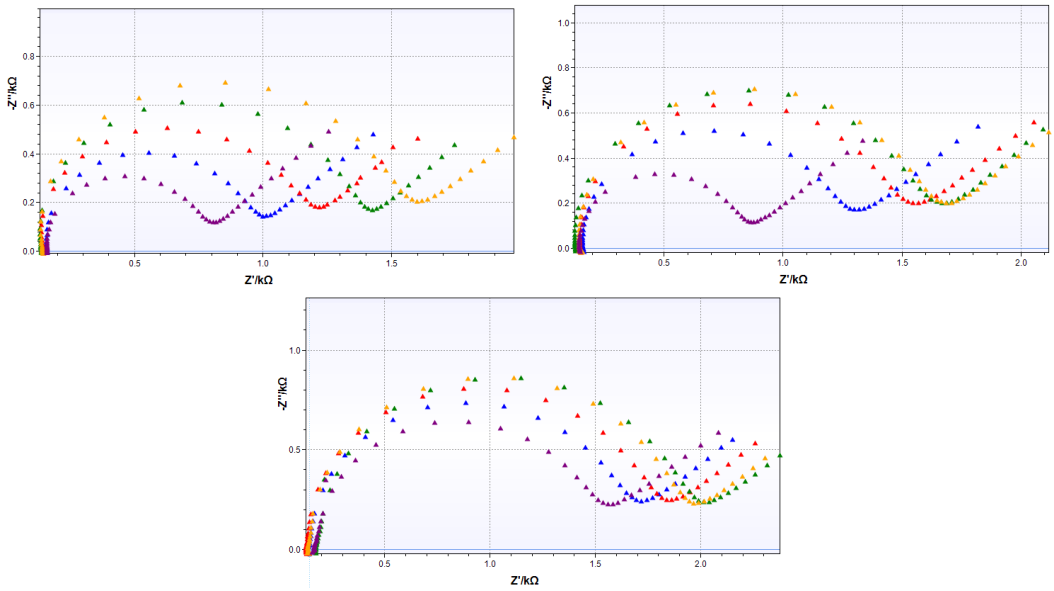

Figure 2.29: The Nyquist plots for impedance of "CEA" part of non-specific analyte experiment. Each plot represents the impedance of single functionalised SPE. Functionalised SPE (Purple), 0 ng/ml CEA (Blue), 1 ng/ml CEA (Red), 10 ng/ml CEA (Green), 100 ng/ml CEA (Yellow).

Table 2.11: Calculated R_{et}, ΔR_{et} and $\%\Delta R_{et}$ values for "CEA" part of non-specific analyte experiment.

		Baseline	0 ng/ml	1 ng/ml	10 ng/ml	100 ng/ml
R_{et} (Ω)	SPE1	506.30	780.65	988.87	1202.4	1714.7
	SPE2	582.13	985.19	1290.8	1417.3	1423.6
	SPE3	613.98	939.39	1000.3	1099.3	1153.1
ΔR_{et} (Ω)	SPE1	N/A	325.41	482.57	696.1	857.9
	SPE2	N/A	403.06	708.67	835.17	841.47
	SPE3	N/A	534.71	678.61	788.81	796.11

Conc. (ng/ml)	$\%\Delta R_{et}$ SPE1	$\%\Delta R_{et}$ SPE2	$\%\Delta R_{et}$ SPE3	Mean	Mean – Mean (0)	SD	%CV
0	54.19	69.24	58.21	60.55	0.00	7.79	12.87
1	95.31	121.74	73.88	96.98	36.43	23.97	24.72
10	137.49	143.47	85.87	122.28	61.73	31.67	25.90
100	169.44	144.55	86.67	133.55	73.00	42.79	31.80

The $\%\Delta R_{et}$ increased from 60.55 to 133.55 by increasing the CEA concentration from 0 ng/ml to 100 ng/ml although the anti-NSE monoclonal antibodies were used to prepare the NSE immunosensor. The obtained data might be the result of unsuccessful functionalisation of whole WEs surface area; or unsuccessful blocking SAM layer end group or surface area by ethanolamine or BSA.

MBs were mixed with various concentration of CEA protein in the second part of experiment before adding the sample to the sensing are of NSE immunosensor. This part of non-specific experiment is called "CEA+MB". The impedance results are presented in Nyquist plot as Figure 2.30. Since the MBs and SPEs were functionalised with two different anti-NSE antibodies which are not specific to CEA protein, higher resistance of electron transfer was not expected. The obtained impedance measurements were used to calculate R_{et}, ΔR_{et}, and $\%\Delta R_{et}$ (Table 2.12).

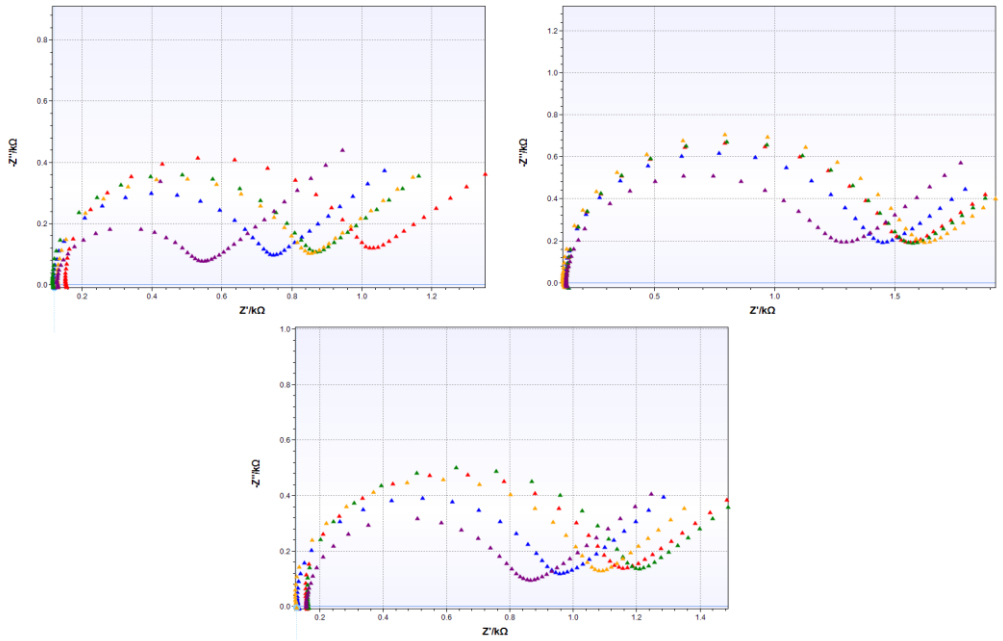

Figure 2.30: The Nyquist plots for impedance of "CEA+MB" part of non-specific analyte experiment. Each plot represents the impedance of single functionalised SPE. Functionalised SPE (Purple), 0 ng/ml CEA (Blue), 1 ng/ml CEA (Red), 10 ng/ml CEA (Green), 100 ng/ml CEA (Yellow).

Table 2.12: Calculated R_{et}, ΔR_{et} and $\%\Delta R_{et}$ values for "CEA+MB" part of non-specific analyte experiment.

		Baseline	0 ng/ml	1 ng/ml	10 ng/ml	100 ng/ml
R_{et} (Ω)	SPE1	923.34	951.23	999.12	932.55	992.47
	SPE2	1043.3	1221.7	1320.7	1335.1	1402.5
	SPE3	633.93	769.01	934.99	977.48	895.85
ΔR_{et} (Ω)	SPE1	N/A	185.53	422.78	307.44	280.05
	SPE2	N/A	178.4	277.4	291.8	359.2
	SPE3	N/A	135.08	301.06	343.55	261.92

Conc. (ng/ml)	$\%\Delta R_{et}$ SPE1	$\%\Delta R_{et}$ SPE2	$\%\Delta R_{et}$ SPE3	Mean	Mean – Mean (0)	SD	%CV
0	47.43*	17.10	21.31	19.20	0.00	2.98	15.50
1	108.09*	26.59	47.49	37.04	17.84	14.78	39.90
10	78.60	27.97	54.19	53.59	34.39	25.32	47.25
100	71.60	34.43	41.32	49.12	39.92	19.77	40.26

*Excluded data from analysis

Although the non-specificity test of NSE immunosensor with use of MBs also resulted in increasing $\%\Delta R_{et}$ after adding CEA antigen (Table 2.12), the percentage of change in resistance of electron is not as large as in the first part of experiment.

The last part of non-specific analyte experiment was "CEA+MB+Platform". The impedance measurement results are presented in Nyquist plot (Figure 2.31). Although Figure 2.31 indicates increase in impedance signal by increasing the concentration of CEA antigen for SPE2, the detection signal did not always increase for SPE1 and SPE3 as the analyte concentration increased such as the impedance signal of 100 ng/ml in SPE1 which is lower than the impedance signal of 10 ng/ml. The calculated R_{et}, ΔR_{et}, and $\%\Delta R_{et}$ values are presented in Table 2.13.

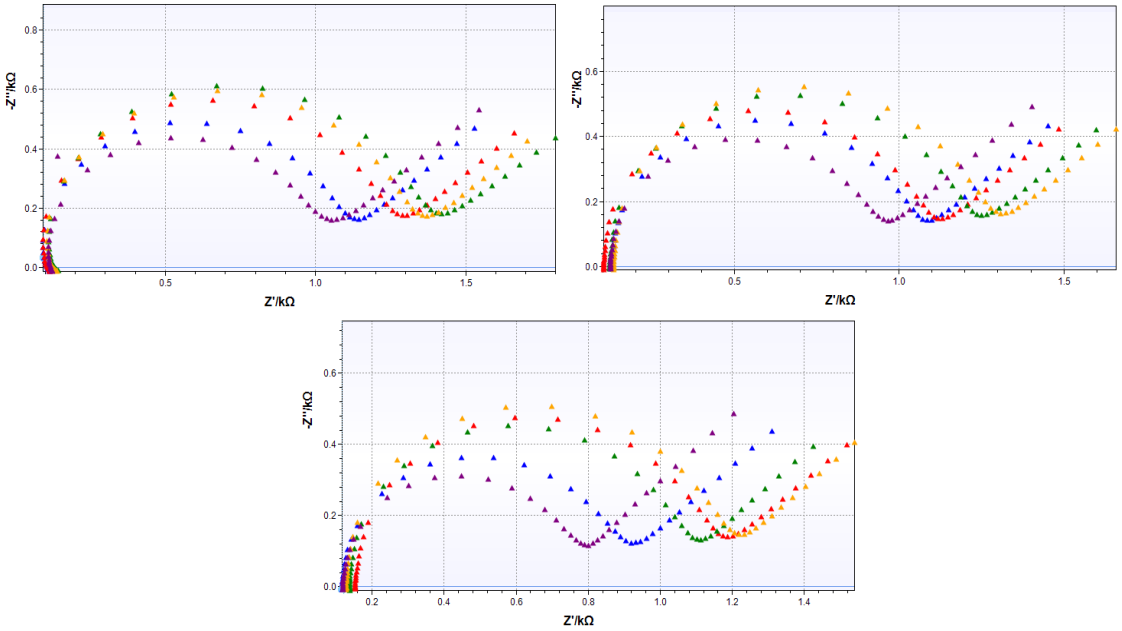

Figure 2.31: The Nyquist plots for impedance of "CEA+MB+Platform" part of non-specific analyte experiment. Each plot represents the impedance of single SPE. Functionalised SPE (Purple), 0 ng/ml CEA (Blue), 1 ng/ml CEA (Red), 10 ng/ml CEA (Green), 100 ng/ml CEA (Yellow).

Table 2.13: Calculated R_{et}, ΔR_{et} and $\%\Delta R_{et}$ values for "CEA+MB+Platform" part of non-specific analyte experiment.

		Baseline	0 ng/ml	1 ng/ml	10 ng/ml	100 ng/ml
R_{et} (Ω)	SPE1	863.06	960.77	1109.7	1210.7	1169.4
	SPE2	766.26	882.38	944.38	1043.6	1092.3
	SPE3	604.33	762.38	947.37	892.97	1006.7
ΔR_{et} (Ω)	SPE1	N/A	97.71	246.64	347.64	306.34
	SPE2	N/A	116.12	178.12	277.34	326.04
	SPE3	N/A	158.05	343.04	288.64	402.37

Conc. (ng/ml)	$\%\Delta R_{et}$ SPE1	$\%\Delta R_{et}$ SPE2	$\%\Delta R_{et}$ SPE3	Mean	Mean – Mean (0)	SD	%CV
0	11.32	15.15	26.15	17.54	0.00	7.70	43.89
1	28.58	23.25	56.76*	25.91	8.37	3.77	14.55
10	40.28	36.19	47.76	41.41	23.87	5.87	14.17
100	35.49	42.55	66.58	48.21	30.67	16.30	33.81

*Excluded data from analysis

The calculated $\%\Delta R_{et}$ values of all three parts of this experiment were used to plot a comparison graph, after normalising to 0 ng/ml mean $\%\Delta R_{et}$ values, Figure 2.32.

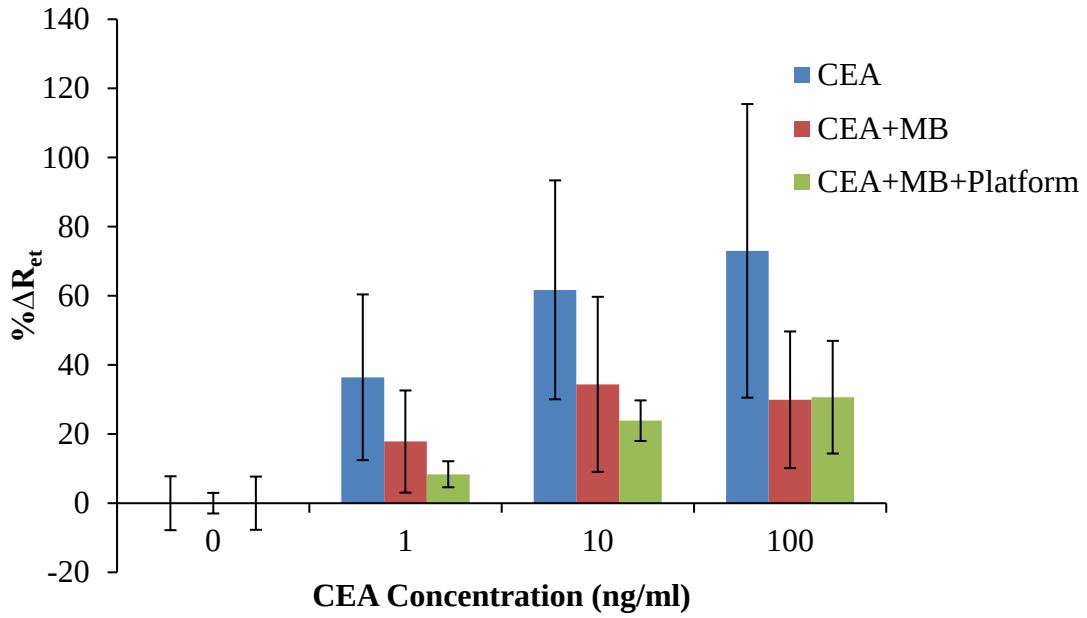

Figure 2.32: The $\%\Delta R_{et}$ of NSE immunosensors against the concentration of CEA protein for non-specific analyte experiment. The bars represent the average ± standard deviation of triplicates.

Figure 2.32 shows the results for each step of the non-specific analyte detection of the NSE immunosensor. The highest signals were obtained by directly adding the CEA sample to the sensing area. Hence these signals might have been obtained because of insufficient blocking of the SAM layer and/or the surface of WEs. The sensor response to various concentrations of CEA decreased by adding functionalised MBs. The lowest impedance responses were obtained after using both MBs and the proposed platform. The low response of the immunosensor to non-specific analytes after applying the platform was probably due to the fact that only MBs were facing the WEs, thus CEA proteins could not attach to the surface of the WEs.

2.3.8.3 Data Comparison

The calculated $\%\Delta R_{et}$ average values of specific binding with use of MBs and proposed platform experiment (Table 2.13) and non-specific binding experiment (Table 2.19) were used to plot a comparison graph, Figure 2.33.

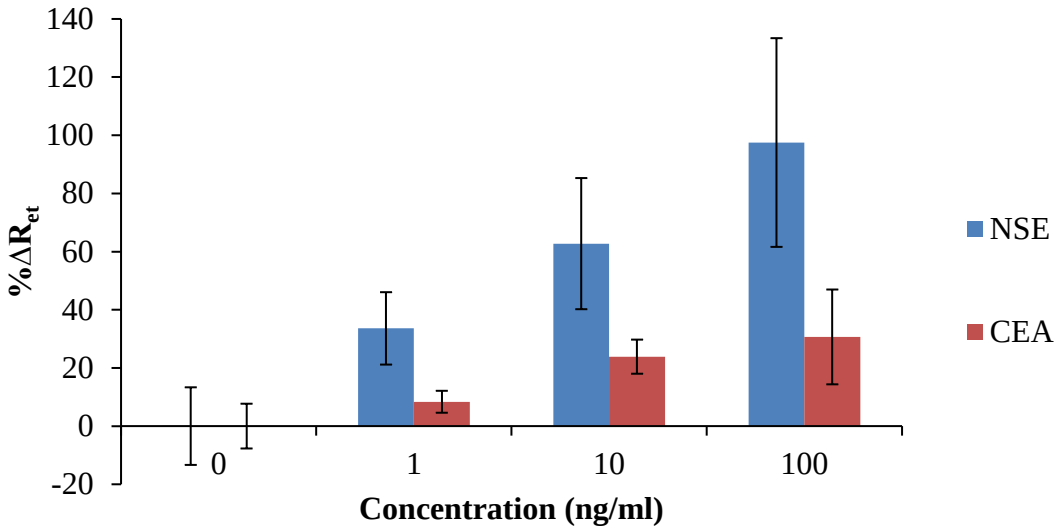

Figure 2.33: Comparison of specificity (Blue) and non-specificity (Red) experiment of NSE immunosensor with use of functionalised magnetic beads and sensing platform. The bars represent the average ± standard deviation of triplicates.

Figure 2.33 clearly shows the increase in immunosensor response by increasing the concentration of both specific and non-specific analytes. However, higher percentage of changes in electron resistance of NSE detection experiment were obtained in compare with the non-specific test with CEA of immunosensor with functionalised MBs and platform. The results can be further improved after performing a fully optimising each step of the immunoassay.

2.4. Conclusions

The work in this chapter was to select the materials, sensors and functionalisation methods to develop the biomarkers biosensors. It was also to confirm the success of the SAM layer formation and the success of the antibody immobilisation process. Two types of antibody immobilisation methods based on formation of SAM layer were tested, cysteamine and 11-MUA. Each step of both antibody immobilisation methods on gold WEs of SPEs were checked by impedance measurements. According to calculated R_{et} values, both methods were successful, though the electrodes become too fragile during the 11-MUA immobilisation method due to the use of ethanol. Therefore, the formation of cysteamine SAM layer method was chosen to be used in this research.

The second part of this chapter reported the experiments performed to choose the best type of SPE. Three types of SPE were tested with gold WE and Ag/ AgCl RE. The functionalised SPEs by monoclonal antibody were tested to detect 0 and 100 ng/ml of analyte. Based on obtained results DRP-220BT shown to have the most increase in signal for 100 ng/ml of analyte in comparison with the other two types of SPEs. Thereby, DRP-220BT was used for the rest of the experiments. However, the experiment was done with single electrode per each type of SPEs.

The third part of the chapter showed that using one functionalised SPE to measure analyte with various concentration not only gives higher response signal but also reduces the amount of error.

Since repeating impedance measurements of a single bare electrode resulted in having reduced R_{et} which indicates cleaning the surface over time, five different methods of electrode cleaning procedure were applied. According to results, cleaning of SPEs with piranha solution and KOH+H_2O_2 are the best two cleaning methods as they reduced the resistance of electron transfer by 97.89% and 96.34%, respectively. As the piranha solution might damage SPEs and there is not much difference in result between these two cleaning methods, placing the SPEs in 50mM KOH in 25% H_2O_2 for 10 minutes followed

by rinsing the SPEs with adequate amount of deionised water and drying by nitrogen gas has been used prior of immobilising antibody on the WEs.

The final and main step of this chapter was to design and test the proposed platform which involves moving the functionalised magnetic nanobeads from the insulating part of SPE to its working electrode. The main purpose of designing the proposed platform was to detect the analyte of interest by using magnetic nanobeads to minimise the washing step and detection time. The platform was tested by both specific and non-specific analyte. The results have shown that using magnetic nanobeads and the proposed platform can result in increasing the detection signal and reducing the experimental error. Nevertheless, the experiments also showed that further optimisation of the immunoassay are required to obtain optimal results and to evidence the real advantages of using the platform.

Chapter 3:

DEVELOPMENT OF NEURON-SPECIFIC ENOLASE (NSE) IMMUNOSENSOR

3.1. Introduction

Lung cancer is the leading cause of cancer incidence and mortality in the world. It can be categorised in two main histological group, small cell lung cancer (SCLC) and non-small cell lung cancer (NSCLC). SCLC is characterised by dissemination at early stage of cancer, and rapid doubling time. Some studies have reported 13% of patient with lung cancer are suffering from SCLC while other studies have reported 10 – 15%, and 15 – 20%. Early diagnosis of SCLC can help in treatment and increasing the survival rate. Blood tumour marker such as neuron-specific enolase (NSE) can be used for early diagnosis and effective treatment of SCLC (Rossi et al., 2013; Xiao et al., 2017; Zhou et al., 2017).

NSE is a type of neuroendocrine enzyme which is known as a potential, specific, sensitive, and reliable blood serum biomarker for early diagnosis of SCLC. Moreover, the concentration of NSE protein in the blood could act as a prognostic factor for cancer therapy. The normal concentration of NSE in blood serum of healthy individual is 5 – 12 ng/ml. SCLC becomes suspicious if the concentration of NSE within the blood serum exceed 24 ng/ml (Yang et al., 2014; Gao et al., 2017; Wei et al., 2017; Zhang et al., 2018).

Electrochemical impedance spectroscopy (EIS) is a sensitive technique which can be used for fast label-free analyte detection with high sensitivity and specificity on the electrode surface. Attachment of analytes to the bio-recognition elements block the electrode surface that results in increasing or decreasing the impedance signal (resistance and/or capacitance) based on the surface charge. The amount of change in impedance signal is proportional to the concentration of target molecule. Immobilisation of bio-recognition to the surface of electrode is a crucial step for successful detection of target analyte. Self-assembled monolayer (SAM) is a low cost, easy, and quick way of immobilising antibody on the surface of electrode which is highly reproduceable and stable (Tang et al., 2007; Shamsipur et al., 2017; Arya et al., 2018).

3.2. Materials and Equipment

All the materials and equipment used in this chapter are listed in Chapter 2, Section 2.1. Additional item that was used here is human blood serum which was purchased from Sigma-Aldrich (Dorset, UK). The PalmSens^3 potentiostat and its corresponded software were used to perform impedance technique to measure the sample concentration with mentioned setting described in Chapter 2, Section 2.2.5, and in the presence of 50 µl of 10 mM $[K_3Fe(CN_6)]/[K_2Fe(CN_6)]$ in 10 mM PBS pH 7.4.

The proposed platform was used in all sample concentration measurements. As explained in Chapter 2, the proposed platform is consisting of 2 magnets which are implanted in two cylinders. The magnetic beads move on the surface of SPEs from non-sensing part to the WE and vice-versa. Figure 3.1 is an illustration of platform principle.

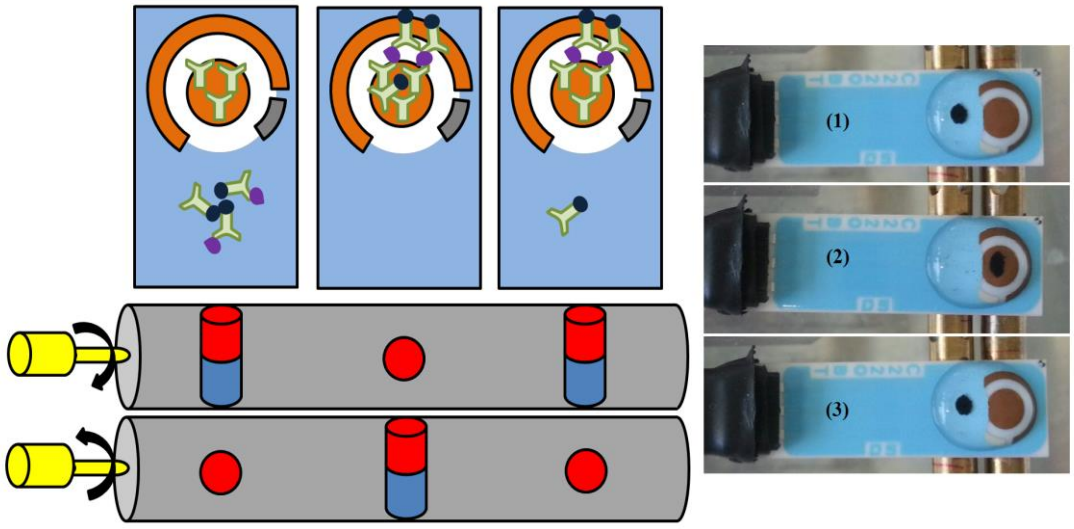

Figure 3.1: The immunosensor platform for lung cancer. After fishing the analyte with functionalised magnetic beads, the magnetic beads were added to non-sensing part of SPE were the platform magnet is perpendicular to SPE (1). The rotation of magnetic cylinders causes movement of magnetic beads to the WE for analyte detection (2) and pull back the unbounded MBs from the WE (3).

3.3. Methods

3.3.1 Functionalisation of Magnetic Beads

The 10-7938 anti-NSE antibody was used to functionalise MBs according to the protocol which is explained in Chapter 2 Section 2.2.2.

3.3.2 Immobilisation of Antibody on the SPEs

Before immobilising the antibodies on the gold WEs, a washing step was applied to all SPEs. The washing step was consisting of dipping SPEs (DRP-220BT) in a solution of 50mM KOH in 25% H_2O_2 for 10 minutes following by rinsing SPEs with dH_2O and the drying with nitrogen gas. NSE immunosensors were prepared with 10-7927 anti-NSE antibody based on the formation of cysteamine SAM layer. The method of immobilisation of antibodies on WEs is described in Chapter 2 Section 2.2.7.1.

3.3.3 Electrochemical Measurements

All EIS measurements were conducted by PalmSens^3 potentiostat with software setting as described in Chapter 2 Section 2.2.4. To compare the EIS results, the R_{et} was calculated for all impedance measurements by the EIS spectrum analyser software.

3.3.4 NSE Assay Development

After preparing different concentration of NSE antigen, 45 µl of each concentration of NSE solutions was mixed with 5 µl of functionalised magnetic beads in a centrifuge tube with vortex and incubated for 20 minutes to allow the formation of MB-Ab-Ag complex. The tube content was washed three times with 50 µl of PBS pH 7.2 using the magnetic rack for beads separation. The whole content of the tube was then transferred to the ceramic part of SPE were the platform magnet pole was faced up. The magnetic beads were pulled to the sensing area (WE) by rotation of magnetic bar, and incubated for 20 minutes. Then, the magnetic bar was rotated again to eliminate the

unbounded MBs from the surface of WE. The SPE was rinsed with PBS (pH 7.4) and dried with nitrogen gas before applying the impedance.

Various concentration of NSE protein sample (0.0 ng/ml to 100 ng/ml) were prepared and measured by NSE immunosensor. The impedance of functionalised SPE was used as a baseline to compare the response signals.

This experiment is different from the "NSE+MB+Platform" experiment, Chapter 2 Section 2.3.7.1 as a washing step was added to wash mixture of MBs with protein sample with use of magnetic rack and PBS buffer prior to adding the sample to the SPEs. This step was added to reduce the error and increase the reproducibility of the sensor platform as it is assumed that the error are the result of binding of undetected antigens by functionalised MBs to the WEs.

3.3.5 Optimisation of Apparatus

As the calculated SD and %CV are high and to achieve better limit of detection, step by step optimisation of the NSE immunoassay was carried out in this chapter.

3.3.5.1 Washing Methods

Applying a washing step to the mixture of MBs and analyte sample shown to reduce the error. Therefore, four methods of washing step were tested to choose the most appropriate method.

After mixing the analyte sample with MBs in a centrifuge tube, a magnet or magnetic rack was used to attract MBs to the wall of the tube and the solution was removed with a pipette. Then 50 µl of PBS pH 7.2 was added and MBs were mixed in the solution by action of vortex. The difference between the tested washing methods was the amount of PBS, the type of magnet, and how many times the washing step was repeated. The methods are as follow:

- Washing the MBs with magnetic rack and 100 µl of PBS for 3 times
- Washing the MBs with magnet and 100 µl of PBS for 3 times
- Washing the MBs with magnetic rack and 50 µl of PBS for 5 times
- Washing the MBs with magnetic rack and 50 µl of PBS for 3 times

All the SPEs were functionalised freshly on the day of experiment and each part of this experiment was repeated three times.

3.3.5.2 SAM Layer Activation

The amino end group of cysteamine SAM layer was activated by adding activation buffer which contained PDITC which is a crosslinking reagent on the WE. In order to get the optimum level of activated SAM layer for attachment of antibodies, the incubation time (30 and 60 minutes) and amount of activation buffer (10 and 20 µl) on the SPE was tested. After confirmation of the success of SPEs functionalisation with anti-NSE antibody, the SPEs were tested to detect and measure various concentration of NSE protein. All the SPEs were functionalised freshly on the day of experiment and each part of this experiment was repeated three times.

3.3.5.3 Blocking of SAM Layer

As previous results Chapter 2 showed that the error of the experiment is high even though it should only recognise specific analyte as monoclonal antibodies were used. These results may be the result of non-specific binding of antigens to the surface of WEs due to an unoptimised blocking of the SAM layer. Hence, testing different reagents to block the thiocyanate end terminals was conducted. 0.1M ethanolamine was prepared in both dH_2O and 10mM PBS, followed by adjusting the pH 7.6 and 8.5. 20 µl of blocking reagents were incubated on WEs for 30 minutes before rinsing the SPEs with 10 mM PBS pH 7.4 and drying them with nitrogen gas. The impedance measurements were applied before and after applying the deactivation of SAM layer step to compare the results and to choose the best blocking solution. All the SPEs were functionalised freshly on the day of experiment and each part of this experiment was repeated three times.

3.3.5.4 Optimisation of the Capture Antibody Concentration

To achieve the optimum concentration of capture antibody on the surface of MBs, three MBs solutions were prepared with 1.2, 2.4, and 3.6 mg/ml concentration of 10-7938 anti-NSE antibody according to the functionalisation of MBs method which is explained in Section 2.2.2.

A 5µl of MBs-Abs were mixed with 45 µl of NSE solutions in a centrifuge tube for 20 minutes to allow formation of MB-Ab-NSE. Then the tube content was washed three times with use of a magnetic rack and 50 µl of PBS buffer, before adding the solution to the immunosensor for analyte detection. The experiment was repeated three times with three freshly made NSE immunosensors each prepared solution of MBs with different concentration of capture antibody on their surface. The impedance technique was applied for NSE detection.

3.3.5.5 Optimisation of the Detection Antibody Concentration

Three different concentration as 5, 10, and 20 µg/ml of detection antibody were immobilised on three different SPEs to find the optimum concentration of antibodies on the surface of WEs. The immobilisation of antibody was done according to the formation of cysteamine SAM layer, CHAPTER 2, Section 2.2.6.1. The experiment was repeated three times with freshly prepared NSE immunosensors. Various concentration of NSE protein as 0, 1, 10, 50 ng/ml were prepared and detected by immunosensor to compare the data and to find the optimum detection antibody concentration.

3.3.6 Standard Plot of the Optimised NSE Immunosensor

After confirmation of anti-NSE antibody immobilisation on the WEs, NSE immunosensors were used to generate the calibration curve of NSE protein detection, and also to check the non-specific binding of analyte. The calibration curve was firstly made by detection of 0, 1, 5, 10, 20, 50, and 100 ng/ml of NSE antigen in PBS buffer, and later by detection of the same NSE sample concentrations in human blood serum.

To check the non-specificity detection of NSE immunosensor, various concentration of CEA protein in human blood serum were prepared and tested as 0, 1, 5, 10, 20, 50, and 100 ng/ml.

In all experiments, functionalised MBs with anti-NSE antibody were used. Both experiments were done with three freshly made NSE immunosensors with optimum concentration of capture and detection antibodies.

3.4. Results

3.4.1 NSE Assay Development

The NSE immunosensors were prepared and tested with various NSE concentrations by formation of sandwich assay on top of WEs surface. The functionalised MBs were mixed and incubated with various concentration of samples for 20 minutes. To reduce the experimental error, the analyte was fished and washed three times with use of magnetic rack and PBS (pH 7.4) before adding MBs to the ceramic part of the SPE. The EIS results obtained from this experiment are presented in Figure 3.2.

The attachment of analytes to the surface of WE reduce the electron transfer from the redox probe to the electrode which results in increasing the impedance. It can be observed from Figure 3.2 that by increasing the concentration of NSE protein higher signals were obtained which is due to the recognition of more NSE molecules by the immunosensor.

The EIS spectrum analyser software was used to calculate R_{et} for all impedance signals, the R_{et} was then used to calculate the $\%\Delta R_{et}$ and further data analysis. The calculation results are summarised in Table 3.1.

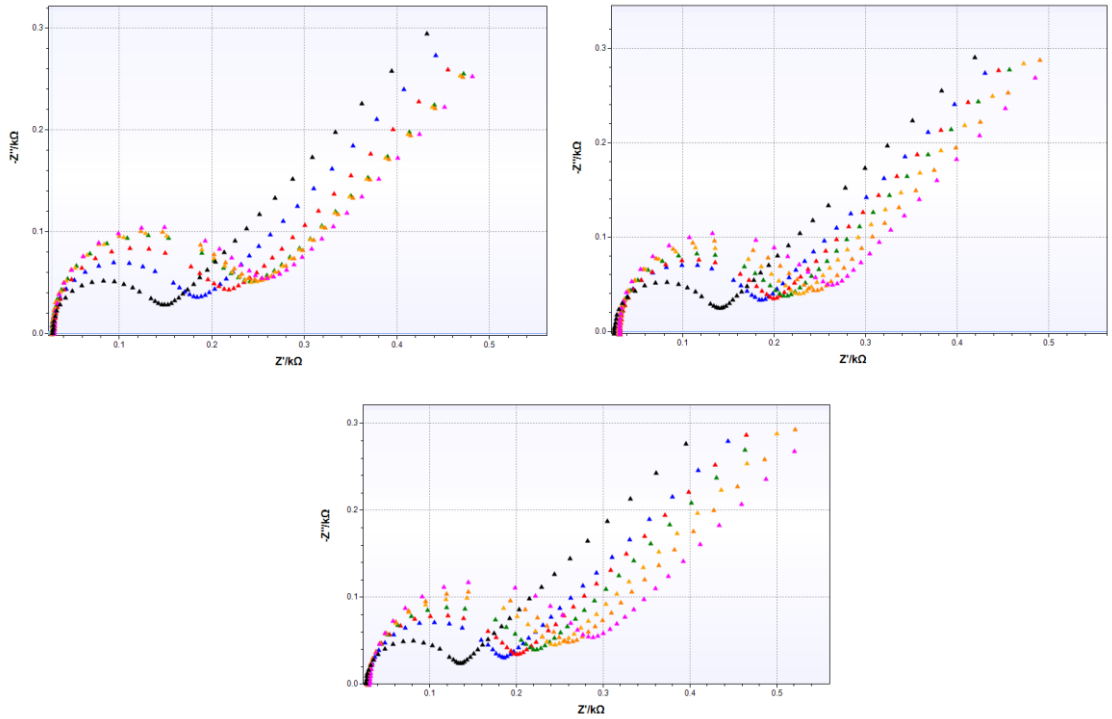

Figure 3.2: The Nyquist plots for impedance of NSE protein detection by NSE immunosensor. Each graph represents the impedance measurements of single NSE immunosensor. Functionalised SPE (Black), 0 ng/ml (Blue), 1 ng/ml (Red), 10 ng/ml (Green), 20 ng/ml (Yellow), 50 ng/ml (Orange), 100 ng/ml (Pink).

It can be seen in Table 3.1 that increasing in concentration of NSE protein resulted in rising the mean values of $\%\Delta R_{et}$. Although lower impedance signals were obtained in this experiment in compare with previous test of immunosensor (Chapter 2 Section 2.3.8.1), both SD and %CV (Table 3.1) were improved in compare with the previous experiment (Table 2.18). For instance, in previous experiment for 100 ng/ml of analyte sample detection the SD and %CV were calculated as 35.88 and 28.38, respectively; which were reduced in this experiment to 19.13 and 17.85. The percentage of changes in ΔR_{et} (Table 3.1 and 2.18) were used to plot a comparison graph against the concentration of NSE (ng/ml) (Figure 3.3) after normalising to zero. The results in Figure 3.3, clearly show the reduction in $\%\Delta R_{et}$ and in error bars, after adding the washing step. Since the only difference between those two experiments is applied washing step to the mixture of MBs and analyte sample before incubating the sample mixture on the immunosensor surface. It is assumed that undetected NSE by functionalised MBs were eliminated from the sample. Hence the obtained results from three NSE immunosensor are in closer range.

Table 3.1: Calculated R_{et}, ΔR_{et}, and $\%\Delta R_{et}$ values of fished NSE protein detection experiment.

		Baseline	0 ng/ml	1 ng/ml	10 ng/ml	20 ng/ml	50 ng/ml	100 ng/ml
R_{et} (Ω)	SPE1	104.06	138.06	159.99	183.95	19.70	196.28	203.28
	SPE2	101.65	130.71	145.39	158.39	171.10	184.64	200.16
	SPE3	94.13	134.34	149.07	162.80	179.97	194.98	215.78
ΔR_{et} (Ω)	SPE1	N/A	34.00	55.93	79.89	86.64	92.22	99.22
	SPE2	N/A	29.06	43.74	56.74	69.45	82.99	98.51
	SPE3	N/A	40.21	54.94	68.67	85.84	100.85	121.65

Conc. (ng/ml)	$\%\Delta R_{et}$ SPE1	$\%\Delta R_{et}$ SPE2	$\%\Delta R_{et}$ SPE3	Mean (Ω)	Mean – Mean (0)	SD	%CV
0	32.67	28.59	42.71	34.66	0.00	7.27	20.97
1	53.75	43.03	58.36	51.71	17.05	7.87	15.21
10	76.77	55.82	72.95	68.51	33.85	11.16	16.29
20	83.26	68.32	91.19	80.92	46.26	11.61	14.35
50	88.62	81.64	107.13	92.46	57.80	13.17	14.25
100	95.35	96.91	129.23	107.16	72.50	19.13	17.85

The experimental data, Table 3.1, was also used to establish the NSE immunosensor linear range response (Figure 3.4). As shown in Figure 3.4, the linear response is plotted by using $\%\Delta R_{et}$ and concentration in logarithmic format, with correlation coefficient of the quantified samples of $R^2 = 0.9512$. The LoD value of 0.81 ng/ml was calculated based on Equation 1; and with use of the slope of calibration curve.

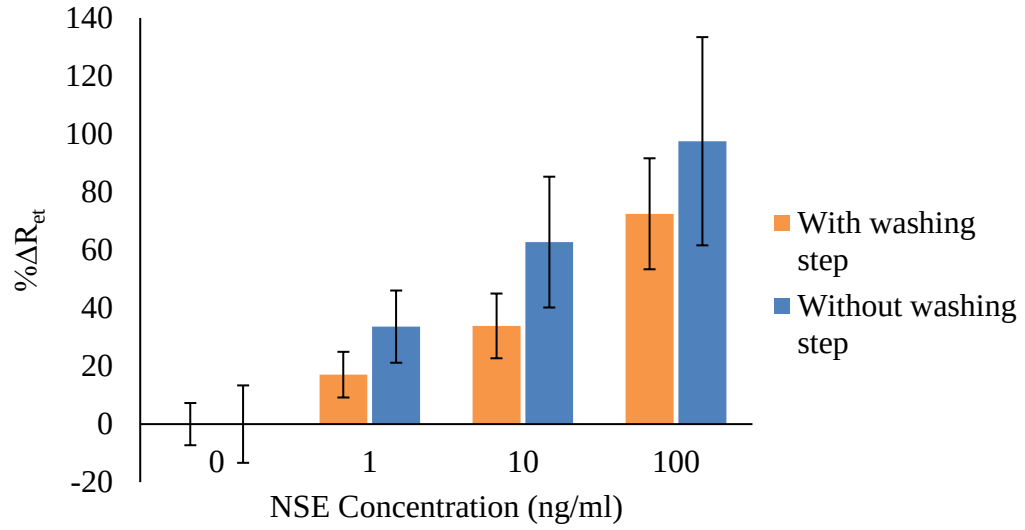

Figure 3.3: The comparison graph of NSE immunosensor results with and without applying a washing step to the mixture of MBs and analyte sample before analyte measurement. The bars represent the average ± standard deviation of triplicates.

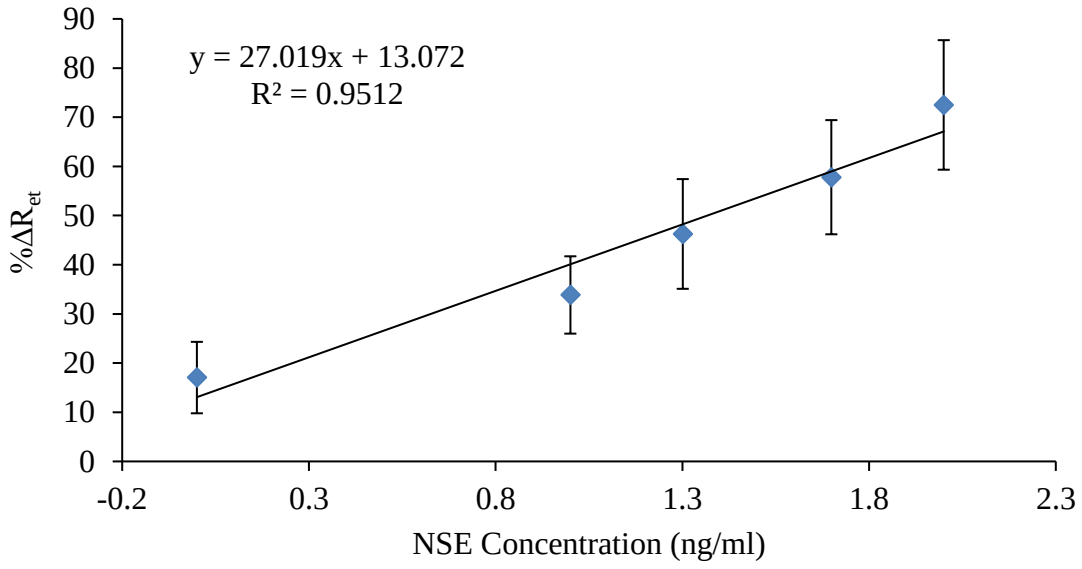

Figure 3.4: The linear range response of NSE immunosensor representing $\%\Delta R_{et}$ versus the $\log_{10}$ of NSE concentrations (1 – 100 ng/ml). The bars represent the average ± standard deviation of triplicates.

3.4.2 Optimisation of Apparatus

The obtained results of testing NSE immunosensors still showed to have large error bars (Figure 3.4). Therefore, further optimisation studies have been conducted to try to reduce the error and increase detection limit.

3.4.2.1 Washing Methods

Applying a washing step to the mixture of MBs-Abs-NSE concentrations prior of adding them to the NSE immunosensor shown to reduce the experimental error. Hence, washing step with different numbers of applying cycles, amount of PBS, and magnets were tested. Various NSE samples with 0, 1, 10, 50 ng/ml concentrations were prepared and measured by NSE immunosensors to compare the effects of washing methods. The impedance results of this experiment are presented in the Nyquist plot format in Figures 3.5 – 3.8. The EIS spectrum analyser software was used to simulate the impedance data and to calculate the R_{et}. The calculated R_{et}, ΔR_{et}, and $\%\Delta R_{et}$ are presented in Table 3.2 – 3.5.

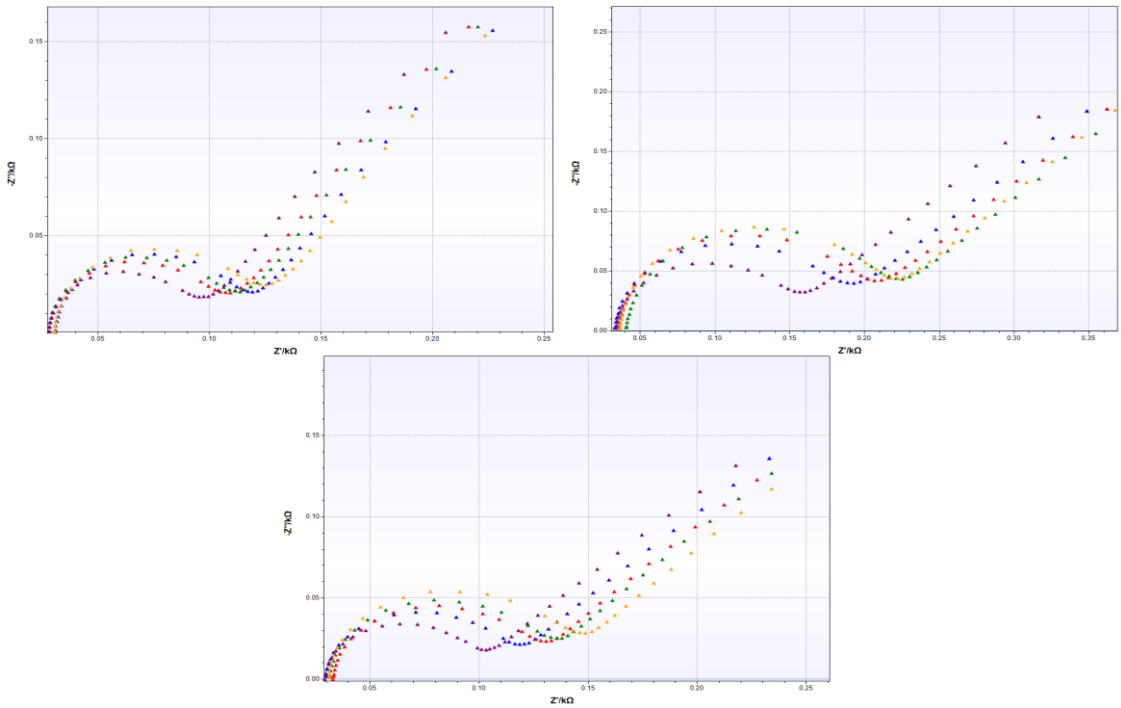

Figure 3.5: The Nyquist plots of NSE immunosensors. The NSE samples were washed 3 times with 100 µl of PBS buffer and use of magnetic rack. Each plot represents the impedance of single immunosensor. Functionalised SPE (Purple), 0 ng/ml NSE (Blue), 1 ng/ml NSE (Red), 10 ng/ml NSE (Green), 50 ng/ml NSE (Yellow).

Table 3.2: Calculated R_{et}, ΔR_{et}, and $\%\Delta R_{et}$ values of washing NSE samples 3 times with 100 µl of PBS buffer and use of magnetic rack.

		Baseline	0 ng/ml	1 ng/ml	10 ng/ml	50 ng/ml
R_{et} (Ω)	SPE1	58.57	69.05	71.65	75.52	91.11
	SPE2	106.17	136.51	148.52	157.60	159.39
	SPE3	61.69	74.85	80.96	87.08	97.39
ΔR_{et} (Ω)	SPE1	N/A	10.48	13.08	16.95	28.93
	SPE2	N/A	30.34	39.89	48.44	50.13
	SPE3	N/A	12.89	19.00	25.12	35.40

Conc. (ng/ml)	$\%\Delta R_{et}$ SPE1	$\%\Delta R_{et}$ SPE2	$\%\Delta R_{et}$ SPE3	Mean	Mean – Mean (0)	SD	%CV
0	17.89	28.58	20.81	22.43	0.00	5.53	24.64
1	22.32	39.89	30.67	30.96	8.53	8.79	28.39
10	28.93	48.44	40.54	39.30	16.87	9.81	24.97
50	55.55	50.13	57.14	54.27	31.84	3.68	6.77

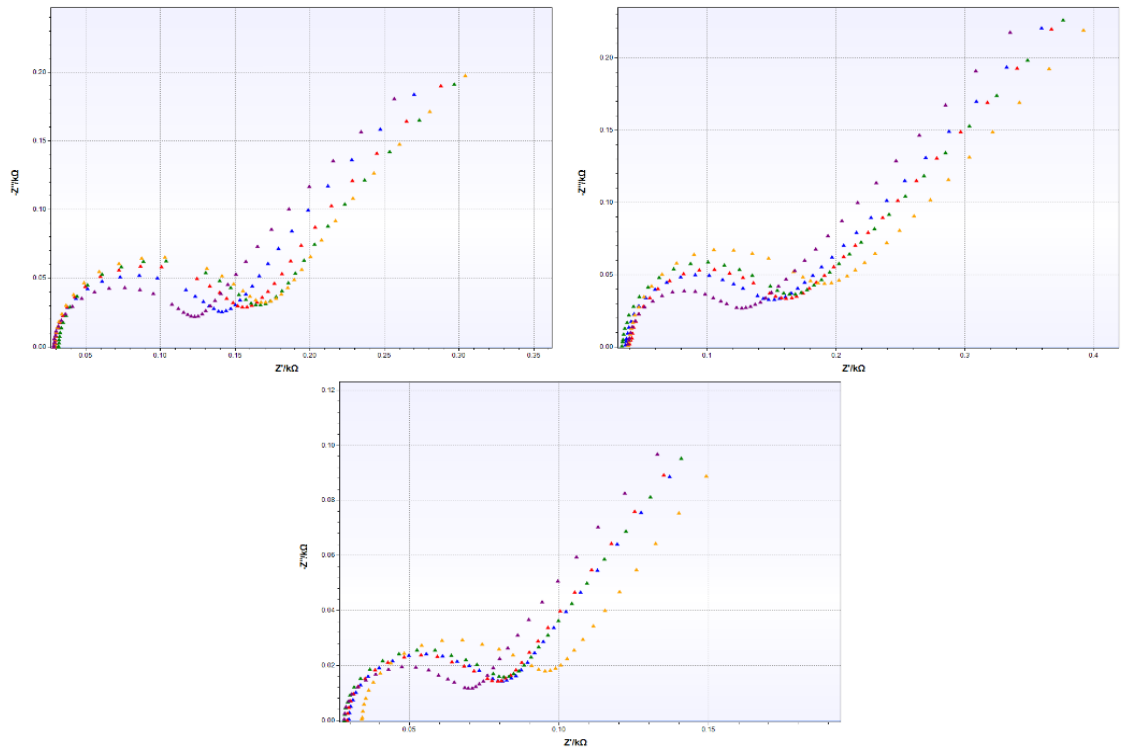

Figure 3.6: The Nyquist plots of NSE immunosensors. The NSE samples were washed 3 times with 100 µl of PBS buffer and use of magnet. Each plot represents the impedance of single immunosensor. Functionalised SPE (Purple), 0 ng/ml NSE (Blue), 1 ng/ml NSE (Red), 10 ng/ml NSE (Green), 50 ng/ml NSE (Yellow).

Table 3.3: Calculated R_{et}, ΔR_{et}, and $\%\Delta R_{et}$ values of washing NSE samples 3 times with 100 µl of PBS buffer and use of magnet.

		Baseline	0 ng/ml	1 ng/ml	10 ng/ml	50 ng/ml
R_{et} (Ω)	SPE1	74.85	90.12	102.49	109.12	114.62
	SPE2	76.42	98.23	104.67	114.07	131.41
	SPE3	29.55	36.15	37.31	38.83	45.07
ΔR_{et} (Ω)	SPE1	N/A	15.27	27.64	34.27	39.77
	SPE2	N/A	21.81	28.25	37.65	54.99
	SPE3	N/A	6.59	7.75	9.27	15.52

Conc. (ng/ml)	$\%\Delta R_{et}$ SPE1	$\%\Delta R_{et}$ SPE2	$\%\Delta R_{et}$ SPE3	Mean	Mean – Mean (0)	SD	%CV
0	20.40	28.54	22.31	23.75	0.00	4.26	17.92
1	36.93	36.96	26.23	33.37	9.62	6.19	18.54
10	45.78	49.27	31.37	42.14	18.39	9.49	22.52
50	53.13	71.96	52.50	59.20	35.45	11.06	18.68

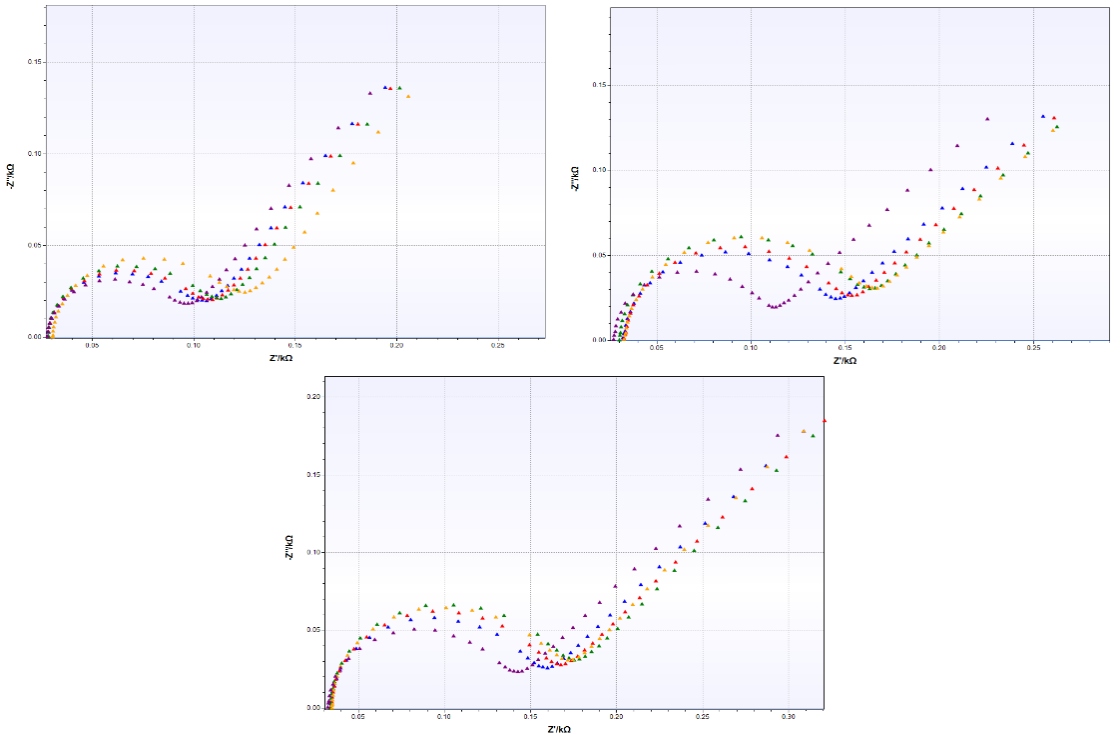

Figure 3.7: The Nyquist plots of NSE immunosensors. The NSE samples were washed 5 times with 50 µl of PBS buffer and use of magnetic rack. Each plot represents the impedance of single immunosensor. Functionalised SPE (Purple), 0 ng/ml NSE (Blue), 1 ng/ml NSE (Red), 10 ng/ml NSE (Green), 50 ng/ml NSE (Yellow).

Table 3.4: Calculated R_{et}, ΔR_{et}, and $\%\Delta R_{et}$ values of washing NSE samples 5 times with 50 µl of PBS buffer and use of magnetic rack.

		Baseline	**0 ng/ml**	**1 ng/ml**	**10 ng/ml**	**50 ng/ml**
R_{et} (Ω)	SPE1	52.58	58.73	61.67	66.10	73.01
	SPE2	84.19	96.68	102.82	112.50	113.78
	SPE3	94.40	107.68	114.65	116.69	116.67
ΔR_{et} (Ω)	SPE1	N/A	6.15	9.09	13.53	20.43
	SPE2	N/A	12.49	18.63	28.31	29.59
	SPE3	N/A	13.28	20.25	22.29	22.27

Conc. (ng/ml)	**$\%\Delta R_{et}$ SPE1**	**$\%\Delta R_{et}$ SPE2**	**$\%\Delta R_{et}$ SPE3**	**Mean**	**Mean – Mean (0)**	**SD**	**%CV**
0	11.70	14.84	14.07	13.54	0.00	1.64	12.09
1	17.29	22.13	21.46	20.29	6.75	2.62	12.92
10	25.73	33.63	23.62	27.66	14.12	5.28	19.08
50	38.86	35.15	23.60	34.24	19.00	7.96	24.46

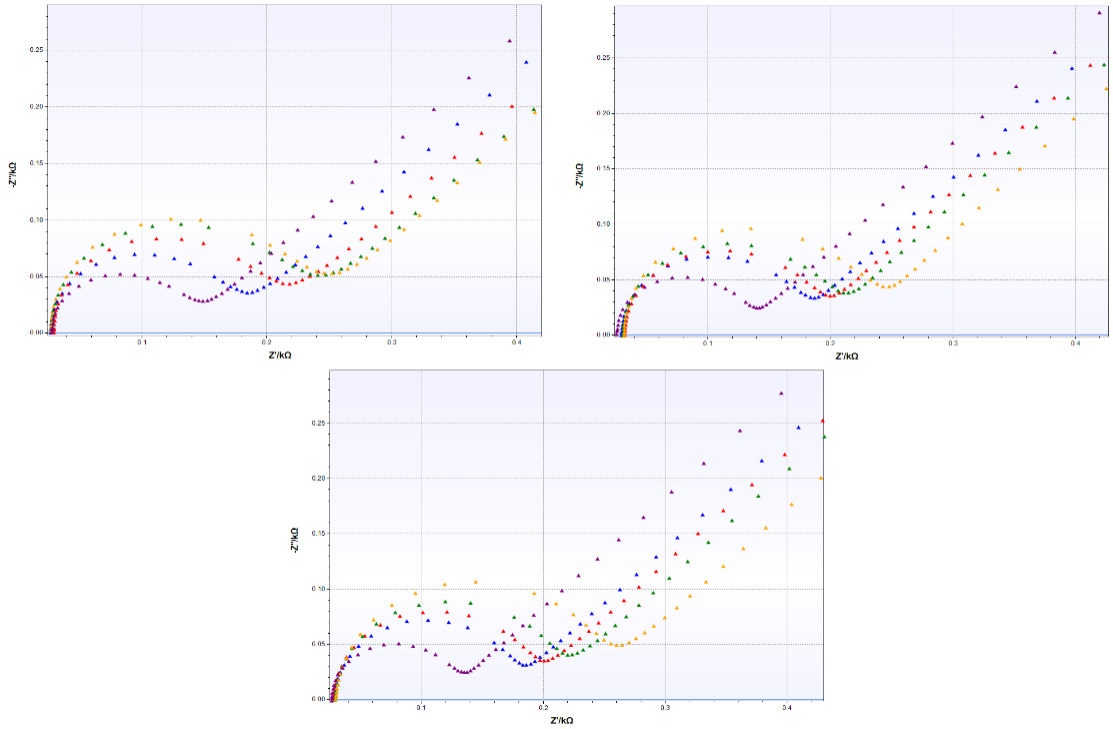

Figure 3.8: The Nyquist plots of NSE immunosensors. The NSE samples were washed 3 times with 50 µl of PBS buffer and use of magnet. Each plot represents the impedance of single immunosensor. Functionalised SPE (Purple), 0 ng/ml NSE (Blue), 1 ng/ml NSE (Red), 10 ng/ml NSE (Green), 50 ng/ml NSE (Yellow).

Table 3.5: Calculated R_{et}, ΔR_{et}, and $\%\Delta R_{et}$ values of washing NSE samples 3 times with 50 µl of PBS buffer and use of magnetic rack.

		Baseline	0 ng/ml	1 ng/ml	10 ng/ml	50 ng/ml
R_{et} (Ω)	SPE1	104.06	138.06	159.99	183.95	196.28
	SPE2	101.65	130.71	145.39	158.39	184.64
	SPE3	94.13	134.34	149.09	162.80	194.98
ΔR_{et} (Ω)	SPE1	N/A	34	55.93	79.89	92.22
	SPE2	N/A	29.06	43.74	56.74	82.99
	SPE3	N/A	40.21	54.94	68.67	100.85

Conc. (ng/ml)	$\%\Delta R_{et}$ SPE1	$\%\Delta R_{et}$ SPE2	$\%\Delta R_{et}$ SPE3	Mean	Mean – Mean (0)	SD	%CV
0	32.67	28.59	42.71	34.66	0.00	7.27	20.97
1	53.75	43.03	58.36	51.71	17.05	7.87	15.21
10	76.77	55.82	72.95	68.51	33.85	11.16	16.29
50	88.62	81.64	107.13	92.46	57.80	13.17	14.25

A comparison graph was prepared (Figure 3.9) based on calculated percentage of change in resistance of electron transfer against the concentration of NSE protein after normalising to zero.

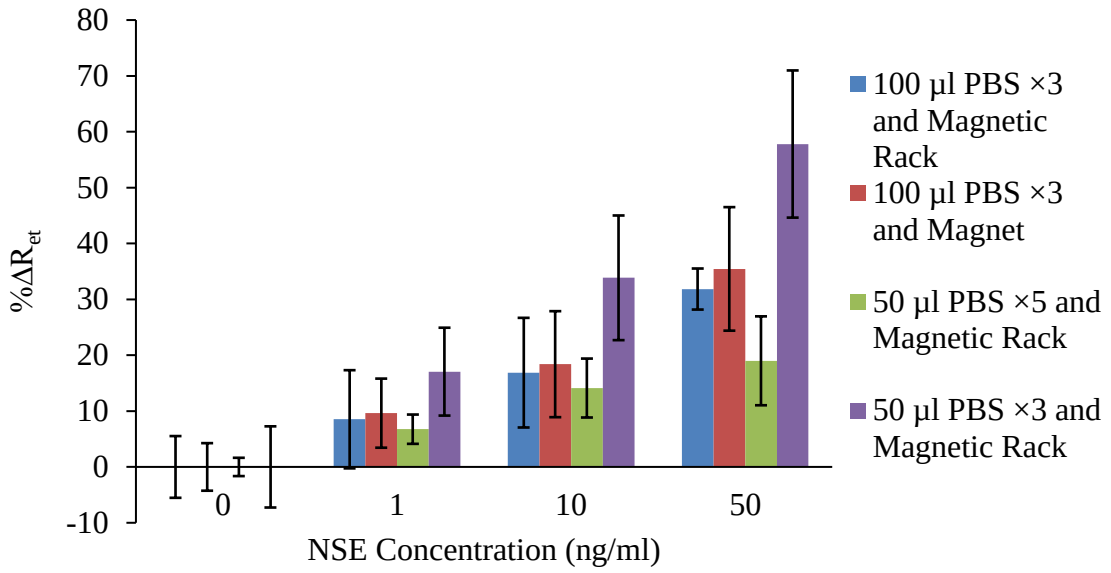

Figure 3.9: The comparison graph of NSE immunosensor response with various washing methods of the MBs and NSE samples mixture in PBS buffer prior of analyte measurement. The bars represent the average ± standard deviation of triplicates.

As Figure 3.9 shows, washing of mixed MBs in NSE samples with 50 µl of PBS for 5 times has resulted in obtaining the lowest detection signals with smaller error bars in comparison with the other types of washing methods. Applying a washing step for 5 times may have eliminated some NSE proteins from the sample. As the highest measurement signals were achieved by washing MBs with the 50 µl of PBS but applying the washing step for 3 times.

Both washing types with 100 µl of PBS have shown to result in lower $\%\Delta R_{et}$ for analyte detection in comparison with 50 µl of PBS repeated tor 3 times. 5 µl of MBs was mixed with 45 µl of NSE concentrations in a centrifuge tube. Since the amount of tube content was more in washing methods with 100 µl of PBS, longer time was required to separate MBs from the sample solution. Hence, some detected NSE proteins by MBs

might have removed from the sample during the washing step. Since all the experiments were done by placing the magnet on the surface of centrifuge tubes for the same period, higher measurement signals have been achieved by washing the MBs 3 times with 50 µl of PBS.

As Figure 3.9 presents, the almost same amount (length) of error bars were obtained for all type of MBs washing except washing of MBs with 50 µl of PBS for 5 times. However, the lowest %CV (Table 3.2 – 3.5) are obtained by washing the MBs with 50 µl of PBS for 3 times. In addition, the highest sensor response was obtained by washing MBs with use of magnetic rack and 50 µl of PBS for 3 times. Therefore, this type of washing was chosen and applied to the mixture of MBs and protein samples before adding MBs to the surface of SPEs.

3.4.2.2 SAM Layer Activation

After formation of SAM layer by incubating 10 mM cysteamine hydrochloride on top of WEs, the activation solution which contained 1,4-phenylene diisothiocyanate (PDITC) was used to activate the amino group of SAM layer. This experiment was designed to achieve the optimum level of activated SAM layer for attachment of antibodies by testing the incubation time (30 and 60 minutes) and the amount of activation buffer (10 and 20 µl).

The prepared NSE immunosensors were used to measure the amount of NSE samples, 0, 1, 10, 50 ng/ml. The impedance results of this experiment are presented in the Nyquist plot format in Figures 3.10 – 3.12. The EIS spectrum analyser software was used to simulate the impedance data and to calculate the R_{et}. The calculated R_{et}, ΔR_{et}, and $\%\Delta R_{et}$ are presented in Table 3.6 – 3.8.

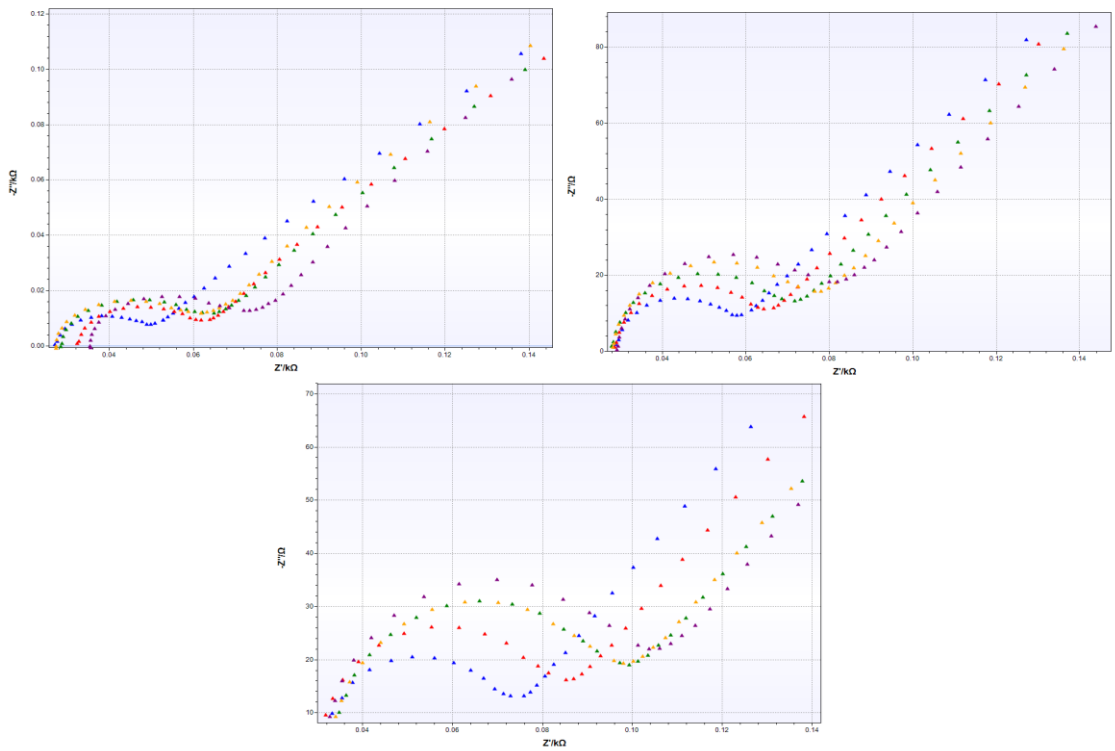

Figure 3.10: The Nyquist plots of NSE immunosensors made by activation of SAM layer by incubation of 10 µl of PDITC for 30 minutes on top of WEs. Each plot represents the impedance of single immunosensor. Functionalised SPE (Blue), 0 ng/ml NSE (Red), 1 ng/ml NSE (Green), 10 ng/ml NSE (Yellow), 50 ng/ml NSE (Purple).

Table 3.6: Calculated R_{et}, ΔR_{et}, and $\%\Delta R_{et}$ values of NSE sample measurement with prepared NSE immunosensor which their SAM layer was activated in 10µl of PDITC for 30 minutes.

		Baseline	0 ng/ml	1 ng/ml	10 ng/ml	50 ng/ml
R_{et} (Ω)	SPE1	16.05	21.25	24.45	25.38	25.68
	SPE2	22.41	28.78	34.36	38.41	39.70
	SPE3	36.53	47.05	54.62	55.64	61.55
ΔR_{et} (Ω)	SPE1	N/A	5.20	8.40	9.33	9.63
	SPE2	N/A	6.37	11.95	16.00	71.41
	SPE3	N/A	10.52	18.09	19.11	25.02

Conc. (ng/ml)	$\%\Delta R_{et}$ SPE1	$\%\Delta R_{et}$ SPE2	$\%\Delta R_{et}$ SPE3	Mean	Mean – Mean (0)	SD	%CV
0	32.42	28.43	28.80	29.88	0.00	2.20	7.38
1	52.34	53.31	49.52	51.72	21.84	1.97	3.81
10	58.13	71.41	52.31	60.62	30.74	9.79	16.15
50	60.00	77.16	68.49	68.55	38.67	8.58	12.52

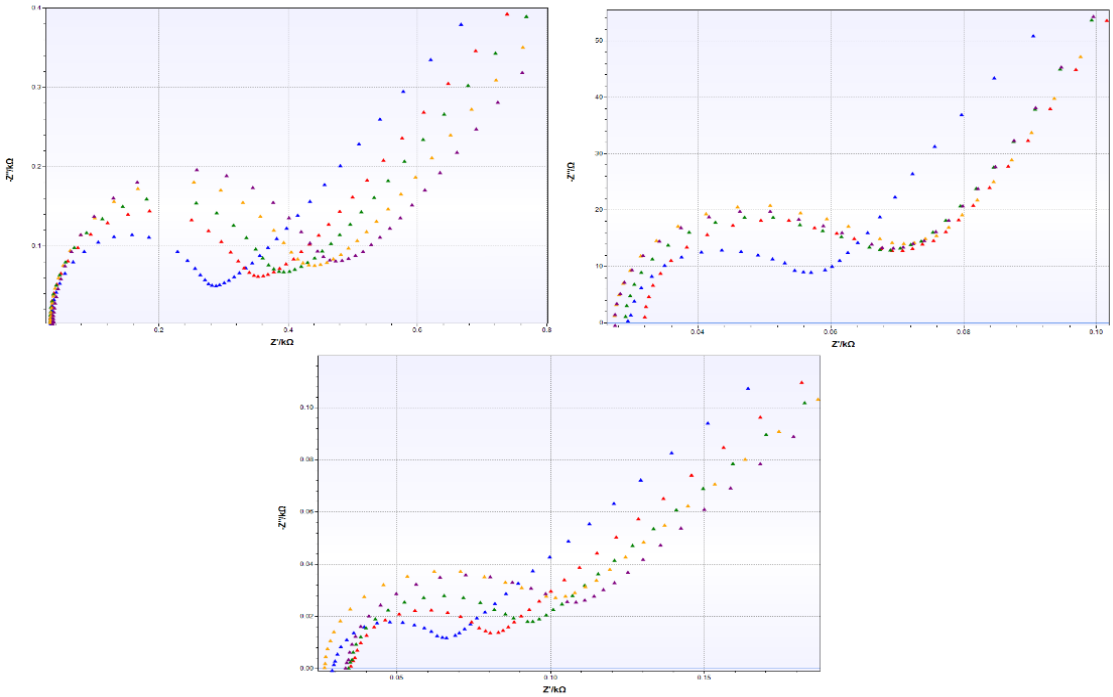

Figure 3.11: The Nyquist plots of NSE immunosensors made by activation of SAM layer by incubation of 20 µl of PDITC for 30 minutes on top of WEs. Each plot represents the impedance of single immunosensor. Functionalised SPE (Blue), 0 ng/ml NSE (Red), 1 ng/ml NSE (Green), 10 ng/ml NSE (Yellow), 50 ng/ml NSE (Purple).

Table 3.7: Calculated R_{et}, ΔR_{et}, and $\%\Delta R_{et}$ values of NSE sample measurement with prepared NSE immunosensor which their SAM layer was activated in 20 µl of PDITC for 30 minutes.

		Baseline	0 ng/ml	1 ng/ml	10 ng/ml	50 ng/ml
R_{et} (Ω)	SPE1	223.99	271.16	296.33	326.95	395.31
	SPE2	19.11	26.49	27.78	31.14	31.21
	SPE3	31.18	39.43	49.59	62.41	65.03
ΔR_{et} (Ω)	SPE1	N/A	47.17	72.34	102.96	171.32
	SPE2	N/A	7.38	8.67	12.03	12.10
	SPE3	N/A	8.25	18.41	31.23	33.85

Conc. (ng/ml)	$\%\Delta R_{et}$ SPE1	$\%\Delta R_{et}$ SPE2	$\%\Delta R_{et}$ SPE3	Mean	Mean – Mean (0)	SD	%CV
0	21.06	38.63	26.47	28.72	0.00	9.00	31.33
1	32.30	45.36	59.03	45.56	16.84	13.37	29.34
10	45.97	62.95	100.16	69.69	40.97	27.72	39.77
50	76.49	63.32	108.56	82.79	54.07	23.27	28.10

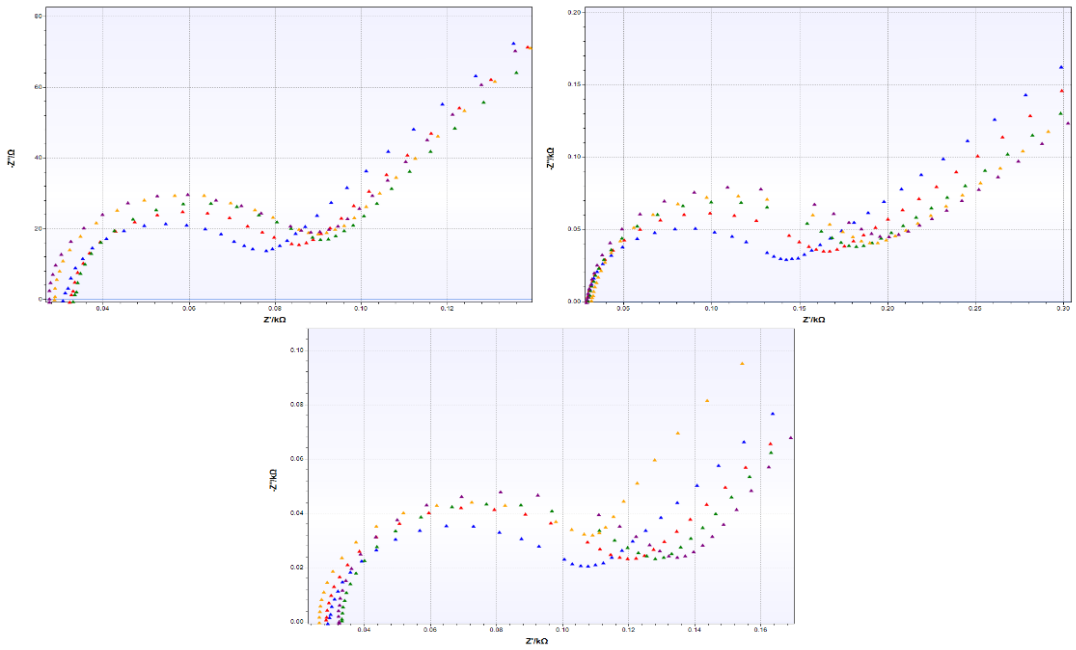

Figure 3.12: The Nyquist plots of NSE immunosensors made by activation of SAM layer by incubation of 10 µl of PDITC for 60 minutes on top of WEs. Each plot represents the impedance of single immunosensor. Functionalised SPE (Blue), 0 ng/ml NSE (Red), 1 ng/ml NSE (Green), 10 ng/ml NSE (Yellow), 50 ng/ml NSE (Purple).

Table 3.8: Calculated R_{et}, ΔR_{et}, and $\%\Delta R_{et}$ values of NSE sample measurement with prepared NSE immunosensor which their SAM layer was activated in 10 µl of PDITC for 60 minutes.

		Baseline	0 ng/ml	1 ng/ml	10 ng/ml	50 ng/ml
R_{et} (Ω)	SPE1	37.44	42.11	45.90	48.85	49.37
	SPE2	100.44	119.72	134.55	140.07	150.39
	SPE3	63.83	74.03	75.09	61.92	80.46
ΔR_{et} (Ω)	SPE1	N/A	4.67	8.46	11.41	11.93
	SPE2	N/A	19.28	34.11	39.63	49.95
	SPE3	N/A	11.20	12.26	-0.91*	17.63

Conc. (ng/ml)	$\%\Delta R_{et}$ SPE1	$\%\Delta R_{et}$ SPE2	$\%\Delta R_{et}$ SPE3	Mean	Mean – Mean (0)	SD	%CV
0	12.46	19.20	17.54	16.40	0.00	3.51	21.41
1	22.60	33.96	19.21	25.26	8.86	7.73	30.59
10	30.48	39.46	-1.42*	34.97	18.57	6.35	18.16
50	31.86	49.73	27.63	36.41	20.01	11.73	32.22

* Excluded data from analysis

A comparison graph was made (Figure 3.13) based on sensor response (%ΔR_{et}) against the concentration of NSE protein after normalising by subtracting %ΔR_{et} of zero from the mean values. The lowest change in impedance measurements were obtained by incubation of SPEs in 10 µl of activation solution for 60 minutes. As the other activation solution with the same volume but shorter incubation time (30 minutes) have resulted in higher impedance change, it is assumed that increasing the time of incubation results surface saturation which results in steric hindrance problem.

Activation of cysteamine SAM layer has shown to reduce the amount of electron transfer (Chapter 2, Section 2.3.4.1). Thus, the amount of activated SAM layer is proportional to the R_{et} value. As Figure 3.13 represents the highest change in electrode impedance were obtained by activating SAM layer with 20 µl of activation solution which is probably related to the amount of available PDITC molecules. Therefore, the SAM layers were activated by 20 µl of activation solution for further experiments.

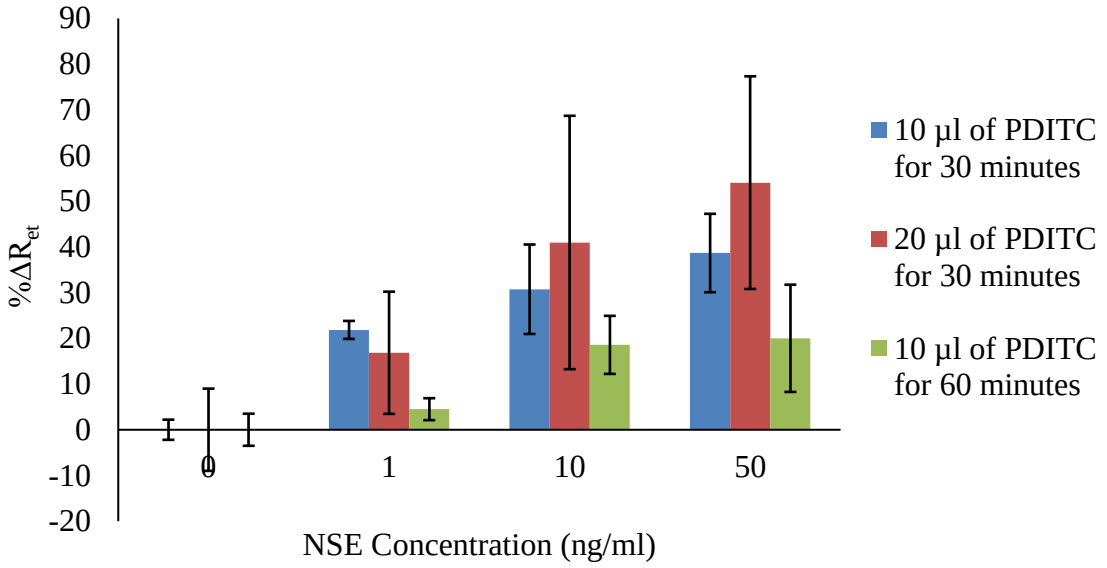

Figure 3.13: The comparison graph of NSE detection by NSE immunosensors which their SAM layers are activated by incubation in different amount of PDITC for different incubation time. The bars represent the average ± standard deviation of triplicates.

3.4.2.3 Blocking of SAM Layer

Poor blockage of immunosensor surface will result in binding of unwanted materials to the sensing area which causes false positive results and also increases the experimental error. This experiment was designed to check the effectiveness of ethanolamine in deactivating available thiocyanate terminals of SAM layer and blocking of the immunosensor surface. Four 0.1 M ethanolamine solutions were prepared as: ethanolamine in dH_2O pH 7.6, ethanolamine in dH_2O pH 8.5, ethanolamine in PBS pH 7.6, and ethanolamine in PBS pH 8.5. EIS was used to measure the impedance of SPEs before and after incubation of blocking solution on WEs. The impedance results are presented in Figure 3.14, and calculated R_{et}, ΔR_{et}, and $\%\Delta R_{et}$ are presented in Table 3.9.

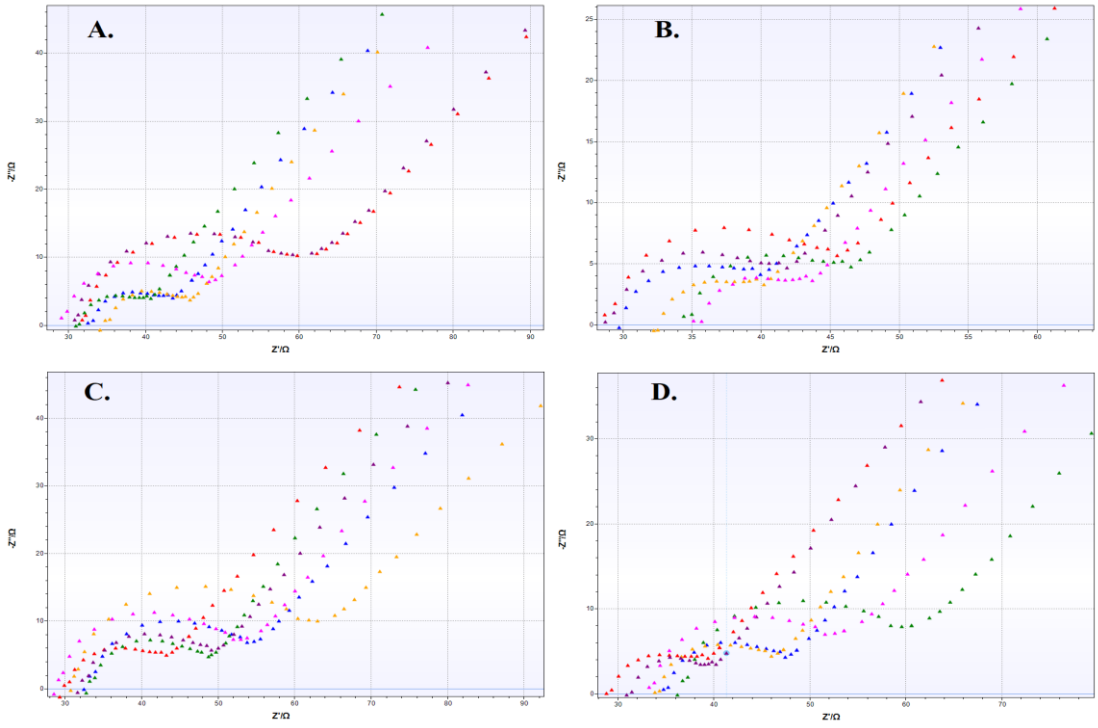

Figure 3.14: The Nyquist plots of Impedance measurements before and after applying ethanolamine to block the surface of NSE immunosensors. (A) Ethanolamine in dH_2O pH 7.6; (B) Ethanolamine in dH_2O pH 8.5; (C) Ethanolamine in PBS pH 7.6; (D) Ethanolamine in PBS pH 8.5. Blue, Red, and Green graphs represent impedance measurements of SPEs before applying ethanolamine. Yellow, purple, and pink graphs represent of SPEs after incubation of ethanolamine on WEs. Three SPEs were tested for each blocking solution.

Deactivation and blocking of SAM layer by incubating ethanolamine solution on WEs result in increasing or decreasing of impedance of electrode (Figure 3.14). As blocking of the SPE surface will cause changes in electron transfer from the redox probe to the surface of the electrode, the blocking reagent solution which causes the highest change in percentage of ΔR_{et} was considered the best blocking reagent for this experiment.

Table 3.9: Calculated R_{et}, ΔR_{et}, and $\%\Delta R_{et}$ values of SPEs before and after incubation of various blocking reagents on WEs.

		PBS 7.6	dH2O 7.6	PBS 8.5	dH2O 8.5
R_{et} (Ω) Before	SPE1	13.90	10.87	13.30	9.43
	SPE2	24.55	33.92	10.12	17.94
	SPE3	15.99	10.98	27.95	13.33
R_{et} (Ω) After	SPE1	18.98	11.02	12.30	6.15
	SPE2	37.68	34.08	8.27	12.59
	SPE3	26.59	12.98	22.52	8.23

Blocking Solution	**$\%\Delta R_{et}$ SPE1**	**$\%\Delta R_{et}$ SPE2**	**$\%\Delta R_{et}$ SPE3**	**Mean**	**SD**
Ethanolamine in PBS pH 7.6	36.57	53.47	66.32	**52.12**	14.92
Ethanolamine in dH_2O pH 7.6	1.32	0.48	18.14	**6.65**	9.96
Ethanolamine in PBS pH 8.5	7.50	18.29	19.41	**15.07**	6.58
Ethanolamine in dH_2O pH 8.5	34.80	29.83	38.24	**34.29**	4.23

The ethanolamine solution prepared in PBS with pH adjusted to 7.6 has shown to have the highest change in impedance which means the best reagent for blockage of the electrode surface among the tested solutions. Therefore, the blocking solution of ethanolamine in PBS with pH 7.6 was used for further experiments.

3.4.2.4 Optimisation of the Capture Antibody Concentration on MBs

To achieve the best concentration of capture antibody on the surface of MBs, three MBs solutions with antibody concentration of 1.2, 2.4, and 3.6 mg/ml were investigated. The obtained EIS results are presented in Figures 3.15 – 3.17; and calculated R_{et}, ΔR_{et}, and $\%\Delta R_{et}$ are shown in Tables 3.10 – 3.12.

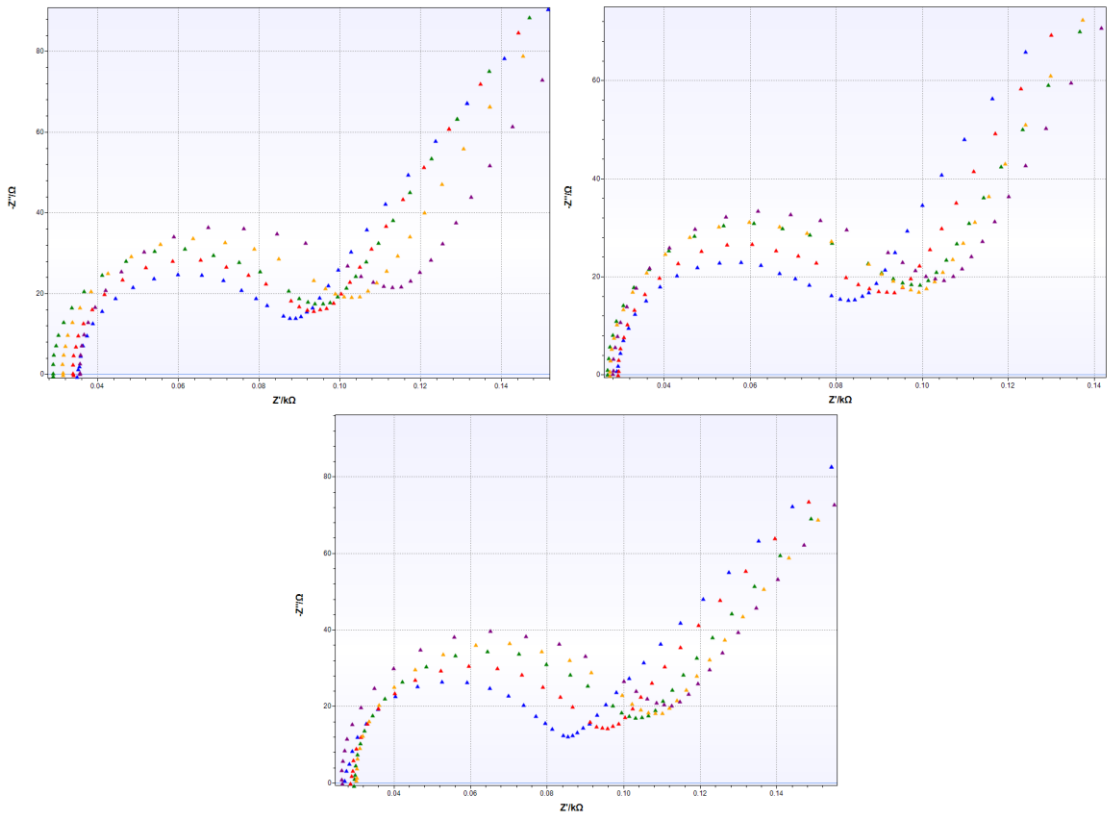

Figure 3.15: The Nyquist plots of Impedance measurements of protein detection by NSE immunosensor with use of prepared MBs with 1.2 mg/ml of 10-7938 anti-NSE antibody. Each plot represents the impedance of single immunosensor. Functionalised SPE (Blue), 0 ng/ml NSE (Red), 1 ng/ml NSE (Green), 10 ng/ml NSE (Yellow), 50 ng/ml NSE (Purple).

Table 3.10: Calculated R_{et}, ΔR_{et}, and $\%\Delta R_{et}$ values of NSE sample measurements with use of prepared MBs with 1.2 mg/ml of capture antibody.

		Baseline	0 ng/ml	1 ng/ml	10 ng/ml	50 ng/ml
R_{et} (Ω)	SPE1	39.84	44.60	51.21	53.43	57.51
	SPE2	39.83	45.58	52.86	53.16	57.74
	SPE3	49.03	54.25	60.08	62.91	68.34
ΔR_{et} (Ω)	SPE1	N/A	4.76	11.37	13.59	17.67
	SPE2	N/A	5.75	13.03	13.33	17.91
	SPE3	N/A	5.22	11.05	13.88	19.31

Conc. (ng/ml)	$\%\Delta R_{et}$ SPE1	$\%\Delta R_{et}$ SPE2	$\%\Delta R_{et}$ SPE3	Mean	Mean – Mean (0)	SD	%CV
0	11.95	14.44	10.65	12.35	0.00	1.93	15.60
1	28.54	32.71	22.54	27.93	15.58	5.11	18.30
10	34.11	33.47	28.31	31.96	19.61	3.18	9.95
50	44.35	44.97	39.38	42.90	30.55	3.06	7.14

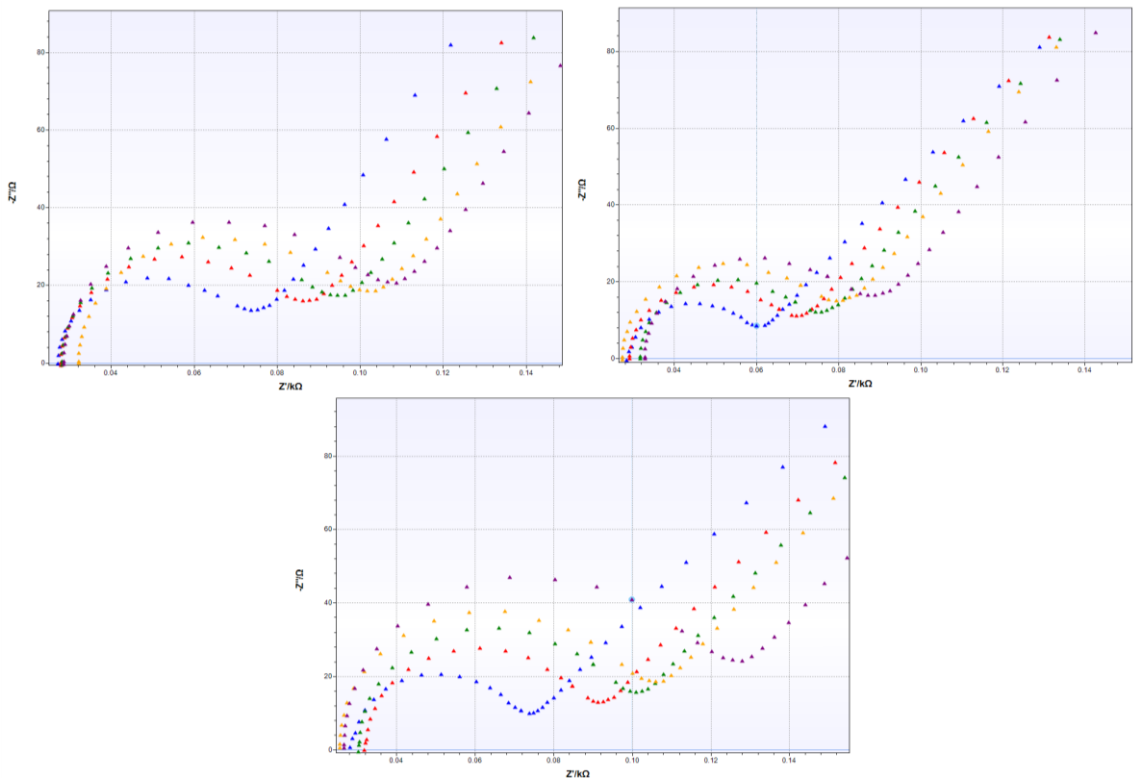

Figure 3.16: The Nyquist plots of Impedance measurements of protein detection by NSE immunosensor with use of prepared MBs with 2.4 mg/ml of 10-7938 anti-NSE antibody. Each plot represents the impedance of single immunosensor. Functionalised SPE (Blue), 0 ng/ml NSE (Red), 1 ng/ml NSE (Green), 10 ng/ml NSE (Yellow), 50 ng/ml NSE (Purple).

Table 3.11: Calculated R_{et}, ΔR_{et}, and $\%\Delta R_{et}$ values of NSE sample measurements with use of prepared MBs with 2.4 mg/ml of capture antibody.

		Baseline	0 ng/ml	1 ng/ml	10 ng/ml	50 ng/ml
R_{et} (Ω)	SPE1	33.91	44.00	50.16	55.73	60.48
	SPE2	24.36	30.60	37.80	39.85	42.06
	SPE3	37.99	49.43	57.97	65.78	88.33
ΔR_{et} (Ω)	SPE1	N/A	10.09	16.25	21.82	26.57
	SPE2	N/A	6.24	13.44	15.49	17.70
	SPE3	N/A	11.44	19.98	27.79	50.34*

Conc. (ng/ml)	$\%\Delta R_{et}$ SPE1	$\%\Delta R_{et}$ SPE2	$\%\Delta R_{et}$ SPE3	Mean	Mean – Mean (0)	SD	%CV
0	29.76	25.62	30.11	28.50	0.00	2.50	8.76
1	47.92	55.17	52.59	51.89	23.39	3.67	7.08
10	64.35	63.59	73.15	67.03	38.53	5.31	7.93
50	78.35	72.66	132.51*	75.51	47.01	4.02	5.33

* Excluded data from analysis

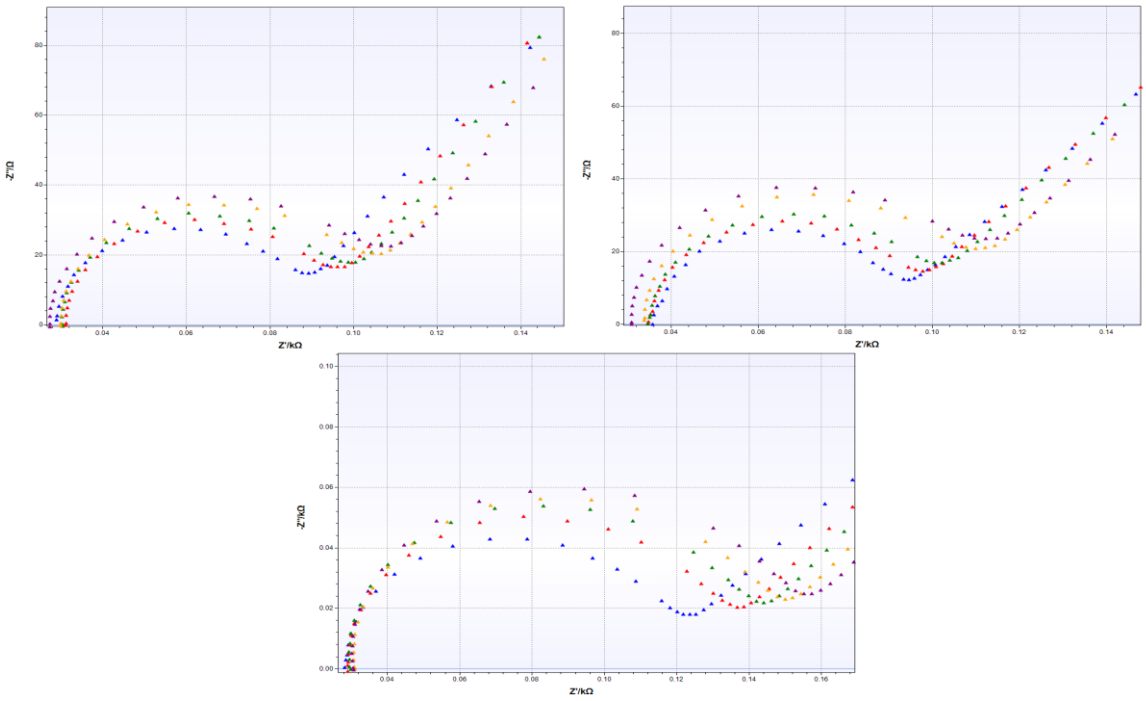

Figure 3.17: The Nyquist plots of Impedance measurements of protein detection by NSE immunosensor with use of prepared MBs with 3.6 mg/ml of 10-7938 anti-NSE antibody. Each plot represents the impedance of single immunosensor. Functionalised SPE (Blue), 0 ng/ml NSE (Red), 1 ng/ml NSE (Green), 10 ng/ml NSE (Yellow), 50 ng/ml NSE (Purple).

Table 3.12: Calculated R_{et}, ΔR_{et}, and $\%\Delta R_{et}$ values of NSE sample measurements with use of prepared MBs with 3.6 mg/ml of capture antibody.

		Baseline	0 ng/ml	1 ng/ml	10 ng/ml	50 ng/ml
R_{et} (Ω)	SPE1	46.30	48.15	51.15	56.68	61.17
	SPE2	48.97	51.64	54.21	62.56	65.35
	SPE3	81.64	92.35	97.71	101.99	107.38
ΔR_{et} (Ω)	SPE1	N/A	1.85	4.85	10.37	14.87
	SPE2	N/A	2.73	5.30	13.65	16.44
	SPE3	N/A	10.71	16.07	20.35	25.74

Conc. (ng/ml)	$\%\Delta R_{et}$ SPE1	$\%\Delta R_{et}$ SPE2	$\%\Delta R_{et}$ SPE3	Mean	Mean – Mean (0)	SD	%CV
0	4.00	5.58	13.12	7.57	0.00	4.87	64.41
1	10.48	10.84	19.68	13.67	6.10	5.21	38.13
10	22.40	27.91	24.93	25.08	17.51	2.76	11.00
50	32.12	33.61	31.35	32.36	24.79	1.15	3.55

All prepared MBs with various concentration of antibody were able to separate NSE protein from different analyte concentrations in PBS, as the impedance signal of NSE immunosensor increased with respect to increasing the concentration of the analyte Figure 3.15 – 3.17. In order to choose the optimum concentration of antibody on the surface of MBs, a comparison graph (Figure 3.18) was plotted according to the $\%\Delta R_{et}$ (Table 3.10 – 3.12) against the concentration of NSE protein (ng/ml).

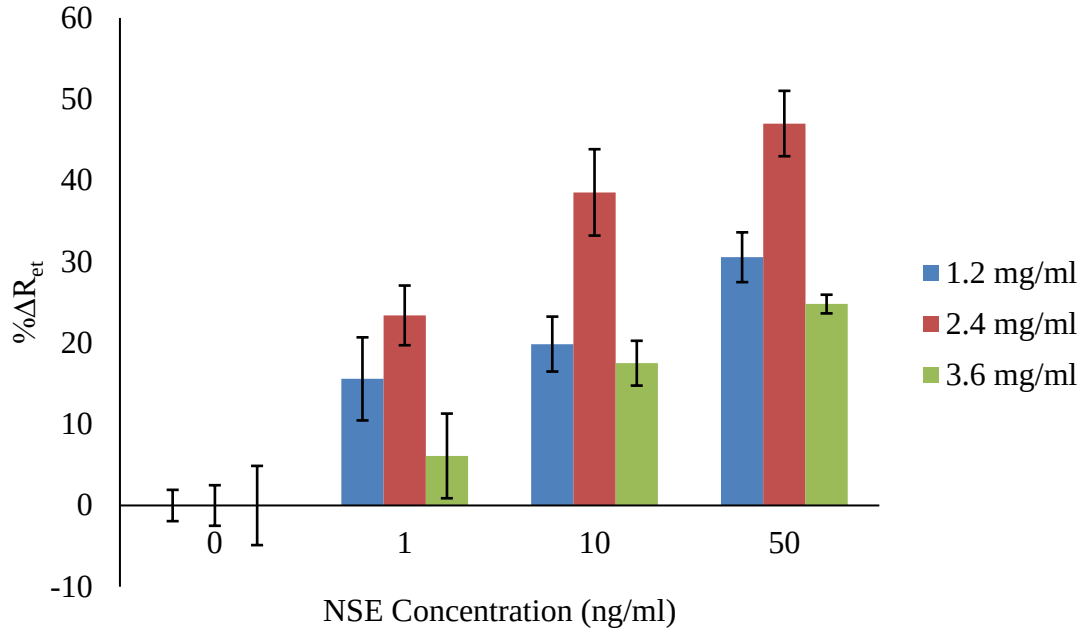

Figure 3.18: The comparison of NSE detection by use of MBs with various concentration of antibody on their surfaces. The bars represent the average ± standard deviation of triplicates.

As Figure 3.18 shows that increasing the concentration of antibody on the surface of MBs from 1.2 mg/ml to 2.4 mg/ml resulted in increasing the signal change. The reason for this is increasing the chance of analyte being captured by the MBs. Increasing the concentration of antibody does not always rises the detection signal due to the effect of steric hindrance. As presenting too many antibodies on the surface of MBs hinder the attachment of analytes, further increase of capture antibody concentration from 2.4 mg/ml to 3.6 mg/ml caused reduction of changes in impedance signals. For instance, the mean $\%\Delta R_{et}$ value for detection of 10 ng/ml of NSE were calculated as 31.96 for analyte detection by MBs with 1.2 mg/ml of antibody while the value increased to 67.03 as the detection antibody concentration increased to 2.4 mg/ml, and further increase of antibody concentration to 3.6 mg/ml reduced the value to 25.08.

The highest changes in percentage of electron transfer were obtained by use of MBs with the antibody concentration of 2.4 mg/ml on their surface. Hence, MBs were prepared with 2.4 mg/ml concentration of antibody for further experiments.

3.4.2.5 Optimisation of Detection Antibody Concentration on SPE

To develop an efficient immunoassay, the optimisation of antibody concentration on the surface of sensor is crucial (Altintas et al., 2011). To determine the best concentration of antibody for preparing NSE immunosensors, various concentration of 10-7937 anti-NSE antibody (detection antibody) as 5, 10, and 20 µg/ml were tested. The obtained experimental results are presented as Nyquist plots in Figure 3.19 – 3.21; and the calculated R_{et}, ΔR_{et}, and $\%\Delta R_{et}$ are represented in Table 3.13 – 3.15

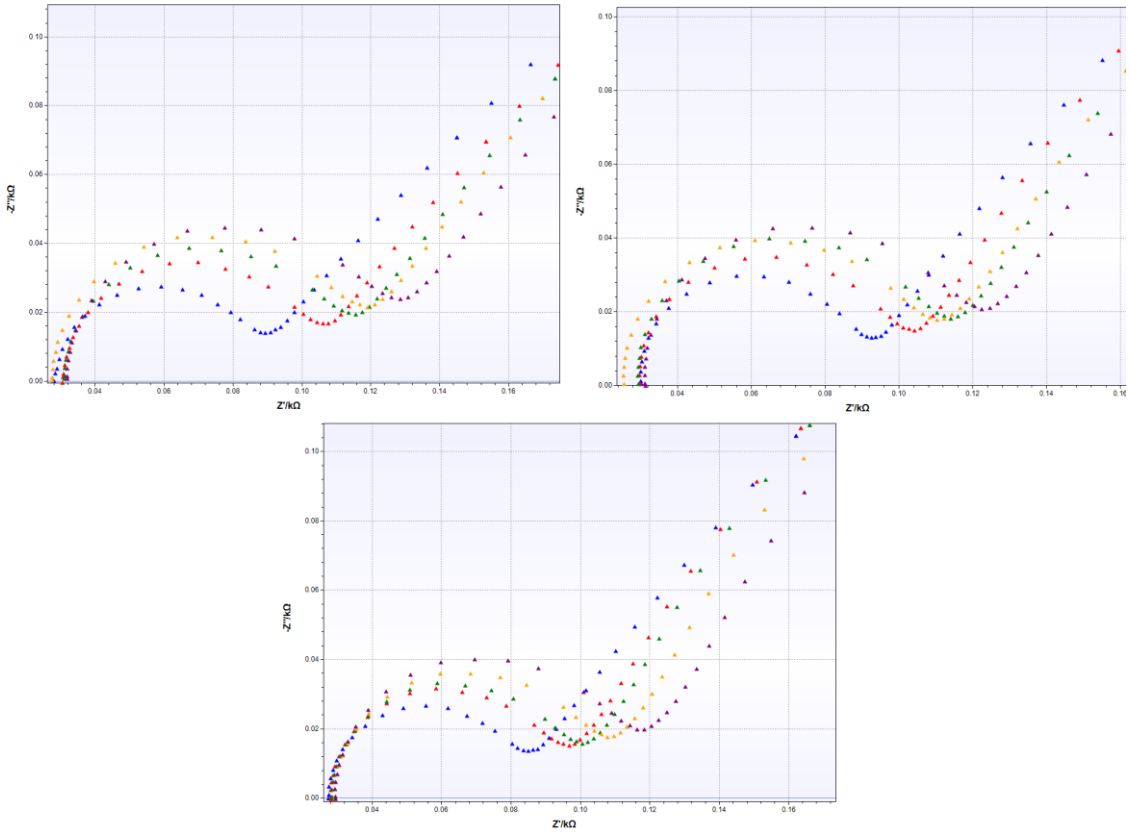

Figure 3.19: The Nyquist plots of Impedance measurements of protein detection by prepared NSE immunosensor with use of 5 µg/ml of 10-7937 anti-NSE antibody. Each plot represents the impedance of single immunosensor. Functionalised SPE (Blue), 0 ng/ml NSE (Red), 1 ng/ml NSE (Green), 10 ng/ml NSE (Yellow), 50 ng/ml NSE (Purple).

Table 3.13: Calculated R_{et}, ΔR_{et}, and $\%\Delta R_{et}$ values of NSE sample measurements with use of prepared NSE immunosensors with 5 µg/ml of detection antibody.

		Baseline	0 ng/ml	1 ng/ml	10 ng/ml	50 ng/ml
R_{et} (Ω)	SPE1	50.24	61.37	67.52	73.55	77.30
	SPE2	50.71	58.77	67.50	68.65	72.64
	SPE3	45.59	52.78	55.74	61.26	68.74
ΔR_{et} (Ω)	SPE1	N/A	11.13	17.28	23.31	27.06
	SPE2	N/A	8.06	16.79	17.94	21.93
	SPE3	N/A	7.19	10.15	15.67	23.15

Conc. (ng/ml)	$\%\Delta R_{et}$ SPE1	$\%\Delta R_{et}$ SPE2	$\%\Delta R_{et}$ SPE3	Mean	Mean – Mean (0)	SD	%CV
0	22.15	15.89	15.77	17.94	0.00	3.65	20.35
1	34.39	33.11	22.26	29.92	11.98	6.66	22.27
10	46.40	35.38	34.37	38.72	20.78	6.67	17.24
50	53.86	43.25	50.78	49.30	31.36	5.46	11.07

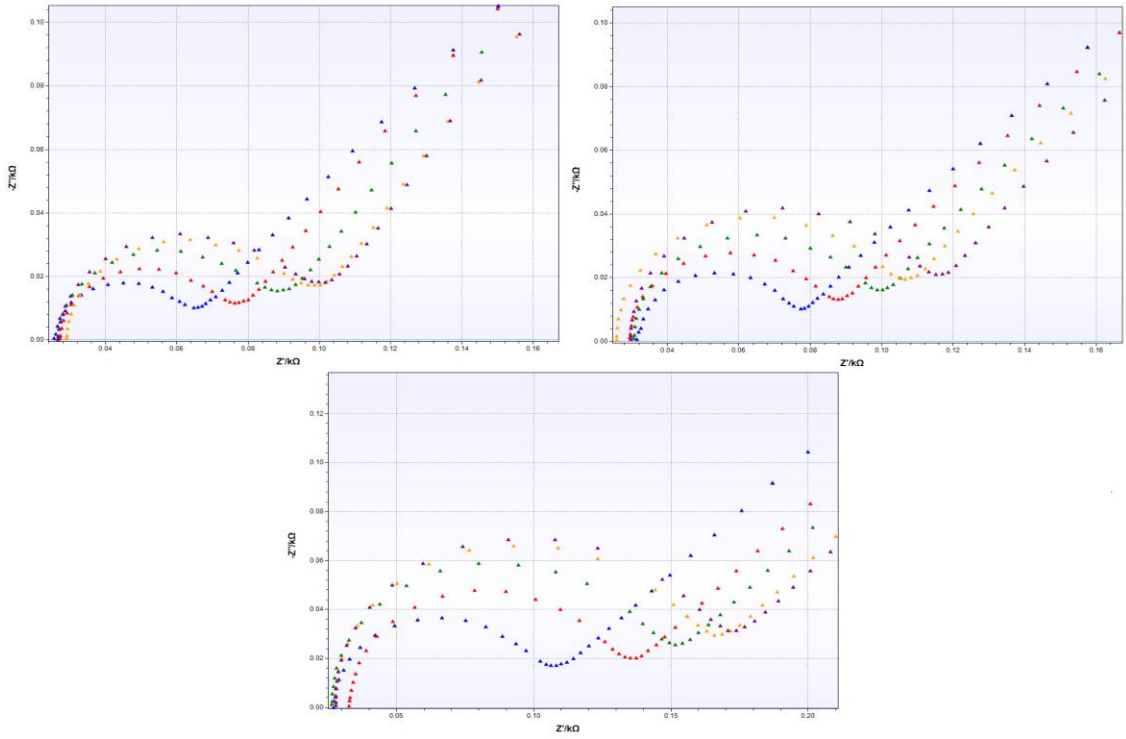

Figure 3.20: The Nyquist plots of Impedance measurements of protein detection by prepared NSE immunosensor with use of 10 µg/ml of 10-7937 anti-NSE antibody. Each plot represents the impedance of single immunosensor. Functionalised SPE (Blue), 0 ng/ml NSE (Red), 1 ng/ml NSE (Green), 10 ng/ml NSE (Yellow), 50 ng/ml NSE (Purple).

Table 3.14: Calculated R_{et}, ΔR_{et}, and $\%\Delta R_{et}$ values of NSE sample measurements with use of prepared NSE immunosensors with 10 µg/ml of detection antibody.

		Baseline	0 ng/ml	1 ng/ml	10 ng/ml	50 ng/ml
R_{et} (Ω)	SPE1	31.07	37.98	47.63	52.65	55.92
	SPE2	37.76	47.61	56.37	66.53	69.78
	SPE3	69.71	89.16	109.04	121.37	125.70
ΔR_{et} (Ω)	SPE1	N/A	6.91	16.56	21.58	24.85
	SPE2	N/A	9.85	18.61	28.77	32.02
	SPE3	N/A	19.45	39.33	51.66	55.99

Conc. (ng/ml)	$\%\Delta R_{et}$ SPE1	$\%\Delta R_{et}$ SPE2	$\%\Delta R_{et}$ SPE3	Mean	Mean – Mean (0)	SD	%CV
0	22.24	26.09	27.90	25.41	0.00	2.89	11.38
1	53.30	49.28	56.42	53.00	27.59	3.58	6.75
10	69.46	76.19	74.11	73.25	47.84	3.45	4.70
50	79.98	84.80	80.32	81.70	56.29	2.69	3.29

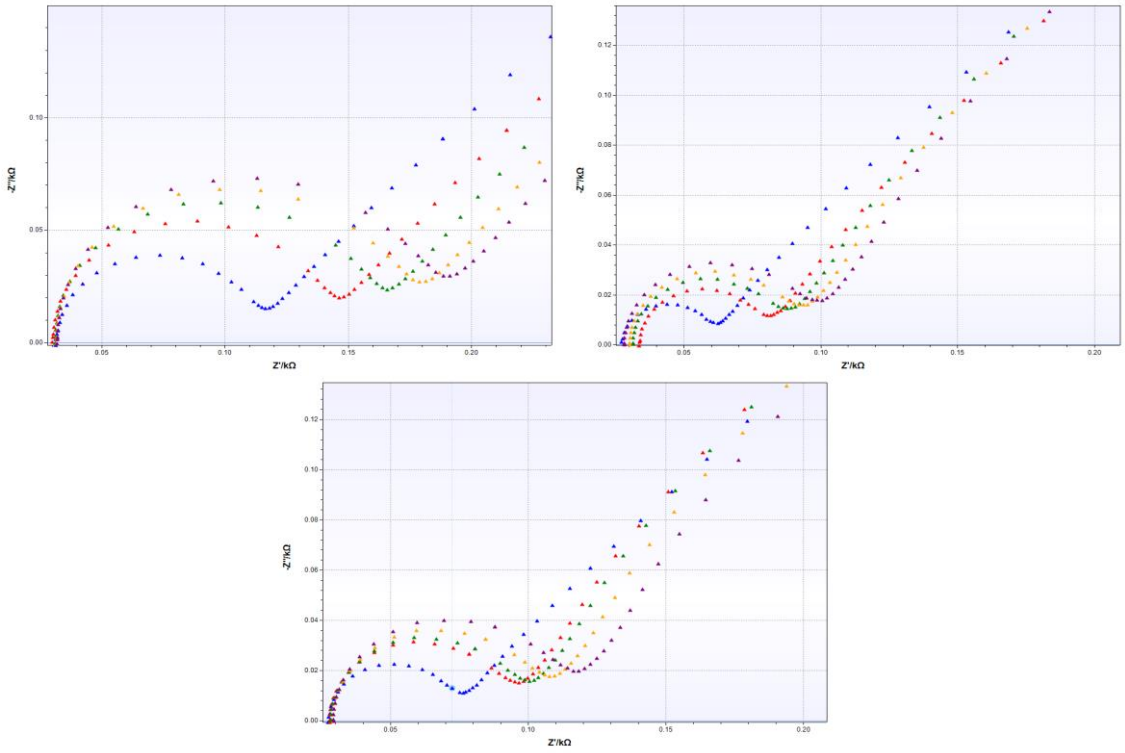

Figure 3.21: The Nyquist plots of Impedance measurements of protein detection by prepared NSE immunosensor with use of 20 µg/ml of 10-7937 anti-NSE antibody. Each plot represents the impedance of single immunosensor. Functionalised SPE (Blue), 0 ng/ml NSE (Red), 1 ng/ml NSE (Green), 10 ng/ml NSE (Yellow), 50 ng/ml NSE (Purple).

Table 3.15: Calculated R_{et}, ΔR_{et}, and $\%\Delta R_{et}$ values of NSE sample measurements with use of prepared NSE immunosensors with 20 µg/ml of detection antibody.

		Baseline	0 ng/ml	1 ng/ml	10 ng/ml	50 ng/ml
R_{et} (Ω)	SPE1	72.33	99.88	115.33	126.85	135.52
	SPE2	27.79	36.46	42.24	47.37	53.46
	SPE3	36.69	46.79	53.67	59.09	67.49
ΔR_{et} (Ω)	SPE1	N/A	27.55	43.00	54.52	63.19
	SPE2	N/A	8.67	14.45	19.58	25.67
	SPE3	N/A	10.10	16.98	22.40	30.80

Conc. (ng/ml)	$\%\Delta R_{et}$ SPE1	$\%\Delta R_{et}$ SPE2	$\%\Delta R_{et}$ SPE3	Mean	Mean – Mean (0)	SD	%CV
0	38.09	31.20	27.53	32.27	0.00	5.36	16.61
1	59.45	52.00	46.28	52.58	20.31	6.60	12.56
10	75.38	70.46	61.05	68.96	36.69	7.28	10.56
50	87.36	92.37	83.95	87.89	55.62	4.24	4.82

In order to choose the best concentration of 10-7937 anti-NSE antibody for the NSE immunosensor preparation, a comparison graph was plotted based on the $\%\Delta R_{et}$ (Table 3.13 – 3.15) against the concentration of NSE protein (ng/ml).

Figure 3.22 represents, the lowest signals were obtained by prepared immunosensors with 5 µg/ml of antibody. As the concentration of antibody increased to 10 or 20 µg/ml, higher percentage of changes in R_{et} were obtained. The NSE immunosensors with 10 µg/ml concentration of antibody were able to achieve the highest percentage of changes in impedance of electrode for detection of NSE samples in comparison with the other two antibody concentration. Thereby, 10 µg/ml was chosen as an optimum concentration for detection antibody.

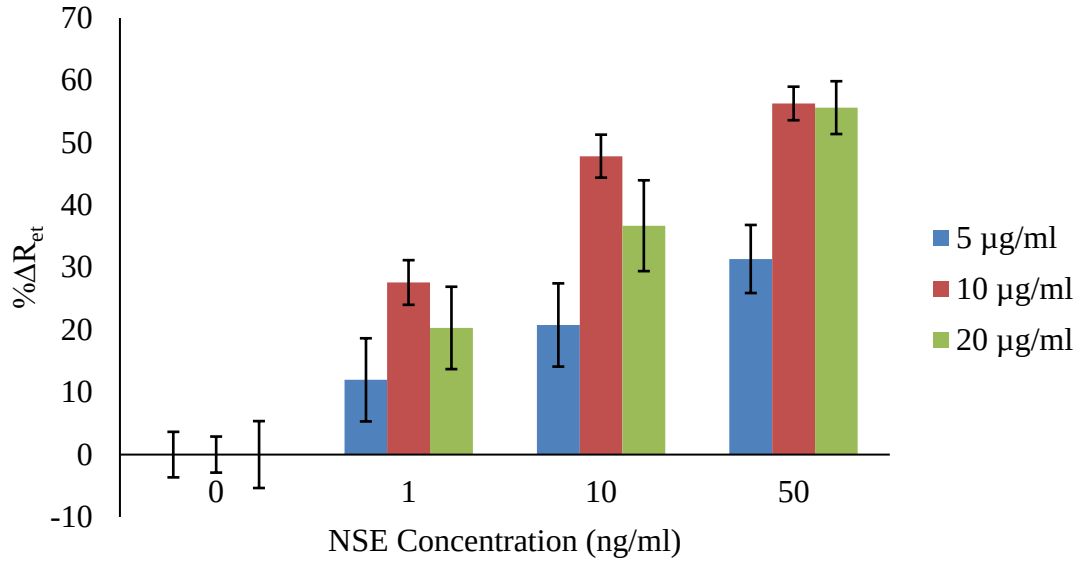

Figure 3.22: The comparison graph of NSE detection with use of prepared NSE immunosensors with various concentration of antibody on their surfaces. The bars represent the average ± standard deviation of triplicates.

3.4.3 Standard Plot of Optimised NSE Immunosensor

Once the experimental error was controlled by testing and optimising each step of antibody immobilisation on the surface of SPEs, and after selecting the optimum concentration of antibodies on both SPE and MBs. The NSE immunosensors were used to detect various NSE concentrations in buffer and human serum, and also to detect CEA protein as a non-specific analyte.

3.4.3.1 NSE Detection in Buffer

The NSE immunosensor was tested by measuring different concentrations of NSE protein samples (0 – 100 ng/ml) in PBS buffer pH 7.4 to create a standard curve. After mixing NSE samples with functionalised MBs, and fishing the analyte. The amounts of protein were measured by NSE immunosensor and use of EIS technique. Figure 3.23 represents the experimental impedance results in the Nyquist plots. The EIS spectrum analyser software was used to simulate the impedance graphs and calculate the R_{et}, ΔR_{et}, and $\%\Delta R_{et}$ which are shown in Table 3.16.

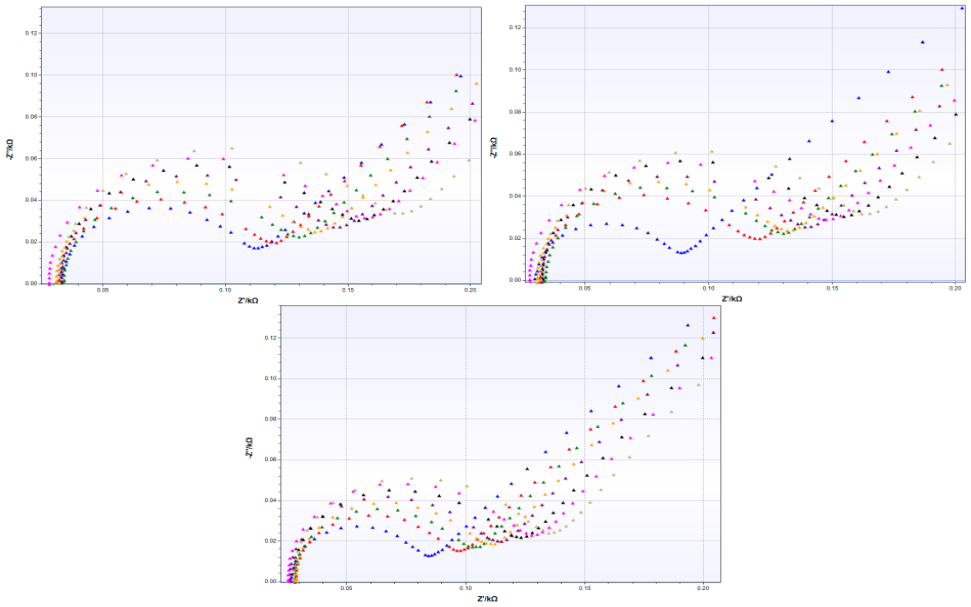

Figure 3.23: The Nyquist plots for impedance of NSE protein detection in PBS buffer by NSE immunosensors. Each graph represents the impedance measurements of single NSE immunosensor. Functionalised SPE (Blue), 0 ng/ml (Red), 1 ng/ml (Green), 5 ng/ml (Yellow), 10 ng/ml (Purple), 20 ng/ml (Black), 50 ng/ml (Pink), 100 ng/ml (Khaki).

Table 3.16: Calculated R_{et}, ΔR_{et}, and $\%\Delta R_{et}$ values for impedance measurements of NSE protein detection in PBS buffer.

		Baseline	0 ng/ml	1 ng/ml	5 ng/ml	10 ng/ml	20 ng/ml	50 ng/ml	100 ng/ml
R_{et} (Ω)	SPE1	67.58	72.45	79.06	88.05	93.40	100.66	108.16	115.75
	SPE2	48.79	53.79	58.83	68.76	69.85	76.30	80.71	86.96
	SPE3	52.12	57.33	62.18	67.25	72.70	78.94	85.46	89.87
ΔR_{et} (Ω)	SPE1	N/A	4.87	11.48	20.47	25.82	33.08	40.58	48.17
	SPE2	N/A	5.00	10.04	19.97	21.06	27.51	31.92	38.17
	SPE3	N/A	5.21	10.06	15.13	20.58	26.82	33.34	37.75

Conc. (ng/ml)	$\%\Delta R_{et}$ SPE1	$\%\Delta R_{et}$ SPE2	$\%\Delta R_{et}$ SPE3	Mean	Mean – Mean (0)	SD	%CV
0	7.21	10.25	10.00	9.15	0.00	1.69	18.43
1	16.99	20.58	19.30	18.96	9.81	1.82	9.59
5	30.29	40.93	29.03	33.42	24.27	6.54	19.56
10	38.21	43.16	39.49	40.29	31.14	2.57	6.38
20	48.95	56.38	51.46	52.26	43.11	3.78	7.24
50	60.05	65.42	63.97	63.15	54.00	2.78	4.40
100	71.28	78.23	72.43	73.98	64.83	3.73	5.04

The standard curve (Figure 3.24) was created based on the calculated $\%\Delta R_{et}$ (Table 3.16) versus the concentration of NSE antigen after normalising the results by subtracting the $\%\Delta R_{et}$ of 0 ng/ml. As Figure 3.24 shows, increasing the concentration of NSE protein results in increasing the impedance of electrode which indicates that increasing the signal is proportional to the analyte concentration. Additionally, comparing these results with the obtained results before applying optimisations (Section 3.4.1) shows improvement in the error bars, though lower response signals were obtained.

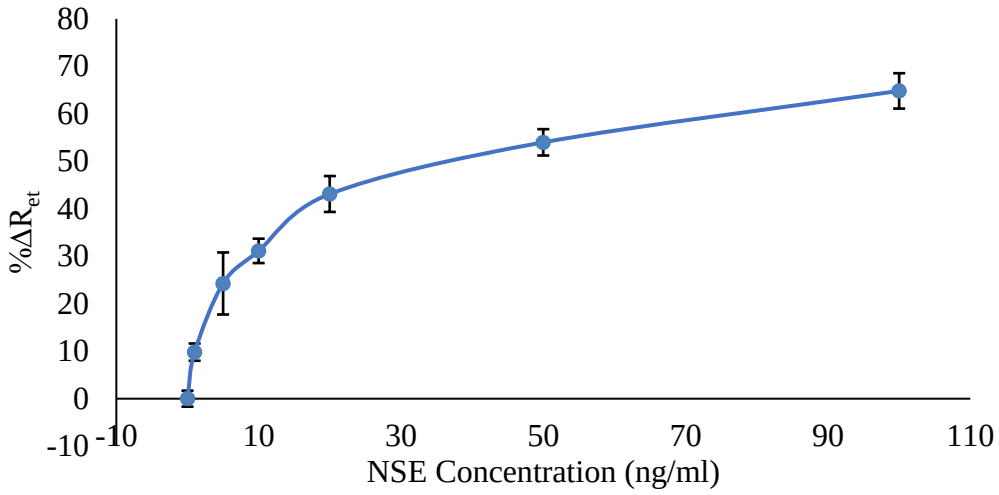

Figure 3.24: Standardised NSE immunosensor response plot created for detection of different NSE concentrations (0.0 – 100 ng/ml) in PBS buffer. The bars represent the average ± standard deviation of triplicates.

The linear range response of NSE immunosensor in PBS buffer was plotted by using sensor response ($\%\Delta R_{et}$) and the concentration of NSE protein in logarithmic format, Figure 3.25. Figure 3.25 shows logarithmically increases of sensor response by increasing the concentration of NSE antigen. The LoD value was calculated as low as 0.18 ng/ml based on Equation 1. The obtained LoD is lower than the calculated LoD before applying optimisation which was 0.81 ng/ml. Moreover, the optimised NSE immunosensor showed a stronger correlation coefficient (0.9848) than unoptimised immunosensor 0.9512.

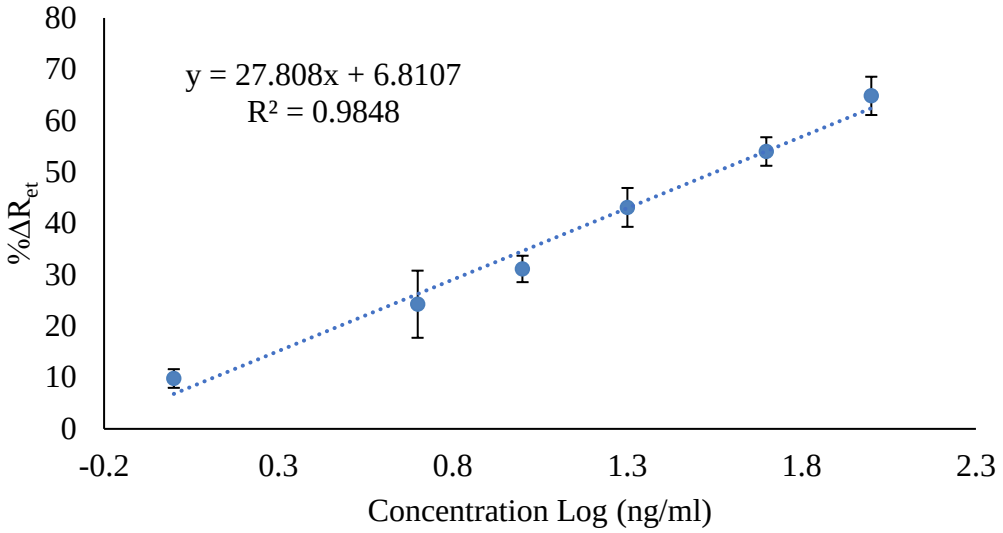

Figure 3.25: The linear range response of NSE immunosensor representing $\%\Delta R_{et}$ versus the $\log_{10}$ of NSE concentrations (1 – 100 ng/ml) in PBS buffer. The bars represent the average ± standard deviation of triplicates.

3.4.3.2 NSE Detection in Human Serum Samples

Once the optimisation steps have reduced the experimental error and improved the LoD of NSE protein in PBS, detection of various concentrations of NSE antigen in human blood serum was tested. This experiment was done by testing the response of NSE immunosensor to range of NSE protein concentrations (0.0 – 100 ng/ml) spiked in human serum. The functionalised MBs were used to fish the analyte from the sample and to move the NSE antigen to the WEs surface to form sandwich assay. The concentration of NSE protein was measured by using of the EIS technique. The experimental results are presented in Nyquist plots in Figure 3.26. The EIS spectrum analyser software was used to simulate the impedance graphs and to calculate the R_{et}. Table 3.17 represents the calculated R_{et}, ΔR_{et}, and $\%\Delta R_{et}$.

The standard curve (Figure 3.27) was then created based on the calculated $\%\Delta R_{et}$ (Table 3.17) against the concentration of NSE antigen after normalising the results by subtracting the $\%\Delta R_{et}$ of 0 ng/ml.

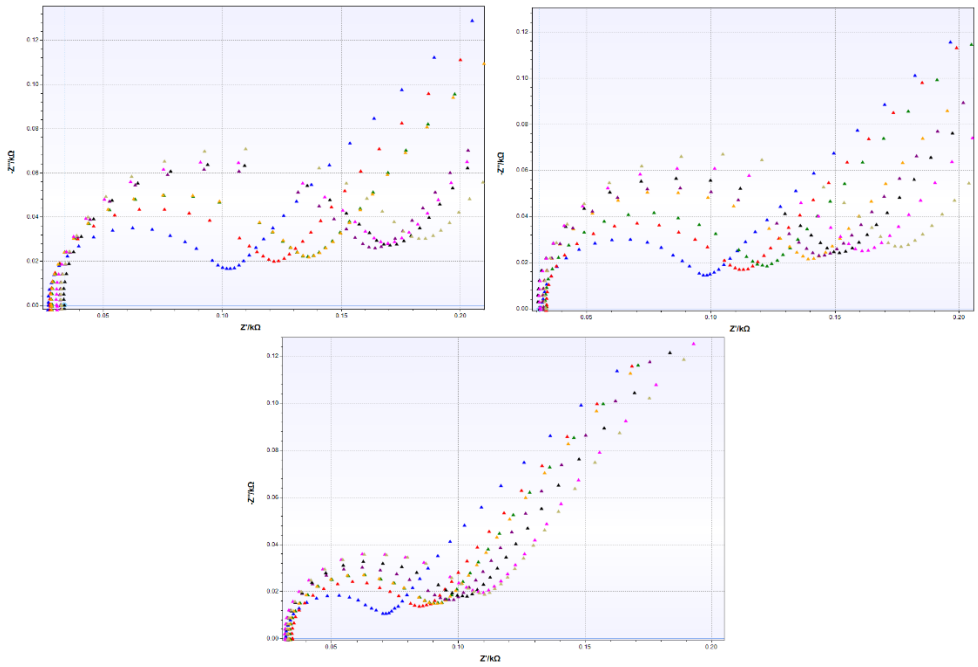

Figure 3.26: The Nyquist plots for impedance of NSE protein detection in Serum by NSE immunosensors. Each graph represents the impedance measurements of single NSE immunosensor. Functionalised SPE (Blue), 0 ng/ml (Red), 1 ng/ml (Green), 5 ng/ml (Yellow), 10 ng/ml (Purple), 20 ng/ml (Black), 50 ng/ml (Pink), 100 ng/ml (Khaki).

Table 3.17: Calculated R_{et}, ΔR_{et}, and $\%\Delta R_{et}$ values for impedance measurements of NSE protein detection in serum.

		Baseline	0 ng/ml	1 ng/ml	5 ng/ml	10 ng/ml	20 ng/ml	50 ng/ml	100 ng/ml
R_{et} (Ω)	SPE1	62.52	77.96	89.38	103.17	111.54	115.65	117.28	128.38
	SPE2	54.90	65.08	72.78	90.61	94.16	102.49	109.52	117.31
	SPE3	30.54	39.69	44.38	47.88	53.51	55.52	60.88	61.10
ΔR_{et} (Ω)	SPE1	N/A	15.44	26.86	40.65	49.02	53.13	54.76	65.86
	SPE2	N/A	10.18	17.88	35.71	39.26	47.59	54.62	62.41
	SPE3	N/A	9.15	13.84	17.34	22.97	24.98	30.34	30.56

Conc. (ng/ml)	$\%\Delta R_{et}$ SPE1	$\%\Delta R_{et}$ SPE2	$\%\Delta R_{et}$ SPE3	Mean	Mean – Mean (0)	SD	%CV
0	24.70	18.54	29.96	24.40	0.00	5.71	23.42
1	42.96	32.57	45.32	40.28	15.88	6.78	16.84
5	65.02	65.05	56.78	62.28	37.88	4.77	7.65
10	78.41	71.51	75.21	75.04	50.64	3.45	4.60
20	84.98	86.68	81.79	84.49	60.09	2.48	2.94
50	87.59	99.49	99.35	95.48	71.08	6.83	7.16
100	105.34	113.68	100.07	106.36	81.96	6.86	6.45

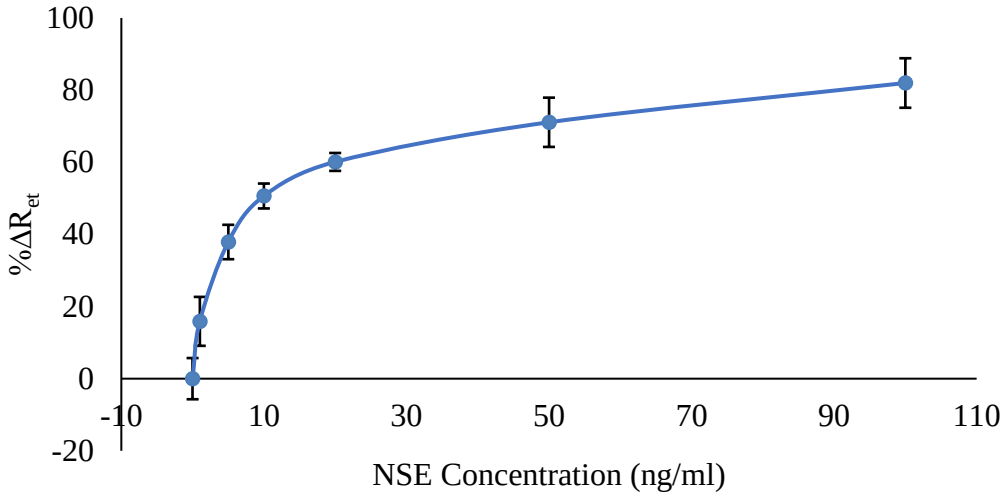

Figure 3.27: Standardised NSE immunosensor response plot created for detection of different NSE concentrations (0.0 – 100 ng/ml) in serum. The bars represent the average ± standard deviation of triplicates.

Like the immunosensor response to NSE concentrations in PBS (Figure 3.24), the impedance of electrode increased by increasing the concentration of NSE antigen in serum (Figure 3.27). This due to the formation of sandwich assay on the surface of WEs which block the surface and reduces the transfer of electron from the redox probe to the electrode surface.

The $\%\Delta R_{et}$ and the logarithmic format of NSE concentrations were used to plot the linear range response of NSE immunosensor, Figure 3.28. it can be observed in Figure 3.28 that the sensor response logarithmically increases by increasing the analyte concentration with correlation coefficient of the quantified samples of 0.9977. The LoD value was calculated as low as 0.52 ng/ml based on Equation 1. Although the achieved LoD is higher than the LoD of NSE detection in PBS buffer which was 0.18 ng/ml; the obtained LoD is lower than the cut-off value which is 12.5 ng/ml.

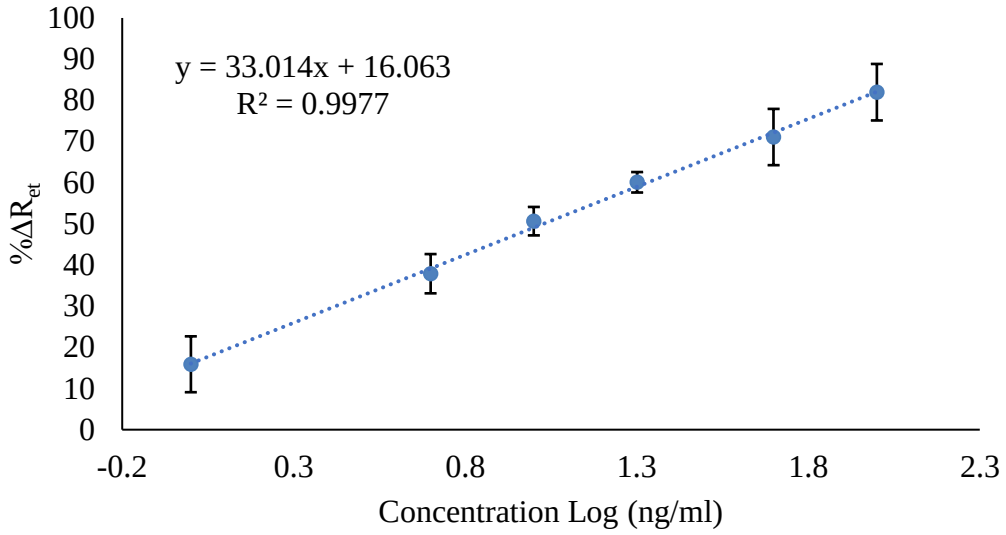

Figure 3.28: The linear range response of NSE immunosensor representing $\%\Delta R_{et}$ versus the $\log_{10}$ of NSE concentrations (1 – 100 ng/ml) in serum. The bars represent the average ± standard deviation of triplicates.

3.4.3.3 Non-Specificity Evaluation

Since the immunosensor were able to detect NSE protein in both PBS buffer and serum samples, non-specificity or cross-reactivity test was done to check whether the sensor signal generation is only due to binding of molecule of interest. This experiment was done by measuring various CEA concentrations (0.0 – 100 ng/ml) spiked in human serum with NSE immunosensor. The analyte measurements were done by EIS technique and the results are presented in Figure 3.29 and Table 3.18.

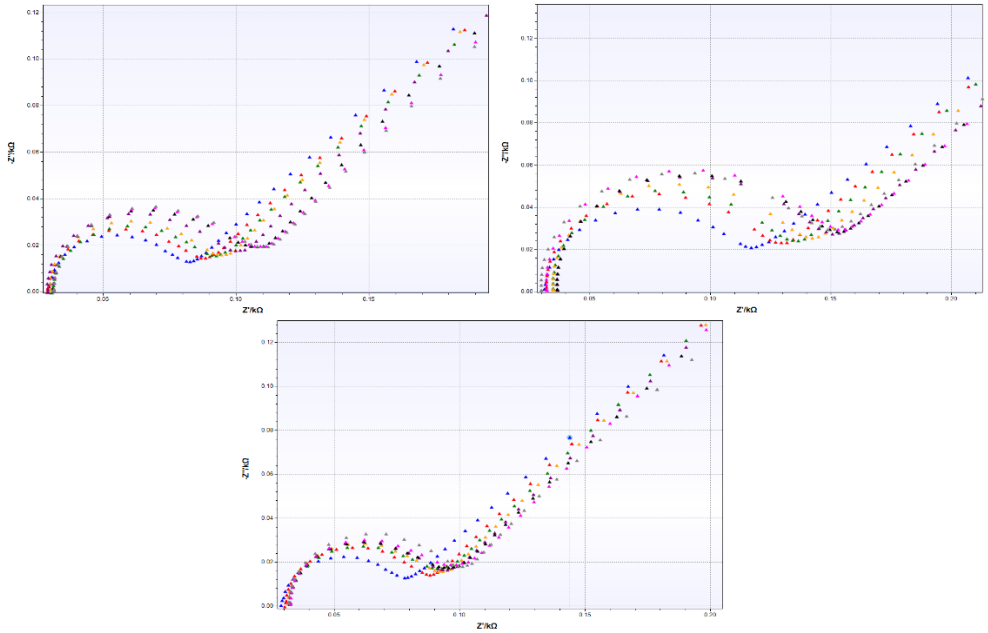

Figure 3.29: The Nyquist plots for impedance of CEA protein detection in serum by NSE immunosensors. Each graph represents the impedance measurements of single NSE immunosensor. Functionalised SPE (Blue), 0 ng/ml (Red), 1 ng/ml (Green), 5 ng/ml (Yellow), 10 ng/ml (Purple), 20 ng/ml (Black), 50 ng/ml (Pink), 100 ng/ml (Grey).

Table 3.18: Calculated R_{et}, ΔR_{et}, and $\%\Delta R_{et}$ values for NSE immunosensor impedance measurements for cross-reactivity test in serum.

		Baseline	0 ng/ml	1 ng/ml	5 ng/ml	10 ng/ml	20 ng/ml	50 ng/ml	100 ng/ml
R_{et} (Ω)	SPE1	43.81	48.64	50.17	54.12	55.91	57.68	61.65	63.04
	SPE2	74.61	84.05	85.74	91.56	97.92	99.30	102.57	104.39
	SPE3	40.88	47.11	48.08	49.87	51.16	52.41	53.67	56.91
ΔR_{et} (Ω)	SPE1	N/A	4.83	6.36	10.31	12.10	13.87	17.84	19.23
	SPE2	N/A	9.44	11.13	16.95	23.31	24.69	27.96	29.78
	SPE3	N/A	6.23	7.20	8.99	10.28	11.53	12.79	16.03

Conc. (ng/ml)	$\%\Delta R_{et}$ SPE1	$\%\Delta R_{et}$ SPE2	$\%\Delta R_{et}$ SPE3	Mean	Mean – Mean (0)	SD	%CV
0	11.02	12.65	15.24	12.97	0.00	2.13	16.41
1	14.52	14.92	17.61	15.68	2.71	1.68	10.73
5	23.53	22.72	21.99	22.75	9.78	0.77	3.39
10	27.62	31.24	25.15	28.00	15.03	3.06	10.94
20	31.66	33.09	28.20	30.98	18.01	2.51	8.11
50	40.72	37.47	31.29	36.49	23.52	4.79	13.13
100	43.89	39.91	39.21	41.00	28.03	2.52	6.16

The obtained results from 3.17 and 3.18 were compared by plotting a comparison graph of $\%\Delta R_{et}$ versus the analyte concentration which is presented in Figure 3.30. As it can be observed from the comparison graph, the NSE immunosensor response increased with increase in analyte concentration. Although the sensor responded to CEA analyte concentration, the generated signals are not as great as the sensor response to NSE antigen binding. For instance, the highest $\%\Delta R_{et}$ for CEA detection was 28.03% which was achieved for detection of 100 ng/ml of CEA while $\%\Delta R_{et}$ of 37.88% was achieved for detection of 5 ng/ml of NSE protein.

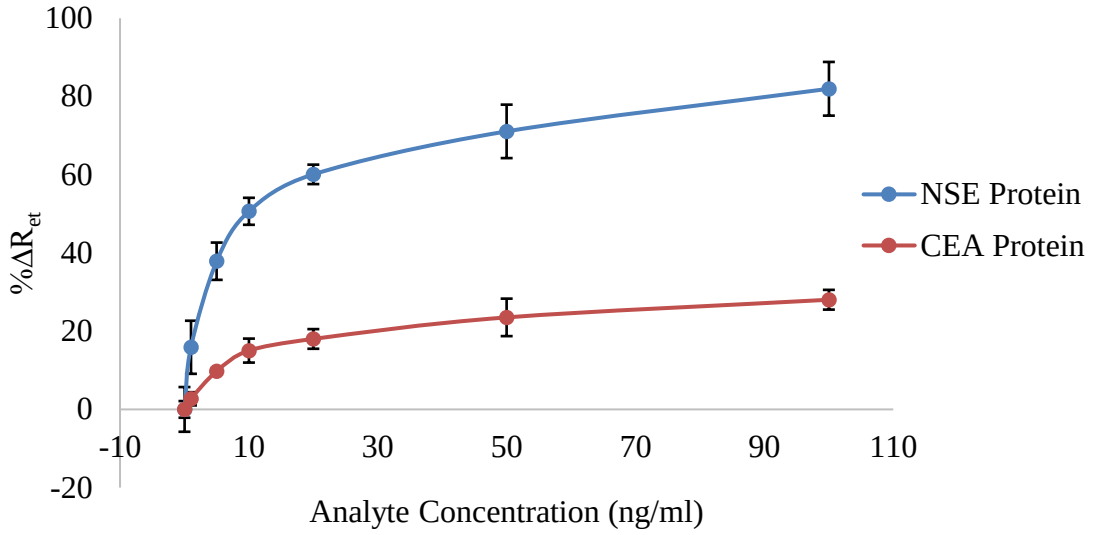

Figure 3.30: Investing the response of NSE immunosensor to various concentration of specific (NSE protein) and non-specific (CEA protein) analyte. The bars represent the average ± standard deviation of triplicates.

3.5. Discussion and Conclusions

NSE is known to be a reliable, sensitive and specific biomarker for SCLC. Thus, it is a suitable biomarker to be used as part of biosensor for detection of lung cancer and specially to distinguish between SCLC and NSCLC.

According to Chapter 2, the proposed platform has shown to be effective in amplifying the detection signal. The NSE immunosensor was constructed by immobilising anti-NSE monoclonal antibody on the SPEs working electrode through formation of SAM layer. The MBs were functionalised with another type of monoclonal antibody. Functionalised MBs were used to detect, to fish the analyte from samples and move the antigen to the sensing area by action of sensing platform. The detection of NSE protein with use of MBs and the proposed platform has not been reported by other researchers.

After confirmation of anti-NSE antibody immobilisation on the WEs, the immunosensors were used to detect various NSE concentration. The sensor was successfully measured various concentrations in PBS buffer with low LoD. The plotted standardised curve showed to have high level of experimental error. Although applying a washing step to the mixture of MBs and antigen sample prior of analyte detection has reduced the amount of error, the error was significantly high. Therefore, the activation of SAM layer and blockage of SAM layer was tested. Deactivation and blockage of SAM layer by ethanolamine in PBS with adjusted pH to 7.6 have shown to be the best blocking reagent among the tested solutions.

The NSE immunosensors were used to measure various concentrations of NSE antigen in PBS buffer after optimising the antibody concentration on both SPEs and MBs surfaces. The obtained standardised curve after optimisations proves the success of optimisations as the error bars were significantly reduced and lower LoD was obtained in compare with the standardised curve before optimisations, 0.18 and 0.81 ng/ml, respectively.

The NSE immunosensor was also tested to measure both specific (NSE antigen) and non-specific (CEA protein) analytes spiked in 100 % serum. The achieved LoD was 0.52 ng/ml which is lower than the cat-off value of 12.5 ng/ml. Additionally, from the sensor response, it is possible to distinguish between 100 ng/ml of CEA and 5 ng/ml of NSE.

There is a limited number of studies reported in literature that describe the detection of NSE protein by biosensors and they are summarised in Chapter1, in Table 1.4. Among them, few studies have obtained higher LoDs than the one obtained in this project for detection in serum (Geißler et al., 2013; Shan & Ma, 2016). Only Barton et al. (2008) have used electrochemical impedance spectroscopy to measure the analyte concentration. They have reported a linear detection range of 1 – 50 pg/ml in buffer and have achieved a LoD of 0.5 pg/ml. Nevertheless, it is not possible to fully compare their assay with the assay developed in this work as they do not mention either the assay time or the amounts of reagents used for analyte detection.

According the results obtained in this study, the developed NSE immunosensor with use of MBs and the proposed platform were successful in detecting specific analyte in both PBS buffer and serum; and has the potential to be used as part of early lung cancer diagnosis.

Chapter 4:

DEVELOPMENT OF CARCINOEMBRYONIC ANTIGEN (CEA) IMMUNOSENSOR

4.1. Introduction

Non-small cell lung cancer (NSCLC) is responsible for 80% to 90% of lung cancer incidence (Kashyap et al., 2015; Wei et al., 2017). The most effective treatment method of NSCLC is surgery, however, most patients (75%) cannot be treated by surgery due to late diagnosis which reduces the 5-year survival rate and increases the chance of cancer recurring (Gao et al., 2017). Thus, it is crucial to diagnose NSCLC at its early stages to increase the survival chance. Cancer biomarkers are valuable as measuring their concentration within body fluids, *e.g.* serum, can be used for early detection and to monitor therapy. Detecting and measuring of cancer biomarker in medical centres is an expensive and time-consuming analysis which requires highly trained people (Fan et al., 2017). Biosensor are low-cost and non-invasive analytical tools which can be used for early diagnosis of lung cancer and simultaneously monitoring the biomarker concentration level.

Carcinoembryonic antigen (CEA) is a cell surface glycoprotein. CEA is known as the most specific and reliable biomarker with a cut-off value of 5 ng/ml for diagnosis of cancer such as NSCLC, breast, colorectal, ovarian, and colon. The concentration level of CEA arises in serum after cancer incidence and during its progression. Thereby, detection and measurement of CEA concentration level in serum can help in early diagnosis and monitoring the treatment (Feng et al., 2016; Gu et al., 2018; Justino et al., 2016).

The electrochemical impedance spectroscopy (EIS) measure the analyte concentration by applying decades of frequency and measuring the total impedance which is consists of a real (Z′) and an imaginary (Z″) part. The EIS is a sensitive and rapid technique which can be used for label-free analyte detection (Cui et al., 2018). Attachment of specific analyte to the surface antibody changes the surface chemistry which lead in change of electron transfer from the redox probe to the electrode surface. The change in impedance of electrode is proportional to the amount of detected analyte. Thus, it can be used to measure the analyte concentration.

This chapter illustrate the development and optimisation of CEA immunosensor for lung cancer with use of a platform (described in Chapter 2). A standardised plot was obtained by applying some of the optimisation steps from the Chapter 3, such as: washing method, SAM layer activation, and blocking of the SAM layer. The concentration of antibody was optimised for both magnetic nanobeads (MBs) and CEA immunosensor. Then, the optimised immunosensor was used to detect the CEA protein within the PBS buffer and to plot a standardised plot to compare the results with the previous set of data. In the last step, CEA immunosensor was used to measure the various concentrations of CEA and NSE proteins spiked in serum as specific and non-specific antigens, respectively.

4.2. Materials and Equipment

All the materials and equipment used in this chapter are the same as listed in Chapter 2, Section 2.1 with an additional item of human blood serum which was purchased from Sigma-Aldrich (Dorset, UK). The PalmSens^3 potentiostat and its corresponded software were used to perform impedance technique to measure the sample concentration with the same mentioned setting in Chapter 2, Section 2.2.5, such as frequency range of 50 kHz – 0.1 Hz and applied potential of 0.12 V. All impedance measurements were carried out in the presence of 50 µl of 10 mM $[K_3Fe(CN_6)]/[K_2Fe(CN_6)]$ in 10 mM PBS pH 7.4.

The proposed platform was used in all sample concentration measurements. As described in Chapter 2, the proposed platform is consisting of 2 cylinders with an implanted magnet. As it explained before, the functionalised MBs were transferred by the action of platform from the non-sensing part of SPEs to the WEs where specific antibodies were immobilised. After incubating Functionalised MBs on the gold WEs, unbound MBs were pulled away from the sensing area by rotation of cylinders which were placed underneath of SPEs. Figure 3.1 (Chapter 3) is an illustration of platform principle.

4.3. Methods

4.3.1 Functionalisation of Magnetic Beads

The 2.4 mg/ml of 12-140-10 monoclonal anti-CEA antibody was used to functionalise MBs according to the protocol which is explained in Chapter 2, Section 2.2.2.

4.3.2 Immobilisation of Antibody on the SPEs

All SPEs were cleaned before immobilising the antibody on the WEs. The washing step was consisting of dipping SPEs in a solution of 50 mM KOH in 25% H_2O_2 for 10 minutes following by rinsing SPEs with dH_2O and drying them with nitrogen gas. CEA immunosensor were prepared with 10 µg/ml of 12-140-01 anti-CEA antibody based on the formation of cysteamine SAM layer. The method of immobilisation of antibodies on WEs is explained in Chapter 2, Section 2.2.7.1.

4.3.3 Electrochemical Measurement

EIS measurements were conducted by Auto GillAC and PalmSens^3 potentiostat with their corresponding software as described in Chapter 2, Section 2.2.4. To compare the EIS results, the R_{et} was calculated for all impedance measurements by the EIS spectrum analyser software.

4.3.4 CEA Assay Development

The magnetic beads were functionalised with 12-140-10 anti-CEA antibody, and CEA immunosensors were prepared by 12-140-01 anti-CEA antibody according to the methods which were explained in Chapter 2, section 2.2.2 and 2.2.6.1, respectively.

After preparing various CEA concentrations (0.0 – 100 ng/ml), 45 µl of each concentration sample was mixed with 5 µl of functionalised magnetic beads in a

centrifuge tube with action of vortex and incubated for 20 minutes to allow forming of MB-Ab-CEA complex. The tube content was then washed three times with 50 µl of PBS pH 7.2 and use of magnetic rack. The whole content of the tube was then transferred to insulating part of SPE were the platform magnet pole was faced up. The magnetic beads were pulled to the sensing area (WE) by rotation of magnetic bar, and incubated for 20 minutes. Then, the magnetic bar was rotated again to eliminate the unbounded MBs from the surface of the WE. The SPE was rinsed with PBS pH 7.4 and dried with nitrogen gas before applying the impedance.

All concentration measurement of CEA protein samples (0.0 ng/ml to 100 ng/ml) were done by use of freshly made CEA immunosensors, sensing platform, and EIS technique. The CEA concentration measurement was done before and after applying some optimisations such as type of blocking agent.

4.3.5 Optimisation of the CEA immunosensor

4.3.5.1 Optimisation of the Capture Antibody Concentration

To achieve the optimum concentration of capture antibody on the surface of MBs, three MBs solutions were prepared with various concentrations of 12-140-10 anti-CEA antibody (1.2, 2.4, and 3.6 mg/ml) according to the functionalisation of MBs method which is explained in Chapter 2, Section 2.2.2.

A 5 µl of MBs were mixed with 45 µl of CEA solutions in a centrifuge tube for 20 minutes to allow formation of MB-Ab-CEA. Then the tube content was washed three times with use of a magnetic rack and 50 µl of PBS buffer, before adding the solution to the immunosensor for analyte detection. The experiment was repeated three times with three freshly made CEA immunosensors each prepared solution of MBs with different concentration of capture antibody on their surface.

4.3.5.2 Optimisation of the Detection Antibody Concentration

Three different concentration as 5, 10, and 20 µg/ml of detection antibody were immobilised on three different SPEs to find the optimum concentration of antibodies on the surface of WEs. The immobilisation of antibody was done according to the formation of cysteamine SAM layer, Chapter2, Section 2.2.7.1. The experiment was repeated three times with freshly prepared CEA immunosensors. Various concentration of CEA protein as 0, 1, 10, 50 ng/ml were prepared and detected by immunosensor to compare the data and to find the optimum detection antibody concentration.

4.3.6 Standard Plot of the Optimised CEA Immunosensor

After confirmation of anti-CEA antibody immobilisation on the WEs and optimisation of capture and detection antibody on the surface of MBs and SPEs, the CEA immunosensors were used to generate the standardised curve of CEA protein detection, and also to check the non-specificity binding of analyte. The calibration curve was firstly made by detection of 0, 1, 5, 10, 20, 50, and 100 ng/ml of CEA antigen in PBS buffer, and later by detection of the same CEA concentrations in 100 % human blood serum.

The non-specificity test of CEA immunosensor was performed by preparing and testing various NSE protein concentrations (0, 1, 5, 10, 20, 50, and 100 ng/ml) in human blood serum.

In all experiments, functionalised MBs with anti-CEA antibody were used. Both experiments were done with three freshly made CEA immunosensors with the optimum concentration of capture and detection antibodies.

4.4. Results

4.4.1. CEA Assay Development

CEA assay were conducted using 2.4 mg/ml of antibody on the surface of MBs and 10 µg/ml of antibody on the surface of gold WEs. The CEA immunosensors were first prepared by the original method (Chapter 2, Section 2.2.7.1), and then were prepared by applying some optimisation such as steps as changing the SAM layer deactivation solution. Three triplicates were prepared and tested for different CEA concentrations.

The impedance measurements of samples with various CEA protein concentrations were done in triplicate with Auto GillAC instrument and the R_{et} values for sensors were calculated by ACM analysis V4 software. Table 4.1 presents the calculated values of R_{et} values, the amount (ΔR_{et}) and percentages of changes ($\%\Delta R_{et}$) in comparison with the baseline, which is the R_{et} value of functionalised SPE before applying the sample to the electrode surface. Functionalised SPEs have shown to have different amounts of resistance in their baselines. Consequently, to have a better comparison, ΔR_{et} was used to calculate the percentage of change in electron resistance of each electrode. The average values of $\%\Delta R_{et}$ (Table 4.1) was used to plot a graph (Figure 4.1A) against the protein concentration after normalising the values by subtracting the blank.

Some optimisations like the amount and incubation time of activation buffer, blocking agent and applying a washing step to the mixture of MBs and protein were used to improve the NSE assay. Therefore, those optimisation steps were applied to measure CEA concentrations. The calculated R_{et}, ΔR_{et}, and $\%\Delta R_{et}$ values are presented in Table 4.2. Figure 4.1B represent the standardised graph of CEA detection (0.0 – 100 ng/ml) by applying some optimisation steps.

Table 4.1: Calculated R_{et}, ΔR_{et}, and $\%\Delta R_{et}$ values for impedance measurements of CEA protein detection before applying optimisation steps.

		Baseline	0 ng/ml	1 ng/ml	10 ng/ml	100 ng/ml
R_{et} (Ω)	SPE1	50.85	56.45	67.16	69.23	78.53
	SPE2	156.9	193.7	222.0	247.5	233.0
	SPE3	190.7	233.6	249.2	279.8	270.4
ΔR_{et} (Ω)	SPE1	N/A	5.60	16.31	18.38	27.68
	SPE2	N/A	36.80	65.10	90.60	76.10
	SPE3	N/A	42.90	58.50	89.10	79.70

Conc. (ng/ml)	$\%\Delta R_{et}$ SPE1	$\%\Delta R_{et}$ SPE2	$\%\Delta R_{et}$ SPE3	Mean (Ω)	Mean – Mean (0)	SD	%CV
0	11.01	23.45	22.50	18.99	0.00	6.92	36.47
1	32.07	41.49	30.68	34.75	15.76	5.88	16.93
10	36.15	57.74	46.72	46.87	27.88	10.80	23.03
100	54.43	48.50	41.79	48.24	29.25	6.32	13.11

Table 4.2: Calculated R_{et}, ΔR_{et}, and $\%\Delta R_{et}$ values for impedance measurements of CEA protein detection after applying optimisation steps.

		Baseline	0 ng/ml	1 ng/ml	5 ng/ml	10 ng/ml	20 ng/ml	50 ng/ml	100 ng/ml
R_{et} (Ω)	SPE1	24.36	30.28	32.03	34.51	35.34	37.45	38.80	39.21
	SPE2	16.22	18.94	20.91	22.68	23.16	24.26	24.90	26.20
	SPE3	25.60	30.36	31.93	34.95	37.34	39.20	41.12	41.94
ΔR_{et} (Ω)	SPE1	N/A	5.92	7.67	10.15	10.98	13.09	14.44	14.85
	SPE2	N/A	2.72	4.69	6.46	6.94	8.04	8.68	9.98
	SPE3	N/A	4.76	6.33	9.35	11.74	13.60	15.52	16.34

Conc. (ng/ml)	$\%\Delta R_{et}$ SPE1	$\%\Delta R_{et}$ SPE2	$\%\Delta R_{et}$ SPE3	Mean	Mean – Mean (0)	SD	%CV
0	24.30	16.77	18.59	19.89	0.00	19.76	3.93
1	31.49	28.91	24.73	28.38	8.49	12.02	3.41
5	41.67	39.83	36.52	39.34	19.45	6.62	2.61
10	45.07	42.79	45.86	44.57	24.68	3.58	1.60
20	53.74	49.57	53.13	52.14	32.25	4.32	2.25
50	59.28	53.51	60.63	57.81	37.92	6.53	3.78
100	60.96	61.53	63.83	62.11	42.22	2.44	1.52

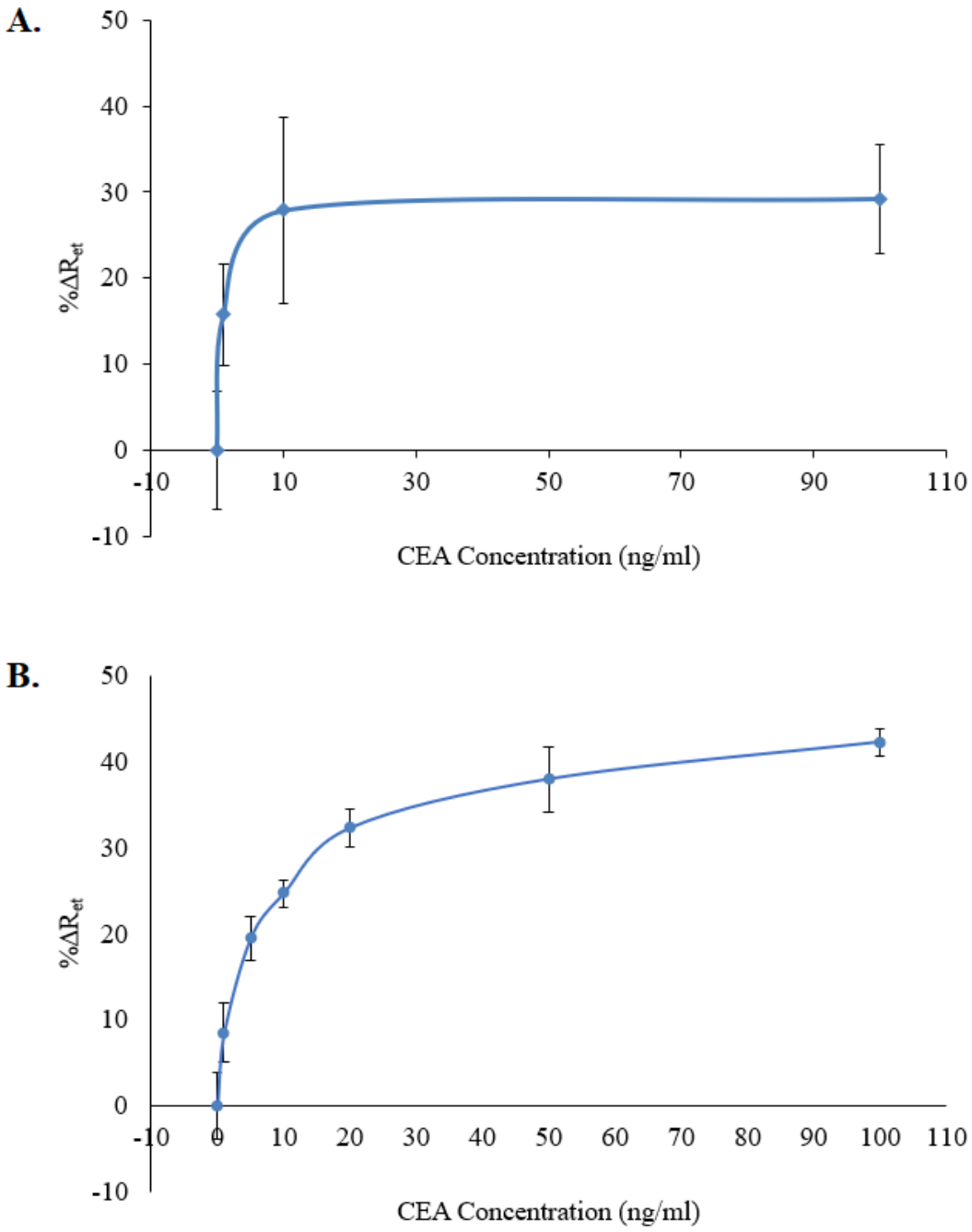

Figure 4.1: CEA antigen detection before (A) and after (B) applying some optimisations as replacing the SAM layer blockage solution with prepared ethanolamine in PBS buffer. The bars represent the average ± standard deviation of triplicates.

According to Figure 4.1A, increase in concentration of protein sample reached a ploto at around 10 ng/ml concentration in an unoptimized assay conditions. The signal clearly was increased by increasing the CEA concentration from 0 ng/ml to 10 ng/ml;

however, it did not increase much for 100 ng/ml CEA concentration. By applying optimisation steps (Figure 4.1B) as applying a washing step to the mixture of MBs and protein samples, and changing the SAM layer blockage solution, the signal clearly enhanced as error bars are reduced in comparison with Figure 4.1A and also, higher change in $\%\Delta R_{et}$ values were obtained.

Figure 4.2, illustrates the linear range response plot of CEA immunosensor $\%\Delta R_{et}$ against CEA concentrations in logarithmic format. It can be observed in Figure 4.3 that the sensor response logarithmically arises by increasing the concentration of CEA protein with correlation coefficient of the quantified samples of 0.9945. The LoD value was calculated as 0.68 ng/ml based on Equation 1 (Chapter 1).

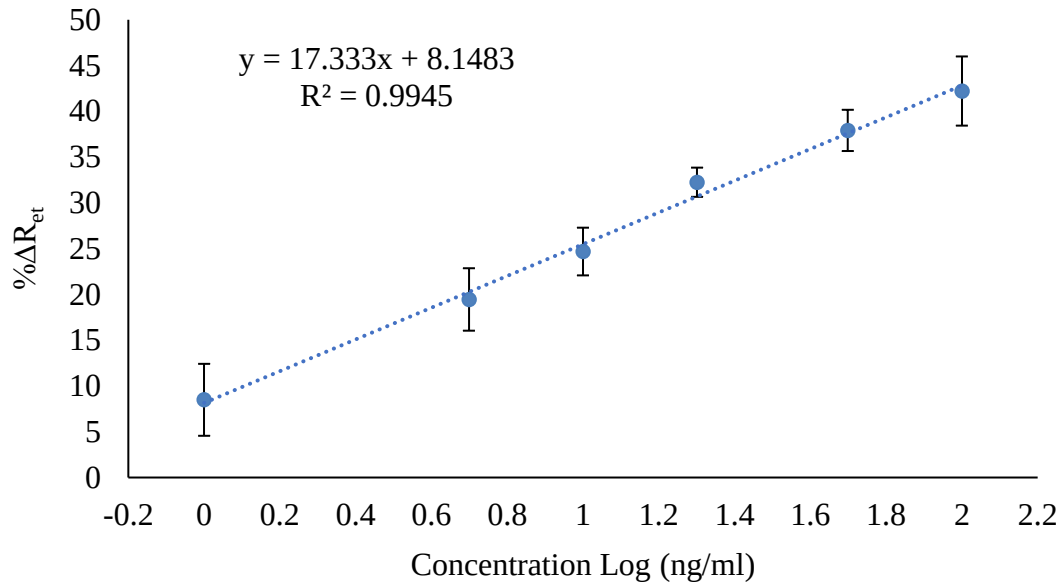

Figure 4.2: The linear range response of CEA immunosensor representing $\%\Delta R_{et}$ versus the $\log_{10}$ of CEA concentrations (1 – 100 ng/ml) in in buffer. The bars represent the average ± standard deviation of triplicates.

4.4.2 Optimisation of the CEA Immunosensor

Although the obtained LoD is below the cut-off value which is 5 ng/ml, in order to enhance the CEA assay and also to achieve a lower LoD value further optimisation experiments were performed.

4.4.2.1 Capture Antibody Concentration on MBs

To determine the optimum concentration of 12-140-10 antibody on the surface of the MBs, three MB solutions with the antibody concentration of 1.2, 2.4, and 3.6 mg/ml were prepared. The experiment was performed by fishing CEA from various sample concentrations (0, 1, 10, and 50 ng/ml) by functionalised MBs and measuring the analyte concentration with CEA immunosensor prepared by immobilising 20 µl of 10 µg/ml of 12-140-01 antibody, and use of EIS technique. The experimental results are presented as Nyquist plots in Figure 4.3 – 4.5. Table 4.3 – 4.5 show calculated R_{et}, ΔR_{et}, and $\%\Delta R_{et}$ values. The obtained mean of $\%\Delta R_{et}$ values for CEA measurement by use of functionalised MBs with different antibody concentrations were used to plot a comparison graph against the concentration of CEA. The comparison plot is presented in Figure 4.6.

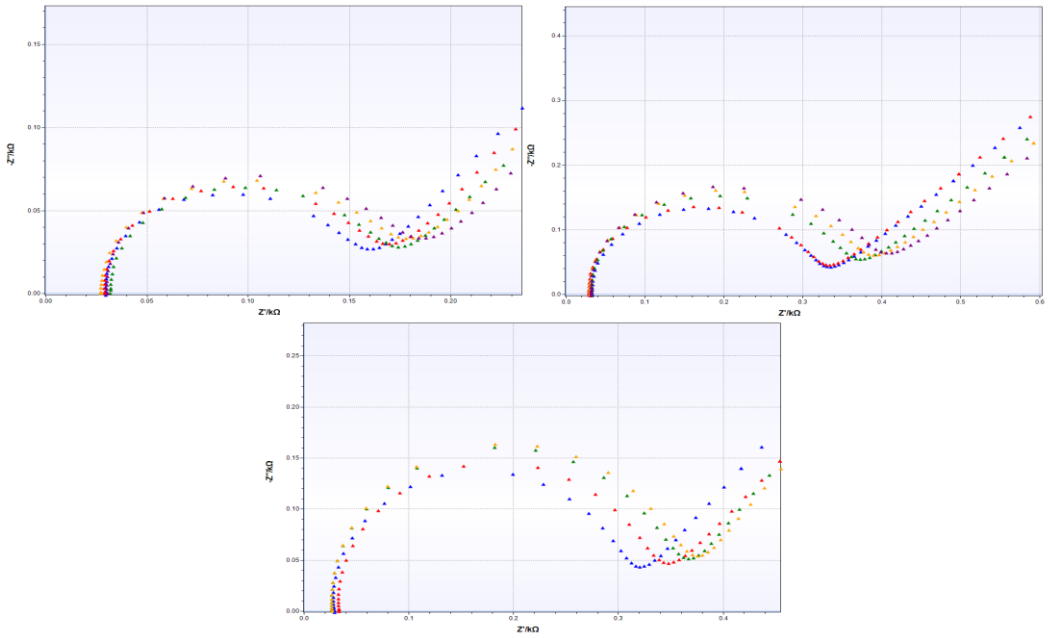

Figure 4.3: The Nyquist plots of Impedance measurements of protein detection by CEA immunosensor with use of prepared MBs with 1.2 mg/ml of 12-140-10 anti-CEA antibody. Each plot represents the impedance of single immunosensor. Functionalised SPE (Blue), 0 ng/ml CEA (Red), 1 ng/ml CEA (Green), 10 ng/ml CEA (Yellow), 50 ng/ml CEA (Purple).

Table 4.3: Calculated R_{et}, ΔR_{et}, and $\%\Delta R_{et}$ values of NSE sample measurements with use of prepared MBs with 1.2 mg/ml of capture antibody.

		Baseline	0 ng/ml	1 ng/ml	10 ng/ml	50 ng/ml
R_{et} (Ω)	SPE1	110.96	118.82	123.38	127.61	131.90
	SPE2	270.68	277.04	309.84	326.35	340.68
	SPE3	264.54	284.56	291.44	306.17	312.20
ΔR_{et} (Ω)	SPE1	N/A	7.86	12.42	16.65	15.01
	SPE2	N/A	6.36	39.16	55.67	10.00
	SPE3	N/A	20.02	26.90	41.63	47.66

Conc. (ng/ml)	$\%\Delta R_{et}$ SPE1	$\%\Delta R_{et}$ SPE2	$\%\Delta R_{et}$ SPE3	Mean	Mean – Mean (0)	SD	%CV
0	7.08	2.35	7.57	5.67	0.00	2.88	50.87
1	11.19	14.47	10.17	11.94	6.27	2.25	18.81
10	15.01	20.57	15.74	17.11	11.44	3.02	17.65
50	18.87	25.86	18.02	20.92	15.25	4.30	20.58

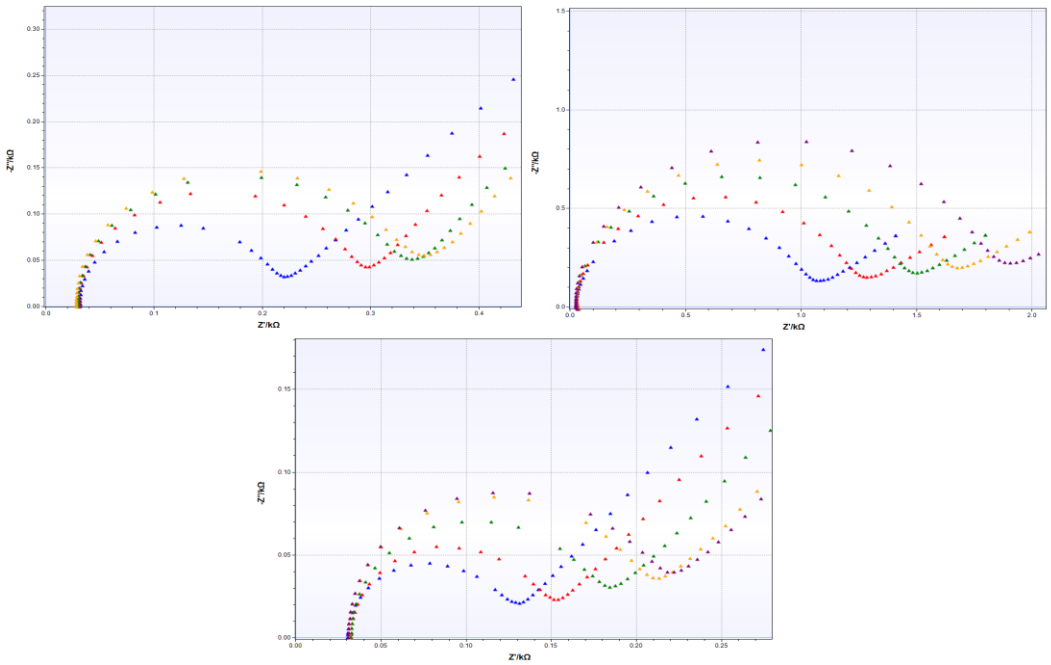

Figure 4.4: The Nyquist plots of Impedance measurements of protein detection by CEA immunosensor with use of prepared MBs with 2.4 mg/ml of 12-140-10 anti-CEA antibody. Each plot represents the impedance of single immunosensor. Functionalised SPE (Blue), 0 ng/ml CEA (Red), 1 ng/ml CEA (Green), 10 ng/ml CEA (Yellow), 50 ng/ml CEA (Purple).

Table 4.4: Calculated R_{et}, ΔR_{et}, and $\%\Delta R_{et}$ values of NSE sample measurements with use of prepared MBs with 2.4 mg/ml of capture antibody.

		Baseline	0 ng/ml	1 ng/ml	10 ng/ml	50 ng/ml
R_{et} (Ω)	SPE1	168.77	199.72	234.30	270.09	282.36
	SPE2	951.60	1147.90	1351.40	1515.50	1719.40
	SPE3	96.06	115.11	132.74	159.42	166.64
ΔR_{et} (Ω)	SPE1	N/A	30.95	65.53	101.32	113.59
	SPE2	N/A	196.30	399.80	563.90	767.80
	SPE3	N/A	19.05	36.68	63.36	70.58

Conc. (ng/ml)	$\%\Delta R_{et}$ SPE1	$\%\Delta R_{et}$ SPE2	$\%\Delta R_{et}$ SPE3	Mean	Mean – Mean (0)	SD	%CV
0	18.34	20.63	19.83	19.60	0.00	1.16	5.93
1	38.83	42.01	38.18	39.67	20.07	2.05	5.16
10	60.03	59.26	65.96	61.75	42.15	3.67	5.94
50	67.30	80.69	73.47	73.82	54.22	6.70	9.08

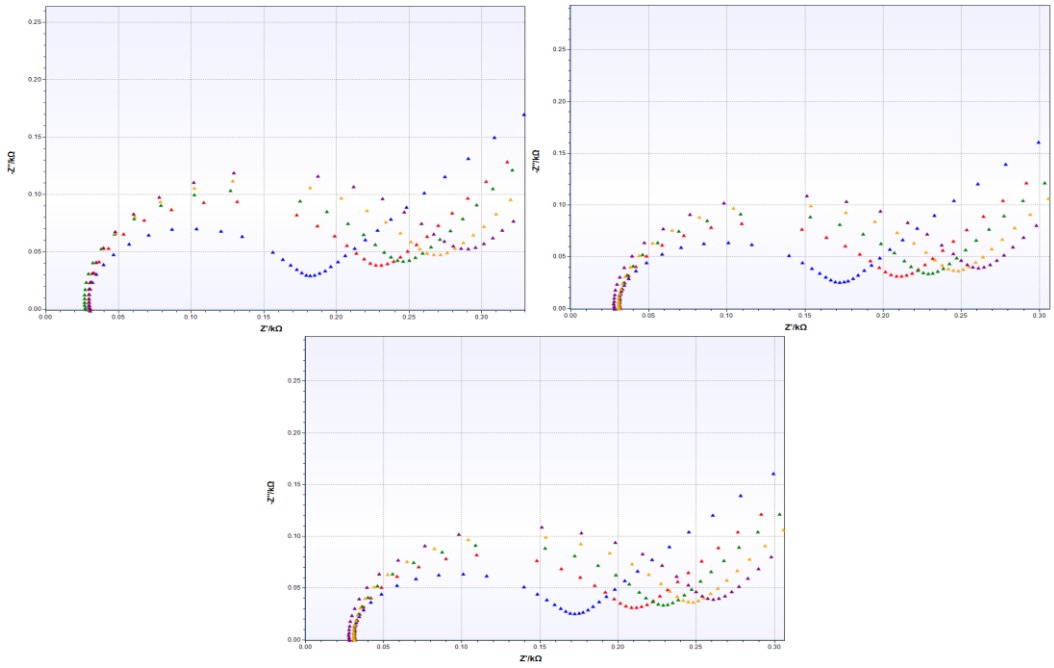

Figure 4.5: The Nyquist plots of Impedance measurements of protein detection by CEA immunosensor with use of prepared MBs with 3.6 mg/ml of 12-140-10 anti-CEA antibody. Each plot represents the impedance of single immunosensor. Functionalised SPE (Blue), 0 ng/ml CEA (Red), 1 ng/ml CEA (Green), 10 ng/ml CEA (Yellow), 50 ng/ml CEA (Purple).

Table 4.5: Calculated R_{et}, ΔR_{et}, and $\%\Delta R_{et}$ values of NSE sample measurements with use of prepared MBs with 3.6 mg/ml of capture antibody.

		Baseline	0 ng/ml	1 ng/ml	10 ng/ml	50 ng/ml
R_{et} (Ω)	SPE1	135.51	168.94	191.51	208.53	225.10
	SPE2	303.43	373.74	449.50	480.45	507.41
	SPE3	120.43	153.91	171.59	187.92	205.90
ΔR_{et} (Ω)	SPE1	N/A	33.43	56.00	73.02	89.59
	SPE2	N/A	70.31	146.07	177.02	203.98
	SPE3	N/A	33.48	51.16	67.49	85.47

Conc. (ng/ml)	$\%\Delta R_{et}$ SPE1	$\%\Delta R_{et}$ SPE2	$\%\Delta R_{et}$ SPE3	Mean	Mean – Mean (0)	SD	%CV
0	24.67	23.17	27.80	25.21	0.00	2.36	9.37
1	41.33	48.14	42.80	43.98	18.77	3.65	8.29
10	53.89	58.34	56.04	56.09	30.88	2.23	3.97
50	66.11	67.22	70.97	68.10	42.89	2.55	3.74

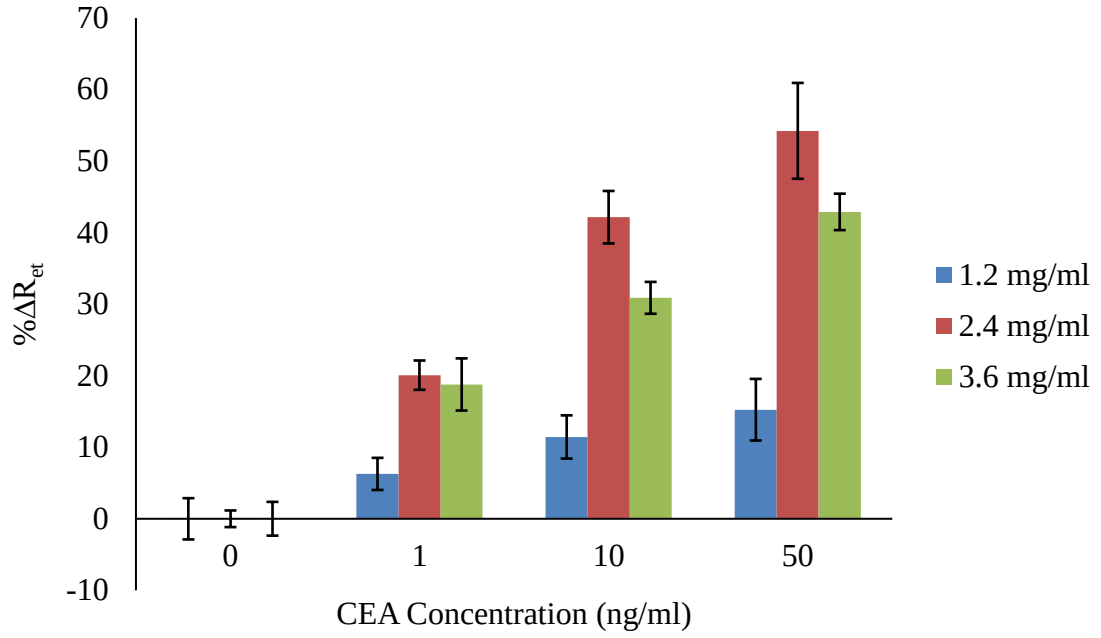

Figure 4.6: The comparison of CEA detection by use of MBs with various concentration of antibody on their surfaces. The bars represent the average ± standard deviation of triplicates.

According to Figure 4.6, changes in impedance signals were obtained by increasing the analyte concentration in all three parts of this experiment. The lowest changes in sensor response were obtained when the MBs with 1.2 mg/ml of antibody on their surface was used. As the antibody concentration increased from 1.2 to 2.4 mg/ml higher changes in immunosensor response were achieved. Further increase of antibody concentration from 2.4 to 3.6 mg/ml resulted in reduction of changes in resistance of electron transfer which might be due to steric hindrance effect.

The results of analyte measurement by CEA immunosensor and use of functionalised MBs with various antibody concentrations show that the highest changes in $\%\Delta R_{et}$ values were obtained by using prepared MBs with antibody concentration of 2.4 mg/ml. Therefore, from the tested concentrations (1.2, 2.4, and 3.6 mg/ml) 2.4 mg/ml was chosen as an optimum concentration for further experiments.

4.4.2.2 Detection Antibody Concentration on SPE

To achieve the optimum concentration level detection antibody, three concentrations of 12-140-01 anti-CEA antibody as 5, 10, and 20 µg/ml were used to prepare CEA immunosensor. After preparation of CEA immunosensors, they have been used to detect various concentration of CEA within the PBS buffer. The experimental results are presented as Nyquist plots in Figure 4.7 – 4.9; and the calculated R_{et}, ΔR_{et}, and $\%\Delta R_{et}$ values are represented in Table 4.6 – 4.8. In order to compare the results, a comparison graph was plotted based on the mean of $\%\Delta R_{et}$ values after normalising to zero against the CEA concentration (ng/ml).

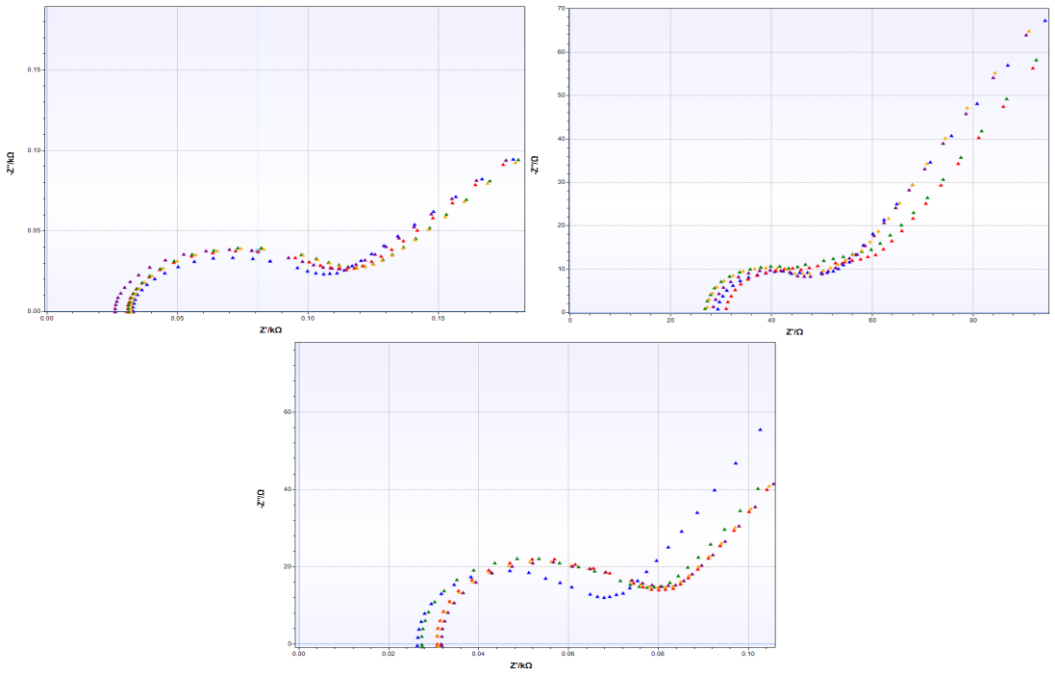

Figure 4.7: The Nyquist plots of Impedance measurements of CEA detection by prepared CEA immunosensor with use of 5 µg/ml of 12-140-01 anti-CEA antibody. Each plot represents the impedance of single immunosensor. Functionalised SPE (Blue), 0 ng/ml NSE (Red), 1 ng/ml NSE (Green), 10 ng/ml NSE (Yellow), 50 ng/ml NSE (Purple).

Table 4.6: Calculated R_{et}, ΔR_{et}, and $\%\Delta R_{et}$ values of NSE sample measurements with use of prepared NSE immunosensors with 5 µg/ml of detection antibody.

		Baseline	0 ng/ml	1 ng/ml	10 ng/ml	50 ng/ml
R_{et} (Ω)	SPE1	59.46	65.69	68.43	69.18	70.19
	SPE2	16.23	16.81	17.16	18.15	19.26
	SPE3	33.31	36.28	37.08	37.62	39.35
ΔR_{et} (Ω)	SPE1	N/A	6.23	8.97	9.72	10.73
	SPE2	N/A	0.58	0.93	1.92	3.03
	SPE3	N/A	2.97	3.77	431	6.04

Conc. (ng/ml)	$\%\Delta R_{et}$ SPE1	$\%\Delta R_{et}$ SPE2	$\%\Delta R_{et}$ SPE3	Mean	Mean – Mean (0)	SD	%CV
0	10.48	3.57	8.92	7.66	0.00	3.62	47.29
1	15.09	5.73	11.32	10.71	3.05	4.71	43.94
10	16.35	11.83	12.94	13.71	6.05	2.35	17.17
50	18.05	18.67	18.13	18.28	10.62	0.34	1.85

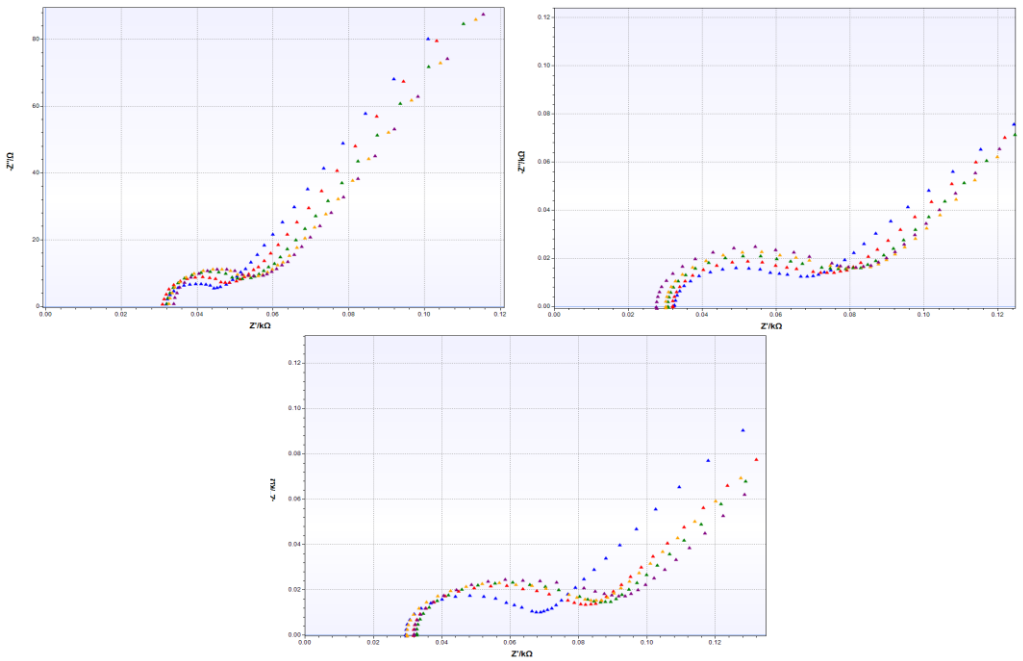

Figure 4.8: The Nyquist plots of Impedance measurements of CEA detection by prepared CEA immunosensor with use of 10 µg/ml of 12-140-01 anti-CEA antibody. Each plot represents the impedance of single immunosensor. Functionalised SPE (Blue), 0 ng/ml NSE (Red), 1 ng/ml NSE (Green), 10 ng/ml NSE (Yellow), 50 ng/ml NSE (Purple).

Table 4.7: Calculated R_{et}, ΔR_{et}, and $\%\Delta R_{et}$ values of NSE sample measurements with use of prepared NSE immunosensors with 10 µg/ml of detection antibody.

		Baseline	0 ng/ml	1 ng/ml	10 ng/ml	50 ng/ml
R_{et} (Ω)	SPE1	11.33	14.22	16.18	17.40	17.63
	SPE2	27.15	33.86	36.22	38.92	42.90
	SPE3	39.68	38.81	40.29	43.03	44.25
ΔR_{et} (Ω)	SPE1	N/A	2.89	4.85	6.07	6.30
	SPE2	N/A	6.71	9.07	11.77	15.75
	SPE3	N/A	9.13	10.61	13.35	14.57

Conc. (ng/ml)	$\%\Delta R_{et}$ SPE1	$\%\Delta R_{et}$ SPE2	$\%\Delta R_{et}$ SPE3	Mean	Mean – Mean (0)	SD	%CV
0	25.51	24.71	30.76	26.99	0.00	3.29	12.17
1	42.81	33.41	35.75	37.32	10.33	4.89	13.11
10	53.57	43.35	44.98	47.30	20.31	5.49	11.61
50	55.60	58.01	46.46	53.36	26.37	6.09	11.42

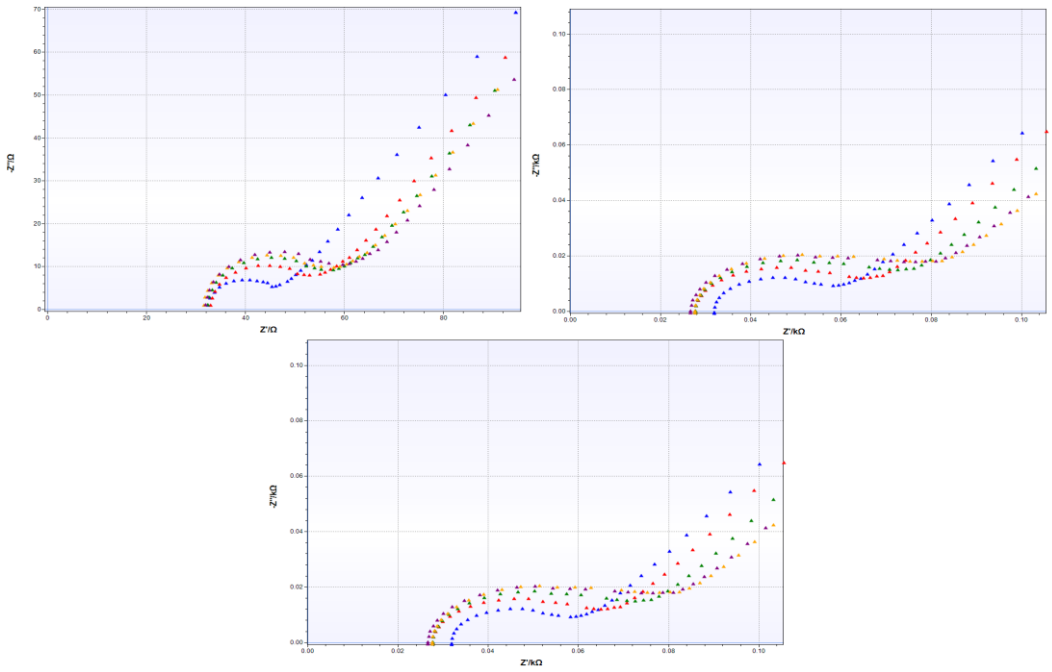

Figure 4.9: The Nyquist plots of Impedance measurements of CEA detection by prepared CEA immunosensor with use of 20 µg/ml of 12-140-01 anti-CEA antibody. Each plot represents the impedance of single immunosensor. Functionalised SPE (Blue), 0 ng/ml NSE (Red), 1 ng/ml NSE (Green), 10 ng/ml NSE (Yellow), 50 ng/ml NSE (Purple).

Table 4.8: Calculated R_{et}, ΔR_{et}, and $\%\Delta R_{et}$ values of NSE sample measurements with use of prepared NSE immunosensors with 20 µg/ml of detection antibody.

		Baseline	0 ng/ml	1 ng/ml	10 ng/ml	50 ng/ml
R_{et} (Ω)	SPE1	11.41	16.80	19.52	20.58	21.54
	SPE2	21.61	32.35	36.36	37.43	38.68
	SPE3	20.23	27.76	33.60	36.17	36.36
ΔR_{et} (Ω)	SPE1	N/A	5.39	8.11	9.17	10.13
	SPE2	N/A	10.74	14.75	15.82	17.07
	SPE3	N/A	7.53	13.37	15.94	16.13

Conc. (ng/ml)	$\%\Delta R_{et}$ SPE1	$\%\Delta R_{et}$ SPE2	$\%\Delta R_{et}$ SPE3	Mean	Mean – Mean (0)	SD	%CV
0	47.24	49.70	37.22	44.72	0.00	6.61	14.78
1	78.00	68.26	61.59	69.28	24.56	8.25	11.91
10	88.78	73.21	78.79	80.26	35.54	7.89	9.83
50	92.29	78.99	79.73	83.67	38.95	7.47	8.93

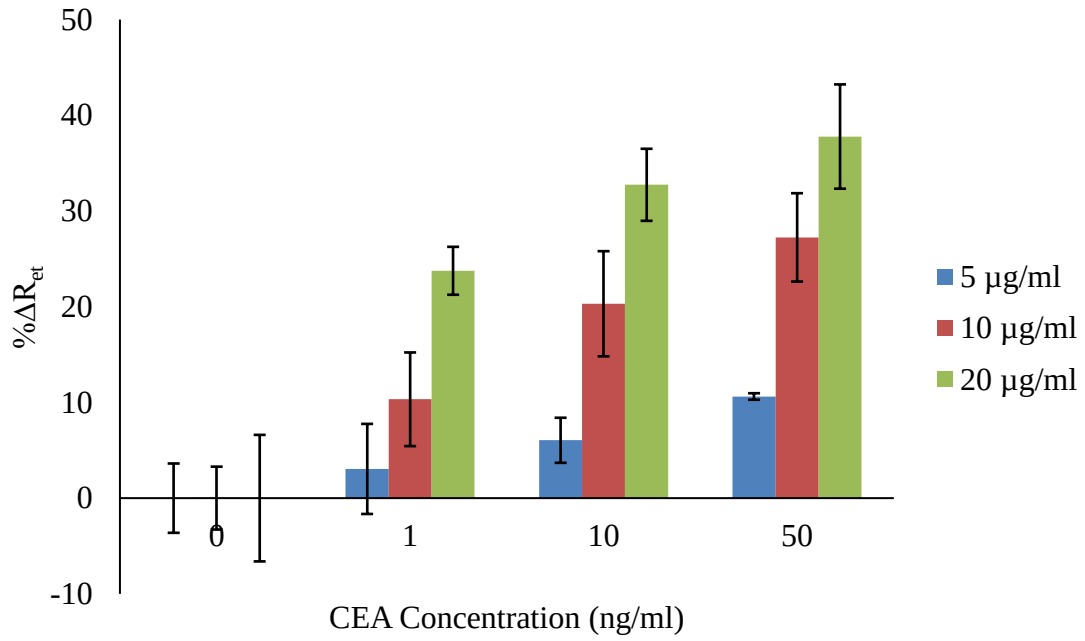

Figure 4.10: The comparison of CEA detection with use of prepared NSE immunosensors with various concentration of antibody on their surfaces. The bars represent the average ± standard deviation of triplicates.

Figure 4.10, shows the percentage of changes in resistance of electron transfer by measuring the analyte concentration. The lowest signals were obtained by immobilising 5 µg/ml of 12-140-01 antibody on the surface of WEs. As the concentration of immobilised antibody on the surface of CEA immunosensor increased, higher changes in detection signals were obtained. For instance, the obtained values for measurement of 1 ng/ml with use of 5 µg/ml of antibody was calculated as 3.05% after normalising to zero; while it raised to 10.33% and 24.56% by increasing the antibody concentration to 10 µg/ml and 20 µg/ml, respectively.

The biggest changes in percentages of ΔRet are achieved by using prepared CEA immunosensors with antibody concentration of 20 µg/ml on their surfaces, which suggest 20 µg/ml as the optimum antibody concentration of the concentrations tested. Although further increase of detection antibody concentration might result in more enhanced signals, due to economical reason higher antibody concentrations were not tested. Therefore, 20 µg/ml was chosen as an optimum concentration of 12-140-01 antibody for further experiments.

4.4.3. Standard Plot of Optimised CEA Immunosensor

After testing some optimisation steps from CHAPTER 3, and choosing the optimum concentration of antibodies on both MBs and immunosensors, the CEA immunosensor was used to measure the CEA concentrations in PBS buffer and later in spiked serum samples. The CEA immunosensors were also used to measure NSE protein in spiked serum samples as non-specific analyte to check sensor cross-reactivity.

4.4.3.1 CEA Detection in Buffer

Various CEA concentration in PBS buffer (0 – 100 ng/ml) were measured by CEA immunosensors to create a standard curve. Functionalised MBs (2.4 mg/ml of 12-140-10 antibody) were used to fish the analyte from the sample and 20 µg/ml of 12-140-01 was used on the sensor surface. The protein concentrations were measured by EIS technique

and the experimental results are presented as Nyquist plots in Figure 4.11; and calculated R_{et}, ΔR_{et}, and $\%\Delta R_{et}$ values are shown in Table 4.9.

After normalising the mean $\%\Delta R_{et}$ values (Table 4.9) to zero, they were used to plot standard curve against the CEA concentration (Figure 4.12) and also to plot the linear range response of CEA immunosensor in buffer versus the logarithmic format of CEA concentration (Figure 4.13).

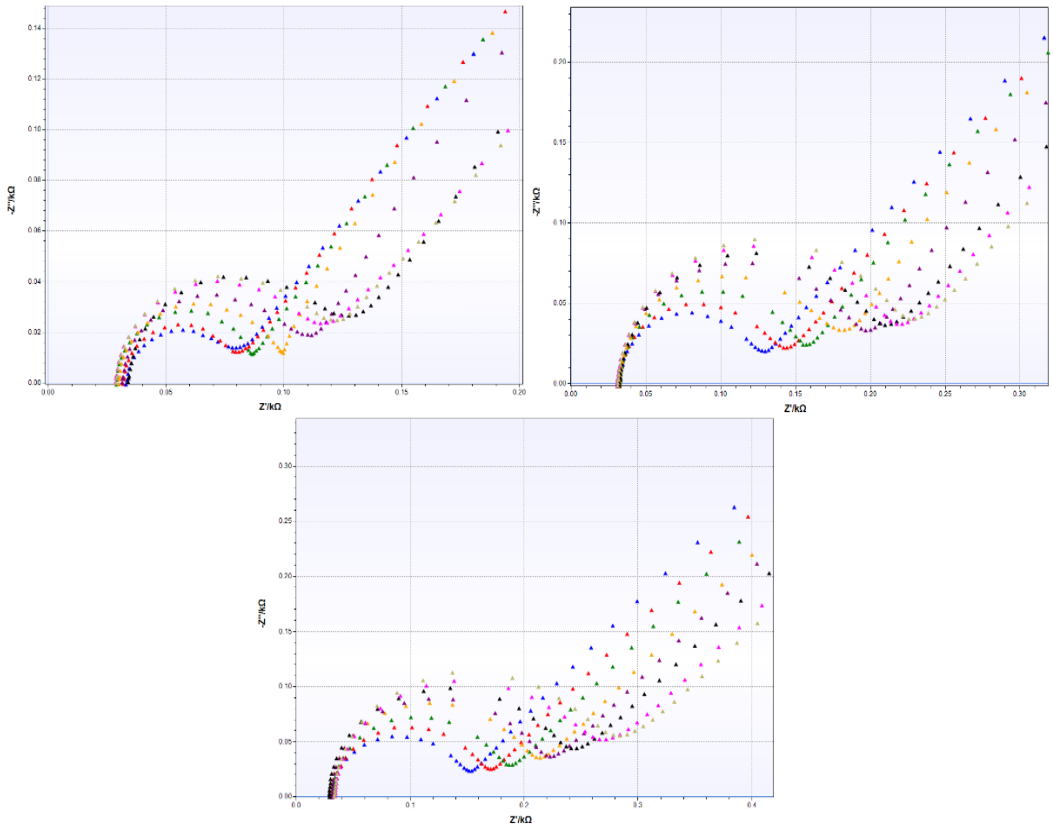

Figure 4.11: The Nyquist plots for impedance of CEA protein detection in PBS buffer by CEA immunosensors. Each graph represents the impedance measurements of single NSE immunosensor. Functionalised SPE (Blue), 0 ng/ml (Red), 1 ng/ml (Green), 5 ng/ml (Yellow), 10 ng/ml (Purple), 20 ng/ml (Black), 50 ng/ml (Pink), 100 ng/ml (Khaki).

Table 4.9: Calculated R_{et}, ΔR_{et}, and $\%\Delta R_{et}$ values for impedance measurements of CEA protein detection in PBS buffer.

		Baseline	0 ng/ml	1 ng/ml	5 ng/ml	10 ng/ml	20 ng/ml	50 ng/ml	100 ng/ml
R_{et} (Ω)	SPE1	35.01	38.06	46.21	55.08	61.90	67.51	73.80	76.46
	SPE2	81.09	92.71	104.7	123.0	139.2	153.2	163.5	171.0
	SPE3	102.96	119.3	137.0	161.4	170.5	189.9	207.0	225.0
ΔR_{et} (Ω)	SPE1	N/A	3.05	11.20	20.07	26.89	32.50	38.79	41.45
	SPE2	N/A	11.62	23.59	41.90	58.12	72.10	82.36	89.87
	SPE3	N/A	16.30	33.33	58.42	67.54	86.92	104.08	122.04

Conc. (ng/ml)	$\%\Delta R_{et}$ SPE1	$\%\Delta R_{et}$ SPE2	$\%\Delta R_{et}$ SPE3	Mean	Mean – Mean (0)	SD	%CV
0	8.71	14.33	15.83	12.96	0.00	3.75	28.96
1	31.99	29.09	32.37	31.15	18.19	1.79	5.76
5	57.33	51.67	56.74	55.25	42.29	3.11	5.63
10	76.81	71.67	65.60	71.36	58.40	5.61	7.86
20	92.83	88.91	84.42	88.72	75.76	4.21	4.74
50	110.80	101.57	101.09	104.49	91.53	5.47	5.24
100	118.39	110.83	114.54	114.59	101.63	3.78	3.30

According to Figure 4.12, increasing the concentration CEA protein has caused increase in impedance measurements. Also, comparing the standardised curve with the standardised curve before optimising the antibody concentration on the surface of immunosensor (Section 4.4.1) indicates the enhancement of sensor response. The linear range response of CEA sensor response (Figure 4.13) also indicates logarithmically raise sensor response by increasing the analyte concentration. The LoD was calculated based on Equation 1 as 0.26 ng/ml with correlation coeffiecient of 0.9924. The obtained LoD is lower than the calculated LoD of CEA immunosensor before optimisations (0.68 ng/ml), though the correlation coefficient is almost the same (un-optimised value = 0.9945). The sensor response was stable with lower error bars, showing excellent sensitivity and reproducibility.

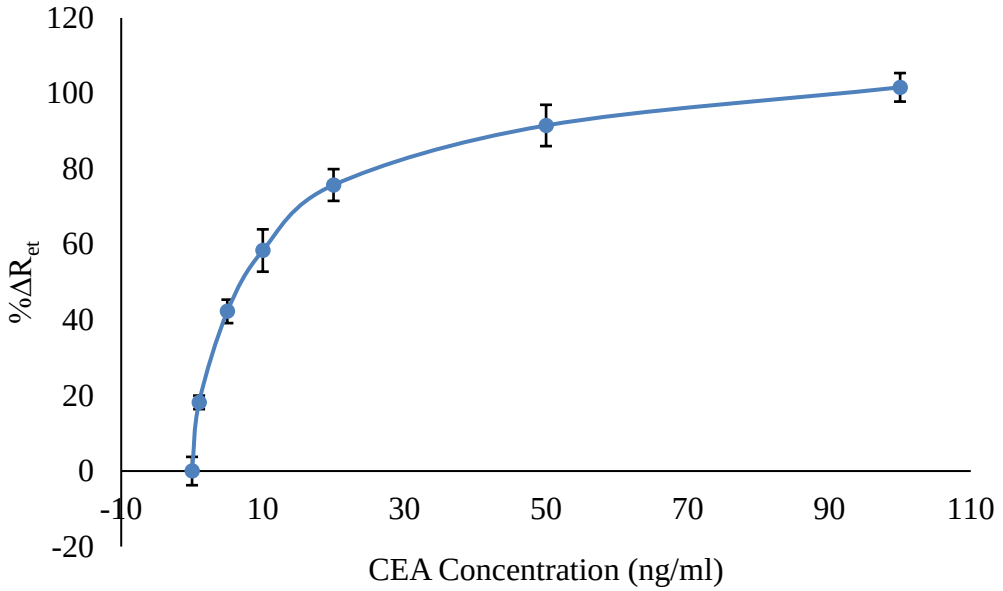

Figure 4.12: Standardised CEA immunosensor response plot created for detection of different CEA concentrations (0.0 – 100 ng/ml) in PBS buffer. The bars represent the average ± standard deviation of triplicates.

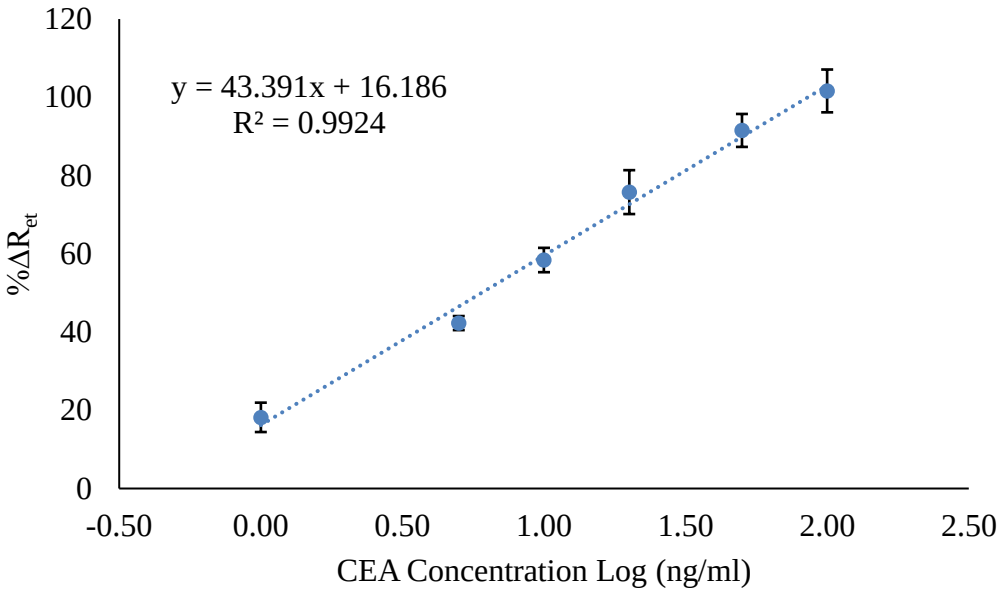

Figure 4.13: The linear range response of CEA immunosensor representing $\%\Delta R_{et}$ versus the $\log_{10}$ of CEA concentrations (1 – 100 ng/ml) in PBS buffer. The bars represent the average ± standard deviation of triplicates.

4.4.3.2 CEA Detection in Human Serum Samples

After improvement of CEA immunosensor response in PBS buffer by optimising the sensor, the immunosensor response was checked with various concentration of CEA protein (0 – 100 ng/ml) spiked in 100 % serum with use of functionalised MBs and sensing platform. The experimental data are presented as Nyquist plots in Figure 4.14 and Table 4.10.

Increasing the concentration of CEA has resulted in increase of the real component of the impedance. This caused due to the binding of MB-CEA complex to the surface antibodies which block the WEs surface and reduces transfer of electrons to the electrode. A standardised curve (Figure 4.15) was then created based on the calculated $\%\Delta R_{et}$ (Table 4.10) after normalising to zero, against the CEA concentrations.

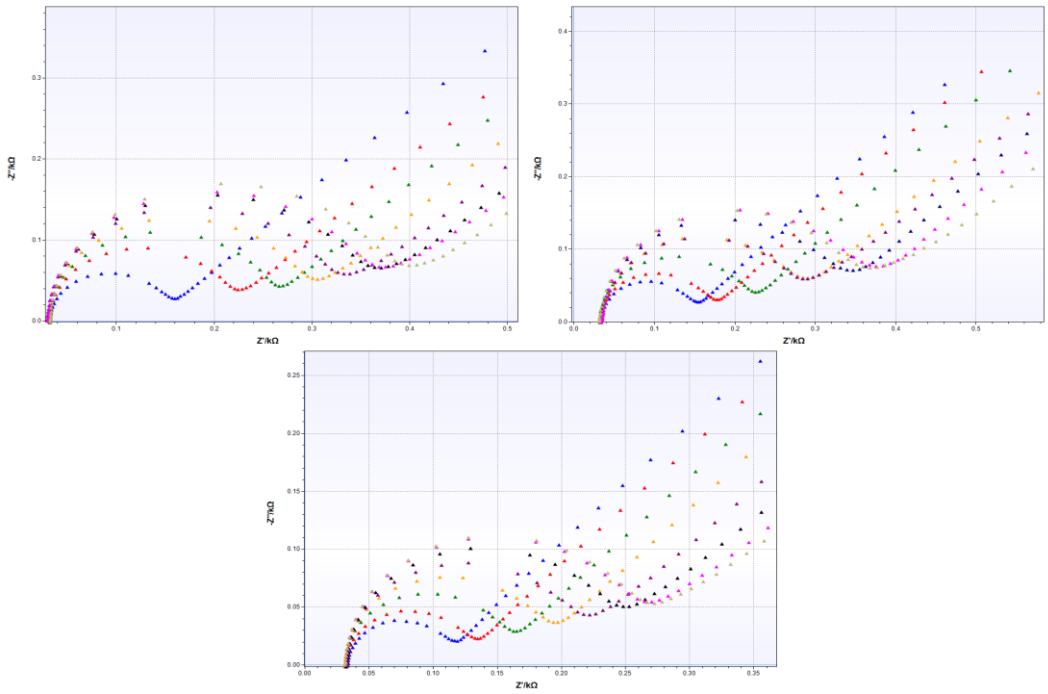

Figure 4.14: The Nyquist plots for impedance of CEA protein detection in Serum by CEA immunosensors. Each graph represents the impedance measurements of single CEA immunosensor. Functionalised SPE (Blue), 0 ng/ml (Red), 1 ng/ml (Green), 5 ng/ml (Yellow), 10 ng/ml (Purple), 20 ng/ml (Black), 50 ng/ml (Pink), 100 ng/ml (Khaki).

Table 4.10: Calculated R_{et}, ΔR_{et}, and $\%\Delta R_{et}$ values for impedance measurements of CEA protein detection in serum.

		Baseline	0 ng/ml	1 ng/ml	5 ng/ml	10 ng/ml	20 ng/ml	50 ng/ml	100 ng/ml
R_{et} (Ω)	SPE1	110.3	171.7	209.8	245.8	277.0	304.7	313.5	335.5
	SPE2	100.9	126.2	169.5	224.5	228.4	273.8	301.1	308.0
	SPE3	68.94	86.00	114.6	142.6	168.3	194.1	213.6	219.2
ΔR_{et} (Ω)	SPE1	N/A	61.56	99.53	135.5	166.66	194.4	203.2	225.2
	SPE2	N/A	25.25	98.59	123.54	127.51	172.90	200.2	207.0
	SPE3	N/A	17.10	45.65	73.63	99.38	125.12	144.7	150.3

Conc. (ng/ml)	$\%\Delta R_{et}$ SPE1	$\%\Delta R_{et}$ SPE2	$\%\Delta R_{et}$ SPE3	Mean	Mean – Mean (0)	SD	%CV
0	55.81	25.02	24.80	35.21	0.00	17.84	50.66
1	90.24	67.96	66.22	74.81	39.60	13.39	17.90
5	122.86	122.40	106.80	117.35	82.14	9.14	7.79
10	151.10	126.34	144.15	140.53	105.32	12.77	9.09
20	176.20	171.31	181.49	176.33	141.12	5.09	2.89
50	184.24	198.34	209.82	197.47	162.26	12.81	6.49
100	204.17	205.13	217.94	209.08	173.87	7.69	3.68

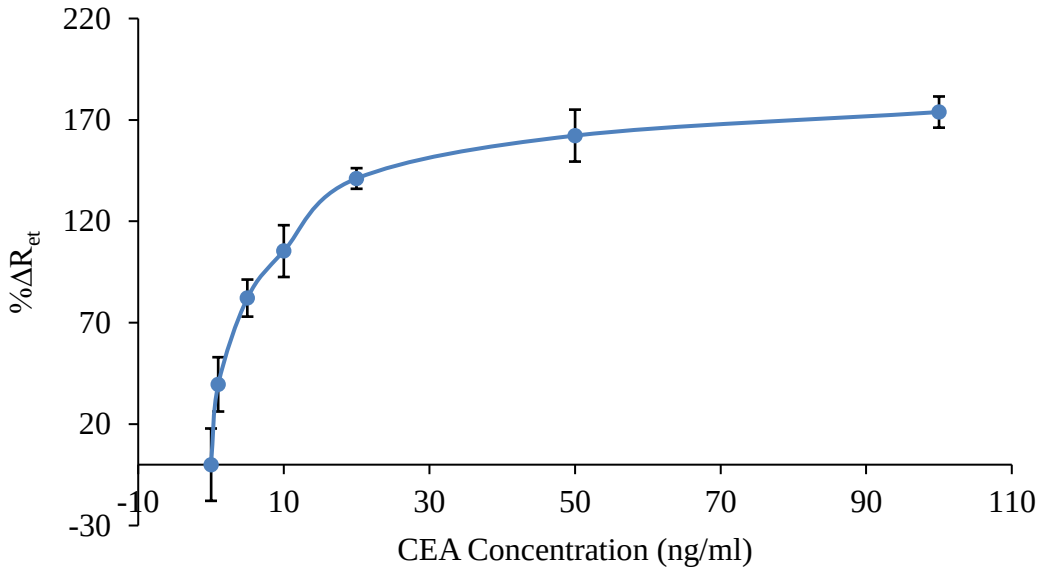

Figure 4.15: Standardised CEA immunosensor response plot created for detection of different CEA concentrations (0.0 – 100 ng/ml) in serum. The bars represent the average ± standard deviation of triplicates.

It can be observed from Figure 4.15 that the CEA immunosensor response to various concentrations of antigen in serum has raised by measuring higher analyte concentrations. Therefore, CEA immunosensor were successful in measuring the CEA concentrations spiked in 100 % serum.

Figure 4.16 represents the linear range response of CEA immunosensor. The linear range response was plotted based on the $\%\Delta R_{et}$ and the logarithmic format of CEA concentrations. As Figure 4.17 shows, the percentage of changes in R_{et} logarithmically increases by increasing the analyte concentration with correlation coefficient of the quantified samples of 0.9839 and calculated LoD value of 0.76 ng/ml. The obtained LoD for analyte detection in serum is slightly higher than calculated LoD of CEA detection in buffer which was 0.26 ng/ml. However, the LoD value is lower than the cut-off value which is 5 ng/ml.

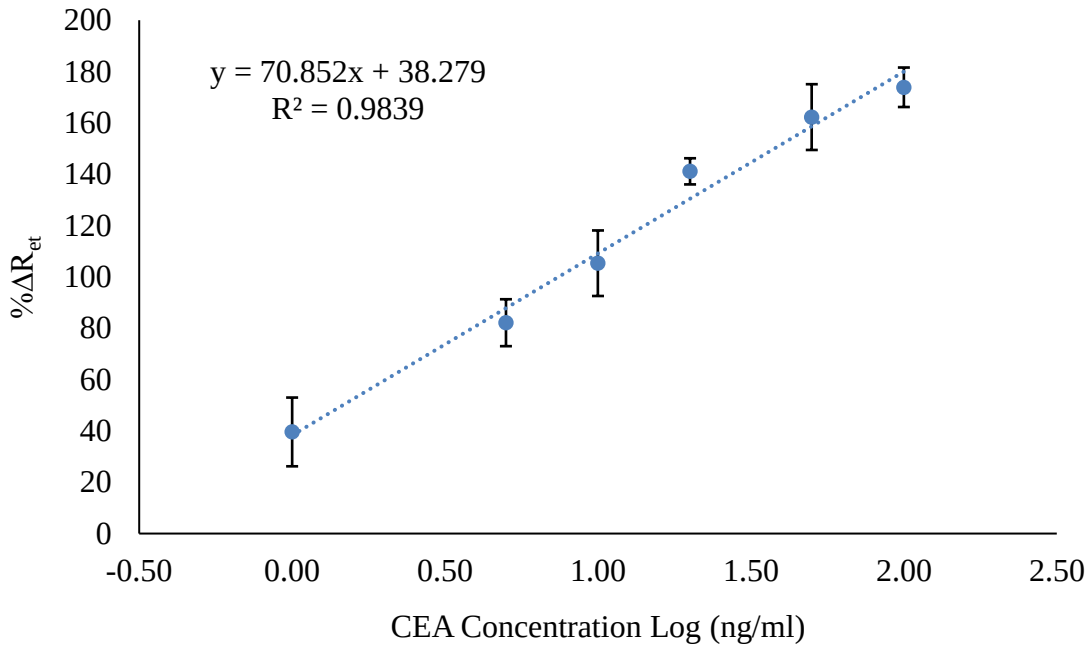

Figure 4.16: The linear range response of CEA immunosensor representing $\%\Delta R_{et}$ versus the $\log_{10}$ of CEA concentrations (1 – 100 ng/ml) in serum. The bars represent the average ± standard deviation of triplicates.

4.4.3.3 Specificity Test

The CEA immunosensor have successfully detected the different concentrations of CEA analyte in both PBS buffer and 100 % serum. To confirm the specificity of the sensor the assay was repeated using NSE protein as the analyte on the CEA immunosensor. The experiment was carried out by measuring various concentrations of NSE protein (0.0 – 100 ng/ml) spiked in 100 % by the CEA immunosensor. The experimental results are presented as Nyquist plot in Figure 4.17, and Table 4.11 represents the calculated $\%\Delta R_{et}$ values.

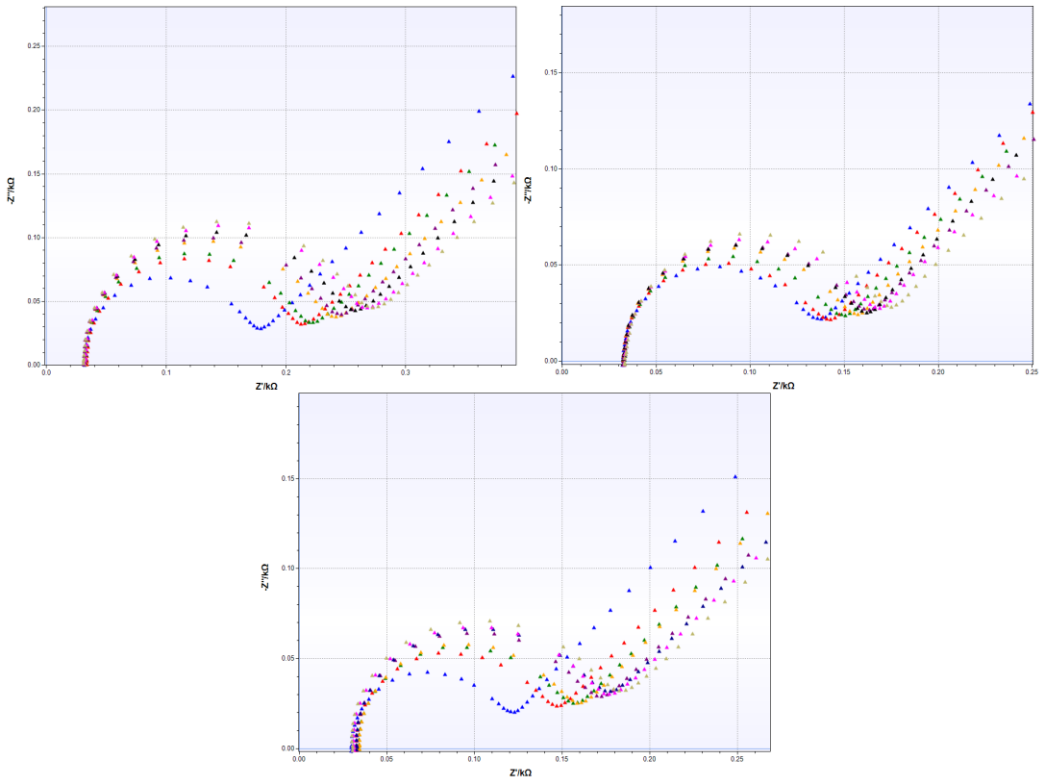

Figure 4.17: The Nyquist plots for impedance of NSE protein detection in serum by CEA immunosensors. Each graph represents the impedance measurements of single CEA immunosensor. Functionalised SPE (Blue), 0 ng/ml (Red), 1 ng/ml (Green), 5 ng/ml (Yellow), 10 ng/ml (Purple), 20 ng/ml (Black), 50 ng/ml (Pink), 100 ng/ml (Khaki).

Table 4.11: Calculated R_{et}, ΔR_{et}, and $\%\Delta R_{et}$ values for CEA immunosensor impedance measurements of cross-reactivity test in serum.

		Baseline	0 ng/ml	1 ng/ml	5 ng/ml	10 ng/ml	20 ng/ml	50 ng/ml	100 ng/ml
R_{et} (Ω)	SPE1	130.34	161.9	170.8	188.7	192.7	202.3	212.7	219.9
	SPE2	74.45	94.99	100.8	107.4	112.7	112.1	119.1	124.8
	SPE3	77.57	99.08	106.8	109.3	121.9	126.6	128.8	136.1
ΔR_{et} (Ω)	SPE1	N/A	31.52	40.46	58.38	62.34	71.96	82.36	89.49
	SPE2	N/A	20.54	26.37	32.95	38.20	37.66	44.60	20.38
	SPE3	N/A	20.30	28.06	30.48	43.11	47.80	19.98	57.34

Conc. (ng/ml)	$\%\Delta R_{et}$ SPE1	$\%\Delta R_{et}$ SPE2	$\%\Delta R_{et}$ SPE3	Mean	Mean – Mean (0)	SD	%CV
0	24.18	27.59	25.77	25.85	0.00	1.70	6.59
1	31.04	35.42	35.62	34.03	8.18	2.59	7.60
5	44.79	44.26	38.69	42.58	16.73	3.38	7.94
10	47.83	51.31	54.72	51.29	25.44	3.45	6.72
20	55.21	50.58	60.68	55.49	29.64	5.05	9.10
50	63.19	59.91	63.44	62.18	36.33	1.97	3.17
100	68.66	67.67	72.78	69.70	43.85	2.71	3.89

The calculated $\%\Delta R_{et}$ values of specific (CEA protein, Table 4.10) and non-specific (NSE protein, Table 4.11) analyte detection in serum by CEA immunosensor were compared in Figure 4.18. It can be observed from the comparison graph (Figure 4.18) that increasing NSE antigen concentration has resulted in increase of sensor response, even though it is not specific analyte to the sensor. The generated signals for measurement of NSE protein concentration are very low in comparison with CEA antigen measurement. As an example, the highest changes in $\%\Delta R_{et}$ of NSE protein measurement after normalising to zero was calculated as 43.85% which was obtained for the 100 ng/ml of NSE, while $\%\Delta R_{et}$ of 39.60% and 82.14% were achieved for detection of 1 ng/ml and 5 ng/ml of CEA protein, respectively.

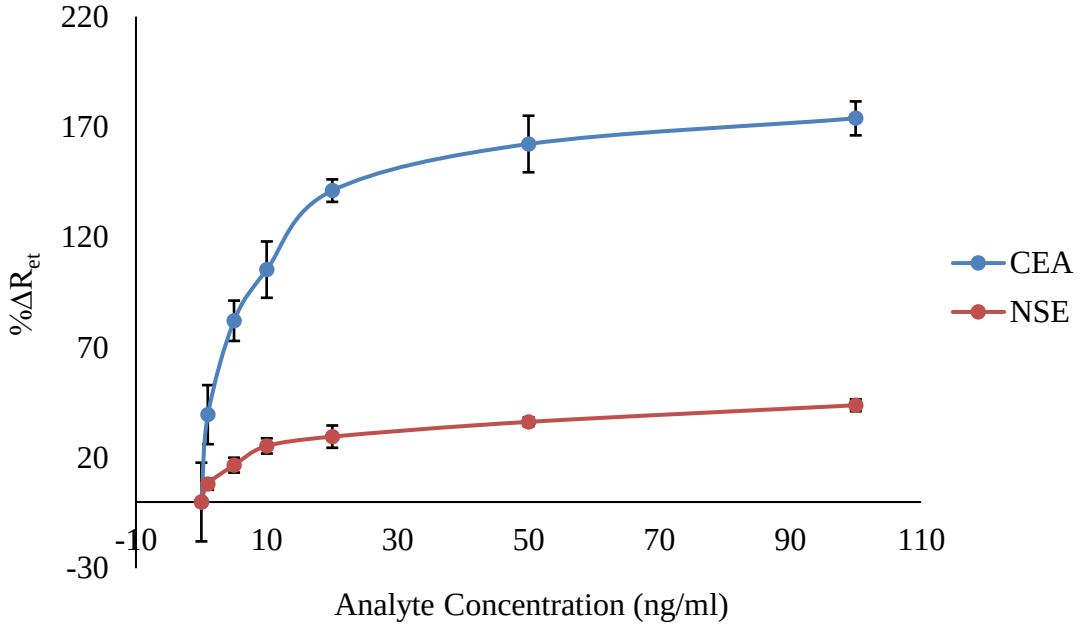

Figure 4.18: Investing the response of CEA immunosensor to various concentration of specific (CEA protein) and non-specific (NSE protein) analyte. The bars represent the average ± standard deviation of triplicates.

4.5. Discussion and Conclusions

CEA is cell surface glycoprotein which is known as reliable, sensitive and specific biomarker of lung cancer. According to the literature, this protein is not normally presents in the body of healthy individuals, however, it's concentration level may reach up to 100 ng/ml in the blood of patients with lung cancer. The cut-off value of CEA antigen has indicated in literature as 5 ng/ml.

The primary anti-CEA monoclonal antibody was immobilised on the surface of gold working electrode CEA immunosensor through formation of SAM layer. MBs were functionalised with the secondary anti-CEA monoclonal antibody. The aim of using specific functionalised MBs to CEA protein was to fish the analyte from the sample solution; to transfer the analyte to sensing area; and also, to increase the sensitivity of the assay. The detection of CEA protein within the serum by using MBs and the proposed platform has not been reported by other researchers. As explained in Chapter 2, using of

proposed platform and functionalised MBs have shown to be successful in amplifying the sensor response.

Once the immobilisation of CEA protein was confirmed by measuring the impedance of SPEs before and after each step of immobilisation process, the CEA immunosensors were used to measure various CEA protein concentration in PBS buffer pH 7.4. According to Chapter 3, some optimisation steps of anti-NSE antibody immobilisation process such as adjusting the ethanolamine solution have shown to be effective in enhancing the detection signals. Hence, the CEA immunosensor was used to measure different CEA concentration in PBS buffer before and after applying those optimisations. According to the obtained results, using ethanolamine solution in PBS with adjusted pH to 7.6 as a deactivation solution has reduced the level of experimental error.

The concentration level of anti-CEA antibodies on the surface of both MBs and SPEs were checked to find the optimum level. After optimising the concentration level of 12-140-01 antibody on the surface of immunosensor, the CEA immunosensors were used to measure CEA protein samples in PBS buffer. A standardised curve of CEA detection in buffer was plotted which proves the success of CEA immunosensor optimisation as achieved LoD was lower than the standardised curve before optimising the assay, 0.26 ng/ml and 0.68 ng/ml, respectively. Additionally, optimising the antibody concentration on the sensing area has also amplified the sensor response. Although increasing the concentration of antibody on the surface of WEs has resulted in improvement of CEA immunosensor response, higher antibody concentration effect was not checked due to economical reasons.

Once the CEA immunosensor was successfully measured CEA protein in PBS buffer, the CEA immunosensor was tested by measuring the CEA protein and NSE protein spiked in 100 % human serum as specific and non-specific analytes, respectively. The sensor was successful in measuring various CEA protein concentrations spiked in 100 % serum and the LoD was calculated as low as 0.76 ng/ml which is lower than the cut-off value which is 5 ng/ml. According to non-specificity experiment results, the percentage of changes in sensor response after normalising to zero for measurement of

100 ng/ml of NSE was 43.85%, while the calculated value for measuring 5 ng/ml of CEA was 82.14%. Therefore, it is possible to distinguish 5 ng/ml of specific antigen (CEA) and 100 ng/ml of non-specific protein (NSE).

The list of CEA biosensors already developed and reported in literature is presented in Chapter 1, in Table 1.2. Most of the examples describe testing of the developed immunosensors only in buffer, achieving in general low LoDs. The immunosensor developed in this project is benefiting from shorter assay times in comparison with most of the examples reported in Table 1.2. For instance, Hou et al. (2013) assay time is more than one hour, and Zhou et al. (2014) assay time is one hour; while the assay time of our CEA immunosensor is 40 minutes. Only in the study done by Pan & Yang in 2007, they have measured CEA protein by EIS technique using functionalised MBs. They have detected CEA in PBS buffer with an incubation time of 30 minutes and have achieved a LoD as low as 0.5 ng/ml, which is higher than the one obtained in this thesis (0.26 ng/ml). Although in Pan & Yang (2007) study, they have reported a lower incubation time than the immunosensor developed in this project, their LoD in buffer is higher and in addition their sensing platform required higher amounts of reagents (e.g. PBS buffer) in comparison with the immunosensor developed in this project. Among the examples reported in Table 1.2, only Jin et al. (2014) have reported detection of CEA with the use of MBs in serum achieving a LoD of 5 ng/ml, which is much higher than the one reported in this thesis (0.76 ng/ml).

According to the results obtained in this Chapter, the developed CEA immunosensor with use of functionalised MBs and the proposed platform were successful in detecting CEA protein in both PBS buffer and 100 % serum; and thereby, has the potential to be used as part of early lung cancer diagnosis.

Chapter 5:

CONCLUSIONS & FUTURE WORK

5.1. General Conclusions

Lung cancer is the most dangerous type of cancer in the world. Cancer research UK has reported 46,403 new cases and 35,895 deaths from lung cancer within the UK in 2014 (Cancer Research UK, 2018). The traditional methods of lung cancer diagnosis are mostly invasive and are not able to detect the disease at its early stage which has the highest cancer therapeutic potential. Early diagnosis of lung cancer can improve the poor survival rate of patients and also reduce the cost of treatment. Early diagnosis of lung cancer may be possible through detection of biomarkers as their concentration level within the body fluid changes after disease onset, *e.g.* carcinoembryonic antigen for lung cancer. Biosensors are analytical devices which can be used for rapid and simultaneous measurement of analyte concentration with high level of sensitivity and specificity. In recent years numerous studies have been carried out to develop a biosensor for lung cancer detection (Sun & Ma, 2012; He et al., 2013; Zhou et al., 2014; Cheng et al., 2015; Shan & Ma, 2016; Wei et al., 2017). It is for this reason that this project is focused on development of rapid, portable, highly sensitive and specific multi-analyte biosensor to screen lung cancer biomarkers.

This thesis details the development of electrochemical impedance spectroscopy (EIS) immunosensor for lung cancer detection. Carcinoembryonic antigen (CEA) and neuron-specific enolase (NSE) are two chosen protein biomarkers for this study as they believed to be good biomarkers for early detection of lung cancer. CEA is cell surface glycoprotein, and it is known as the most reliable biomarker for detection of non-small cell lung cancer (NSCLC). CEA protein is not normally present in the blood of healthy individuals while high concentration level can be detected in people with various type of cancer such as NSCLC. NSE is glycolytic enzyme and is known to be a reliable, sensitive and specific biomarker associated with small cell lung cancer (SCLC). The normal concentration level NSE protein has been reported to be between 5 to 12 ng/ml in blood of healthy individual while in SCLC patients the concentration level exceeds this level. Different studies have reported different cut-off value for CEA and NSE antigens, though most studies have indicated the cut-off value of 5 ng/ml and 12.5 ng/ml for CEA and NSE, respectively.

The detection and measurement of CEA and NSE concentrations were done by formation of sandwich assay on the surface of gold working electrodes (WEs). Two types of monoclonal antibodies were used for both type of immunosensors in order to increase their specificity. The magnetic nanobeads were functionalised with capture antibody while the detection antibodies were immobilised on the surface of WEs.

The self-assembled monolayer (SAM layer) was used to immobilise capture antibodies on the WEs because of its high stability and easy formation. The initial part of this project was to choose the type of SAM layer. Thus, two types of SAM layer were investigated as cysteamine and 11-mercaptoundecanoic acid (11-MUA). The success of both methods was confirmed by applying impedance measurement before and after each step of antibody immobilisation process. Since the SPEs were damaged by the action of ethanol presented in 11-MUA solution, cysteamine SAM layer formation was selected to prepare immunosensors.

After selecting the method of antibody immobilisation on the gold WEs, three types of SPEs were investigated. Three different CEA immunosensors were prepared by using each type of SPEs. The SPE investigation was conducted by measuring the 0 and 100 ng/ml of CEA protein. Out of three tested type of SPEs (DRP-220AT, DRP-220BT, and DRP-250AT), DRP-220BT has shown to have the broadest range. That is why DRP-220BT SPE type was chosen for further experiments.

The results of continuously measuring the impedance of bare SPEs showed reduction of electron transfer resistance (R_{et}). Therefore, it was assumed that SPEs are not clean as applying impedance measurements have resulted in increase of electron transfer from the redox probe to the fold WEs. Also, contamination of SPEs may have effect on the quality of SAM layer and eventually the sensitivity of the immunosensors. Hence, various cleaning methods were investigated in order to find out the most appropriate cleaning process for the chosen type of SPE. Cleaning the electrodes with potassium hydroxide (KOH) in 25% hydrogen peroxide (H_2O_2) was the best cleaning method with reduction in impedance signal of bare SPEs by 96.34%. Thus, the KOH in

25% H_2O_2 was chosen as the most successful cleaning procedure and was used to clean all SPEs prior of functionalisation process.

The initial aim of this project was to design and test a platform. We proposed a magnetic sensing platform integrated with an impedimetric immunosensor. The main purpose of designing the proposed platform was to detect the analyte of interest by using MBs to minimise the washing step and detection time. After building the proposed platform and preparing NSE immunosensors, the effect of platform was tested. The experiment was conducted in two parts of specificity and non-specificity tests and each part was consisting three steps as:

- Measuring various concentrations of NSE
- Measuring various concentrations of MBs-NSE
- Measuring various concentrations of MBs-NSE by use of proposed platform

The fabricated NSE-SPEs could detect various concentration of NSE proteins which prove the success of antibody immobilisation process. Adding functionalised magnetic beads to the analyte sample enhanced the experimental signals which is probably due to the formation of sandwich assay on top of working electrode. As an example, the $\%\Delta R_{et}$ of 100 ng/ml was 55.56 Ω while it increased to 91.59 Ω after use of magnetic beads. The sensing platform was used for the last part of experiment which improved the $\%\Delta R_{et}$, *e.g.* 97.51 Ω was the calculated change in R_{et} of 100 ng/ml. The non-specificity results also show increasing in $\%\Delta R_{et}$ by increasing the analyte concentration, though the increase in change of R_{et} is not as great as the specificity results. The results have shown that using magnetic nanobeads and the proposed platform can result in increasing the detection signal and reducing the experimental error. However, the experimental data also showed that further optimisation of the immunosensors are required in order to evidence the real advantages of using the platform.

5.1.1 Neuron-Specific Enolase Immunosensor

The first immunosensor developed in this project was NSE immunosensor. The initial challenge of NSE immunosensor development was to control the experimental error as it was significantly high. The experimental error was controlled by changing the deactivation and blockage solution of SAM layer. The new deactivation and blockage solution of SAM layer was 0.1 M ethanolamine prepared in 10 mM PBS buffer with adjusted pH of 7.6.

Various concentrations of antibody on the surface of MBs were assessed as 1.2, 2.4, and 3.6 mg/ml, and the best reading were obtained by utilising antibody concentration of 2.4 mg/ml. The concentration of antibody on the gold WEs surface was also investigated by testing 5, 10, and 20 µg/ml of antibody, which resulted in 10 µg/ml giving the highest sensor response.

The NSE immunosensor was used to measure various NSE concentrations (0 – 100 ng/ml) in PBS buffer pH 7.4 before and after optimisation and also to measure the analyte concentration spiked in 100 % human serum. The summery of the NSE immunosensor results is presented in Table 5.1.

Table 5.1: The summary of NSE immunosensor response.

	Before optimisation, in PBS	**After optimisation, in PBS**	**Spiked in 100 % serum**
Linear Range	1 – 100 ng/ml	1 – 100 ng/ml	1 – 100 ng/ml
Equation	y = 27.019x + 13.072	y = 27.808x + 6.8107	y = 33.014x + 16.063
R^2	0.9512	0.9848	0.9977
LoD	0.81 ng/ml	0.18 ng/ml	0.52 ng/ml

5.1.2 Carcinoembryonic Antigen Immunosensor

The second immunosensor developed in this project was CEA immunosensor. Since changing the deactivation and blockage solution of SAM layer showed to improve the results by reducing the experimental error for NSE immunosensors, CEA immunosensors were prepared by 0.1 M ethanolamine in PBS pH 7.6. The CEA immunosensors were used to measure various CEA concentrations before optimisations. Then, different antibody concentrations were assessed to find out the optimum concentration level to be immobilised on the surfaces of MBs. It was found that the best concentration level for anti-CEA antibody is 2.4 mg/ml out of 1.2, 2.4, and 3.6 mg/ml. Different concentrations of antibody (5, 10, and 20 µg/ml) were tested to find out the best concentration of immobilised anti-CEA antibody on the surface of gold WEs. The best results were obtained by use of 20 µg/ml antibody. Although the results show that increasing the concentration of antibody raises the immunosensor response, higher antibody concentrations were not investigated as due to economical reason.

The CEA immunosensor was used to measure various concentrations of CEA in PBS buffer pH 7.4 (0 – 100 ng/ml) before optimisation, after optimisation, and was also used to measure the analyte concentration spiked in 100 % human serum. The summery of the CEA immunosensor results is presented in Table 5.2.

Table 5.2: The summary of CEA immunosensor response.

	Before optimisation, in PBS	**After optimisation, in PBS**	**Spiked in 100 % serum**
Linear Range	1 – 100 ng/ml	1 – 100 ng/ml	1 – 100 ng/ml
Equation	y = 17.333x + 8.1483	y = 43.391x + 16.186	y = 70.852x + 38.279
R^2	0.9945	0.9924	0.9839
LoD	0.68 ng/ml	0.26 ng/ml	0.76 ng/ml

5.2. Challenges

Developed platform and immunosensors have shown to be able to detect analytes of interest and to have the LoD values of less than the cut-off value. Regardless of the project success, there were some challenges in this project which are listed below.

- It is very difficult to have the same concentration of MBs solution due to their nano-size.

- To capture the analyte, magnetic field was applied to the mixture of MBs and analyte samples which results in aggregation of MBs. Dispersing MBs into the solution is time consuming and difficult as lots of vortex is required.

- EIS spectrum analyser software which is a free software was used to simulate the experimental results to calculate the R_{et} values. It is quick and easy to use, and it also presents the percentage of error. Although we tried to keep the same percentage of error (~ 5%) for all impedance results, some R_{et} values may have calculated with less or higher percentage of error.

5.3. Proposed Future Work

According to the results achieved in this project two impedimetric immunosensors were developed which successfully detected lung cancer biomarkers in buffer and human serum, within the cut-off range. Nonetheless, there are several experiments which can lead in further improvement of developed immunosensors in this study.

1. ***Testing the stability of the immunosensors***

The immunosensors were always prepared freshly on the day of experiment. Thus, the storage stability of the immunosensors was not tested. This experiment can be carrying out by immobilising the detection antibodies on gold WEs and test their sensitivity by daily measuring various analyte concentrations over a length of time. The

functionalised SPEs should be stored at 4oC between analyte measurements. In case of obtaining low level of stability, using reagent stabiliser may be needed.

2. Testing magnetic nanobeads concentration and volume

Although the antibody concentration on the surface of MBs was tested, the effect of the MBs concentration and volume on the assay were not tested. Investigating different concentration and volume of the MBs may result in using less amount of MBs which makes the assay cheaper.

3. Testing the incubation time

The functionalised MBs were mixed and incubated with analyte samples for 20 minutes. Also, fished analytes were incubated for 20 minutes on the gold WEs before removing unbound MBs and applying impedance. Testing the incubation time of analyte detection by functionalised MBs, and immobilised antibody on the WEs can improve the assay sensitivity or reduce the analyte detection duration.

4. Testing the immunosensors sensitivity by removing the washing step

After mixing the functionalised MBs with protein sample, a washing step was applied to remove any unbound materials to the MBs. The initial experiment showed having a washing step can reduce the experimental error. However, the obtained later results showed changing the deactivation and blockage solution is effective in controlling the error. Therefore, removing a washing step may not have the same effect as before, and also it can result in reduction of assay time.

5. Testing larger size magnets in platform

As it explained in Chapter 2, a magnet is implanted in each cylinder of platform to move the functionalised MBs and their attached analytes to the sensing area, and to remove unbound MBs from the WEs. The proposed platform was able to move the MBs, though due to its small size magnets only small area of WEs were used for detection of analytes of interest, testing larger size magnet may results in using larger surface area of gold WEs and eventually may results in improvement of the assay. However, use of

larger magnet means having different magnetic field which may reduce the assay sensitivity due to MBs agglomeration.

6. Testing the impedimetric immunosensors with patient samples

The developed immunosensors were only used for detection of analytes in PBS buffer and spiked analytes in 100 % serum. Therefore, it is necessary to test the developed immunosensors with real samples from patients and healthy individuals ethically provided from hospitals.

7. Analyte detection in presence of other biomarkers

The non-specificity test of both immunosensors were carried out by spiking a non-specific biomarker in 100 % human blood serum. The results showed huge signal difference between the specific and non-specific analyte detection. Due to time constraints immunosensors were not tested to detect specific analyte in the presence of non-specific analyte(s).

8. Development of multi-analyte detection immunosensor

The developed immunosensors in this study have shown to be able to detect single analyte concentrations with an acceptable sensitivity and within the cut-off range. Thus, they can be further developed for multi-biomarker detection. Since early diagnosis of lung cancer is not possible detection of only type of biomarker, development of multi-analyte detection immunosensor is required for lung cancer detection. The array of electrode which is commercially available can be used to produce immunosensors by immobilising different type antibodies for different type of biomarkers. However, a new design of proposed platform and appropriate potentiostat are required.

5.4. Final Conclusions

As explained in Chapter 1, lung cancer is responsible for most of the cancer-related deaths in the world. Diagnosis of lung cancer at its early stages can reduce the cost of treatment and increase the chance of survival. Therefore, it is crucial to diagnose lung

cancer as early as possible. Since the current methods of cancer diagnosis are mostly reliable on tissue biopsy and are not very specific. The overall output of this study includes the design of the magnetic actuator sensing platform which was successfully tested by developed NSE and CEA immunosensors. Both immunosensors successfully detected and measured their corresponding biomarker concentrations with low LoD values. To the best of our knowledge, no one has reported the use of a magnetic platform as the one developed in this thesis.

REFERENCES:

Acero Sánchez, J.L., Fragoso, A., Joda, H., Suárez, G., McNeil, C.J., O'Sullivan, C.K., 2016. Site-directed introduction of disulfide groups on antibodies for highly sensitive immunosensors. Anal. Bioanal. Chem. 408, 5337–5346.

Ag, D., Bongartz, R., Dogan, L.E., Seleci, M., Walter, J.-G., Demirkol, D.O., Stahl, F., Ozcelik, S., Timur, S., Scheper, T., 2014. Biofunctional quantum dots as fluorescence probe for cell-specific targeting. Colloids Surfaces B Biointerfaces 114, 96–103.

Ahmad, A., Moore, E., 2012. Electrochemical immunosensor modified with self-assembled monolayer of 11-mercaptoundecanoic acid on gold electrodes for detection of benzo[a]pyrene in water. Analyst 137, 5839–44.

Ali, A., Ahmad, M., Akhtar, M.N., Shaukat, S.F., Mustafa, G., Atif, M., Farooq, W.A., 2016. Magnetic nanoparticles (Fe3O4 & Co3O4) and their applications in urea biosensing. Russ. J. Appl. Chem. 89, 517–534.

Ali, W., Moghaddam, F.J., Raza, M.U., Bui, L., Sayles, B., Kim, Y.-T., Iqbal, S.M., 2016. Electromechanical transducer for rapid detection, discrimination and quantification of lung cancer cells. Nanotechnology 27, 195101.

Altintas, Z., Kallempudi, S.S., Sezerman, U., Gurbuz, Y., 2012. A novel magnetic particle-modified electrochemical sensor for immunosensor applications. Sensors Actuators B Chem. 174, 187–194.

Altintas, Z., Tothill, I., 2013. Biomarkers and biosensors for the early diagnosis of lung cancer. Elsevier 188, 988–998.

Altintas, Z., Uludag, Y., Gurbuz, Y., Tothill, I.E., 2011. Surface plasmon resonance based immunosensor for the detection of the cancer biomarker carcinoembryonic antigen. Talanta 86, 377–83.

Anderson, J.E., Hansen, L.L., Mooren, F.C., Post, M., Hug, H., Zuse, A., Los, M., 2006. Methods and biomarkers for the diagnosis and prognosis of cancer and other diseases: towards personalized medicine. Drug Resist. Updat. 9, 198–210.

Aono, K., Aki, S., Sueyoshi, K., Hisamoto, H., Endo, T., 2016. Development of optical biosensor based on photonic crystal made of TiO_2 using liquid phase deposition. Jpn. J. Appl. Phys. 55, 08RE01.

Arai, T., Inoue, Y., Sugimoto, C., Inoue, Y., Nakao, K., Takeuchi, N., Matsumuro, A., Hirose, M., Nakata, K., Hayashi, S., 2014. CYFRA 21-1 as a disease severity

marker for autoimmune pulmonary alveolar proteinosis. Respirology 19, 246–52.

Arduini, F., Micheli, L., Moscone, D., Palleschi, G., Piermarini, S., Ricci, F., Volpe, G., 2016. Electrochemical biosensors based on nanomodified screen-printed electrodes: Recent applications in clinical analysis. TrAC Trends Anal. Chem. 79, 114–126.

Arrieta, O., Saavedra-Perez, D., Kuri, R., Aviles-Salas, A., Martinez, L., Mendoza-Posada, D., Castillo, P., Astorga, A., Guzman, E., De la Garza, J., 2009. Brain metastasis development and poor survival associated with carcinoembryonic antigen (CEA) level in advanced non-small cell lung cancer: a prospective analysis. BMC Cancer 9, 119.

Arya, S.K., Bhansali, S., 2011. Lung cancer and its early detection using biomarker-based biosensors. Chem. Rev. 111, 6783–809.

Arya, S.K., Zhurauski, P., Jolly, P., Batistuti, M.R., Mulato, M., Estrela, P., 2018. Capacitive aptasensor based on interdigitated electrode for breast cancer detection in undiluted human serum. Biosens. Bioelectron. 102, 106–112.

Ates, M., 2011. Review study of electrochemical impedance spectroscopy and equivalent electrical circuits of conducting polymers on carbon surfaces. Prog. Org. Coatings 71, 1–10.

Atkinson, A.J., Colburn, W.A., DeGruttola, V.G., DeMets, D.L., Downing, G.J., Hoth, D.F., Oates, J.A., Peck, C.C., Schooley, R.T., Spilker, B.A., Woodcock, J., Zeger, S.L., 2001. Biomarkers and surrogate endpoints: preferred definitions and conceptual framework. Clin. Pharmacol. Ther. 69, 89–95.

Aydın, E.B., Sezgintürk, M.K., 2017. A sensitive and disposable electrochemical immunosensor for detection of SOX2, a biomarker of cancer. Talanta 172, 162–170.

Barton, A.C., Davis, F., Higson, S.P.J., 2008. Labeless Immunosensor Assay for the Stroke Marker Protein Neuron Specific Enolase Based upon an Alternating Current Impedance Protocol. Anal. Chem. 80, 9411–9416.

Bondarenko, A.S., Ragoisha, G.A., 2008. EIS Spectrum Analyser [WWW Document]. URL http://www.abc.chemistry.bsu.by/vi/analyser/

Brabender, J., Danenberg, K.D., Metzger, R., Schneider, P.M., Park, J.M., Salonga, D., Hölscher, A.H., Danenberg, P. V., 2001. Epidermal growth factor receptor and

HER2-neu mRNA expression in non-small cell lung cancer is correlated with survival 7, 1850–1855.

Byers, L.A., Rudin, C.M., 2015. Small cell lung cancer: Where do we go from here? Cancer 121, 664–672.

Cagle, P.T., Allen, T.C., Olsen, R.J., 2013. Lung cancer biomarkers: present status and future developments. Arch. Pathol. Lab. Med. 137, 1191–8.

Cancer Research UK, 2014a. Worldwide cancer incidence statistics [WWW Document]. URL http://www.cancerresearchuk.org/cancer-info/cancerstats/world/incidence/ (accessed 3.12.14).

Cancer Research UK, 2014b. Worldwide cancer mortality statistics [WWW Document]. URL http://www.cancerresearchuk.org/cancer-info/cancerstats/world/mortality/ (accessed 3.12.14).

Cancer Research UK, 2014c. Worldwide cancer statistics [WWW Document]. URL http://www.cancerresearchuk.org/cancer-info/cancerstats/world/ (accessed 3.12.14).

Cancer Research UK, 2017. Symptoms of advanced cancer | Lung cancer | Cancer Research UK [WWW Document]. URL http://www.cancerresearchuk.org/about-cancer/lung-cancer/advanced/symptoms (accessed 10.9.17).

Cancer Research UK, 2018. Lung cancer statistics | Cancer Research UK [WWW Document]. URL http://www.cancerresearchuk.org/health-professional/cancer-statistics/statistics-by-cancer-type/lung-cancer (accessed 1.9.18).

Carter, L., Chuah, K., Tavallaie, R., Barfidokht, A., Parker, S.G., Gooding, J.J., 2015. Switching “on and off” faradaic electrochemistry at an otherwise passivated electrode using gold-coated magnetic nanoparticles, Electrochemistry Communications.

Cecchet, F., Marcaccio, M., Margotti, M., Paolucci, F., Rapino, S., Rudolf, P., 2006. Redox mediation at 11-mercaptoundecanoic acid self-assembled monolayers on gold. J. Phys. Chem. B 110, 2241–2248.

Chen, H.-Y., Yu, S.-L., Li, K.-C., Yang, P.-C., 2012. Biomarkers and transcriptome profiling of lung cancer. Respirology 17, 620–6.

Chen, M., Hou, C., Huo, D., Yang, M., Fa, H., Tota, J.E.., Ramanakumar, A. V., Franco, E.L.., Holdenrieder, S.., Pawel, J. von;, Dankelmann, E.., Duell, T..,

Faderl, B.., Markus, A.., Siakavara, M.., Wagner, H.., Feldmann, K., Hoffmann, H., Raith, H., Nagel, D., Stieber, P., Barlési, F., Gimenez, C., Torre, J.-P., Doddoli, C., Mancini, J., Greillier, L., Roux, F., Kleisbauer, J.-P., Pujol, J.L., Boher, J.M., Grenier, J., Quantin, X., Reinmuth, N., Brandt, B., Semik, M., Kunze, W.P., Achatzy, R., Scheld, H.H., Broermann, P., Berdel, W.E., Macha, H.N., Thomas, M., Hokland, P., Pallisgaard, N., Olesen, L.H., Norgaard, J.M., Pallisgaard, N., Bukh, A., Hokland, P., Tamaki, H., Mishima, M., Kawakami, M., Tsuboi, A., Kim, E.H., Hosen, N., Ikegame, K., Murakami, M., Fujioka, T., Masuda, T., Taniguchi, Y., Nishida, S., Osumi, K., Soma, T., Oji, Y., Oka, Y., Kawase, I., Sugiyama, H., Ogawa, H., Feng, K.J., Yang, Y.H., Wang, Z.J., Jiang, J.H., Shen, G.L., Yu, R.Q., Huang, K.-J., Liu, Y.-J., Wang, H.-B., Wang, Y.-Y., Singh, A., Sinsinbar, G., Choudhary, M., Kumar, V., Pasricha, R., Verma, H.N., Singh, S.P., Arora, K., Yola, M.L., Eren, T., Atar, N., Zhu, L., Luo, L., Wang, Z., Wang, J., Zhang, S., Zhang, Y., Monterroso, S.C.C., Carapuca, H.M., Duarte, A.C., Katano, H., Uematsu, K., Maruyama, C., Hamano, Y., Gupta, V.K., Yola, M.L., Qureshi, M.S., Solak, A.O., Atar, N., Üstündağ, Z., He, H.Y., Klinowski, J., Forster, M., Lerf, A., Song, Y.J., Qu, K.G., Zhao, C., Ren, J.S., Qu, X.G., Muti, M., Sharma, S., Erdem, A., Papakonstantinou, P., Huang, K.J., Niu, D.J., Sun, J.Y., Han, C.H., Wu, Z.W., Li, Y.L., Xiong, X.Q., Park, K.W., Jung, J.H., He, H., Gao, C., Wang, X.W., Liu, S.Q., Wang, H.Y., Tu, F.Y., Fang, D., Li, Y.H., Guo, C.X., Wang, M., Chen, T., Lou, X.W., Li, C.M., Zhu, C.Z., Fang, Y.X., Wen, D., Dong, S.J., Jiang, L.C., Zhang, W.D., Li, T., Ai, X.P., Yang, H.X., Alizadeh, T., Mirzagholipur, S., Wang, X.L., Liu, E.L., Zhang, X.L., Cote, L.J., Kim, F., Huang, J.X., Kovtyukhova, N.I., Ollivier, P.J., Martin, B.R., Mallouk, T.E., Chizhik, S.A., Buzaneva, E. V., Gorchinskiy, A.D., Wang, M.X., Liu, Q., Sun, H.F., Stach, E.A., Zhang, H.Y., Stanciu, L., Xie, J., Sun, X.M., Liu, Z., Welsher, K., Robinson, J.T., Goodwin, A., Zaric, S., Dai, H.J., Hallbeck, M., Hermanson, O., Blomqvist, A., Zhang, Y.C., Su, L., Manuzzi, D., Monteros, H.V.E. de los, Jia, W.Z., Huo, D.Q., Hou, C.J., Lei, Y., Chang, Y., Lye, M.L., Zeng, H.C., Zhao, W., Wu, X.Q., Lu, Z.Q., Hou, W.J., Li, H.X., Dubal, D.P., Dhawale, D.S., Salunkhe, R.R., Jamdade, V.S., Lokhande, C.D., Pendashteh, A., Mousavi, M.F., Rahmanifar, M.S., Niu, S., Zhao, M., Ren, R., Zhang, S., Bo, Y., Yang, H., Hu, Y., Yao, T., Huang, S., Jayakumar, K.,

Rajesh, R., Dharuman, V., Venkatasan, R., Hahn, J.H., Pandian, S.K., Campos-Ferreira, D.S., Nascimento, G.A., Souza, E. V., Souto-Maior, M.A., Arruda, M.S., Zanforlin, D.M., Ekert, M.H., Bruneska, D., Lima-Filho, J.L., Peng, H.-P., Hu, Y., Liu, P., Deng, Y.-N., Wang, P., Chen, W., Liu, A.-L., Chen, Y.-Z., Lin, X.-H., 2015. A highly sensitive electrochemical DNA biosensor for rapid detection of CYFRA21-1, a marker of non-small cell lung cancer. Anal. Methods 7, 9466–9473.

Chen, Z., Liang, R., Guo, X., Liang, J., Deng, Q., Li, M., An, T., Liu, T., Wu, Y., 2017. Simultaneous quantitation of cytokeratin-19 fragment and carcinoembryonic antigen in human serum via quantum dot-doped nanoparticles. Biosens. Bioelectron. 91, 60–65.

Cheng, H., Hu, Y., 2012. Influence of chain ordering on frictional properties of self-assembled monolayers (SAMs) in nano-lubrication. Adv. Colloid Interface Sci. 171–172, 53–65.

Cheng, S., Hideshima, S., Kuroiwa, S., Nakanishi, T., Osaka, T., 2015. Label-free detection of tumor markers using field effect transistor (FET)-based biosensors for lung cancer diagnosis. Sensors Actuators B Chem. 212, 329–334.

Cheng, Y., Lee, S.-C., Harn, H.-J., Chen, C.-J., Chen, C.-J., Chen, J.-C., Yu, C.-P., 2003. Prognostic prediction of the immunohistochemical expression of p53 and p16 in resected non-small cell lung cancer. Eur. J. Cardio-Thoracic Surg. 23, 221–228.

Chung, C., Christianson, M., 2014. Predictive and prognostic biomarkers with therapeutic targets in breast, colorectal, and non-small cell lung cancers: A systemic review of current development, evidence, and recommendation. J. Oncol. Pharm. Pract. 20, 11–28.

Cooper, M.A., 2002. Optical biosensors in drug discovery. Nat. Rev. Drug Discov. 1, 515–528.

Cui, F., Xu, Y., Wang, R., Liu, H., Chen, L., Zhang, Q., Mu, X., 2018. Label-free impedimetric glycan biosensor for quantitative evaluation interactions between pathogenic bacteria and mannose. Biosens. Bioelectron. 103, 94–98.

Daniels, J.S., Pourmand, N., 2007. Label-Free Impedance Biosensors: Opportunities and Challenges. Electroanalysis 19, 1239–1257.

Du, D., Zou, Z., Shin, Y., Wang, J., Wu, H., Engelhard, M.H., Liu, J., Aksay, I.A., Lin, Y., 2010. Sensitive Immunosensor for Cancer Biomarker Based on Dual Signal Amplification Strategy of Graphene Sheets and Multienzyme Functionalized Carbon Nanospheres. Anal. Chem. 82, 2989–2995.

Elshafey, R., Tlili, C., Abulrob, A., Tavares, A.C., Zourob, M., 2013. Label-free impedimetric immunosensor for ultrasensitive detection of cancer marker Murine double minute 2 in brain tissue. Biosens. Bioelectron. 39, 220–5.

Ensafi, A., Taei, M., Rahmani, H.., Khayamian, T., 2011. Sensitive DNA impedance biosensor for detection of cancer, chronic lymphocytic leukemia, based on gold nanoparticles/gold modified electrode. Electrochim. Acta 56, 8176–8183.

Ettinger, D.S., Wood, D.E., Akerley, W., Bazhenova, L.A., Borghaei, H., Camidge, D.R., Cheney, R.T., Chirieac, L.R., D'Amico, T.A., Demmy, T.L., Dilling, T.J., Dobelbower, M.C., Govindan, R., Grannis, F.W., Horn, L., Jahan, T.M., Komaki, R., Krug, L.M., Lackner, R.P., Lanuti, M., Lilenbaum, R., Lin, J., Loo, B.W., Martins, R., Otterson, G.A., Patel, J.D., Pisters, K.M., Reckamp, K., Riely, G.J., Rohren, E., Schild, S.E., Shapiro, T.A., Swanson, S.J., Tauer, K., Yang, S.C., Gregory, K., Hughes, M., National comprehensive cancer network, 2015. Non-Small Cell Lung Cancer, Version 6.2015. J. Natl. Compr. Canc. Netw. 13, 515–24.

Fan, Y., Liu, J., Wang, Y., Luo, J., Xu, H., Xu, S., Cai, X., 2017. A wireless point-of-care testing system for the detection of neuron-specific enolase with microfluidic paper-based analytical devices. Biosens. Bioelectron. 95, 60–66.

Feng, T., Qiao, X., Wang, H., Sun, Z., Hong, C., 2016. A sandwich-type electrochemical immunosensor for carcinoembryonic antigen based on signal amplification strategy of optimized ferrocene functionalized Fe3O4@SiO2 as labels. Biosens. Bioelectron. 79, 48–54.

Fernandez-Sanchez, C., McNeil, C.J., Rawson, K., 2005. Electrochemical impedance spectroscopy studies of polymer degradation: application to biosensor development. TrAC Trends Anal. Chem. 24, 37–48.

Fischer, L.M., Tenje, M., Heiskanen, A.R., Masuda, N., Castillo, J., Bentien, A., Émneus, J., Jakobsen, M.H., Boisen, A., 2009. Gold cleaning methods for electrochemical detection applications. Microelectron. Eng. 86, 1282–1285.

Foa, P., Fornier, M., Miceli, R., Seregni, E., Santambrogio, L., Nosotti, M., Cataldo, I.,

Sala, M., Caldiera, S., Bombardieri, E., 1999. Tumour markers CEA, NSE, SCC, TPA and CYFRA 21.1 in resectable non-small cell lung cancer. Anticancer Res. 19, 3613–8.

Fragoso, A., Laboria, N., Botero, M.L., Bejarano, D., Latta, D., Hansen-Hagge, T.E., Kemmner, W., Katakis, I., Gärtner, C., Drese, K., O'Sullivan, C.K., 2010. Development of an integrated microsystem for the multiplexed detection of breast cancer markers in serum using electrochemical immunosensors. Proc. SPIE- Int. Soc. Opt. Eng. 7593, 75930K–75930K–9.

Früh, M., De Ruysscher, D., Popat, S., Crinò, L., Peters, S., Felip, E., 2013. Small-cell lung cancer (SCLC): ESMO Clinical Practice Guidelines for diagnosis, treatment and follow-up. Ann. Oncol. 24 Suppl 6, vi99-105.

Gao, W., Wang, W., Yao, S., Wu, S., Zhang, H., Zhang, J., Jing, F., Mao, H., Jin, Q., Cong, H., Jia, C., Zhang, G., Zhao, J., 2017. Highly sensitive detection of multiple tumor markers for lung cancer using gold nanoparticle probes and microarrays. Anal. Chim. Acta 958, 77–84.

Gao, X., Zhang, Y., Chen, H., Chen, Z., Lin, X., 2011. Amperometric immunosensor for carcinoembryonic antigen detection with carbon nanotube-based film decorated with gold nanoclusters. Anal. Biochem. 414, 70–76.

Gautschi, O., Ratschiller, D., Gugger, M., Betticher, D., Heighway, J., 2007. Cyclin D1 in non-small cell lung cancer: A key driver of malignant transformation. Lung Cancer 55, 1–14.

Geißler, D., Stufler, S., Löhmannsröben, H.-G., Hildebrandt, N., 2013. Six-Color Time-Resolved Förster Resonance Energy Transfer for Ultrasensitive Multiplexed Biosensing. J. Am. Chem. Soc. 135, 1102–1109.

Giouroudi, I., Kokkinis, G., 2017. Recent Advances in Magnetic Microfluidic Biosensors. Nanomaterials 7, 171.

Gooding, J.J., Ciampi, S., 2011. The molecular level modification of surfaces: from self-assembled monolayers to complex molecular assemblies. Chem. Soc. Rev. 40, 2704.

Gorodkiewicz, E., Charkiewicz, R., Rakowska, A., Bajko, P., Chyczewski, L., Niklinski, J., 2012. SPR imaging biosensor for podoplanin: sensor development and application to biological materials. Microchim. Acta 176, 337–343.

Grass, R.N., Athanassiou, E.K., Stark, W.J., 2007. Covalently Functionalized Cobalt Nanoparticles as a Platform for Magnetic Separations in Organic Synthesis. Angew. Chemie Int. Ed. 46, 4909–4912.

Grieshaber, D., MacKenzie, R., Vörös, J., Reimhult, E., 2008. Electrochemical Biosensors - Sensor Principles and Architectures. Sensors 8, 1400–1458.

Grunnet, M., Sorensen, J.B., 2012. Carcinoembryonic antigen (CEA) as tumor marker in lung cancer. Lung Cancer 76, 138–43.

Gu, H.-M., Shi, J.-Q., Wang, X., Deng, S.-P., 2012. A fast graphical similarity algorithm for pattern recognition for data from a voltammetric electronic tongue. Anal. Methods 4, 1284.

Gu, X., She, Z., Ma, T., Tian, S., Kraatz, H.-B., 2018. Electrochemical detection of carcinoembryonic antigen. Biosens. Bioelectron. 102, 610–616.

Han, J., Zhuo, Y., Chai, Y., Yuan, Y.-L., Yuan, R., 2012. Novel electrochemical catalysis as signal amplified strategy for label-free detection of neuron-specific enolase. Biosens. Bioelectron. 31, 399–405.

Harmsma, M., Schutte, B., Ramaekers, F.C.S., 2013. Serum markers in small cell lung cancer: Opportunities for improvement. Biochim. Biophys. Acta - Rev. Cancer 1836, 255–272.

He, A., Liu, T.-C., Dong, Z.-N., Ren, Z.-Q., Hou, J.-Y., Li, M., Wu, Y.-S., 2013. A novel immunoassay for the quantization of CYFRA 21-1 in human serum. J. Clin. Lab. Anal. 27, 277–83.

Hensing, T. a, Salgia, R., 2013. Molecular biomarkers for future screening of lung cancer. J. Surg. Oncol. 108, 327–33.

Holdenrieder, S., 2016. Biomarkers along the continuum of care in lung cancer. Scand. J. Clin. Lab. Invest. 76, S40–S45.

Holmes, J.L., Davis, F., Collyer, S.D., Higson, S.P.J., 2011. A new application of scanning electrochemical microscopy for the label-free interrogation of antibody–antigen interactions. Anal. Chim. Acta 689, 206–211.

Holzinger, M., Le Goff, A., Cosnier, S., 2014. Nanomaterials for biosensing applications: a review. Front. Chem. 2, 63.

Hou, L., Cui, Y., Xu, M., Gao, Z., Huang, J., Tang, D., 2013. Graphene oxide-labeled sandwich-type impedimetric immunoassay with sensitive enhancement based on

enzymatic 4-chloro-1-naphthol oxidation. Biosens. Bioelectron. 47, 149–156.

Indovina, P., Marcelli, E., 2013. Mass spectrometry-based proteomics: The road to lung cancer biomarker discovery. Mass Spectrom. … 32, 129–142.

Ito, G., Uchiyama, M., Kondo, M., Mori, S., Usami, N., Maeda, O., Kawabe, T., Hasegawa, Y., Shimokata, K., Sekido, Y., 2004. Krüppel-Like Factor 6 Is Frequently Down-Regulated and Induces Apoptosis in Non-Small Cell Lung Cancer Cells. Cancer Res. 64, 3838–3843.

Jadhav, S.A., 2011. Self-assembled monolayers (SAMs) of carboxylic acids: an overview. Cent. Eur. J. Chem. 9, 369–378.

Jin, B., Wang, P., Mao, H., Hu, B., Zhang, H., Cheng, Z., Wu, Z., Bian, X., Jia, F., Jin, Q., Zhao, J., 2014. Multi-nanomaterial electrochemical biosensor based on label-free graphene for detecting cancer biomarkers. Biosens. Bioelectron. 55, 464–469.

Jumper, C., Cobos, E., Lox, C., 2004. Determination of the serum matrix metalloproteinase-9 (MMP-9) and tissue inhibitor of matrix metalloproteinase-1 (TIMP-1) in patients with either advanced small-cell lung cancer or non-small-cell lung cancer prior to treatment. Respir. Med. 98, 173–7.

Justino, C.I.L., Duarte, A.C., Rocha-Santos, T.A.P., 2016. Critical overview on the application of sensors and biosensors for clinical analysis. TrAC Trends Anal. Chem. 85, 36–60.

Justino, C.I.L., Rocha-Santos, T.A., Duarte, A.C., 2010. Review of analytical figures of merit of sensors and biosensors in clinical applications. TrAC Trends Anal. Chem. 29, 1172–1183.

K'Owino, I.O., Sadik, O.A., 2005. Impedance Spectroscopy: A Powerful Tool for Rapid Biomolecular Screening and Cell Culture Monitoring. Electroanalysis 17, 2101–2113.

Kalari, S., Jung, M., Kernstine, K.H., Takahashi, T., Pfeifer, G.P., 2013. The DNA methylation landscape of small cell lung cancer suggests a differentiation defect of neuroendocrine cells. Oncogene 32, 3559–3568.

Kashyap, A., Bujamma, D., Babu M, N., 2015. Bioinformatics of Non Small Cell Lung Cancer and the Ras Proto-Oncogene, SpringerBriefs in Applied Sciences and Technology. Springer Singapore, Singapore.

Katz, E., Willner, I., 2003. Probing Biomolecular Interactions at Conductive and

Semiconductive Surfaces by Impedance Spectroscopy: Routes to Impedimetric Immunosensors, DNA-Sensors, and Enzyme Biosensors. Electroanalysis 15, 913–947.

Kaufman, H.L., Hörig, H., Medina, F.A., Golding, S., Conkright, W.A., 2000. Strategies for cancer therapy using carcinoembryonic antigen vaccines. Expert Rev. Mol. Med. 2, 1–24.

Kazemi, S.H., Shanehsaz, M., Ghaemmaghami, M., 2015. Non-Faradaic electrochemical impedance spectroscopy as a reliable and facile method: Determination of the potassium ion concentration using a guanine rich aptasensor. Mater. Sci. Eng. C 52, 151–154.

Kim, Y.J., Rahman, M., Lee, J.-J., 2013. Ultrasensitive and label-free detection of annexin A3 based on quartz crystal microbalance. Sensors Actuators B Chem. 177, 172–177.

Kimmel, D.W., LeBlanc, G., Meschievitz, M.E., Cliffel, D.E., 2012. Electrochemical sensors and biosensors. Anal. Chem. 84, 685–707.

Ko, S., Han, G., Lee, J.K., 2015. Surface organic chemistry for application to organic electronics. Tetrahedron Lett. 56, 3721–3731.

Kosaka, N., Iguchi, H., Ochiya, T., 2010. Circulating microRNA in body fluid: a new potential biomarker for cancer diagnosis and prognosis. Cancer Sci. 101, 2087–2092.

Kristiansen, G., Yu, Y., Petersen, S., Kaufmann, O., Schluns, K., Dietel, M., Petersen, I., 2001. Overexpression of c-erbB2 protein correlates with disease-stage and chromosomal gain at the c-erbB2 locus in non-small cell lung cancer. Eur. J. Cancer 37, 1089–1095.

Kulpa, J., Wójcik, E., Reinfuss, M., Kołodziejski, L., 2002. Carcinoembryonic antigen, squamous cell carcinoma antigen, CYFRA 21-1, and neuron-specific enolase in squamous cell lung cancer patients. Clin. Chem. 48, 1931–7.

Kumar, S., Sharma, J.G., Maji, S., Malhotra, B.D., 2016. Nanostructured zirconia decorated reduced graphene oxide based efficient biosensing platform for non-invasive oral cancer detection. Biosens. Bioelectron. 78, 497–504.

Lei, J., Lei, C., Wang, T., Yang, Z., Zhou, Y., 2013. Detection of targeted carcinoembryonic antigens using a micro-fluxgate-based biosensor. Appl. Phys.

Lett. 103, 203705.

Li, C., Hong, W., 2013. Research status and funding trends of lung cancer biomarkers. J. Thorac. Dis. 5, 698–705.

Li, F., Gooneratne, C., Kosel, J., 2012. Magnetic biosensor system to detect biological targets. In: 2012 International Conference on Electromagnetics in Advanced Applications. IEEE, pp. 1238–1241.

Li, H., Cao, Z., Zhang, Y., Lau, C., Lu, J., 2010. Combination of quantum dot fluorescence with enzyme chemiluminescence for multiplexed detection of lung cancer biomarkers. Anal. Methods 2, 1236.

Li, H., Ziao, Q., Lv, J., Lei, Q., Huang, Y., 2017. Dopamine modified hyperbranched TiO2 arrays based ultrasensitive photoelectrochemical immunosensor for detecting neuron specific enolase. Anal. Biochem. 531, 48–55.

Li, J., Li, S., Yang, C.F., 2012. Electrochemical Biosensors for Cancer Biomarker Detection. Electroanalysis 24, 2213–2229.

Li, R., Todd, N.W., Qiu, Q., Fan, T., Zhao, R.Y., Rodgers, W.H., Fang, H.-B., Katz, R.L., Stass, S.A., Jiang, F., 2007. Genetic deletions in sputum as diagnostic markers for early detection of stage I non-small cell lung cancer. Clin. Cancer Res. 13, 482–7.

Li, Y., Chen, Y., Deng, D., Luo, L., He, H., Wang, Z., 2017. Water-dispersible graphene/amphiphilic pyrene derivative nanocomposite: High AuNPs loading capacity for CEA electrochemical immunosensing. Sensors Actuators B Chem. 248, 966–972.

Li, Y., Jing, Y., Srinivasan, B., Yao, X., Hugger, M.A., Xing, C., Wang, J.-P., Häfeli, U., Schütt, W., Zborowski, M., 2010. Biomarker Quantification in Unprocessed Human Sera by Using A New Nanomagnetic Protein Assay. pp. 237–243.

Li, Y., Jing, Y., Yao, X., Srinivasan, B., Xu, Y., Xing, C., Wang, J.-P., 2009. Biomarkers identification and detection based on GMR sensor and sub 13 nm magnetic nanoparticles. In: 2009 Annual International Conference of the IEEE Engineering in Medicine and Biology Society. IEEE, pp. 5432–5435.

Li, Y., Wu, S., Chen, Y., Lu, Q., Wang, L., 2011. Formation of Au nanoflowers on cysteamine monolayer and their electrocatalytic oxidation of nitrite. Anal. Methods 3, 1399.

Lin, D., Wu, J., Ju, H., Yan, F., 2014. Nanogold/mesoporous carbon foam-mediated silver enhancement for graphene-enhanced electrochemical immunosensing of carcinoembryonic antigen. Biosens. Bioelectron. 52, 153–158.

Lin, P.-C., Lin, J.-K., Lin, C.-C., Wang, H.-S., Yang, S.-H., Jiang, J.-K., Lan, Y.-T., Lin, T.-C., Li, A.F.-Y., Chen, W.-S., Chang, S.-C., 2012. Carbohydrate antigen 19-9 is a valuable prognostic factor in colorectal cancer patients with normal levels of carcinoembryonic antigen and may help predict lung metastasis. Int. J. Colorectal Dis. 27, 1333–1338.

Lindholm-Sethson, B., Nyström, J., Malmsten, M., Ringstad, L., Nelson, A., Geladi, P., 2010. Electrochemical impedance spectroscopy in label-free biosensor applications: multivariate data analysis for an objective interpretation. Anal. Bioanal. Chem. 398, 2341–9.

Little, C.D., Nau, M.M., Carney, D.N., Gazdar, A.F., Minna, J.D., 1983. Amplification and expression of the c-myc oncogene in human lung cancer cell lines. Nature 306, 194–196.

Liu, D., Nakano, J., Ishikawa, S., Yokomise, H., Ueno, M., Kadota, K., Urushihara, M., Huang, C., 2007. Overexpression of matrix metalloproteinase-7 (MMP-7) correlates with tumor proliferation, and a poor prognosis in non-small cell lung cancer. Lung Cancer 58, 384–391.

Liu, W.-J., Tan, X.-H., Guo, B.-P., Ke, Q., Sun, J., Cen, H., 2013. Associations Between RASSF1A Promoter Methylation and NSCLC: A Meta-analysis of Published Data. Asian Pacific J. Cancer Prev. 14, 3719–3724.

Liu, X., Qin, Y., Deng, C., Xiang, J., Li, Y., 2015. A simple and sensitive impedimetric aptasensor for the detection of tumor markers based on gold nanoparticles signal amplification. Talanta 132, 150–154.

Llandro, J., Palfreyman, J.J., Ionescu, A., Barnes, C.H.W., 2010. Magnetic biosensor technologies for medical applications: a review. Med. Biol. Eng. Comput. 48, 977–98.

Luo, J., Qu, S., Liu, J., Wang, B., Cai, X., 2013. Rapid detection of Cyfra 21-1 by optical-biosensing based on chemiluminescence immunoassay using bio-functionlized magnetic nanocomposites. Chinese Sci. Bull. 58, 2567–2569.

Luo, X., Davis, J.J., 2013. Electrical biosensors and the label free detection of protein

disease biomarkers. Chem. Soc. Rev. 42, 5944.

Mandler, D., Kraus-Ophir, S., 2011. Self-assembled monolayers (SAMs) for electrochemical sensing. J. Solid State Electrochem. 15, 1535–1558.

Manzanares-Palenzuela, L., Martin-Fernandez, B., Sanchez-Paniagua Lopez, M., Lopez-Ruiz, B., 2015. Electrochemical genosensors as innovative tools for detection of genetically modified organisms. TrAC Trends Anal. Chem. 66, 19–31.

Martin, F., Santolaria, F., Batista, N., Milena, A., Gonzalez-Reimers, E., Brito, M.J., Oramas, J., 1999. Cytokine levels (IL-6 AND IFN-γ), acute phase response and nutritional status as prognostic factors in lung cancer. Cytokine 11, 80–86.

MedicineNet, 2010. Lung Cancer Picture [WWW Document]. URL https://www.medicinenet.com/image-collection/lung_cancer_picture/picture.htm (accessed 1.5.18).

Meyer, M.H.F., Stehr, M., Bhuju, S., Krause, H.-J., Hartmann, M., Miethe, P., Singh, M., Keusgen, M., 2007. Magnetic biosensor for the detection of Yersinia pestis. J. Microbiol. Methods 68, 218–24.

Mitsudomi, T., Kosaka, T., Endoh, H., Horio, Y., Hida, T., Mori, S., Hatooka, S., Shinoda, M., Takahashi, T., Yatabe, Y., 2005. Mutations of the epidermal growth factor receptor gene predict prolonged survival after gefitinib treatment in patients with non-small-cell lung cancer with postoperative recurrence. J. Clin. Oncol. 23, 2513–20.

Monošík, R., Streďanský, M., Šturdík, E., 2012. Biosensors - classification, characterization and new trends. Acta Chim. Slovaca 5, 109–120.

Moreira, F.T.C., Ferreira, J.M.S., Puga, J.R.T., Sales, G.F., 2016. Screen-printed electrode produced by printed-circuit board technology. Application to cancer biomarker detection by means of plastic antibody as sensing material. Sensors Actuators B Chem. 223, 927–935.

Muluneh, M., Issadore, D., 2014. Microchip-based detection of magnetically labeled cancer biomarkers. Adv. Drug Deliv. Rev. 66, 101–109.

Muñoz, J., Montes, R., Baeza, M., 2017. Trends in electrochemical impedance spectroscopy involving nanocomposite transducers: Characterization, architecture surface and bio-sensing. TrAC Trends Anal. Chem. 97, 201–215.

Najlah, M., Ahmed, Z., Iqbal, M., Wang, Z., Tawari, P., Wang, W., McConville, C.,

2017. Development and characterisation of disulfiram-loaded PLGA nanoparticles for the treatment of non-small cell lung cancer. Eur. J. Pharm. Biopharm. 112, 224–233.

Nathalie, H.-V., Chris, P., Serge, G., Catherine, C., Benjamin, B., Claire, B., Christelle, P., Briollais, L., Pascale, R., Marie-Lise, J., Yves, C., 2009. High kallikrein-related peptidase 6 in non-small cell lung cancer cells: an indicator of tumour proliferation and poor prognosis. J. Cell. Mol. Med. 13, 4014–4022.

Nau, M.M., Brooks, B.J., Battey, J., Sausville, E., Gazdar, A.F., Kirsch, I.R., McBride, O.W., Bertness, V., Hollis, G.F., Minna, J.D., 1985. L-myc, a new myc-related gene amplified and expressed in human small cell lung cancer. Nature 318, 69–73.

Nau, M.M., Brooks, B.J., Carney, D.N., Gazdar, A.F., Battey, J.F., Sausville, E.A., Minna, J.D., 1986. Human small-cell lung cancers show amplification and expression of the N-myc gene 83, 1092–1096.

Newman, J.D., Setford, S.J., 2006. Enzymatic biosensors. Mol. Biotechnol. 32, 249–68.

Newman, J.D., Turner, A.P.F., 2005. Home blood glucose biosensors: a commercial perspective. Biosens. Bioelectron. 20, 2435–53.

Okamura, K., Takayama, K., Izumi, M., Harada, T., Furuyama, K., Nakanishi, Y., 2013. Diagnostic value of CEA and CYFRA 21-1 tumor markers in primary lung cancer. Lung Cancer 80, 45–9.

Ono, A., Takahashi, T., Mori, K., Akamatsu, H., Shukuya, T., Taira, T., Kenmotsu, H., Naito, T., Murakami, H., Nakajima, T., Endo, M., Yamamoto, N., 2013. Prognostic impact of serum CYFRA 21-1 in patients with advanced lung adenocarcinoma: a retrospective study. BMC Cancer 13, 354.

Pan, J., Yang, Q., 2007. Antibody-functionalized magnetic nanoparticles for the detection of carcinoembryonic antigen using a flow-injection electrochemical device. Anal. Bioanal. Chem. 388, 279–286.

Patching, S.G., 2014. Surface plasmon resonance spectroscopy for characterisation of membrane protein–ligand interactions and its potential for drug discovery ☆. BBA - Biomembr. 1838, 43–55.

Patra, H.K., Turner, A.P.F., 2014. The potential legacy of cancer nanotechnology: cellular selection. Trends Biotechnol. 32, 21–31.

Perumal, V., Hashim, U., 2014. Advances in biosensors: Principle, architecture and

applications. J. Appl. Biomed. 12, 1–15.

Petrovic, M., Mitrovic, S., Stankovic, V., Jurisic, V., Atkinson, H.D., 2012. Neuroendocrine Markers-Useful Predictors of Therapeutic Responses in Non-resectable Non-small Cell Lung Cancer. Lab. Med. 43, 6–10.

Piletsky, S.A., Turner, A.P.F., 2002. Electrochemical Sensors Based on Molecularly Imprinted Polymers. Electroanalysis 14, 317–323.

Planque, C., Monte, M. de, Guyetant, S., Rollin, J., Desmazes, C., Panel, V., Lemarie, E., Courty, Y., 2005. KLK5 and KLK7, two members of the human tissue kallikrein family, are differentially expressed in lung cancer. Biochem. Biophys. Res. Commun. 329, 1260–1266.

Prodromidis, M.I., 2010. Impedimetric immunosensors—A review. Electrochim. Acta 55, 4227–4233.

Pujol, J.L., Molinier, O., Ebert, W., Dayrès, J.P., Barlesi, F., Buccheri, G., Paesmans, M., Quoix, E., Moro-Sibilot, D., Szturmowicz, M., Bréchet, J.M., Muley, T., Grenier, J., 2004. CYFRA 21-1 is a prognostic determinant in non-small-cell lung cancer: Results of a meta-analysis in 2063 patients. Br. J. Cancer 90, 2097–2105.

Rajesh, Sharma, V., Tanwar, V.K., Mishra, S.K., Biradar, A.M., 2010. Electrochemical impedance immunosensor for the detection of cardiac biomarker Myogobin (Mb) in aqueous solution. Thin Solid Films 519, 1167–1170.

Ramadan, Q., Christophe, L., Teo, W., Li, S., Feng, H.H., 2010. Flow-through immunomagnetic separation system for waterborne pathogen isolation and detection: application to Giardia and Cryptosporidium cell isolation. Anal. Chim. Acta 673, 101–8.

Ramadan, Q., Gijs, M. a M., 2011. Simultaneous sample washing and concentration using a “trapping-and-releasing” mechanism of magnetic beads on a microfluidic chip. Analyst 136, 1157–66.

Ribaut, C., Loyez, M., Larrieu, J., Chevineau, S., Lambert, P., Remmelink, M., Wattiez, R., cau, 2017. Cancer biomarker sensing using packaged plasmonic optical fiber gratings: Towards in vivo diagnosis. Biosens. Bioelectron. 92, 449–456.

Ribaut, C., Voisin, V., Malachovská, V., Dubois, V., Mégret, P., Wattiez, R., Caucheteur, C., 2016. Small biomolecule immunosensing with plasmonic optical fiber grating sensor. Biosens. Bioelectron. 77, 315–322.

Ríos, A., Zougagh, M., Bouri, M., 2013. Magnetic (nano)materials as an useful tool for sample preparation in analytical methods. A review. Anal. Methods 5, 4558.

Rocha-Santos, T.A.P., 2014. Sensors and biosensors based on magnetic nanoparticles. TrAC Trends Anal. Chem. 62, 28–36.

Rossi, A., Martelli, O., Di Maio, M., 2013. Treatment of patients with small-cell lung cancer: from meta-analyses to clinical practice. Cancer Treat. Rev. 39, 498–506.

Ruffert, C., 2016. Magnetic Bead—Magic Bullet. Micromachines 7, 21.

Samanta, D., Sarkar, A., 2011. Immobilization of bio-macromolecules on self-assembled monolayers: methods and sensor applications. Chem. Soc. Rev. 40, 2567.

Sankiewicz, A., Lukaszewski, Z., Trojanowska, K., Gorodkiewicz, E., 2016. Determination of collagen type IV by Surface Plasmon Resonance Imaging using a specific biosensor. Anal. Biochem. 515, 40–46.

Sasaki, H., Yukiue, H., Kobayashi, Y., Tanahashi, M., Moriyama, S., Nakashima, Y., Fukai, I., Kiriyama, M., Yamakawa, Y., Fuji, Y., 2001. Expression of the cdc25B gene as a prognosis marker in non-small cell lung cancer. Cancer Lett. 173, 187–192.

Sawabata, N., Ohta, M., Takeda, S., Hirano, H., Okumura, Y., Asada, H., Maeda, H., 2002. Serum carcinoembryonic antigen level in surgically resected clinical stage I patients with non-small cell lung cancer. Ann. Thorac. Surg. 74, 174–9.

Schmaltz, T., Sforazzini, G., Reichert, T., Frauenrath, H., 2017. Self-Assembled Monolayers as Patterning Tool for Organic Electronic Devices. Adv. Mater. 29, 1605286.

Shamsipur, M., Pishabadi, A., Molaabasi, F., Hosseinkhani, S., 2017. Impedimetric monitoring of apoptosis using cytochrome-aptamer bioconjugated silver nanocluster. Biosens. Bioelectron. 90, 195–202.

Shan, C., Yang, H., Song, J., Han, D., Ivaska, A., Niu, L., 2009. Direct Electrochemistry of Glucose Oxidase and Biosensing for Glucose Based on Graphene. Anal. Chem. 81, 2378–2382.

Shan, J., Ma, Z., 2016. Simultaneous detection of five biomarkers of lung cancer by electrochemical immunoassay. Microchim. Acta 183, 2889–2897.

Sharma, R., Agrawal, V.V., Sharma, P., Varshney, R., Sinha, R.K., Malhotra, B.D., 2012. Aptamer based electrochemical sensor for detection of human lung adenocarcinoma A549 cells. J. Phys. Conf. Ser. 358, 12001.

Shin, Y., Soo, R.A., Yoon, J., Promoda Perera, A., Yoon, Y.-J., Park, M.K., 2015. Rapid and label-free amplification and detection assay for genotyping of cancer biomarker. Biosens. Bioelectron. 68, 107–114.

Silvestri, G.A., Tanoue, L., Margolis, M., Barker, J., Detterbeck, F., 2003. The Noninvasive Staging of Non-small Cell Lung Cancer*: The Guidelines. Chest 123, 147S–156S.

Slebos, R.J.C., Kibbelaar, R.E., Dalesio, O., Kooistra, A., Stam, J., Meijer, C.J.L.M., Wagenaar, S.S., Vanderschueren, R.G.J.R.A., van Zandwijk, N., Mooi, W.J., Bos, J.L., Rodenhuis, S., 1990. K- *ras* Oncogene Activation as a Prognostic Marker in Adenocarcinoma of the Lung. N. Engl. J. Med. 323, 561–565.

Sobczak-Kupiec, A., Venkatesan, J., AlAnezi, A. alhathal, Walzcyk, D., Forooqi, A., Malina, D., Hoseseini, S.H., 2016. Magnetic nanomaterials and sensors for biological detection. Nanomedicine Nanotechnology, Biol. Med. 12, 2459–2473.

Song, J., Liu, Z., Zhong, W., Huang, Y., Ma, Z., Dong, D., Liang, C., Tian, J., 2016. Non-small cell lung cancer: quantitative phenotypic analysis of CT images as a potential marker of prognosis. Sci. Rep. 6, 38282.

Song, S., Wang, L., Li, J., Fan, C., Zhao, J., 2008. Aptamer-based biosensors. TrAC Trends Anal. Chem. 27, 108–117.

Špringer, T., Homola, J., 2012. Biofunctionalized gold nanoparticles for SPR-biosensor-based detection of CEA in blood plasma. Anal. Bioanal. Chem. 404, 2869–75.

Srinivasan, B., Li, Y., Jing, Y., Xu, Y., Yao, X., Xing, C., Wang, J.-P., 2009. A Detection System Based on Giant Magnetoresistive Sensors and High-Moment Magnetic Nanoparticles Demonstrates Zeptomole Sensitivity: Potential for Personalized Medicine. Angew. Chemie Int. Ed. 48, 2764–2767.

Su, F., Xu, C., Taya, M., Murayama, K., Shinohara, Y., Nishimura, S.-I., 2008. Detection of Carcinoembryonic Antigens Using a Surface Plasmon Resonance Biosensor. Sensors 8, 4282–4295.

Su, L., Jia, W., Hou, C., Lei, Y., 2011. Microbial biosensors: a review. Biosens. Bioelectron. 26, 1788–99.

Sun, G., Ding, Y., Ma, C., Zhang, Y., Ge, S., Yu, J., Song, X., 2014. Paper-based electrochemical immunosensor for carcinoembryonic antigen based on three dimensional flower-like gold electrode and gold-silver bimetallic nanoparticles. Electrochim. Acta 147, 650–656.

Sun, X., Ma, Z., 2012. Highly stable electrochemical immunosensor for carcinoembryonic antigen. Biosens. Bioelectron. 35, 470–474.

Swellam, M., Ragab, H.M., Abdalla, N.A., El-Asmar, A.B.H., 2008. Soluble cytokeratin-19 and E-selectin biomarkers: Their relevance for lung cancer detection when tested independently or in combinations. Cancer Biomarkers 4, 43–54.

Tamanaha, C.R., Mulvaney, S.P., Rife, J.C., Whitman, L.J., 2008. Magnetic labeling, detection, and system integration. Biosens. Bioelectron. 24, 1–13.

Tang, H., Chen, J., Nie, L., Kuang, Y., Yao, S., 2007. A label-free electrochemical immunoassay for carcinoembryonic antigen (CEA) based on gold nanoparticles (AuNPs) and nonconductive polymer film. Biosens. Bioelectron. 22, 1061–1067.

Teotia, pradeep kumar, Kaler, R.S., 2017. 1-D grating based SPR biosensor for the detection of lung cancer biomarkers using Vroman effect. Opt. Commun.

Thakur, A., Qiu, G., NG, S., Guan, J., Yue, J., Lee, Y., Wu, M.L., 2017. Direct detection of two different tumor-derived extracellular vesicles by SAM-AuNIs LSPR biosensor. Biosens. Bioelectron. 94, 400–407.

Thévenot, D.R., Toth, K., Durst, R.A., Wilson, G.S., 2001. Electrochemical biosensors: recommended definitions and classification. Biosens. Bioelectron. 16, 121–131.

Tian, T., Liu, H., Li, L., Yu, J., Ge, S., Song, X., Yan, M., 2017a. Paper-based biosensor for noninvasive detection of epidermal growth factor receptor mutations in non-small cell lung cancer patients. Sensors Actuators, B Chem. 251, 440–445.

Tian, T., Liu, H., Li, L., Yu, J., Ge, S., Song, X., Yan, M., 2017b. Non-small-cell lung cancers: a heterogeneous set of diseases. Sensors Actuators B Chem. 251, 440–445.

Tothill, I.E., 2009. Biosensors for cancer markers diagnosis. Semin. Cell Dev. Biol. 20, 55–62.

Wang, H., Han, H., Ma, Z., 2017. Conductive hydrogel composed of 1,3,5-

benzenetricarboxylic acid and Fe3 + used as enhanced electrochemical immunosensing substrate for tumor biomarker. Bioelectrochemistry 114, 48–53.

Wang, H., Ma, Z., 2017. Amperometric immunoassay for the tumor marker neuron-specific enolase using a glassy carbon electrode modified with a nanocomposite consisting of polyresorcinol and of gold and platinum nanoparticles. Microchim. Acta 184, 3247–3253.

Wang, J., 2006. Electrochemical biosensors: Towards point-of-care cancer diagnostics. Biosens. Bioelectron. 21, 1887–1892.

Wang, R., Chen, X., Ma, J., Ma, Z., 2013. Ultrasensitive detection of carcinoembryonic antigen by a simple label-free immunosensor. Sensors Actuators B Chem. 176, 1044–1050.

Wang, T., Zhou, Y., Lei, C., Luo, J., Xie, S., Pu, H., 2017. Magnetic impedance biosensor: A review. Biosens. Bioelectron. 90, 418–435.

Watson, S., Nie, M., Wang, L., Stokes, K., 2015. Challenges and developments of self-assembled monolayers and polymer brushes as a green lubrication solution for tribological applications. RSC Adv. 5, 89698–89730.

Wei, Z., Zhang, J., Zhang, A., Wang, Y., Cai, X., 2017. Electrochemical Detecting Lung Cancer-Associated Antigen Based on Graphene-Gold Nanocomposite. Molecules 22, 392.

WHO, 2017. WHO | Cancer [WWW Document]. WHO. URL http://www.who.int/mediacentre/factsheets/fs297/en/ (accessed 8.20.17).

Xiao, K., Wang, K., Qin, W., Hou, Y., Lu, W., Xu, H., Wo, Y., Cui, D., 2017. Use of quantum dot beads-labeled monoclonal antibody to improve the sensitivity of a quantitative and simultaneous immunochromatographic assay for neuron specific enolase and carcinoembryonic antigen. Talanta 164, 463–469.

Xu, R.H., Liao, C.Z., Luo, Y., Xu, W.L., Li, K., Chen, J.X., Huang, Y.F., Chen, Y.C., Zhu, L., Yuan, W. Bin, 2014. Optimal cut-off values for CYFRA 21-1 expression in NSCLC patients depend on the presence of benign pulmonary diseases. Clin. Chim. Acta. 440C, 188–192.

Xu, Y., Wang, E., 2012. Electrochemical biosensors based on magnetic micro/nano particles. Electrochim. Acta 84, 62–73.

Yáñez-Sedeño, P., Campuzano, S., Pingarrón, J., 2016. Magnetic Particles Coupled to

Disposable Screen Printed Transducers for Electrochemical Biosensing. Sensors 16, 1585.

Yang, H., Mi, R., Wang, Q., Wei, X., Yin, Q., Chen, L., Zhu, X., Song, Y., 2014. Expression of neuron-specific enolase in multiple myeloma and implications for clinical diagnosis and treatment. PLoS One 9, e94304.

Yang, H., Zhou, H., Hao, H., Gong, Q., Nie, K., 2016. Detection of Escherichia coli with a label-free impedimetric biosensor based on lectin functionalized mixed self-assembled monolayer. Sensors Actuators, B Chem. 229, 297–304.

Yang, T., Vdovenko, M., Jin, X., Sakharov, I.Y., Zhao, S., 2014. Highly sensitive microfluidic competitive enzyme immunoassay based on chemiluminescence resonance energy transfer for the detection of neuron-specific enolase. Electrophoresis 35, 2022–8.

Yeh, C.-H., Su, K.-F., Lin, Y.-C., Shen, P.-L., 2013. Using the biosensor based on impedance measurement and sandwich immunoassay for carcinoembryonic antigen detection. 2013 Ieee Sensors 1–3.

Yoshimoto, T., Higashino, K., Hada, T., Tamura, S., Nakanishi, K., Mitsunobu, M., Uematsu, K., Matsuoka, T., Taketa, K., 1987. A primary lung carcinoma producing alpha-fetoprotein, carcinoembryonic antigen, and human chorionic gonadotropin. Immunohistochemical and biochemical studies. Cancer 60, 2744–2750.

Yu, D., Du, K., Liu, T., Chen, G., 2013. Prognostic Value of Tumor Markers, NSE, CA125 and SCC, in Operable NSCLC Patients. Int. J. Mol. Sci. 14, 11145–56.

Yu, S., Cao, X., 2012. Electrochemical immunoassay based on gold nanoparticles and reduced graphene oxide functionalized carbon ionic liquid electrode. Microchem. J. 103, 125–130.

Yu, T., Cheng, W., Li, Q., Luo, C., Yan, L., Zhang, D., Yin, Y., Ding, S., Ju, H., 2012. Electrochemical immunosensor for competitive detection of neuron specific enolase using functional carbon nanotubes and gold nanoprobe. Talanta 93, 433–438.

Yu, X., Wang, Y., Chen, X., Wu, K., Chen, D., Ma, M., Huang, Z., Wu, W., Li, C., 2015. White-Light-Exciting, Layer-by-Layer-Assembled ZnCdHgSe Quantum Dots/Polymerized Ionic Liquid Hybrid Film for Highly Sensitive Photoelectrochemical Immunosensing of Neuron Specific Enolase. Anal. Chem.

87, 4237–4244.

Zelada-Guillén, G.A., Bhosale, S. V, Riu, J., Rius, F.X., 2010. Real-time potentiometric detection of bacteria in complex samples. Anal. Chem. 82, 9254–60.

Zeng, Y., Bao, J., Zhao, Y., Huo, D., Chen, M., Yang, M., Fa, H., Hou, C., 2017. A sensitive label-free electrochemical immunosensor for detection of CYFRA21-1 based on 3D-G@Au. Talanta.

Zhang, Q., Li, X., Qian, C., Dou, L., Cui, F., Chen, X., 2018. Label-free electrochemical immunoassay for neuron specific enolase based on 3D macroporous reduced graphene oxide/polyaniline film. Anal. Biochem. 540–541, 1–8.

Zhang, Y., Yang, D., Weng, L., Wang, L., 2013. Early lung cancer diagnosis by biosensors. Int. J. Mol. Sci. 14, 15479–509.

Zhou, J., Du, L., Zou, Y., Hu, N., Wang, P., 2014. An ultrasensitive electrochemical immunosensor for carcinoembryonic antigen detection based on staphylococcal protein A—Au nanoparticle modified gold electrode. Sensors Actuators B Chem. 197, 220–227.

Zhou, L., Huang, J., Yu, B., You, T., 2016. A novel self-enhanced electrochemiluminescence immunosensor based on hollow Ru-SiO2@PEI nanoparticles for NSE analysis. Sci. Rep. 6, 22234.

Zhou, M., Wang, Z., Yao, Y., Zhou, H., Liu, M., Sun, J., 2017. Neuron-specific enolase and response to initial therapy are important prognostic factors in patients with small cell lung cancer. Clin. Transl. Oncol. 19, 865–873.

Zhou, X., Gua, S., Gao, J., Zhao, J., Xue, S., Xu, W., 2017. Glucose oxidase-initiated cascade catalysis for sensitive impedimetric aptasensor based on metal-organic frameworks functionalized with Pt nanoparticles and hemin/G-quadruplex as mimicking peroxidases. Biosens. Bioelectron. 98, 83–90.

Zhou, X., Xue, S., Jing, P., Xu, W., 2016. A sensitive impedimetric platform biosensing protein: Insoluble precipitates based on the biocatalysis of manganese(III) meso-tetrakis (4-N-methylpyridiniumyl)-porphyrinin in HCR-assisted dsDNA. Biosens. Bioelectron. 86, 656–663.

Zhu, L., Jia, N., Huang, B., Tan, L., Yang, S., Yao, S., 2013. Electrochemical immunoassay for carcinoembryonic antigen using gold nanoparticle–graphene

composite modified glassy carbon electrode. Talanta 116, 809–815.

Zhu, Q., Chai, Y., Yuan, R., Zhuo, Y., Han, J., Li, Y., Liao, N., 2013. Amperometric immunosensor for simultaneous detection of three analytes in one interface using dual functionalized graphene sheets integrated with redox-probes as tracer matrixes. Biosens. Bioelectron. 43, 440–5.

APPENDIX:

Appendix 1: Platform Drawing

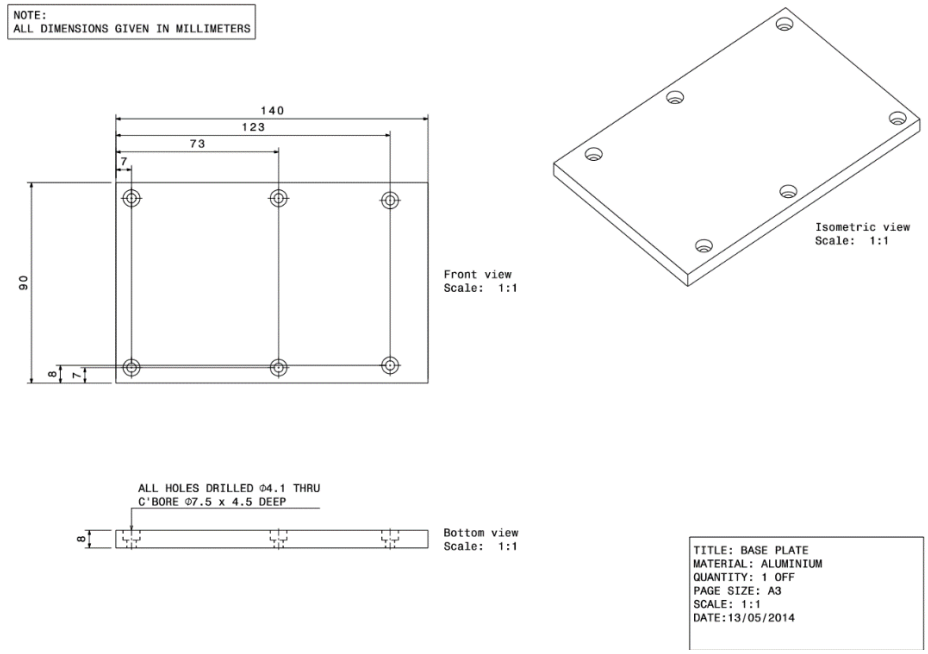

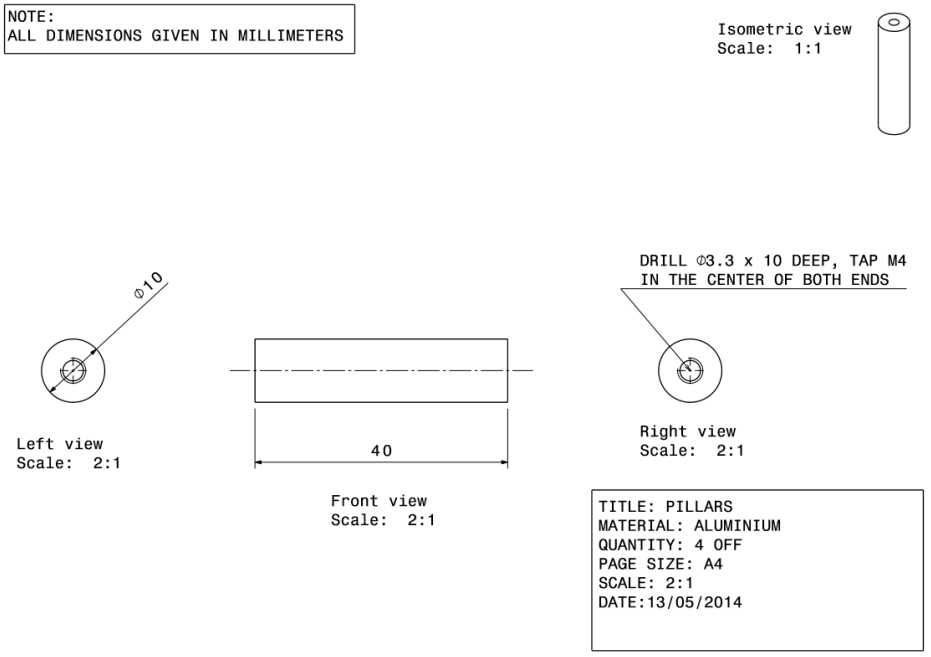

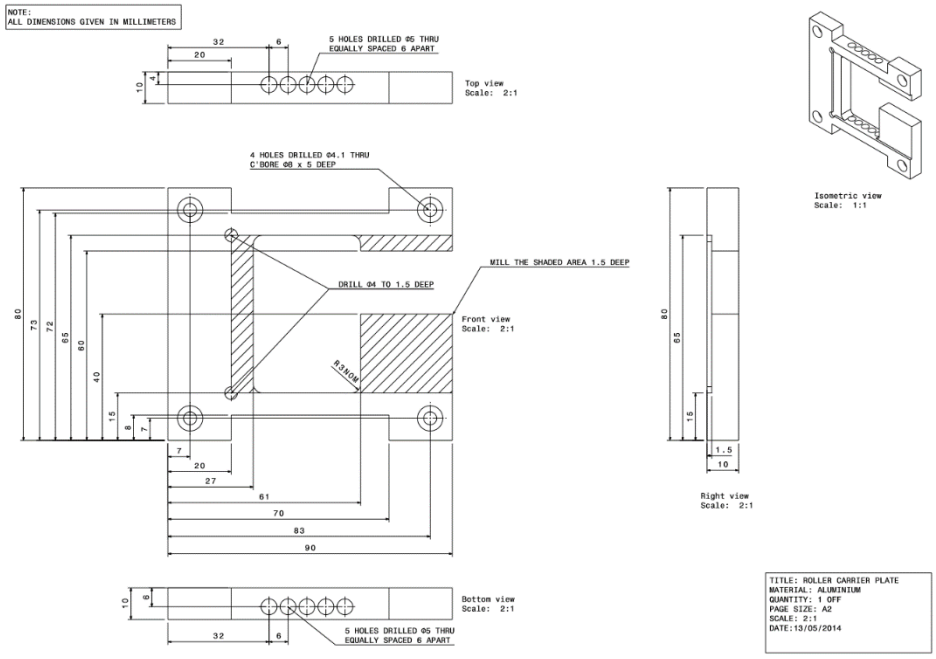

NOTE:
ALL DIMENSIONS GIVEN IN MILLIMETERS

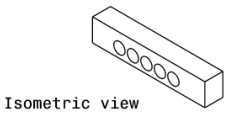

Isometric view
Scale: 1:1

Top view
Scale: 1:1

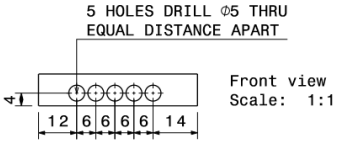

Front view
Scale: 1:1

Right view
Scale: 1:1

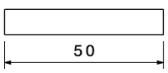

Bottom view
Scale: 1:1

TITLE: PLASTIC BEARING BLOCK
MATERIAL: PLASTIC
QUANTITY: 2 OFF
PAGE SIZE: A4
SCALE: 1:1
DATE:13/05/2014

Appendix 2: Arduino Uno Code

```
#include <Adafruit_MotorShield.h>
#include <Wire.h>
#include "utility/Adafruit_PWMServoDriver.h"


Adafruit_MotorShield AFMS = Adafruit_MotorShield();

Adafruit_StepperMotor *Motor1 = AFMS.getStepper(48,2);

void setup () {
  Serial.begin(9600);
  Serial.println("Stepper Motor");
  AFMS.begin();
  Motor1->setSpeed (100);

}

void loop () {
  Serial.println ("Microstep");
  Motor1->step(24, FORWARD, MICROSTEP);
  // 36 STEPS FOR MINE CYLINDAR
  Motor1->release ();
  delay(15000);
  Motor1->step(24, FORWARD, MICROSTEP);
  Motor1->release ();
  delay(15000);
}
```

Appendix 3: Publications

Electrochemical Impedance Spectroscopy Biosensor for Neuron-specific Enolase (NSE) Biomarker for Lung Cancer

*M. Arabnejad, I. Chianella and I.E. Tothill**

Cranfield University, Cranfield, Bedfordshire, MK43 0AL, England, UK

Introduction

Lung cancer was the most prevalent cancer in the world in 2012, causing 13% (1.8 million) of cancer incidence and 19% (1.6 million) of cancer deaths. The rate of lung cancer mortality is increasing annually. The current diagnosis methods based on cell morphology have two main disadvantages: the methods are invasive as they rely on tissue biopsy; and are not able to detect lung cancer at an early stage of the disease. Early detection is vital for patients survival and administration of the effective therapeutics since disease symptoms do not appear in patients till late cancer stages. A non-invasive and early diagnosis of lung cancer is possible via detection of protein biomarkers within body fluids (e.g. serum or blood) as the level of these molecules changes due to disease presence and progression. Enolase is a glycolytic enzyme that consists of αα, ββ, γγ, αγ, and βγ isozymes. Neuron-specific enolases (NSE), containing the γ subunit, has been associated with lung cancer. While the normal concentration range of NSE in serum of healthy individuals is between 5 to 12 ng/ml, higher concentrations are found in individuals with lung cancer. The aim of this study is to develop Electrochemical Impedance Spectroscopy (EIS) biosensors to detect and quantify NSE.

Methodology

The sensing platform includes magnetic manipulation, screen printed electrodes (SPE), and magnetic nanobeads. The magnetic nanobeads are functionalised with antibodies to capture the analyte from the sample, and to move them over the sensing area where another antibody against the analyte is attached forming a sandwich assay. Moreover, magnetic nanobeads are used to increase the chance of antigen-antibody complex formation. The PalmSens3 Potentiostat (PalmSens BV, Netherlands) is used for Electrochemical Impedance Spectroscopy measurements.

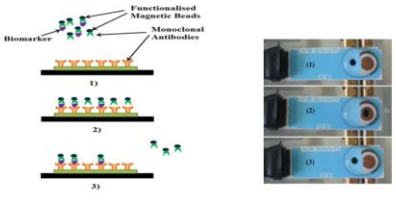

Figure 1: The working mechanism of sensing platform

Results

Figure 2: The obtained average of Ret value of before and after applying cleaning methods followed by calculation of % of reduction in Ret.

Methods	HCl	KOH+ H_2O_2	Oven	Piranha Solution	Ultrasonic Bath
Mean1 (Ret Before Cleaning)	561.35	762.05	209.14	181.99	339.75
Mean2 (Ret After Cleaning)	310.51	27.88	1685.83	3.84	761.19
M1 – M2	250.84	734.18	-1476.69	178.15	-421.44
% of R_{ct} Reduction	44.68	96.34	-706.07	97.89	-124.05

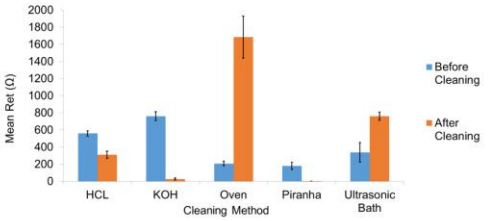

Figure 3: Comparison bar chart showing the deference in the impedance signal of SPE before and after applying various cleaning methods, before immobilising the antibodies on the surface of the electrodes (n=3).

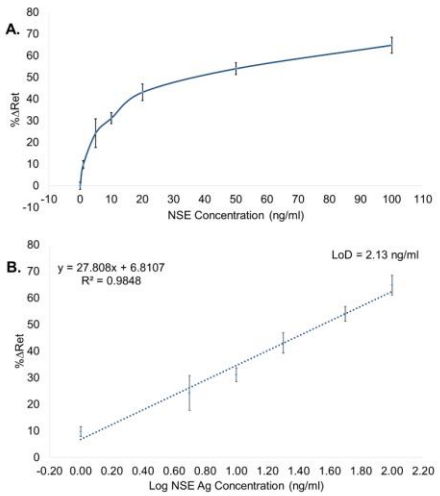

Figure 4: (A) Standardised curve response of impedance immunosensor versus NSE protein concentration (n=3). (B) Linear regression plot (n=3).

Conclusion

Cleaning the electrodes with potassium hydroxide in 25% hydrogen peroxide (KOH+H2O2) was the best cleaning method with reduction in impedance signal by 96%. Thus, the KOH+H2O2 was chosen as the most successful cleaning procedure and was used to clean all SPEs prior of functionalisation process. As shown by the linear regression plot, the platform successfully detected increasing concentrations of NSE protein with a coefficient of correlation of 0.9848 and a detection limit of 2.13 ng/ml.

**Corresponding Authors: Prof Ibtisam E.Tothill*

i.tothill@cranfield.ac.uk

www.cranfield.ac.uk